Comportement rhéologique des boues activées : Mesures, modélisation et impact sur le transfert d'oxygène dans les bioréacteurs aérés

Camilo Duran Quintero

Université Fédérale

Toulouse Midi-Pyrénées

THÈSE

En vue de l'obtention du

DOCTORAT DE L'UNIVERSITÉ DE TOULOUSE

Délivré par :

Institut National des Sciences Appliquées de Toulouse (INSA de Toulouse)

Présentée et soutenue par :
Camilo DURAN QUINTERO

le 11 Décembre 2015

Titre :

COMPORTEMENT RHEOLOGIQUE DES BOUES ACTIVEES : MESURES, MODELISATION ET IMPACT SUR LE TRANSFERT D'OXYGENE DANS LES BIOREACTEURS AERES

École doctorale et discipline ou spécialité :
ED MEGEP : Génie des procédés et de l'Environnement

Unité de recherche :
Hydrosystèmes et Bioprocédés (HBAN), Irstea - Antony

Directeur/trice(s) de Thèse :

Arnaud COCKX Maître de Conférences – INSA (Toulouse)
Sylvie GILLOT Directrice de Recherche – Irstea (Lyon)

Jury :

Olivier BREMOND Invité – Suez Environnement (France)
Pierre BUFFIERE Rapporteur – INSA (Lyon)
Yannick FAYOLLE Encadrant de thèse – Irstea (Antony)
Gilles HEBRARD Examinateur – INSA (Toulouse)
Olivier POTIER Examinateur – LRGP-ENSGSI (Nancy)
Christophe VIAL Rapporteur – IP-Polytech (Clermont Ferrand)

REMERCIEMENTS

J'ai réalisé mes travaux de thèse au sein de l'équipe Epure de l'Unité de Recherche Hydrosystèmes et Bioprocédés (HBAN) de Irstea Antony. L'accomplissement de ce travail est le fruit de la collaboration, la participation et de l'effort de nombreuses personnes sur qui j'ai eu la chance de compter et auxquelles je tiens à adresser ma gratitude sincère.

Je remercie tout d'abord M. Michel Penel, directeur régional d'Irstea Antony ainsi que M. Didier Pont et Mme. Nathalie Touze-Foltz, directeurs successifs de l'Unité de Recherche HBAN, pour leur accueil et leur contribution au bon déroulement de ma thèse.

Je tiens à remercier tout particulièrement les personnes qui ont dirigé et encadré ce projet :

Je remercie très sincèrement Mme. Sylvie Gillot pour avoir guidé ce travail avec beaucoup d'engagement, pour avoir apporté toute son expertise scientifique remarquable dans toutes les étapes et pour son exigence.

De même, je remercie M. Arnaud Cockx pour m'avoir fait confiance depuis mon stage de recherche pour entreprendre ce projet, pour ses conseils avisés et pour sa participation enrichissante aux multiples discussions scientifiques d'avancement du projet.

Aussi, j'adresse un immense merci à M. Yannick Fayolle pour s'être impliqué autant dans ce projet, pour sa disponibilité sans bornes, pour sa confiance et pour la qualité scientifique et humaine de son encadrement. De même je lui remercie pour son soutien désintéressé dans les moments les plus durs.

Mes remerciements sont aussi adressés à M. Gilles Hebrard, M. Olivier Bremond et M. Jean-Christophe Baudez pour leur participation aux comités de thèse qui a fait évoluer positivement ce travail. Je dois remercier en particulier M. Baudez pour nous avoir proposé le défi de la mise en œuvre du rhéomètre capillaire.

Je remercie également les professeurs M. Pierre Buffièrè et M. Christophe Vial pour avoir accepté d'évaluer mon travail en qualité de rapporteurs, ainsi que M. Olivier Potier pour sa participation au Jury en tant qu'examinateur et pour les corrections qu'ils ont apporté au manuscrit. De même, à tous les membres du jury je les remercie pour leurs analyses, retours et questions intéressantes qui ont eu lieu lors de ma soutenance de thèse.

Je souhaite aussi remercier toutes les personnes ayant contribué au déroulement de mon travail expérimental, tant lors des mesures réalisées au laboratoire que lors des différentes campagnes effectuées sur le terrain, où malgré des conditions climatiques rarement clémentes et une

dynamique de travail souvent épuisante, leur enthousiasme et bonne humeur me firent toujours sentir que ce projet était le leur aussi.

Ainsi, je remercie vivement M. Pierre Mauricrace pour tout le savoir faire précieux qu'il a apporté à la préparation et au développement technique et logistique des campagnes de mesure sur le terrain et au laboratoire. Sa participation et son assistance ont été déterminantes pour minimiser les inévitables pannes lors des expérimentations. Outre la qualité de son travail, sa compagnie chaleureuse et agréable m'a apporté de la sérénité à tout moment.

Egalement, j'adresse un grand merci à Sylvain Pageot pour son apport très important à la réalisation de l'ensemble de mes travaux expérimentaux, toujours avec détente et camaraderie sans perdre de vue la rigueur nécessaire pour réussir cette étape. De même je le remercie pour tous les échanges scientifiques et sportifs que nous avons pu partager, mais surtout je voudrais le remercier pour son amitié simple et sincère au long de ces années.

De même, je remercie vivement Yoan Pechaud pour sa participation impliquée et sa posture réflexive lors de la réalisation des expériences et pour les multiples discussions qui ont contribué à faire avancer de façon significative les divers aspects scientifiques. Je lui remercie aussi pour son amitié et pour les bons moments partagés.

Mes remerciements son également adressés aux stagiaires Virginie Clérima, Kevin Gerbel et Florian Maillard avec qui j'ai partagé des moments amicaux et chaleureux et dont leur travail investi a fait avancer de façon importante la partie expérimentale de ce projet.

De même, je tiens à remercier M. Joel Zancanaro (Suez Environnement) pour nous avoir facilité l'accès de notre équipe terrain aux stations de traitement d'eau et pour s'être rendu disponible pour partager des renseignements divers. Aussi, ces remerciements sont adresses à Larry, Benjamin, Olivier, Cyril, Jean-Luc, exploitants des stations d'épuration qui nous ont accueilli dans leurs installations avec ouverture et bonne humeur.

J'adresse aussi une pensée particulière à Graziella Alvarez et Fatou Ndoye de Irstea GPAN pour avoir partagé amplement divers renseignements concernant la construction du rheometre tubulaire. Je leur suis redevable de leur collaboration et leur exprime toute ma gratitude.

Je remercie aussi aux membres de l'Equipe Chimie de HBAN, notamment Mme. Nina Pourette, pour la réalisation des analyses de cations.

Je tiens à remercier aussi Mme. Michelle Lebel, Mme. Elizabeth Riant, Mme. Nathalie Camus, Mme. Laurence Tanton et M. Roger Martins pour leur support logistique et leur gentillesse ayant contribué au déroulement de ce projet dans les meilleures conditions.

Aux amis et collègues de l'équipe EPURE, Nadège Durban, Julien Bollon, M. Alain Heduit, Ahlem Filali, M. Jean-Jacques Pernelle, Anne Goubet, Elodie Suard, David Delage, Lauriane Juzan, Stéphane Bons, Cyril Marcilhac et Vincent Landreau, je leur adresse aussi un grand merci pour leur accueil, leur écoute, leur encouragements, leurs conseils et pour tous les moments chaleureux partagés aussi en dehors du travail.

Egalement, je remercie toutes les personnes des différentes équipes de recherche avec qui j'ai pu échanger spontanément dans les couloirs de Irstea et lors des participations aux diverses activités au sein de l'association ASSCR (Frisbee, Football, Volleyball, Apiculture, Potagers) et grâce à qui le quotidien a été très plaisant à vivre (Valérie, Cédric, Pierre, David, Damien, Charles, Florent, Simon S., Simon P., Vazken, Michäel, Alfred, Hocine, Marc, François, Remy, Theo, Louise, Julien T., Laure, Pascal, Olivier, Carolina, Oscar, Hajer).

Je remercie profondément Claire Vanouche et les amis de Toulouse (Antoine, Olivier, Philippe, Laura, Lucie, Bruno, Cathy, Marie Claude, Yolanda, Cécile, Gilles, Bernard, Alain, Pascal, Sophie, Antonia, Amandine, Papit, Lina et Diana) qui m'ont accueilli en France bras grands ouverts et puis accompagné avec énormément de générosité et d'ouverture. De même, je remercie mes cousines Catalina et Paola et leurs familles pour leur affection, leur vitalité contagieuse, leur attitude « rien n'est impossible » et les très belles aventures partagées.

J'adresse aussi une pensée particulière à mes amis du Lycée (Mincho, Pipe, Corduroy, Gambito, Guguen et Oscar) et de l'Université en Colombie (María, Chihiro, Germán, Pat, Andru, Josuelo, Richard, Carolina, Lucho, Jorge) que je ne vois plus beaucoup mais dont le seul fait de me souvenir a été un motif de joie pendant ces années.

Finalement, je remercie infiniment mes parents, pour leur amour, protection et générosité et pour avoir été un exemple d'honnêteté, dévouement et travail. De même, je remercie mes chères sœurs Liliana et Valentina, mes grands-parents, Doña Alma, Carla, ainsi que toute ma famille, qui a rempli ma vie de beaux souvenirs et qui n'a jamais cessé de me soutenir. A JuanPi, merci pour le bonheur qu'il nous apporte. Et à Erika, pour sa compréhension, sa douceur et sa joie, je lui adresse ma gratitude la plus profonde.

RESUME

Le but principal de cette étude était d'évaluer et de mieux comprendre l'impact de la vitesse superficielle de gaz et des propriétés de boues activées (BA), sur leur comportement rhéologique et le transfert de l'oxygène dans des bioréacteurs.

Tout d'abord, la rhéologie des BA a été évaluée à l'aide d'un rhéomètre tubulaire, conçu et construit dans ce travail. Des mesures rhéologiques ont été effectuées avec des BA provenant de cinq stations d'épuration (STEP) et avec des concentrations en MES comprises entre 2.3 et 10.2 g L^{-1}. Selon ces résultats, la rhéologie des BA est significativement déterminée par la concentration en matière en suspension (MES) mais d'autres caractéristiques liées à leur origine, tel que la taille, la cohésion et la densité du floc, peuvent aussi influencer la viscosité apparente des boues. Basé sur les rheogrames expérimentaux, le modèle rhéologique issu de cette étude est comparé à des modèles rhéologiques existants.

Deuxièmement, le transfert d'oxygène a été évalué dans une colonne à bulles (Hc=4.4 m, Dc=0.29 m) installée dans deux STEP: une installation classique et un bioréacteur à membrane. La colonne, alternativement équipée d'un diffuseur fines ou grosses bulles (FB, GB), a été alimentée en continu avec des BA extraites du réacteur d'aération, ou de la boucle de recirculation ou du réacteur membranaire. Pour des MES comprises entre 3.0 et 10.4 g L^{-1}, le coefficient $k_L a$ a été plus faible dans les BA que dans l'eau propre et encore réduit avec une augmentation des MES. Cette diminution est en partie attribuable à la réduction observée de la rétention de gaz (ε_G), associée à une augmentation de la viscosité apparente des boues, celle-ci entrainant une réduction de l'aire interfaciale spécifique (a) due à la coalescence de bulles et à la formation de bulles plus grosses. Aussi, la concentration des tensioactifs non ioniques, a montré un effet négatif sur le coefficient $k_L a$ lors des tests d'oxygénation effectués en aération FB et faibles concentrations en MES. Cet impact n'a pas été observé dans des conditions d'aération GB, ce qui a été expliqué par le taux de renouvellement d'interface plus élevé généré par ces dernières.

Enfin, le taux de cisaillement moyen exercé par l'essaim de bulles dans la colonne pendant les tests d'oxygénation a été théoriquement évalué compte tenu des conditions d'opération. Par la suite, des corrélations empiriques ont été construites en utilisant des nombres adimensionnels et expriment le coefficient $k_L a$ en fonction de la vitesse superficielle de gaz et la viscosité apparente, tout en considérant sa dépendance du taux de cisaillement. Enfin, le facteur alpha est défini comme une loi de puissance décroissante en fonction de la viscosité apparente, pour des systèmes à faible chargé.

Mots-clés: boues activées, rhéologie, rhéomètres tubulaire, transfert d'oxygène, colonne à bulles, hydrodynamique.

ABSTRACT

The main purpose of this study was to evaluate and better understand the impact of superficial gas velocity and activated sludge properties, on activated sludge rheology and oxygen transfer in bioreactors.

First of all, activated sludge rheology was evaluated using a tubular rheometer, designed and constructed in this work. Rheological measurements were performed with activated sludge from five different wastewater treatment plants and with MLSS concentrations between 2.3 and 10.2 g L^{-1}. Results showed that although the sludge rheology is significantly defined by the MLSS concentration, other sludge characteristics related to the sludge origin, such as such as floc size, floc cohesiveness and floc density also influence the sludge apparent viscosity. Existing rheological models were evaluated on the set of obtained experimental flow curves.

Besides, the oxygen transfer is evaluated in a bubble column (Hc=4.4, Dc=0.29 m) installed in two different wastewater treatment plants: a conventional activated sludge plant (CAS) and a membrane bioreactor (MBR). The column, alternatively equipped with a fine or a coarse bubble diffuser (FB, CB), was continuously fed with activated sludge extracted either from the aeration tank, the recirculation loop or the membrane reactor. With MLSS concentrations from 3.0 to 10.4 g L^{-1}, the $k_L a$ coefficient was lower in activated sludge than in clean water and still reduced with an increase of the MLSS concentration. This reduction is partially attributed to the observed reduction of gas holdup (ε_G), associated with an increase in the sludge apparent viscosity (μ_{app}), which leads to a reduction of the specific interfacial area (a) due to bubble coalescence and the formation of larger bubbles. Besides, the concentration of non-ionic surfactants, exhibited a negative effect on the $k_L a$ coefficient for the oxygenation tests performed under FB aeration conditions and low MLSS concentration. This impact was not observed under CB aeration conditions, which was explained by the higher renewal rates generated by coarse bubbles.

Finally, the mean shear rate exerted by the bubble swarm in the column during the oxygen transfer tests was theoretically evaluated considering the operating conditions. Subsequently, empirical correlations were constructed using dimensionless numbers and express the oxygen transfer coefficient as a function of the superficial gas velocity and the apparent viscosity, considering its shear rate dependence. Finally, alpha factor is defined as a power law decreasing function of the apparent viscosity, for low loaded activated sludge systems.

Keywords: Activated sludge, non-Newtonien fluid, rheology, tubular rheometer, oxygen transfer, hydrodynamics, bubble column.

LIST OF CONTENTS

NOTATION

Latin Letters

a	Specific interfacial area	(m^2 m^{-3})
A	Gas-liquid interfacial area	(m^2)
C	Dissolved oxygen concentration in activated sludge	(kg L^{-1})
Cs'	Dissolved oxygen saturation concentration in activated sludge	(kg L^{-1})
C_D	Bubble drag coefficient	(-)
COD_s, COD_t	Soluble /total Chemical Oxygen Demand	(mg L^{-1}) , (g L^{-1})
d_{bs}	Bubble Sauter diameter	(m)
db	Bubble diameter	(m)
D	Capillary tube diameter	(m)
$D_{3/2}$	Mean surface floc diameter	(μm)
$D_{4/3}$	Mean volume floc diameter	(μm)
D_{50}	Median floc diameter	(μm)
D_C	Column diameter	(m)
D_{O_2}	Oxygen diffusion coefficient	(m^2 s^{-1})
Fci	Floc cohesion index	(-)
Fr	Froude number	(-)
g	Standard gravity constant	(m s^{-2})
G	Bubble slip velocity	(m s^{-1})
Ga	Galileo number	(-)
HFV	Hydrostatic floc volume	(mL L^{-1})
Hc	H, column height	(m)
He	Henry's law constant	(-)
J	Mass flux per surface unit	(kg s^{-1} m^{-2})
k_G, k_L	Gas-side (G) / liquid-side (L) mass transfer coefficient	(m h^{-1})
k_La	Volumetric oxygen transfer coefficient	(h^{-1})
k_La'	Volumetric oxygen transfer coefficient in activated sludge	(h^{-1})
k_La_{20}	Volumetric oxygen transfer coefficient at 20°C	(h^{-1})
K_G, K_L	Gas-side (G) / liquid-side (L) global mass transfer coefficient	(m h^{-1})
K	Consistency index	(Pa s^n)
MLSS	Mixed liquor suspended solids	(g L^{-1})
MLVSS	Mixed liquor volatile suspended solids	(g L^{-1})

n	Flow index	(-)
N_T	Transfer number	(-)
OTE_c	Oxygen transfer efficiency	(-)
ΔP	Pressure loss in the capillary tube	(Pa)
$\Delta P/L$	Longitudinal pressure loss in the capillary tube	(Pa m^{-1})
Q	Flow rate in the capillary tube	(m^3 h^{-1})
Q_i	Inlet airflow rate	(m^3 h^{-1})
Q_e	Outlet airflow rate	(m^3 h^{-1})
R	Capillary tube ratio	(m)
Re	Reynolds number	(-)
s	Surface renewal rate	(s^{-1})
S	Reactor`s cross section	(m^2)
Sc	Schmidt number	(-)
St_M	Stanton mass transfer number	(-)
$SOTE$	Standard oxygen transfer efficiency	(-)
t	Time	(s)
t_C	Gas-liquid contact time at the interface	(s)
SVI	Sludge volume index	(mL g^{-1})
T	Temperature	(°C)
U_b	Bubble rise velocity	(m s^{-1})
U_G, U_L	Superficial gas (G) /liquid (L) velocity	(m s^{-1})
V	Aerated volume reactor	(m^3)
$y_{CO2,e}$	Carbon dioxide molar fraction at the outlet air flow	(-)
$y_{CO2,i}$	Carbon dioxide molar fraction at the inlet air flow	(-)
y_e	Oxygen molar fraction at the outlet air flow	(-)
y_i	Oxygen molar fraction at the inlet air flow	(-)
$y_{w,i}$	Water vapor molar fraction at the inlet air flow	(-)
$y_{w,e}$	Water vapor molar fraction at the outlet air flow	(-)

Greek letters

α	Alpha factor	(-)
β	Activated Sludge correction coefficient for oxygen saturation concentration	(-)
ε_G	Overall gas hold-up	(%)
$\dot{\gamma}$	Shear rate	(s^{-1})
μ	Dynamic viscosity	(Pa.s)
μ_{app}	Apparent viscosity	(Pa.s)
μ_∞	Limit viscosity	(Pa.s)
θ	$k_L a$ temperature correction factor	(-)
ρ_G, ρ_L	Gas density, Liquid density	(kg m^{-3})
ρ_{ML}	Density of the mixed liquor	(kg m^{-3})
σ	Static surface tension	(mN m^{-1})
τ	Shear stress	(Pa)
τ_y	Yield shear stress	(Pa)
χ	Bubble eccentricity	(-)

INTRODUCTION

Context and objectives

Sustainable management of water resources is a priority concern for the international community. Environmental regulations issued by the different nations seek to minimize the impact of domestic and industrial disposals on aquatic environments. Due to its efficiency, relatively simple operation and low cost, activated sludge (AS) is the most widely used process for wastewater treatment (Hreiz *et al.,* 2015). In France, close to 80% of the pollution load in wastewater is treated using this technology. However, the energy expenditure related to the air supply and dispersion, required to perform the biological process, can represent up to 70% of the total electrical consumption in the treatment facilities (Descoins *et al.,* 2012). A fine understanding on how the different dimensional and operational parameters impact the aeration efficiency of the system is part of the process optimization.

Studies performed in clean water have shown that the aeration efficiency depends on design parameters such as the reactors geometry and the characteristics of the aeration system (type, layout and depth) as well as on the operating conditions such as superficial gas velocity or liquid circulation velocity (Gillot *et al.* 2005). In order to precise the impact of these variables on hydrodynamics and aeration efficiency in aeration tanks, computational fluid mechanics (CFD) tools have been used to develop modelling protocols to simulate two-phases flows and oxygen transfer in clean water (Cockx *et al.*, 2001, Vermande, 2005, Fayolle *et al.*, 2007).

Under process conditions, the aeration efficiency is always lower compared to its value in clean water (Henkel, 2010). In order to optimise the aeration systems and to adapt the developed CFD models to process conditions, the influence of AS characteristics (rheology, solid content, particle size, physico-chemical properties, etc.) on hydrodynamics and oxygen transfer needs to be further evaluated.

Concerning the soluble phase, measurements carried out in clean water and in clean water with different additives have demonstrated that soluble substances such as surfactants (even at small concentrations i.e. 1 mg L^{-1}), salts and glucose interfere with oxygen transfer through different mechanisms, impacting bubble coalescence, surface tension and oxygen diffusivity (Wagner and Pöpel 1996; Gillot *et al.* 2000; Rosso *et al.* 2006; Germain *et al.* (2007); Hebrard *et al.* 2009; Jamnongwong *et al.* 2010). For Rosso *et al.* (2005), Gillot and Héduit (2008) and Henkel (2010), the negative impact of the soluble substances on oxygen transfer is reduced at higher sludge retention time (SRT > 15 days) due to a more advanced removal or sorption of soluble substances such as surfactants.

Several investigations performed on AS systems have highlighted that increasing the MLSS (mixed liquor suspended solids) concentration (in the range of 2 to 30 g L^{-1}) reduces the volumetric mass transfer coefficient (Cornel *et al.,* 2003; Krampe and Krauth 2003; Jin *et al.,* 2006; Germain *et al.,* 2007; Henkel *et al.* 2009). The presence of solids (biological flocs and particulate material) firstly represents an obstacle for the oxygen transfer at the gas-liquid interface (steric effect, Mena *et al.* 2005). In addition, the MLSS concentration has been identified to play a determining role in the rheological behaviour of activated sludge (Rosenberger *et al.* 2002; Tixier *et al.* 2003; Mori *et al.* 2006; Yang *et al.* 2009), which in turns is a key property governing the bioreactor hydrodynamics and consequently impacting the volumetric oxygen transfer coefficient ($k_L a$). Viscosity can affect the bubble's size at detachment (Kulkarni and Joshi 2005) or their rising velocity and the bubble coalescence phenomena (Mena *et al.* 2005). As activated sludge is a non-Newtonian fluid (Seyssiecq *et al.* 2003; Ratkovich *et al.* 2013), its apparent viscosity depends on the shear rate, which can be exerted by the stirring system and by the air injection. No study has until now evaluated, on the same type of activated sludge, the relationship between the AS physico-chemical properties, its dynamic rheological behaviour, the airflow rate and oxygen transfer. In this context, the main purpose of the PhD was to evaluate the influence of two key parameters of aerated bioreactors (sludge properties and superficial gas velocity) on AS rheological behaviour, hydrodynamics (mean shear rate) and on the volumetric oxygen transfer coefficient. Three research tracks were followed to reach this objective:

1. Studying and modelling the rheological behaviour of AS. Given the data dispersion between the different proposed rheological models in literature, rheological measurements were performed to evaluate the AS rheology. AS from different treatment plants have been considered and several AS properties (MLSS content, floc size, floc cohesiveness and soluble COD, cations, surface tension, sludge volume index) were determined. To perform the rheological measurements, a tubular rheometer adapted to the sludge characteristics was designed and constructed and a dedicated experimental protocol was developed.

2. Studying the impact of operating conditions (airflow rate and bubble diffuser type) and activated sludge properties on oxygen transfer. A bubble column with a liquid depth equivalent to full-scale aeration tanks and fed continuously with AS, was installed on two wastewater treatment plants (WWTPs): a conventional AS plant and a membrane bioreactor (MBR). MLSS concentrations were varied depending on the sampling location of the sludge (aeration tank, recirculation loop, membrane reactor). This column was

alternatively equipped with a fine bubble and a coarse bubble diffuser. Oxygen transfer coefficients and overall gas hold-ups measurements were performed at different aeration rates. In parallel, the sludge physicochemical properties – including rheological behaviour - were determined in order to evaluate their impact on oxygen transfer.

3. Confronting AS rheology and oxygen transfer results. A dynamic representation of the apparent viscosity in the aerated reactor has been introduced by estimating the shear rate prevailing in the bubble column considering the hydrodynamic conditions (superficial gas and liquid velocities, overall gas-hold-up) and AS rheology (function of the AS properties) during the oxygen transfer tests.

Outline of the document

The PhD thesis consists of 6 chapters that are briefly described below.

Chapter 1 proposes a literature review related to the two main subjects of the PhD thesis: oxygen transfer and rheological behaviour of activated sludge. Mechanisms involved in both processes are first presented, and activated sludge properties that may influence them are then analysed.

Experimental material and methods used in this work are presented in **Chapter 2**. In particular, the conception and design of the employed rheometer is described, as well as the bubble column (Dc=0.29 m, Hc=4.4 m) that has been used to characterise oxygen transfer on site. The measurement methods, including the principles of the rheological measurements with a tubular rheometer and oxygen transfer characterisation are also described.

The use of the tubular rheometer has required to develop and adapt a methodology to characterize the rheological behaviour of activated sludge. This methodology is described in **Chapter 3**. The uncertainty of the measurement is first assessed, and the implementation of the apparatus is described, especially the conditions allowing to reach a given accuracy.

In **Chapter 4** are presented the results of the experimental rheological study performed to investigate the rheology of activated sludge samples issued from five different wastewater treatment plants. The AS rheological behaviour is first evaluated by analysing the shape of experimental rheograms. Subsequently, the relationship between the mentioned physicochemical properties of AS and its rheological behaviour is studied. Finally, a rheological model is issued based on the experimental rheograms and the impacting parameters.

Chapter 5 is dedicated to the analysis of oxygen transfer results in clean water and activated sludge obtained in the bubble column mentioned above and the influence of AS physicochemical properties, superficial gas velocity and bubble diffuser type on those results.

Results of the rheological measurements are confronted to oxygen transfer characteristics in **Chapter 6**. The apparent viscosity, integrating the shear-thinning behaviour of activated sludge rheology, is especially investigated and shown to be the key parameter to interpret the impact of operating conditions (as MLSS concentration and superficial gas velocity) on oxygen transfer efficiency in the bubble column.

Chapter I. Literature Review

This literature review begins with an introduction of the activated sludge process. The two main subjects of this work are then addressed: oxygen transfer and rheology. First the oxygen transfer principles and characteristics parameters are identified. After a quick review of the design and operational parameters that affect the oxygen transfer in clean water, a literature analysis on the activated sludge properties and constituents that impact the oxygen transfer is presented. In a second part, after introducing the rheology principles, the rheological models used to represent the activated sludge non-Newtonian behaviour are then presented. The activated sludge properties that may influence the rheological behaviour are then examined.

I.1 Activated sludge (AS) process

The activated sludge process, developed 100 years ago, is a biological wastewater treatment allowing the removal of the suspended and soluble major pollutants of wastewater (organic matter, nitrogen and phosphorus). A simplified conventional activated sludge wastewater treatment (CAS) is depicted on Figure I.1.

Prior to the biological treatment, the raw wastewater follows a series of pretreatments in order to eliminate coarse solids, sand and grease by means of screening, settling, and flotation procedures respectively.

The pretreated wastewater is then sent to the bioreactor where it will be mixed with a culture of suspended and flocculated microorganisms capable of assimilating the soluble carbonaceous, nitrogenous and phosphorus pollution. The resulting mixed liquor is called *activated sludge.* Because the biodegradation requires dissolved oxygen, the bioreactor includes an aeration system. As the bioassimilation proceeds, the biomass population grows and the interstitial water is cleared out of its major pollutants. Finally, to separate the interstitial water from the biological aggregates, the activated sludge is sent to a clarifier. Then the suspended solids settle and are partially recycled to the bioreactor in order to maintain a constant biomass concentration while the treated water exits the clarifier by overflow. The excess sludge is sent to sludge treatment. The residence time of the biomass in the system, also called the mean cell residence time or the sludge age, ranges from 10 to 30 days in systems designed to fully treat nitrogen components. With adequate operating conditions, the conventional activated sludge process (CAS) has the capacity of removing more than 90% of suspended solids, 75% of the organic matter, 70% of the nitrogenous pollution and 80% of the phosphorous pollution contained in the raw wastewater using metallic salts addition (Elskens, 2010).

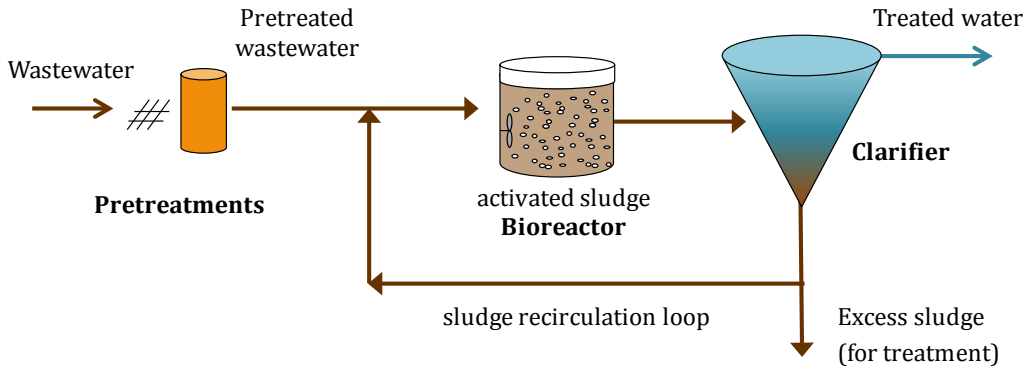

Figure I.1 Schematic of a conventional activated sludge process

Instead of separating the biological aggregates from the treated water using a settling step in the clarifier, an alternative process that incorporates a filtration step was introduced in the late 1960's. This process is known as membrane bioreactor (MBR). The filtration step is performed by means of submerged membrane modules that are incorporated in the aeration tank or in separate basins and designed with large filtration surfaces in order to reach high permeate flows. The use of fine pore membranes (0.05 and 0.4 μm) guarantees an effluent with better quality than the conventional process through the complete removal of suspended solids. Additionally, this configuration allows to increase the biomass concentration therefore reducing the volume of the biological tanks.

I.1.1 Aeration systems

Different technologies have been developed in order to supply oxygen for the biological demand in the bioreactors. These systems can be classified in 3 categories as follows:

- Mechanical surface aerators such as rotating impellers or brush rotors. These devices enlarge the gas-liquid interface by shearing the liquid surface and projecting liquid droplets into the air. Simultaneously, air bubbles are introduced into the mixed liquor.

- Jet aerators: these systems pump out the activated sludge and mixed it with pressurized air before reintroducing it into the reactor through a high velocity jet stream.

- Air injection systems: these devices supply air through gas diffusers installed at the bottom of the reactor. Depending on the orifice diameter, these systems produce fine (~3mm), medium (~4-6mm) or coarse bubbles.

Because of the high performance of the air injection systems in terms of the transferred oxygen per amount of energy consumed (aeration efficiency), especially for the fine bubbles diffusers, the use of these systems in the wastewater treatment plants[1] have been extended since the 90's.

Despite of a better energy performance of the air injection systems, the energy expenditure of the aeration stage can represent up to 70% of the energy consumption in the treatment plant (Fayolle *et al.,* 2010). In order to reduce this energy expenditure, it is necessary to evaluate the performance of the aeration system in relation to the activated sludge characteristics. This requires the determination of the amount of transferred oxygen and hence to understand the gas-liquid mass transfer principles. These are presented in the following paragraphs.

I.2 Principles of gas-liquid mass transfer

In a system where the concentration of species is spatially heterogeneous, the molecules species migrate spontaneously to minimize the concentration differences. This mass flux phenomena, driven by a concentration gradient, is known as the diffusional mass transfer and is described by the Fick's first law. According to this principle, in a system with species A and B, the mass flux of A (J_A) diffusing in the direction z, is related to the concentration gradient of A by means of a proportionality constant called the molecular diffusion coefficient. The first Fick's law is written as:

$$J_A = -D_{AB}\frac{\partial C_A}{\partial z} \qquad \text{I.1}$$

with

J_A mass flux of A (kg s^{-1} m^{-2})

D_{AB} diffusion coefficient of A into B (m^2 s^{-1})

$\partial C_A/\partial z$ concentration gradient of A in the direction z (kg m^{-4})

Assuming that the diffusion of the component A is unidirectional and carried out through a stationary film of thickness e where the concentration gradient is ΔC_A, the A mass flux is written as:

[1] Nowadays also called water resource recovery facilities (WRRF).

$$J_A = \frac{D_{AB}}{e}\Delta C_A \qquad \text{I.2}$$

A transfer coefficient (k) is introduced as a characterization of the film diffusivity in relation to the film thickness:

$$J_A = \frac{D_{AB}}{e}\Delta C = k\Delta C \qquad \text{I.3}$$

In the study of gas-liquid mass transfer it is assumed that both phases are separated by an interface and that diffusional mass transfer occurs inside a gas and a liquid film with thickness e developed at each side of the interface. This representation of the gas-liquid diffusional mass transfer corresponds to the double film model (Lewis et Whitman, 1924). It considers the following assumptions:

- The gas and the liquid films are characterized by the transfer coefficients k_G and k_L respectively;
- At the gas-liquid interface, concentrations are in equilibrium according to the Henry's law;
- Concentrations outside the films are homogenous;

The double film model is represented in Figure I.2.

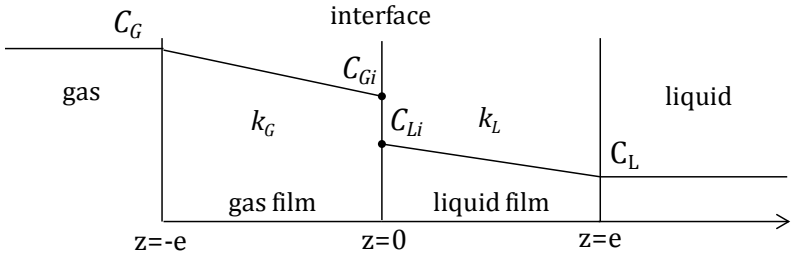

Figure I.2. Double film model (adapted from Roustan, 2003)

In the double film model, the solute mass transfer from a gas phase to a liquid phase is carried out following three steps:

- The solute diffuses through the gas film and reaches the gas-liquid interface

- The gas is absorbed and solubilises into the liquid and a thermodynamic equilibrium is established.
- The solute gas diffuses through the liquid film until it reaches the liquid phase homogenous concentration.

In the gas film, the solute molar flux ($J°$) is written as:

$$J° = k_G(C_G - C_{Gi}) \quad \text{I.4}$$

and in the liquid film, the solute molar flux is:

$$J° = k_L(C_{Li} - C_L) \quad \text{I.5}$$

with

k_G gas-side mass transfer coefficient (m s^{-1})

k_L liquid-side mass transfer coefficient (m s^{-1})

C_G solute molar concentration in the homogenous gas phase (mol m^{-3})

C_{Gi} gas-side molar concentration at the interface (mol m^{-3})

C_{Li} liquid-side molar concentration at the interface (mol m^{-3})

C_L solute molar concentration in the homogenous liquid phase (mol m^{-3})

Because of the experimental difficulty to access the solute concentrations C_{Gi} and C_{Li} at the interface, *global* mass transfer coefficients for the gas and liquid phase in equilibrium, according to the Henry's law ($C_{GS} = He.C_{LS}$), are introduced. The molar flux of transferred solute is respectively written as:

$$J° = K_G(C_G - C_{GS}) \quad \text{I.6}$$

$$J° = K_L(C_{LS} - C_L) \quad \text{I.7}$$

with

K_G gas-side global mass transfer coefficient (m s^{-1})

K_L liquid-side global mass transfer coefficient (m s^{-1})

C_{GS} solute molar concentration in the gas phase in equilibrium with C_L (mol m^{-3})

C_{LS} solute molar saturation concentration in the liquid phase in equilibrium with C_G (mol m^{-3})

Each layer in the double film represents a resistance to mass transfer. With the equilibrium condition at the interface ($C_{GS} = He.C_{LS}$), the global resistance to mass transfer in the gas and the liquid phase are written as:

$$\frac{1}{K_G} = \frac{1}{k_G} + \frac{H_e}{k_L} \quad \text{I.8}$$

$$\frac{1}{K_L} = \frac{1}{k_L} + \frac{1}{He \cdot k_G} \quad \text{I.9}$$

with

He Henry's law constant

$1/K_G$ global resistance to mass transfer in the gas film (s m^{-1})

$1/K_L$ global resistance in the liquid film (s m^{-1})

If the component solubility in the liquid phase is low, the Henry constant (He) is very high. Then the gas-liquid mass transfer is conditioned by the resistance to mass transfer of the liquid film. Thus, the gas-liquid molar flux is written as:

$$J = K_L(C_{LS} - C_L) = k_L(C_{LS} - C_L) \quad \text{I.10}$$

I.2.1 The volumetric oxygen transfer coefficient (k_La)

The determination of oxygen transfer is based on the first Fick's law and the double film model. Because the oxygen solubility in water is low, the mass flow of transferred oxygen is expressed as:

$$F = JA = k_L A\,(Cs - C) \quad \text{I.11}$$

with

F mass flow of transferred oxygen (kg h^{-1})

A gas-liquid interfacial area (m^2)

Cs dissolved oxygen saturation concentration (kg m^{-3})

C dissolved oxygen concentration in the liquid phase (kg m^{-3})

The concept of specific interfacial area is introduced to express the interfacial area per unit of aerated volume ($a = A/V$). The mass flow of transferred oxygen is expressed as follows:

$$F = k_L a\,(Cs - C)V \quad \text{I.12}$$

with

$k_L a$ volumetric oxygen transfer coefficient (h^{-1})

V aerated volume (m^3)

The mass flow of transferred oxygen is therefore expressed as the product of the volumetric oxygen transfer coefficient ($k_L a$) by the gradient concentration ($Cs - C$). $k_L a$ depends on the liquid-side oxygen transfer coefficient (k_L) and the specific interfacial area (a). The dissolved oxygen saturation concentration (Cs) is a function of the atmospheric and hydrostatic pressure and liquid characteristics (including temperature, salts concentration…).

I.2.2 The liquid-side mass transfer coefficient (k_L)

According to the film model, the liquid-side mass transfer coefficient is the ratio of the diffusivity coefficient of the liquid film to the film thickness e (D_{AB}/e). The practical difficulty of using this model is the determination of the thickness of the liquid film. Other theoretical models have therefore been proposed to estimate the liquid-side mass transfer coefficient (k_L). These are presented in Table I.1 for two different intervals of bubble size. Above 2.5 mm of diameter, bubbles are considered to have a mobile and renewable interface which favors the oxygen transfer. On the contrary, for rising bubbles with a diameter lower than 2.5 mm, the bubble interface is considered a rigid surface that is scarcely renewable.

Table I.1. Correlations for estimating the liquid-side mass transfer coefficient (k_L) for different size of bubbles

Model	Equation			Bubble size interval (mm)
Higbie model (1935)	$k_L = 2\sqrt{\frac{D}{\pi \cdot t_c}}$	I.13	D diffusivity coefficient ($m^2\ s^{-1}$) t_c contact time (s)	d_b>2.5
	$t_c = \frac{d_b}{G}$	I.14	d_b bubble diameter (m) G bubble slip velocity ($m\ s^{-1}$)	
Danckwerts (1951)	$k_L = \sqrt{D \cdot s}$	I.15	s surface renewal rate (s^{-1})	
Calderbank and Moo-Young (1961)	$k_L = 0.42\left(\frac{(\rho_L - \rho_G)\mu_L g}{{\rho_L}^2}\right)^{1/3} Sc^{-1/2}$	I.16	ρ_L liquid density ($kg\ m^{-3}$) ρ_G gas density ($kg\ m^{-3}$) μ_L liquid viscosity (Pa s) Sc Schmidt number ($Sc = \mu_L/(\rho_L D)$) D solute diffusivity in the liquid media ($m^2\ s^{-1}$)	d_b>2.5
	${k_L}^{rigid} = 0.31\left(\frac{g\mu_L}{\rho_L}\right)^{1/3} Sc^{-2/3}$	I.17		d_b<2
Frössling (1938)	${k_L}^{rigid} = \frac{D}{d_b}(2 + 0.6Re^{1/2}Sc^{1/3})$	I.18	Re bubble Reynolds number ($Re = U_b d_b \rho_L/\mu_L$) Sc Schmidt number ($Sc = \mu_L/(\rho_L D)$) U_b bubble rise velocity ($m\ s^{-1}$)	d_b<2

The Higbie model (Equation I.13), considers that the diffusional oxygen transfer in the liquid film occurs when liquid elements (eddies) reach the gas-liquid interface and during a short contact time (t_c), attains the concentration equilibrium with the interface. Subsequently the liquid element is replaced by another one that will stay at the interface during the same previous contact time (t_c). For a gas bubble rising freely in a liquid volume, the contact time is equivalent to the time that the bubble takes to cross a distance equal to its diameter.

The Danckwerts model, also called surface renewal model, considers that the contact time at the interface is probably not the same for all liquid elements arriving at the gas-liquid interface. The concept of surface renewal rate (s) is then introduced and the k_L coefficient is expressed as shown in Equation I.15.

Calderbank and Moo-Young (1961) proposed two empirical correlations for k_L expressed as a function of the liquid properties and diffusivity, one for bubbles with mobile interfaces (Equation I.16) and other one for bubbles with rigid interfaces (Equation I.17).

The Frössling empirical model (1938) (Equation I.18), is used for bubbles with a diameter lower than 2×10^{-3} m, which are considered to have a rigid interface. It considers the bubble rise velocity and the liquid properties through the Reynolds and Schmidt numbers respectively.

I.2.3 Specific interfacial area (a)

For spherical bubbles, the specific interfacial area is a function of the bubble diameter and the gas hold-up (ε_G):

$$a = \frac{6}{d_{bs}} \cdot \frac{\varepsilon_G}{(1-\varepsilon_G)} \qquad \text{I.19}$$

where the bubble Sauter diameter (d_{bs}) is the weighed bubble's diameter considering the population bubble size distribution, defined by:

$$d_{bs} = \frac{\sum_i ni \cdot dbi^3}{\sum_i ni \cdot dbi^2} \qquad \text{I.20}$$

with

d_{bs} bubble Sauter diameter (m)

dbi bubble diameter (m)

ni number of bubbles with diameter dbi

For ellipsoidal bubbles with a major axis (A) and a minor axis (b), a bubble equivalent diameter is introduced as follows (Roustan, 2003):

$$db = (A^2 b)^{1/3} \qquad \text{I.21}$$

It corresponds to the diameter of an ellipsoidal bubble having the same volume of a spherical bubble.

The gas hold-up (ε_G) is the gas fraction in the aerated volume, defined as:

$$\varepsilon_G = \frac{V_G}{V_T} = \frac{V_G}{V_G + V_L} \qquad \text{I.22}$$

with

V_G the volume occupied by the gas phase (m^3)

V_T the aerated volume (m^3)

V_L the volume occupied by the liquid phase (m^3)

Considering that for a given bubble volume, ellipsoidal shaped-bubbles have a higher specific interfacial area (a) than spherical bubbles, a correction factor (f_K) is defined to consider the effect of bubble shape on the interfacial area, as follows (Cockx, 1997):

$$a = \frac{6}{d_{bs}} \cdot \frac{\varepsilon_G}{(1-\varepsilon_G)} \cdot f_K \qquad \text{I.23}$$

where the correction factor (f_K) is defined as a function of the bubble eccentricity (χ) which is the ratio of the major axe to the minor axe:

$$f_K = \frac{1}{2\chi^{1/3}}\left(\chi + \frac{\ln(\chi + \sqrt{\chi^2-1}}{\sqrt{\chi^2-1}}\right) \qquad \text{I.24}$$

For bubbles with an eccentricity below 1.66, the shape effect on the interfacial surface is lower than 5% (Fayolle, 2006).

Conclusions

- The correlation used to estimate the flow of transferred oxygen is based on the Fick's law and the double film model. Because of the low oxygen solubility in water, the resistance to oxygen transfer is located in the liquid film. The flow of transferred oxygen depends basically on two parameters: the oxygen transfer coefficient ($k_L a$), and the dissolved oxygen concentration gradient ($Cs - C$). The oxygen transfer coefficient ($k_L a$) is defined by the liquid-side mass transfer coefficient (k_L) and the specific interfacial area (a) which are also function of the oxygen diffusivity in the liquid, bubble size and shape, bubble rise velocity and gas hold-up.

I.2.4 Gas-liquid dispersions

Understanding the flow conditions of a gas-liquid dispersion is a prerequisite in order to evaluate its influence on oxygen transfer phenomena.

I.2.4.1 Gas and liquid velocities

The superficial gas and liquid velocities (U_G and U_L), represent the gas and liquid flow rate per unit of reactor cross section (S). They are of practical use in order to compare the operating conditions for basins of different geometries and are written as follows:

$$U_G = \frac{Q_G}{S} \quad \text{I.25}$$

$$U_L = \frac{Q_L}{S} \quad \text{I.26}$$

with

U_G superficial gas velocity (m s^{-1})

Q_G gas flow rate (m^3 s^{-1})

U_L superficial liquid velocity (m s^{-1})

Q_L liquid flow rate (m^3 s^{-1})

S reactor's cross section (m^2)

In the reactor section, the gas and the liquid phases flow through effective sections: $\varepsilon_G S$ and $\varepsilon_L S$, for gas and liquid respectively. The gas and liquid flow rate through these effective surfaces is actually equivalent to the average bubble rise velocity and liquid velocities:

$$U_b = \frac{U_G}{\varepsilon_G} \quad \text{I.27}$$

$$U_l = \frac{U_L}{\varepsilon_L} \quad \text{I.28}$$

with

U_b average bubble rise velocity (m s^{-1})

ε_G overall gas hold-up (-)

U_l average liquid velocity (m s^{-1})

ε_L overall liquid hold-up (-)

The relative bubble rise velocity compared to the liquid velocity is characterized by the slip velocity which is defined as:

$$G = U_b - U_l = \frac{U_G}{\varepsilon_G} - \frac{U_L}{(1-\varepsilon_G)} \quad \text{I.29}$$

I.2.4.2 Homogenous and heterogeneous regime

Bubble flow regime in bubble columns is characterized by the gas-liquid distribution on the column section. The bubble flow regimes are well described by Zahradník *et al.* (1997) and Mena *et al.* (2005). At low gas velocities and with gas diffusers with small orifices the *homogeneous flow* regime takes place: the interaction between bubbles is small (bubble coalescence and break-up are insignificant), the bubble size distribution is narrow, and the gas hold-up is uniformly distributed in the column section (HoR in Figure I.3 (a)). At higher gas flow rates or with diffusers with large orifices the *heterogeneous* flow regime occurs: bubble coalescence takes place and consequently larger bubbles appear in the dispersion. The bubble size distribution is wider and the gas hold-up profile in the column section is parabolic with a maximum value at the centre (HeR in Figure I.3 (a)). A transitional regime occurs between the homogenous and heterogeneous regimes. It is characterized by the beginning and complete development of liquid circulation patterns in the bubble bed. Affected by the liquid circulation, bubble rise faster and the gas hold-up stops increasing with the superficial gas velocity and declines. Subsequently when the heterogeneous regime is established at higher gas flow rates, the liquid circulation patterns are reduced and the gas hold-up increases again with the superficial gas velocity though with a less pronounced slope. The typical evolution of the gas hold-up with the superficial gas velocity is shown in Figure I.3 (b).

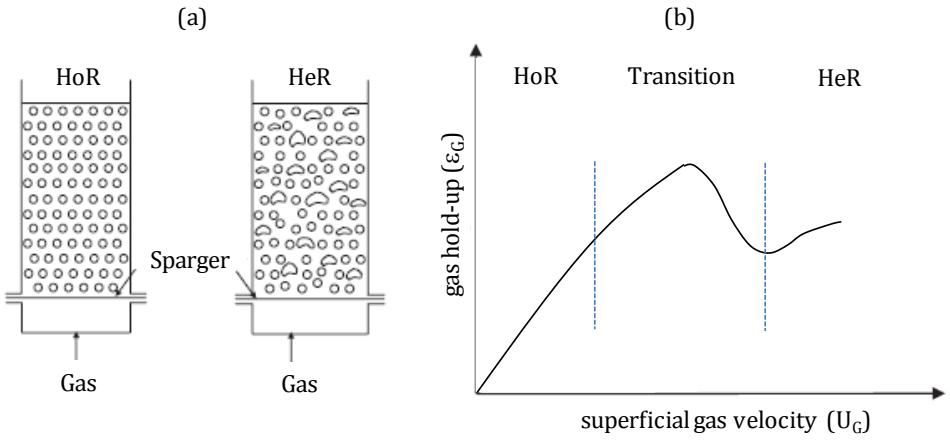

Figure I.3. (a) Representation of homogenous (HeR) and heterogeneous regimes (HeR) in bubble columns; (b) Typical evolution of the gas hold-up with the gas flow rate in the flow regimes. (Zahradník *et al*., 1997, Mena *et al.,* 2005)

I.2.4.2.1 Factors affecting the bubble regime

The study of Zahradník *et al*. (1997) summarized some parameters affecting the formation and stability of bubbling regimes. Design parameters such as distributor type and geometry; reactor geometry as well as system properties such as the electrolytes content and viscosity were studied. The main results are described in the following paragraphs.

I.2.4.2.1.1 Diameter orifice and reactor geometry

To study the distributor influence on bubble regime, 8 different perforated plates (orifices diameters between 10mm and 100μm) were used in an air-water system. It was observed that for orifice diameters bigger than 1.6mm, the homogeneous bubbling regime could not be generated. For orifice diameters smaller than 1mm the flow regime and the maximum gas hold-up presented an increased stability. The results have also shown that for all gas diffusers the fully heterogeneous bubbling regime is developed at a superficial gas velocity higher than 0.125m s^{-1}. Concerning the influence of the reactor geometry, it was observed that decreasing the ratio of the liquid height to the column diameter (H/D) significantly increases the gas hold-up for all distributors, thus accentuating the homogeneous bubbling regime. On the contrary, at high gas flow rates in the heterogeneous regime, the gas hold-up was independent on the ratio (H/D).

I.2.4.2.1.2 Dissolved electrolytes and liquid viscosity

In aqueous solutions of electrolytes (NaCl, KCl, $MgSO_4$, KI) Zahradník *et al*. (1997) observed that the heterogeneous regime was reached at a higher superficial gas velocities compared to the air-

water system. The authors attributed this result to the hindrance of coalescence due to the salt concentration (from 0.036 up to 0.38 mol L^{-1}). On the other hand, the influence of the liquid viscosity was evaluated using saccharose solutions. It was observed that at a given gas flow rate, an increment in the fluid viscosity related to an increase in the saccharose concentration, led to a gas hold-up reduction due to an enhancement of bubble coalescence. The cause-effect link between fluid viscosity and bubble coalescence is explained by Stewart (1995) as follows: an increase in the liquid viscosity reduces the turbulence in the wake of individual rising bubbles and as a consequence neighbour bubbles are drawn into other bubble's wake thus facilitating bubble collision and eventually coalescence.

I.2.4.3 Bubble size

The volume of the bubble at the detachment stage in a quiescent liquid results from the equilibrium between the lifting forces of buoyancy and gas momentum and the restraining forces of surface tension, drag and inertia (Gaddis and Vogelpohl, 1986). From a force balance, the authors proposed a generalized equation to estimate the bubble size of isolated spherical bubbles in a quiescent and infinite media. The obtained correlation is written as follows:

$$d_b = \left[\left(\frac{6 d_o \sigma}{\rho_L g} \right)^{\frac{4}{3}} + \left(\frac{81 \mu_L Q_{Gn}}{\pi g \rho_L} \right) + \left(\frac{135 {Q_{Gn}}^2}{4\pi^2 g} \right)^{\frac{4}{5}} \right]^{\frac{1}{4}} \qquad \text{I.30}$$

According to this correlation, the bubble size is governed by design and operating parameters such as gas flow rate through the nozzle (Q_{Gn}), orifice diameter (d_o) and physicochemical properties such as liquid viscosity (μ_L), density (ρ_L) and surface tension (σ). The authors observed that this theoretical correlation reproduces adequately some experimental data available in the literature for air-water, air-glycerol and air-glucose systems (deviation within ±10%).

Besides, Jamialahmadi *et al.* (2001) studied the effect of these different variables on the size of a bubble formed through a single orifice in distilled water and solutions of distilled water with methanol, ethanol, propanol, isopropanol, glycerol and potassium chloride. The authors observed that the surface tension and the orifice diameter were the main variables affecting the bubble size, though the impact of superficial gas velocity and liquid viscosity was also significant. The authors defined the bubble size as:

$$d_b = f(d_o, U_G, \rho_L, \mu_L, \sigma, g) \quad \text{I.31}$$

Using 900 experimental data gathered from various studies, the mentioned authors proposed the following empirical correlation in terms of the dimensionless numbers to predict the bubble size at formation:

$$\frac{d_b}{d_o} = \left(\frac{5}{{B_{do}}^{1.08}} + \frac{9.261 Fr^{0.36}}{Ga^{0.39}} + 2.147 Fr^{0.51} \right)^{1/3} \quad \text{I.32}$$

with

d_b bubble diameter (m)

d_o orifice diameter(m)

B_{do} Bond number in terms of orifice ($B_{do} = \rho_L g {d_o}^2/\sigma$)

Fr Froude number ($Fr = {U_{Gn}}^2/(d_o g)$)

Ga Galileo number ($Ga = {\rho_L}^2 {d_o}^3 g/{\mu_L}^2$)

U_{Gn} superficial gas velocity through the nozzle section (m^2)

The use of this correlation allowed the authors to reproduce the experimental results with an absolute mean average error of 3.2% (Jamialahmadi *et al.,* 2001).

The two presented correlations predict similar values of bubble diameter at formation in respect to the gas flow rate and clean water properties (see Figure I.4a). Both correlations predict a similar impact of the liquid properties such as surface tension and dynamic viscosity in the bubble diameter (only values predicted with the Jamialahmadi *et al.,* 2001, correlation are presented in Figure I.4b). The effect of the liquid surface tension appears to be more significant at low gas flow rates. At a superficial gas velocity (U_{Gn}) of 1.3 m s^{-1} reducing the liquid surface tension by 7% (from 72.8 down to 68.0 mN m^{-1}) would result in a bubble diameter decrease of 1.7 % (from 3.57 down to 3.51 mm). On the contrary, the impact of viscosity on bubble diameter appears to increase with the gas flow rate and is less significant compared to the one of surface tension. Increasing up to 5 times the dynamic viscosity (from 1 up to 5 mPa.s) at a superficial gas velocity (U_{Gn}) of 1.3 m s^{-1} would result in an increase of bubble diameter by 2.5% (from 3.57 up to 3.63 mm).

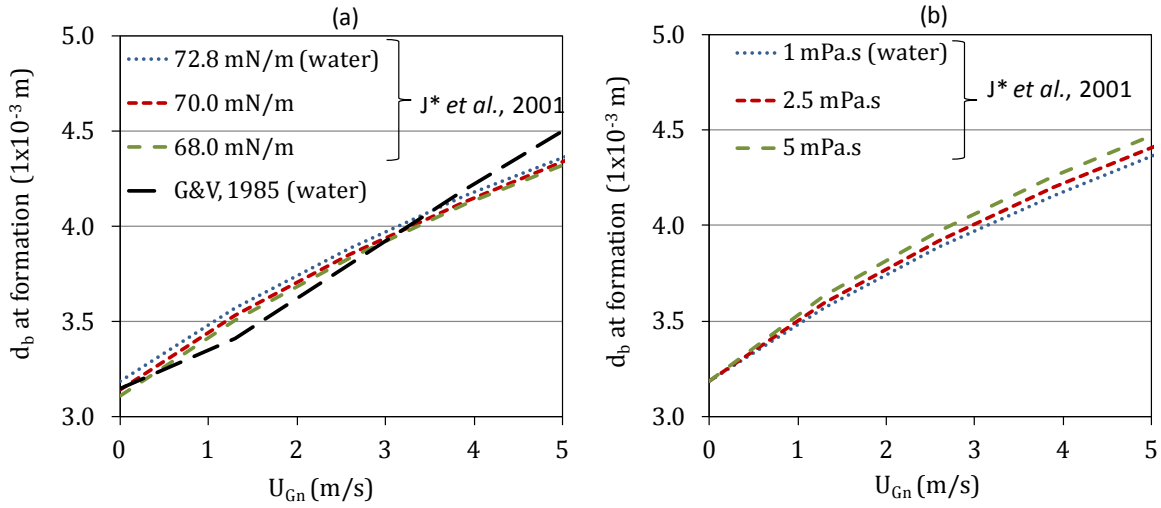

Figure I.4. Estimated diameter for spherical isolated bubbles at the detachment stage for different gas flow rates (expressed in terms of the superficial gas velocity through the nozzle section(U_{Gn}) using the *Jamialahmadi *et al.* (2001) correlation for an orifice diameter of 0.7 mm and different liquid properties: (a) μ=1 mPa.s, ρ=998 kg m^{-3}, surface tension (σ) from 68.0 to 72.8 mN m^{-1}; (b) σ=72.8 mN m^{-1}, ρ=998 kg m^{-3}, dynamic viscosity (μ) from 1 to 10 mPa.s. In Figure (a) the bubble diameter predicted with the correlation from Gaddis and Vogelpohl (1986) is also shown for the same diameter orifice (0.7 mm) and water properties (μ=1 mPa.s, ρ=998 kg m^{-3}, σ=72.8 mN m^{-1}).

I.2.4.4 Bubble terminal velocity

The bubble terminal velocity refers to the velocity that would have an isolated bubble in an infinite motionless media. It can be estimated theoretically from a balance of forces acting on the rising bubble (buoyancy, gravity, drag, added mass, lift, Basset). Because the density of the liquid phase is high compared to the gas phase, the bubble terminal velocity (U_{b^0}) can be written as:

$$U_{b^0} = \sqrt{\frac{4gd_b}{3C_D}} \qquad \text{I.33}$$

with

U_{b^0} bubble terminal velocity (m s^{-1})

g gravity constant (m s^{-2})

d_b bubble diameter (m)

C_D bubble drag coefficient (-)

The terminal bubble velocity is an increasing function of the bubble diameter (d_b) and decreases with the increase of the bubble drag coefficient (C_D). Several empirical correlations have been

proposed to estimate the drag coefficient (Harmathy, 1960; Wallis, 1969; Clift *et al.,* 1978; Ishii and Zuber, 1979; Johansen and Boysan, 1988; Karamanev, 1994). They define it as a function of liquid properties such as density and surface tension, or as a function of the Eötvos number (Eo) or the Reynolds number (Re) which depend also on bubble diameter and the viscosity.

An estimation of the bubble terminal velocity in clean water can be obtained as a function of the bubble equivalent diameter from the diagram established by Clift *et al*. (1978) (Figure I.5).

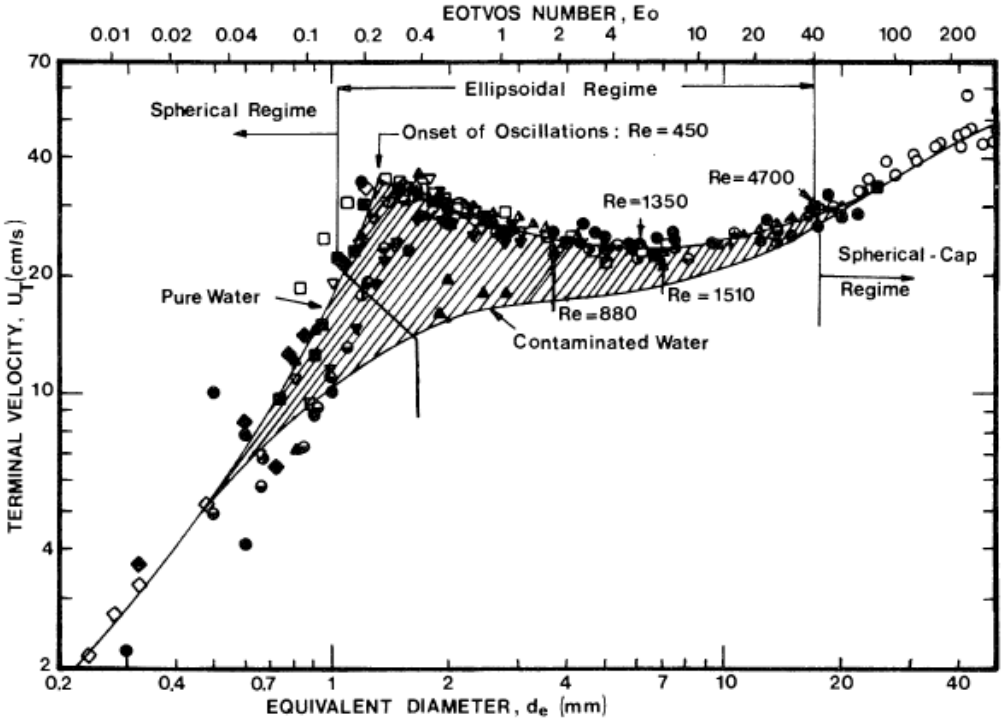

Figure I.5. Bubble terminal velocity in clean water (20°C) and contaminated water as a function of the bubble equivalent diameter (from Clift *et al.,* 1978).

For bubbles rising in clean water with an equivalent diameter between 3 and 7 mm, which is the range of bubble size observed in full scale aeration tanks using fine bubble diffusers (Fayolle, 2006), the terminal velocity would be of approximately 0.23 m s^{-1}.

Because of an increase of the drag coefficient, the bubble terminal velocity in contaminated water is lower than on clean water (Kulkarni and Joshi, 2005). For the same range of bubble equivalent diameter (3-7 mm), the bubble terminal velocity may be reduced down to approximately 0.18 m s^{-1}.

In a homogenous bubble swarm the bubble rise velocity is also function of the gas hold-up. At low gas hold-up values (<4.8%) with minimal interactions between bubbles, the rise velocities in

the bubble swarm would be higher compared to an isolated bubble because some bubbles enter into the wake of other rising bubbles, consequently reducing radial movements and the bubbles drag (Henkel, 2010; Bouche *et al.,* 2012).

However, increasing the gas hold-up would promote the bubble interactions and leads to an increase of the bubble drag coefficient, which counteracts the effect previously mentioned. Riboux *et al.* (2010) and Colombet *et al.* (2011) observed the reduction of the bubble velocity (U_b) with the increase of the overall gas hold-up (ε_G) for a bubble swarm in filtered tap water and described it as follows:

$$U_b = U_{b^0}(1 - {\varepsilon_G}^{0.49}) \qquad \text{I.34}$$

with

U_{b^0} rise velocity of an isolated bubble (m s^{-1})

In the study of Colombet *et al.* (2011), the experimental value for the terminal velocity (U_{b^0}) was 0.32 m s^{-1} for bubbles with a diameter of 2.1 mm in a range of gas hold-up from 0.45% up to 16.5%.

Conclusions

- Characteristics of the gas phase such as bubble size, rise velocity, gas hold-up and flow regime are dependent on design, configuration and operation variables as well as on the liquid properties such as density, surface tension and viscosity. Thus, the oxygen transfer characteristic parameters (k_L and a) depend on the multiple mentioned variables.

I.2.5 Design and operation parameters affecting oxygen transfer in clean water

Several research works have evaluated how design and operating parameters influence the oxygen transfer in clean water. The main results (principally obtained in full scale stirred reactors) are summarized in the next paragraphs.

I.2.5.1 Gas diffusers density and distribution

The gas diffuser density refers to the fraction of the reactor cross sectional area that is covered with membrane diffusers.

Impact on k_La: Oxygen transfer increases for higher gas diffuser densities (Wagner and Pöpel, 1998) and well distributed diffusers on the reactor surface (ASCE, 1992).

Mechanisms: The rising bubble swarm induces an uprising liquid circulation flow associated to drag and buoyancy forces. If the density of gas diffusers is low or gas diffusers are unevenly distributed on the reactor surface, the liquid goes down preferentially in the non-aerated surfaces consequently generating vertical liquid recirculation flows, called 'spiral flows' that end up reducing the gas hold-up and oxygen transfer (Gillot, 1997; Capela, 1999; Fayolle, 2006).

I.2.5.2 Gas diffuser type

Impact on k_La: The oxygen transfer depends on the installed diffuser type: perforated plate, sintered glass porous plate; perforated flexible membrane (Bouaifi *et al.,* 2001).

Mechanisms: The gas diffuser type determines the bubble size and bubble regime and consequently the gas-hold-up, the interfacial area (a) and also the liquid-side transfer coefficient (k_L).

I.2.5.3 Submergence of diffusers

Impact on k_La: The increase of the liquid height above the gas diffusers leads to a reduction of oxygen transfer (Pöpel and Wagner, 1996; Gillot *et al.,* 2005).

Mechanisms: For a given gas flow rate, an increase in the liquid height promotes the development of vertical liquid circulation patterns which lead to a reduction of the gas hold-up.

I.2.5.4 Superficial gas velocity

Impact on k_La: The superficial gas velocity is positively correlated with the oxygen transfer coefficient (Bouaifi *et al.,* 2001; Gillot *et al.,* 2005).

Mechanisms: Primarily an increase of the gas hold-up and consequently of the interfacial area (Bouaifi *et al.,* 2001). The oxygen transfer is higher despite an increase of the bubble size and a reduction of the liquid-side transfer coefficient (Colombet *et al.,* 2011). It must be underlined

that the oxygen transfer efficiency (the ratio of transferred oxygen to supplied oxygen) is reduced with an increase in the superficial gas velocity. The reason for this reduction is that increasing the superficial gas velocity induces large-scale liquid circulations (spiral flows) that result in lower gas hold-up (Gillot, 1997; Capela, 1999; Fayolle, 2006).

I.2.5.5 Liquid circulation velocity

Some wastewater treatment reactors have a geometrical configuration in which a horizontal liquid circulation is induced by means of slow speed submerged impellers (loop reactors). The resulting horizontal liquid velocity has an effect on oxygen transfer.

Impact on k_La: The application of a horizontal velocity induces an increase in oxygen transfer (Déronzier *et al.,* 1996; Gillot *et al.,* 2000; Gillot and Héduit, 2000).

Mechanisms: The liquid circulation velocity neutralizes the 'spiral flows' (Czarnota and Hahn, 1995), leading to an extended gas hold-up and consequently an expanded interfacial area. According, to Fayolle (2006) the liquid circulation reduces slightly the bubble diameter (-10%) but is not enough to explain the whole augmentation of the interfacial area.

I.2.6 Oxygen transfer in activated sludge

Activated sludge is a complex fluid composed of biological aggregates or flocs and interstitial water. For classical activated sludge and MBR sludge, the water content can range from 98.5 to 99.8 w%. Biological aggregates are a heterogeneous mixture of microbial colonies, colloids, organic fibers and particles, inorganic compounds embedded in a network of extracellular polymeric substances (EPS) of biological origin such as proteins, humic acids, polysaccharides, DNA and nucleic acids (Sheng *et al.,* 2008; Wilen, 2008). Interstitial water is composed by soluble organic matter, soluble N and P species, soluble EPS, surfactants and salts. The physicochemical properties of the continuous and dispersed phases define the size of the biological aggregates. Also, because biological flocs are actually shear sensitive, the hydrodynamic conditions associated to the reactor configuration determine the flocculation-breakup equilibrium and consequently the floc size (Spicer *et al.,* 1998; Biggs and Lant, 2000; Bouyer *et al.,* 2001; Wilén *et al.,* 2003; Jin and Lant, 2004; Bouyer *et al.,* 2005; Coufort *et al.,* 2008).

The diverse components of activated sludge and the associated properties have an impact on oxygen transfer. Under the same design and operating conditions, the oxygen transfer capacity

is lower in activated sludge than in clean water. This oxygen transfer depletion is characterised by the alpha factor (α) defined as:

$$\alpha = \frac{k_L a'}{k_L a} \qquad \text{I.35}$$

with

$k_L a'$ oxygen transfer coefficient in polluted water (h^{-1})

$k_L a$ oxygen transfer coefficient clean water (h^{-1})

The magnitude of this reduction is conditioned on how the oxygen transfer characteristic parameters (C_s, k_L and a) are impacted by the various components and properties of activated sludge.

I.2.6.1 Dissolved oxygen saturation concentration in activated sludge (Cs')

The dissolved oxygen saturation concentration in activated sludge (Cs') is considered to be slightly lower compared to the value in clean water (Cs). Under the same operating conditions, this reduction is characterized by means of a coefficient noted β as follows:

$$Cs' = \beta Cs \qquad \text{I.36}$$

The value of the coefficient β ranges between 0.95 and 0.99 depending on the nature of the wastewater influent. A value of β=0.99 is classically used for domestic activated sludge (ASCE, 1996).

The similarity of the Cs values in clean water and activated sludge has been recently confirmed by Jimenez (2013) who measured the dissolved oxygen saturation concentration of activated sludge interstitial water and did not observed any variation compared to clean water, within the margin of experimental error (±2%).

I.2.6.2 Activated sludge properties affecting the oxygen transfer coefficient (k_La')

Activated sludge impact on oxygen transfer results from the multiple effects that the complex floc-interstitial water can produce on the variables defining the liquid mass transfer coefficient (k_L) and the interfacial area (a) such as bubble, size, bubble rising velocity, oxygen diffusion coefficient and gas hold-up.

Several research works have sought to establish what factors determine the decline of oxygen transfer coefficient in activated sludge (k_La'). To better understand the occurring phenomena, the literature results concerning the effects of the solid fraction and the effects of the soluble fraction have been analysed separately. Subsequently, the literature results concerning the influence of global properties of activated sludge, such as the solid residence time (SRT) and the apparent viscosity, on k_La` is also investigated.

I.2.6.2.1 Solid fraction

Out from the context of the activated sludge process, the effect of solids on oxygen transfer has been studied by several authors (Banisi *et al.,* 1995; Freitas and Texeira, 2001; Yang *et al.,* 2001; Dhaouadi *et al.,* 2006; Littlejohns and Daugulis, 2007; Mena *et al.,* 2011). Whether the solids produce a decline or a rise of oxygen transfer seems to depend on the solid characteristics such as size, density, hydrophobicity and concentration. Mena *et al.* (2005) have listed the ways in which solids may affect the flow regime in a bubble column. This list provides a perspective of how activated sludge suspended solids may affect the oxygen transfer.

- Steric effect: Solids occupy a volume around the bubble leading to a decline of the gas-liquid interface area available for oxygen transfer.

- Buoyancy: If the suspended solids have a different density compared to the liquid phase, solids can change the density of the suspension and consequently modify the bubbles rising velocity and the gas hold-up by affecting the buoyancy force acting on the bubbles.

- Viscosity: Solids induce an increase in the suspension viscosity. This increment leads to three overlapping effects (i) the bubble coalescence is favored and consequently the bubble size and bubble rising velocity increase (Mena *et al.,* 2005), (ii) at the bubble formation stage in non-Newtonian fluids, the bubble growth time is extended with the increasing viscosity due to higher viscoelastic stresses exerted on the bubble and consequently bubble size is increased (Kulkarni and Joshi, 2005), (iii) the velocity of the rising bubbles is reduced in viscous liquids due to a higher bubble drag coefficient (Mena

et al., 2005). By affecting the bubble size, rise velocity and the gas hold-up, the viscosity impacts the interfacial area (a) and the liquid-side transfer coefficient (k_L).

- Surface hydrophobicity: Depending on their affinity for the gas and liquid medium, solids will tend or not to concentrate near the gas-liquid interface and consequently affect the available surface for mass transfer as well as the bubbles drag coefficient. The bubble hydrophobicity would condition the steric effect previously mentioned. For Mena *et al.* (2011), hydrophobic solid particles are adsorbed at the gas-liquid interface and play a negative role in the mass transfer. This effect would become important when the solid particles are small compared to the bubble size.

- Bubble rising velocity: Apart from the viscosity effect that can slow down the rising bubbles, solids can also collide with the rising bubbles and consequently affect their trajectory and rising velocity to end up affecting the gas hold-up (Mena *et al.,* 2005).

- Bubble coalescence: As mentioned above, this effect is promoted by the presence of solids in association with the increase of viscosity. However, according to Khare and Joshi (1990) small solid particles (μm) can be adsorbed at the bubble surface (if particles have a surface affinity for the gas-liquid interface) and hinder the bubble coalescence to end up affecting the bubble size, the gas hold-up and the interfacial area.

I.2.6.2.1.1 Activated sludge suspended solids

In activated sludge several works have studied the impact of the **MLSS** (mixed liquor suspended solids) concentration on oxygen transfer. Unanimously, the increase in the MLSS concentration is correlated with the decline of the oxygen transfer and consequently the alpha factor (Cornel *et al.,* 2003; Krampe and Krauth, 2003; Jin *et al.,* 2006; Germain *et al.,* 2007; Henkel *et al.,* 2009; Mineta *et al.,* 2011; Racault *et al.,* 2011). However when results from different research works are compared, the dispersed data makes evident that the oxygen transfer decline compared to clean water is not only determined by the MLSS concentrations (Figure I.6).

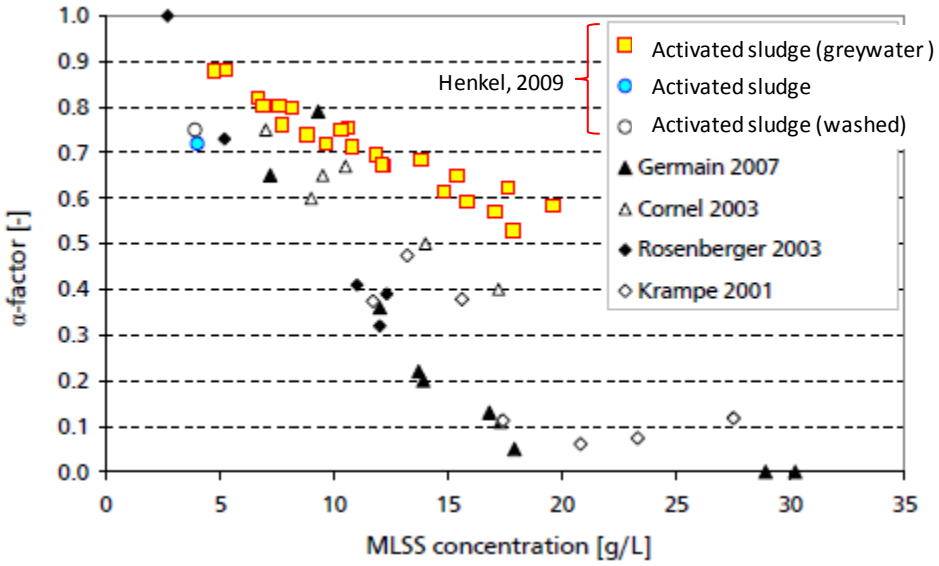

Figure I.6. Alpha factor for different sludge MLSS concentration. Results obtained by different works in MBR. (Image from Henkel *et al.,* 2009). MBR: membrane bioreactor. 'washed': activated sludge with clean water replacing interstitial water.

To understand the impact of the MLSS concentration on oxygen transfer, Jin *et al.* (2006) and Mineta *et al.* (2011) measured the overall gas hold-up in aeration batch tests in an airlift and a bubble column respectively. Overall gas hold-up measurements were based on the determination of the liquid global height corresponding to aerated and non-aerated conditions. For gas fractions ranging from 2 to 15% and from 0.5 to 2% respectively and a MLSS concentration ranging from 2 g L^{-1} to 8 g L^{-1} both authors observed a decrease in the gas hold-up with the MLSS concentration. Furthermore Mineta *et al.* (2011) observed a lower gas hold-up in clean water compared to activated sludge. These studies associated the impact of MLSS concentration on gas hold-up to the effects of viscosity on the the bubble regime.

Considering **MLVSS** (mixed liquor volatile suspended solids) concentration instead of MLSS concentration, Henkel *et al.* (2009) showed that the latter is also correlated with the alpha factor but in contrast to the MLSS concentration, the impact of the MLVSS concentration on the alpha factor seems to be independent of the sludge origin (Figure I.7).

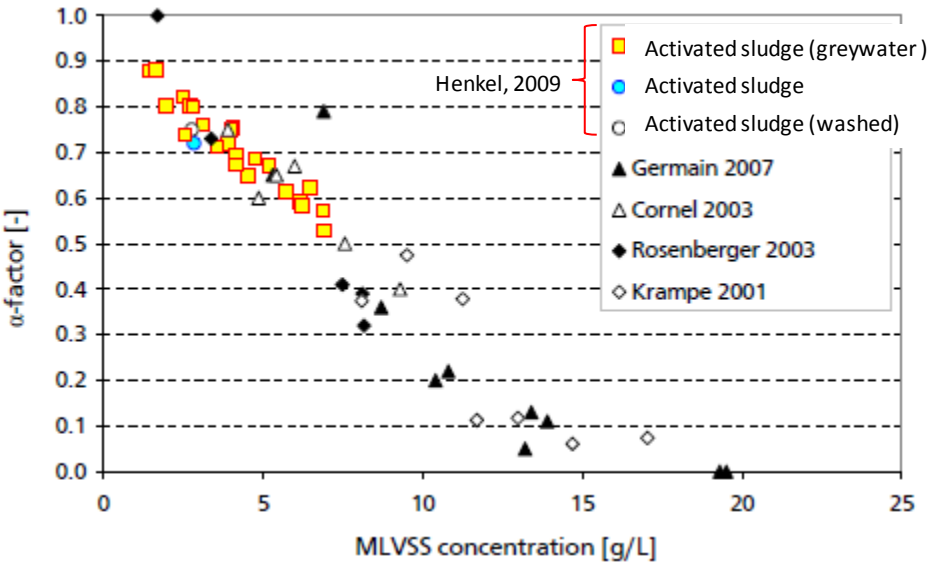

Figure I.7. Alpha factor for different sludge MVLSS concentration. Results from different works (Figure from Henkel *et al.,* 2009). 'washed': activated sludge with clean water replacing interstitial water.

Given the fact that the MLVSS concentration accounts primarily for the sludge biomass which is mainly composed of water (bound water), Henkel *et al.* (2009) hypothesizes that the MLVSS concentration is better correlated with the volume occupied by the floc than the MLSS concentration. Subsequently, the link between the floc volume and the impact on the oxygen transfer would be explained in relation to the steric effect: the floc volume would be a key parameter conditioning the free water available at the bubble surface for an undisturbed oxygen transfer. To establish the correlation between the floc volume and the MVLSS concentration, this author poured 1L of activated sample in a graduated tube, measured the settled volume of flocs after 30 minutes and measured also the corresponding MVLSS concentration. Independently of the type of effluent (greywater or wastewater), a good correlation was observed between the floc volume and the MLVSS concentration, especially at low suspended solids concentration (<6 g L^{-1} MVLSS).

In this context, the author introduced the hydrostatic floc volume **(HFV)** as a sludge property closely related to the MVLSS concentration and potentially characterizing the oxygen transfer and alpha factor decline. The HFV corresponds in practice to the volume of settled suspended solids during 48 h in a graduated cylinder of 1L. The volume of water above the volume of settled solids would represent the available 'free water' at the bubble surface for the oxygen transfer, while the settled volume would be related to the flocs bound water (in cells and EPS). The 48h settling time was fixed in agreement to measurements results showing that beyond that lapse of time, no evolution of the floc volume is observed.

According to Figure I.7, the MLVSS concentration determines the oxygen transfer decline in activated sludge. In order to examine the extent of the proposed correlation between these two variables (alpha and MVLSS concentration), other oxygen transfer data available in the literature, obtained by means of a mass balance method (Racault *et al.,* 2009), were plotted together with the correlation obtained by Henkel (2010) (see Figure I.8). It appears, after this comparison, that the oxygen transfer decline in activated sludge compared to clean water is not only influenced by the MVLSS concentration, and other sludge properties play a role in this impact.

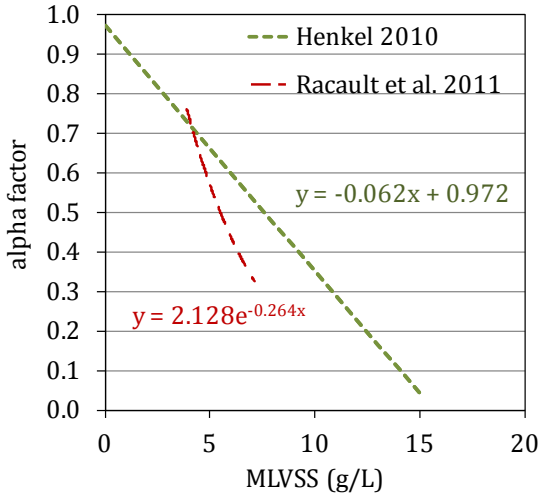

Figure I.8. Decrease of alpha factor with the increase of the MVLSS concentration according to two different models: Henkel (2010) and Racault *et al.* (2011).

I.2.6.2.1.2 Floc size

Similarly to the influence of the floc volume on the oxygen transfer proposed by Henkel (2010), the floc size is a sludge property that could be related to the oxygen transfer depletion. Only the study carried out by Germain *et al.* (2007) has evaluated the effect of this property on oxygen transfer. For 10 activated sludge samples drawn from 7 different wastewater treatment plants (all membrane bioreactors), results showed that the mass median diameter (MMD), in a range from 33 to 90 μm, measured by laser diffraction (Malvern Mastersizer 2000), does not have an influence on the oxygen transfer coefficient.

I.2.6.2.1.3 Bound Extracellular Polymeric Substances (EPS)

EPS are a complex mixture of polymers excreted by the microorganisms, lysis and hydrolysis products, and adsorbed organic matter from the wastewater (Wilén *et al.,* 2003). They constitute the major organic fraction of activated sludge (Frølund *et al.,* 1996). Bound EPS refer to the

fraction of EPS that is part of the biological flocs. Their concentration on activated sludge is of the order of 100 milligrams per gram of MVLSS (Domínguez *et al.,* 2010). Their composition, in decreasing order, is fractioned in proteins, humic acids, polysaccharides and DNA (Wilén *et al.,* 2003). It is known that these substances play a major role in the conformation of biological flocs and can determine the floc structural properties. For instance Urbain *et al.* (1993) and Jin *et al.* (2003) found that, for several sludge origins, the floc-extracted EPS concentration correlates positively with poor settleability. For Mikkelsen and Keiding (2002) who studied the relation of the floc-extracted EPS content with the flocculation and shear sensitivity for various sludge types, the EPS fraction stabilises the floc structure via polymer entanglement, affecting the hydrophobicity and surface charge.

Results from the mentioned studies let infer that floc properties such as floc volume, size or hydrophobicity are related to the EPS content. Because these floc characteristics may impact the oxygen transfer, it seems of interest to determine the relation between the EPS fraction and the oxygen transfer coefficient.

For eight MBR samples from different activated sludge plants, the study of Germain *et al.* (2007) observed that the polysaccahrides EPS content is positively correlated to an increase of the $k_L a$' coefficient while the protein EPS fraction had a negligible impact. To explain this result the authors hypothesized that the EPS polysaccharides content increased the floc size and porosity and thus oxygen diffusivity.

The difficulty of studying the impact of bound EPS on oxygen transfer lies on the lack of a normalized protocol for the measurement of these components, particularly regarding the extraction method before chemical analysis. For instance, Domínguez *et al.* (2010) observed that depending on the applied extraction method (resin, thermal, formaldehyde, formaldehyde + sonication) analysis results of the EPS content could even be multiplied by 6.

Conclusions on the impact of the solid fraction on oxygen transfer

- The different works studying the impact of the solid fraction on oxygen transfer in activated sludge mainly concerned the MLSS concentration. Unanimously an oxygen transfer decline is observed with an increase in MLSS. It is however observed that for activated sludge with the same MLSS concentration but from different origins, the measured oxygen transfer decline compared to clean water is not necessarily the same. This means that other sludge physicochemical properties also play a role on that oxygen transfer depletion.
- It can be inferred from the literature review that other properties associated to the solid fraction such as the suspension viscosity can be of importance in the oxygen transfer. In relation to the steric effect, the floc volume, conditioned on hydrophobicity, could be linked to the decrease of the oxygen transfer. The MVLSS concentration is presented as being closely related to the floc volume and as a sludge property better characterizing the oxygen transfer decline compared to the MLSS concentration. However, a comparison with recent literature results shows that the impact of the MVLSS on oxygen transfer is also dependent on the sludge origin.
- The EPS concentration appears to play an important role on the floc properties and structure and consequently on oxygen transfer. However the lack of a normalized protocol for the measurement of these components seems to be an obstacle for their determination.

I.2.6.2.2 Soluble substances

I.2.6.2.2.1 Surfactants

Surfactants presence in activated sludge is primarily due to the domestic use of detergents. Their average concentration in raw wastewater ranges between 7 and 15 mg L^{-1} (Wagner and Pöpel, 1996) and after biodegradation their concentration in conventional activated sludge is close to 2 mg L^{-1}. The particular structure of these species comprises a hydrophilic group linked to a hydrophobic group (amphiphilicity) and provides these molecules with the capacity of diffusing in polar fluids and adsorb to hydrophobic interfaces. The accumulation of surfactants at the interface leads to the reduction of the interfacial tension. Figure I.9 illustrates the surfactant arrangement at a bubble-water interface. The hydrophobic group, in general a hydrocarbon chain with an aromatic or lineal group, is conventionally represented by a 'tail'. The polar group is a functional group such as carboxylate ($-COO^-$), sulfonate ($-SO_3^-$), etc, and are schematized as a 'head'.

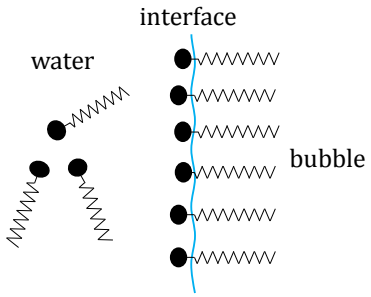

Figure I.9. Schematic of surfactants arrangement at a water-bubble interface.

Depending on the charge of the polar group, surfactants are classified in anionic, non-ionic, cationic or amphoteric (two ionic groups +\-)

The effect of surfactants on oxygen transfer has been widely studied ***in clean water with added surfactants***. Several works having characterized this reduction with the alpha factor are presented in Table I.2.

Table I.2. Literature results of alpha factor in clean water with added surfactant.

Author	Surfactant type	Surfactant name	Concentration range (mg L-1)	Alpha factor	Experimental setup
Wagner *et al.* (1996)	Anionic	AT1	2.5 – 7.5	0.8 - 0.72	50L column; 0.52 m height; FB.
	Anionic	AT2		0.77 - 0.67	
	Non Ionic	NT1		0.75 - 0.65	
Gillot (1997)	Anionic	SDS	1	0.98	400 L oxidation ditch, 0.5 m water height, FB.
	Anionic	SLS		0.97	
	Non Ionic	ELA		0.82	
Capela (1999)	Anionic	SDS	1	1 - 1.02	200 L column, water height between 1.55 - 3 m, FB.
	Non Ionic	ELA		0.82 - 0.64	
				0.47 - 0.81	Three real sites from volumes of 265, 643 et 489 m^3, water height between 2.5 and 6 m, FB
Painmanakul *et al.* (2008)	Anionic	SLS	50-1900	0.79-0.49	0.4 m height column; 0,05 m diameter, isolated bubbles generated with single orifice of 0.29 - 0,48 mm
	Non Ionic	Fatty alcohol benzyl ammonium bromide C12/C18, 10 EO, n-butyl end caped	86-3500	0.45-0.44	
	Cationic	lauryl dimethyl benzyl ammonium bromide	110-2000	0.4-0.40	

FB: fine bubbles aeration

Even at very low concentrations (1mg L^{-1}), surfactants can impact the oxygen transfer and this effect is in most cases negative if not equal. Independently of the surface tension of the surfactant solution (associated to the surface concentration), the magnitude of this influence is related to the surfactant molecule. Two different surfactant solutions that have the same surface tension may not produce the same effect on oxygen transfer. According to Rosso *et al.* (2006), the impact on oxygen transfer is conditioned by the surfactants diffusivity through the liquid film which is related to their molecular weight: light molecules migrate faster than heavy molecules and consequently their impact on oxygen transfer would be more significant.

To explore the different mechanisms involved in the surfactant`s impact on oxygen transfer, several studies have evaluated separately the effect of surfactants on the liquid-side oxygen transfer coefficient (k_L) and on the interfacial area (a) (Wagner and Pöpel, 1996; Capela, 1999; Gillot *et al.,* 2000; Vasconcelos *et al.,* 2003; Rosso *et al.,* 2006; Sardeing *et al.,* 2006; Painmanakul and Hébrard, 2008; Hebrard *et al.,* 2009; Jamnongwong *et al.,* 2010). The results have provided significant comprehension elements on the mechanisms at the origin of the surfactant's impact on oxygen transfer. The following overlapping effects have been proposed when surfactants accumulate at the bubble surface:

- Surfactants reduce both the surface tension and bubble coalescence and consequently the bubble size diminishes leading to an increment of the interfacial area (a).

Simultaneously, smaller bubbles have lower rise velocity thus favouring the gas hold-up (ε_G) and the interfacial area (a).

- Adsorbed surfactants increase the bubbles drag coefficient and slow down the rising bubbles which ends-up with an increment of the gas hold-up (ε_G) and interfacial area (a). In contrast, for a constant bubble size, the reduction of the rising velocity leads to a reduction of the liquid-side oxygen transfer coefficient (k_L), according to the Higbie's model.
- The oxygen diffusivity into the liquid is hindered and consequently the liquid-side oxygen transfer coefficient decreases (k_L).

Whether the oxygen transfer decreases or remains constant in the presence of surfactants depends on how important is the increase of the interfacial area (a) compared to the reduction of the liquid-side oxygen transfer coefficient (k_L).

Vasconcelos *et al.* (2003) and Sardeing *et al.* (2006) found that in presence of surfactants (anionic, cationic, and non-ionic) the liquid-side oxygen transfer coefficient (k_L) lies between the theoretical values for bubbles with mobile (Higbie, 1935; Calderbank and Moo Young, 1961) and rigid interface (Frössling, 1938).

On the other hand, before the adsorbed surfactants have an effect on oxygen transfer, these substances need first to adsorb to the bubble surface. Under this approach, by means of dynamic surface tension measurements (DST) some studies have evaluated the correlation of surfactant's adsorption kinetics with oxygen transfer (Masutani and Stenstrom, 1991; Capela, 1999; Rosso *et al.,* 2006). In fact, surfactants with low adsorption kinetics would take longer to adsorb and saturate the bubble surface and consequently their effect on oxygen transfer would be significant only if the gas-liquid contact time is higher than the adsorption time (*e.g.* reactors with important liquid height). The results from Capela (1999) showed first that different surfactants with an equal concentration (10 mg L^{-1}) have different adsorption times (1 minute for a non-ionic surfactant versus a few seconds for an anionic surfactant). Subsequently, the relatively high adsorption time of the mentioned non-ionic surfactant, helped the author to explain why the oxygen transfer decreased when increasing the liquid height of a bubble column filled with clean water added with non ionic surfactants (1 mg L^{-1}). When increasing the liquid height, surfactants with low adsorption kinetics have enough time to adsorb to the bubble surface and affect the oxygen transfer.

In ***activated sludge*** the impact of anionic surfactants has been studied by Henkel (2010) in two membrane bioreactors fed with synthetic greywater. Even for very high surfactants concentrations in the wastewater influent (between 62 and 70 mg L^{-1}), and for solids retention times (SRTs) ranging between 12 and 80 days, surfactants concentration in the activated sludge remained very low (0.3 mg L^{-1}). According to this author, these concentrations were too low to observe an effect on oxygen transfer. Activated sludge in membrane bioreactor (MBR) has higher solids retention time (SRT) and higher biomass concentration compared to conventional activated sludge systems (CAS). As a result, the degradation of soluble pollution is more complete in MBR systems than in CAS. Consequently the surfactants concentration in conventional activated sludge is probably higher than in MBRs and the impact of surfactants on oxygen transfer might not be insignificant.

I.2.6.2.2.2 Electrolytes

Several studies performed in clean water with added salts have shown that these components have a positive effect on oxygen transfer (Alves *et al.,* 2004; Painmanakul and Hébrard, 2008; Jamnongwong *et al.,* 2010). Because the liquid-side transfer coefficient (k_L) decreases or remains constant in the presence of salts, the enhancement of oxygen transfer can be attributed to a significant increase of the interfacial area (a). However, because these studies are limited to the use of Na_2SO_4 (42.6 g L^{-1}) and NaCl (1.2-100.0 g L^{-1}) respectively, the mechanisms at the origin of this impact are not completely elucidated for the salt species. In fact, the inhibition of bubble coalescence is often the first evoked mechanism to explain the oxygen transfer increase: (i) by means of a smaller bubble size the interfacial area (a) is extended and (ii) because small bubbles have lower rising velocities, the gas hold-up (ε_G) is expanded. However, the study of Craig (2004) has shown that certain anion-cation combinations do not interfere with bubble coalescence and correlates this effect with the ionic strength of the dissolved salts. Besides, the work from Quinn *et al.* (2014) performed with five different dissolved salts provides significant insights on other mechanisms in which electrolytes can affect the oxygen transfer. This author showed that isolated rising bubbles (~2.3 mm) become more spherical as the salt concentration increased, the resulting bubble shape being dependent of the solute type and concentration. Furthermore, it was observed that regardless of the dissolved salt and concentration, the bubble shape seems to determine the bubble rising velocity (Figure I.10)

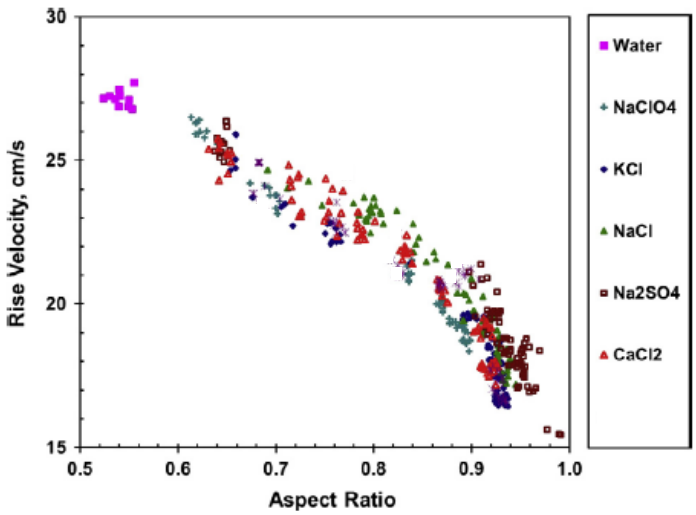

Figure I.10. Relationship between the bubble rise velocity and aspect ratio (the inverse of eccentricity) for water and five different dissolved salts (0.005 M – 2.0 M) (Quinn *et al.,* 2014)

In ***activated sludge*** the effect of dissolved salts on oxygen transfer is not reported in the literature. In activated sludge the electrical conductivity, an indication of the content of dissolved salts, is classically near to 1000 μS cm^{-1} (~1 g L^{-1}). This value is almost twice the clean tap water conductivity (~550 μS cm^{-1}) but inferior to the fixed value of 1500 μS cm^{-1} above which the oxygen transfer measurements in clean water must be performed to avoid the impact of dissolved salts in oxygen transfer (NF EN 12255-15:2004). This suggests that the content of dissolved salts in activated sludge is not significant enough to have a significant impact on oxygen transfer.

I.2.6.2.2.3 Activated sludge interstitial water

Jimenez (2013) studied the impact of soluble substances contained in activated sludge interstitial water on oxygen transfer. By means of an optical technique for flow and concentration visualization (FLIP), the author measured several characteristic variables affecting oxygen transfer of an isolated bubble (~1mm) rising in clean water and in three different activated sludge interstitial waters sampled from: (i) the aerated basin, (ii) the sludge recirculation loop and (iii) the wastewater influent. The results showed a decrease in the oxygen transfer for the three interstitial waters compared to clean water (α factor equal to 0.52, 0.39 and 0.21 respectively). This oxygen transfer reduction was due to the observed liquid-side transfer coefficient (k_L) depletion associated to the decrease of surface tension, eccentricity and bubble rising velocity. Indeed, other variables such as bubble diameter, diffusion coefficient, liquid density and viscosity as well as the interfacial area (a), were not significantly different from one experiment to the other. In activated sludge interstitial water, other mechanisms than

the reduction of the diffusivity, would prevail to explain the value of the liquid-side oxygen transfer coefficient (k_L) but remain not understood: the formation of a surfactants barrier on the gas liquid interface that would inhibit locally the mobility of oxygen molecules in a thin layer around the bubble.

Conclusions on the impact of dissolved substances on oxygen transfer

- In clean water the dissolved substances such as surfactants and electrolytes even at low concentrations have generally a negative impact on oxygen transfer. Dissolved substances in the interstitial water of activated sludge seem to impact negatively the oxygen transfer coefficient. Because the presence of dissolved substances increases or do not modify the interfacial area (a), it is the decline of the liquid-side transfer coefficient (k_L) that explains the depletion of the oxygen transfer coefficient ($k_L a$). However, in activated sludge, surfactants and electrolytes seem to have a non significant impact on oxygen transfer because of their low concentrations. Nevertheless, results available on the literature on this aspect are rare and further examination is required.

I.2.6.2.3 Solids retention time (SRT)

Increasing the solids retention time enhances the degree of biodegradation of the substances impacting negatively the oxygen transfer, principally the surfactants. Therefore a positive correlation between the SRT (also called mean residence time , MCRT) and oxygen transfer has been observed in the literature (Rosso *et al.,* 2005; Gillot and Héduit, 2008; Henkel, 2010)(Figure I.11). However, these authors have observed that for different types of activated sludge, the SRT do not fully explain the decrease of the oxygen transfer coefficient (the alpha value): a given SRT value may correspond to different alpha values (Figure I.11).

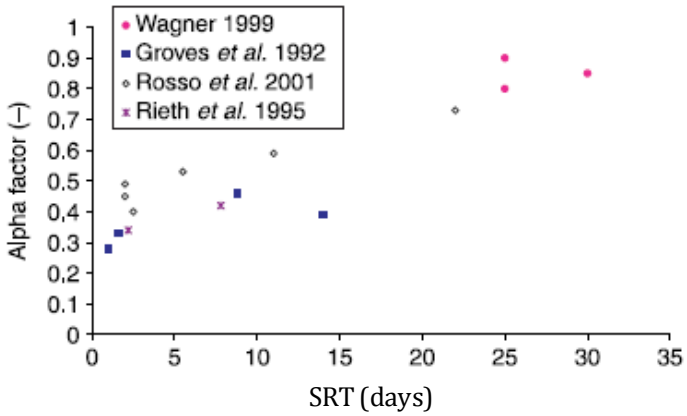

Figure I.11. Alpha factor for different solids retention time (SRT) obtained by different authors (from Gillot and Héduit, 2008).

Therefore other parameters have to be considered in order to upgrade the estimation of the alpha factor. Rosso *et al.* (2005) coupled the gas flow rate with the SRT but still observed an important dispersion of the data in respect to the alpha value (R^2=0.52). Having observed that the reactor's liquid height above the gas diffusers had a negative effect on the oxygen transfer in activated sludge, Gillot and Héduit (2008) have introduced the bubble Equivalent Contact Time (ECT) in order to improve the estimation of the alpha factor. This variable would take into account the fact that bubbles having a longer contact time with the liquid phase are longer exposed to the surfactants absorption at their surface thus leading to an increment in the oxygen transfer depletion. Coupling the SRT with an estimation of the bubble Equivalent Contact Time (a function of the gas flow rate and diffuser submergence), the authors predicted the alpha factor for 14 full-scale wastewater treatment plants operated under extended aeration. Despite the satisfactory modelled results, some assumptions such as a non-significant effect of the activated sludge on bubble size (d_b) and the liquid-side oxygen transfer coefficient (k_L) may require further exploration.

Besides, having observed that the MLVSS (mixed liquor volatile suspended solids) concentration is well correlated with the oxygen transfer decrease in activated sludge (cf. I.2.6.2.1.1) the work from Henkel (2010) coupled the effect of the MLVSS on oxygen transfer with the effect of SRT. The proposed empirical correlation to predict the alpha factor (α) is presented in Equation I.37 and illustrated in the Figure I.12.

$$\alpha = 0.51 - 0.062 \times MLVSS + 0.019 \times SRT \quad \pm 0.114 \qquad \text{I.37}$$

Despite the interest of this model, the impact of activated sludge on the hydrodynamic conditions on oxygen transfer remained unexplored.

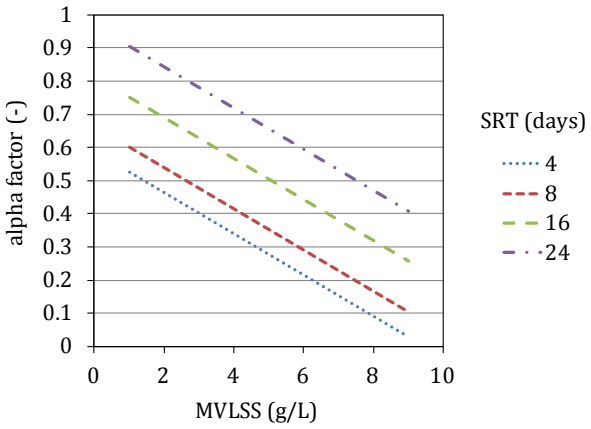

Figure I.12. Alpha factor for different sludge MLVSS concentration and the SRT according to the correlation proposed by Henkel (2010).

I.2.6.2.4 Activated sludge apparent viscosity

Viscosity influences the hydrodynamic conditions of the gas-liquid dispersion. As previously mentioned (cf. I.2.6.2.1), viscosity can impact the bubble size at formation, promote the bubble coalescence and reduce the bubble rising velocity. These multiple effects end up affecting the oxygen transfer characteristics parameters a and k_L. Apart from the context of activated sludge, several works carried out with Newtonian and non-Newtonian fluids have observed that an increase of viscosity leads to a decrease in oxygen transfer (Henzler, 1980; Schumpe and Deckwer, 1987; Chisti and Moo-Young, 1989; Shi *et al.,* 1990; Al-Masry, 1999; Kawase and Kumagai, 1991; Cerri *et al.*, 2008; Thomasi *et al.,* 2010). According to the review completed by Seyssiecq *et al.* (2003), the oxygen transfer coefficient ($k_L a$) in non-Newtonian suspensions decreases as a power law with the increment of apparent viscosity (μ_{app}) as follows:

$$k_L a \propto {\mu_{app}}^{-C} \text{ with } 0.25 < C < 0.84 \qquad \text{I.38}$$

The large range of values of the empirical constant C indicates that the apparent viscosity is not the solely factor that explain the variability of $k_L a$ is quite variable. The viscosity effect is not only related to the physicochemical properties of the aerated suspension but also to the design

and operating conditions that can affect the gas-liquid flow regime such as diffuser type, reactor geometry, superficial gas velocity, etc.

In ***activated sludge***, Krampe and Krauth (2003) have evaluated the effect of sludge apparent viscosity on oxygen transfer in a bubble column. The authors measured the oxygen transfer coefficient in activated sludge with a MLSS concentration range from 8 to 28 g L^{-1} (obtained by diluting the sludge samples) and studied the sludge rheological behaviour. Knowing that based on the bubble size and rising velocity previous works had estimated a shear rate of 40 s^{-1} in the aerated reactor, these authors correlated the apparent viscosity at 40 s^{-1} ($\mu_{app,40}$) to the oxygen transfer coefficient ($k_L a$). Independently of the two types of used diffusers (fine bubbles diffuser and injector for compressed air) the results showed an oxygen transfer depletion with the increase in apparent viscosity ($\mu_{app,40}$). The alpha factor (α) was written as follows:

$$\alpha = {\mu_{app,40}}^{-0.456} \qquad \text{I.39}$$

Despite a high data scattering at the lowest apparent viscosity values, these results highlighted the significant impact of the sludge apparent viscosity on oxygen transfer. According to the authors, apparent viscosity relates more distinctly to the alpha factor than to the MLSS concentration. However this correlation is limited to a shear rate of 40 s^{-1} and although it considers the sludge viscosity, it does not take into account the specific sludge rheological behaviour.

From these results, two aspects appear of interest in order to better evaluate the correlation between the oxygen transfer and the sludge apparent viscosity: (i) determining the range of shear rate prevailing in aerated bioreactors and (ii) considering the specific activated sludge rheology.

I.2.6.2.4.1 Correlations predicting the oxygen transfer coefficient as a function of viscosity

The impact of viscosity (and apparent viscosity) on oxygen transfer has appeared to be significant and many authors have included it in empirical correlations to predict the oxygen transfer in different reactors configurations. These equations are summarized in the review of Garcia-Ochoa and Gomez (2009). For instance, in stirred reactors the oxygen transfer coefficient

($k_L a$) is written as a function of the superficial gas velocity (U_G), viscosity (μ) or apparent viscosity (μ_{app}) and aeration specific power input (P/V):

$$k_L a = A \cdot {U_G}^B \cdot {\mu_{app}}^C \cdot (P/V)^D \quad \text{I.40}$$

where *A, B, C and D* are empirical constants and the power input (P/V) depends on the tank geometry, the stirrer type and geometry and the stirring rate.

In bubble columns the oxygen transfer coefficient ($k_L a$) can be written as:

$$k_L a = A \cdot {U_G}^B \cdot {\mu_{app}}^C \quad \text{I.41}$$

The constants (A , B, C, etc) of these empirical correlations have been studied for Newtonian fluids such as water, glycerol, electrolytes solution as well as for non-Newtonian fluids such as xanthan gum, CMC (carboxymethyl cellulose), PAA (polyacrylamide) and in some cases biological broth (Gabelle *et al.,* 2012). For non-Newtonian fluids, the impact of apparent viscosity requires the estimation of the average shear rate related to the superficial gas velocity in the aerated bioreactor as well as the fluid rheological behaviour. In the domain of activated sludge the empirical constants of this type of correlation are not available in the literature.

Conclusions on the impact of activated sludge on oxygen transfer

- The suspended solids fraction appears to be the main parameter responsible for the oxygen transfer decrease in activated sludge compared to clean water. Multiple effects seem to be behind this impact. An increase in the suspended solid concentration modifies the hydrodynamic conditions by producing an increase in the suspended viscosity. Hence the bubble coalescence and gas phase characteristics such as bubble size, rise velocity and gas hold-up are affected. In association with the steric effect, the floc volume and size are sludge properties that may also explain the oxygen transfer reduction in activated sludge.
- Although it has been observed that the *interstitial water* of activated sludge has a lower liquid-side transfer coefficient than clean water, the impact of soluble substances such as surfactants and dissolved salts on oxygen transfer *in activated sludge* still requires further exploration since the literature results are scarce and not conclusive.
- Nevertheless, from the results that show a positive correlation between the alpha factor and the solids retention time (SRT) it can be inferred that the surfactants have an effect on oxygen transfer. Analytical and empirical correlations have been proposed to predict the alpha factor as a function of the SRT coupled with the equivalent contact time (ECT) or with the mixed volatile liquor suspended solids (MVLSS). However these do not consider the potential effects of activated sludge on the gas-liquid dispersion and the hydrodynamic conditions.
- Besides, a few works have correlated the oxygen transfer reduction to the increase in sludge apparent viscosity determined at fixed shear rate ($40 s^{-1}$). For a better evaluation of apparent viscosity on oxygen transfer it would be necessary to estimate the shear rate prevailing in the aerated bioreactor considering the hydrodynamic conditions such as gas velocities and liquid properties (e.g. sludge rheology).
- Finally, empirical equations correlating the oxygen transfer to the apparent viscosity associated to the hydrodynamic conditions (in terms of superficial gas velocity) and the fluid rheology are proposed in the literature for Newtonian and non-Newtonian fluids, but not in the field of activated sludge.

I.3 Rheology principles

Rheology studies the flow and deformation of matter under the application of a shear force. From the ancient Greek rheo ($\rho\acute{\varepsilon}\omega$) which means flow, the concept of rheology was introduced by Bingham in 1928 to establish a discipline regrouping knowledge from material science and fluid mechanics and allowing to evaluate problems related to the flow of plastic materials and non-Newtonian fluids.

I.3.1 Laminar shear flow

The rheological study of a fluid is performed by developing a **laminar shear flow**. This implies the following assumptions:

1. The material is composed of adjacent layers of infinitely thin thickness.
2. This flow produces a relative slip between the various layers.
3. There is no transfer of matter between the various layers.

When the laminar shear flow takes place, frictional forces tangential to the layers surface (dS) are exerted at the interfaces of the successive layers. These forces, shown in Figure I.13, called elementary shear forces (dF), tend to slow down the neighbour layers moving faster and to accelerate those moving at lower velocities.

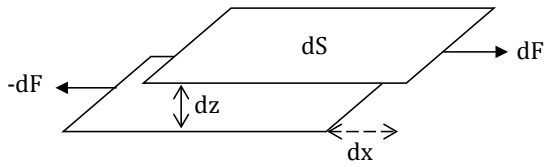

Figure I.13. Shear forces exerted on two adjacent layers in a laminar shear flow

The ratio of the shear force to the unit surface is called **shear stress (τ).**

$$d\tau = \frac{dF}{dS} \text{ or } \tau = \frac{F}{S} \text{ (Pa)} \qquad \text{I.42}$$

The infinitesimal displacement dx of a layer with thickness dz with respect to a neighbor layer is named **shear** or deformation **(γ)**.

$$d\gamma = \frac{dx}{dz} \qquad \text{I.43}$$

The shear velocity, the derivative of shear with respect to time, is called **shear rate ($\dot{\gamma}$).**

$$\dot{\gamma} = \frac{d\gamma}{dt} \quad (s^{-1}) \qquad \text{I.44}$$

According to the Newton's law (1687), the shear stress (τ) is proportional to the shear rate ($\dot{\gamma}$) by means of a proportionally constant initially referred as 'the lack of slipperiness of the fluid elements' and today known as the dynamic viscosity (μ). The Newton's law is expressed as:

$$\tau = \mu\dot{\gamma} \qquad \text{I.45}$$

I.3.2 Rheological measurements

The primary objective of a rheological study consists in determining how the shear stress evolves with the exerted shear rate or vice versa.

When performing rheological measurements, the following assumptions must be considered:

- The flow regime is laminar
- The flow is steady
- The fluid is incompressible
- The system is isothermal
- Wall slip is negligible
- Edge effects are negligible

I.3.2.1 Rheometers

To perform rheological measurements, two types of rheometers are implemented to develop the laminar shear flow: tubular rheometers (Figure I.14) and rotational rheometers. The different geometries induce various shear ranges and are more or less adapted to the fluid characteristics such as viscosity, settleability, sample availability and particle size.

In the *tubular rheometer*, the shear flow is generated by applying a pressure on the fluid entering into a capillary. The shear stress is determined under the assumption that the pressure drop (ΔP) of a fluid flowing inside a tube of radius R and length L, is only due to friction.

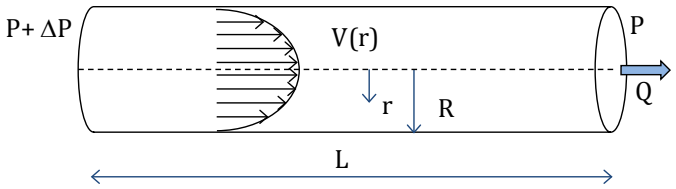

Figure I.14. Tubular rheometer

As in a tube the velocity profile is a function of the radius (r), the shear rate and shear stress are calculated at the tube's wall ($\dot{\gamma}_w$,τ_w) where the shear rate is maximum. By determining the longitudinal pressure loss ($\Delta P/L$) associated to the fluid flow rate (Q) in a tube of a given geometry (L,R), the shear stress (τ_w), shear rate ($\dot{\gamma}_w$) and dynamic viscosity (μ) are estimated according to the Poiseuille's law, with the equations indicated in Table I.3 for Newtonian fluids.

In *rotational rheometers*, the fluid is placed in the gap between a mobile and an immobile surface such as concentric cylinders, plate-plate surfaces and cone-plate surfaces. The laminar shear flow is generated as the mobile surface rotates at a given angular velocity (w) associated to a torque (M). Figure I.15 illustrates the different geometries used in rotational rheometers.

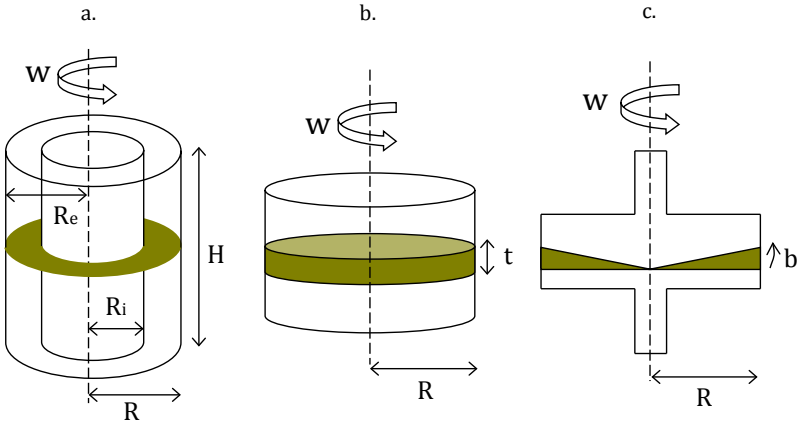

Figure I.15. Geometries of rotational rheometers: a. Concentric cylinder, b. Plate-plate, c. Cone-plate.

The equations to estimate the shear stress, shear rate and dynamic viscosity in capillary and rotational geometries are presented in Table I.3 (for Newtonian fluids).

Table I.3. Equations to calculate the shear rate, shear stress and dynamic viscosity in capillary and rotational rheometers.

Rheometer		Shear rate ($\dot{\gamma}$)	Shear stress (τ)	Viscosity (μ)
Tubular		$\dot{\gamma}_w = \frac{4Q}{\pi R^3}$	$\tau_w = \frac{R}{2}\frac{\Delta P}{L}$	$\mu = \frac{\tau}{\dot{\gamma}} = \frac{\Delta P}{L}\frac{\pi}{8Q}R^4$
Rotational	Concentric cylinder	$\dot{\gamma}_R = \frac{wR}{R_e - R_i}$	$\tau = \frac{F}{S} = \frac{M}{R}\cdot\frac{1}{2\pi RH} = \frac{M}{2\pi R^2 H}$	$\mu = \frac{M(R_e - R_i)}{w(2\pi R^3 H)} = K\frac{M}{w}$
	Plate-Plate	$\dot{\gamma}_R = \frac{wR}{t}$	$\tau = \frac{2M}{\pi R^3}$	$\mu = \frac{2}{\pi R^4}\frac{M}{w} = K\frac{M}{w}$
	Cone -Plate	$\dot{\gamma} = \frac{w}{\beta}$	$\tau = \frac{3M}{2\pi R^3}$	$\mu = \frac{3M\beta}{w(2\pi R^3)} = K\frac{M}{w}$

Rheometer with concentric cylinders geometry are known as the reference apparatus in most of the cases studying rheology of fluid materials (Mori *et al.,* 2007). In this type of geometry, having a higher cylinder surface implies the generation of lower shear stresses. Consequently, the implementation of a geometry with a double concentric cylinder is privileged when a low range of shear stress is required (as for low viscosity fluids). The advantages and drawbacks of using the tubular and the rotational rheometers are listed in Table I.4.

Table I.4. Advantages and drawbacks of tubular and rotational rheometers (Dupuis, 2008; Ratkovich *et al.,* 2013).

	Tubular	Rotational
Advantages	Mechanically simple. Good precision. On line testing. Large range of shear is applicable (with additional tubes) Well established corrections. Low cost.	Low shear range is applicable: Yield stress is easily determined Time dependant effects can be measured (i.e. thixotropy) Small volume sample required. Widely used, commercially available.
Disadvantages	Large volume sample required Difficulty to reach the lowest values of shear stress. Cannot measure time effects (i.e. viscoplasticity, thixotropy).	Centrifugal forces can cause changes on concentration gradient in the measuring gap. Settling may cause sample heterogeneity and therefore measurement errors. Expensive. Plate-plate and cone-plate geometries are not adapted to low viscosity fluids.

When the fluid under study contains solid particles or aggregates it is recommended to consider that particle size should be significantly lower than the space between the two surfaces (Dupuis, 2008) in order to avoid a system blockage and allow the particles to be dragged with the fluid. This is important especially for plate-plate and cone-plate geometries for which the gap between the two surfaces is very small (between 1 mm and 10 μm). Concerning the settling capacity of

some suspensions, geometries with small volumes are best adapted in order to avoid sample heterogeneity during the measurements. At the same time, small geometries may induce wall slip effects (Ratkovich *et al.,* 2013).

Besides, because rheology principles are based on a laminar flow, it is important to survey the flow conditions in the rheometer in order to avoid turbulences or vortices that may induce to measurement errors.

In concentric cylinder geometries (Couette geometry), the critical Reynolds number (Re_c), below which the flow would still be laminar is a function of the mean radius between the rotor and the stator ($\bar{R}$) and the gap length (e) as follows:

$$Re_c = 41.3\sqrt{\frac{\bar{R}}{e}} \qquad \text{I.46}$$

And the Reynolds number is determined by the angular velocity (w), the rotor radius (R_i), the gap length (e) and the fluid density (ρ_L) and viscosity (μ_L) as follows:

$$Re_c = \frac{eR_i w\rho_L}{\mu_L} \qquad \text{I.47}$$

In capillary rheometers a laminar flow is considered to occur at a Reynolds number below approximately 2000. In a capillary tube the Reynolds number is function of the fluid velocity (U), tube diameter (D), and fluid density (ρ_L) and viscosity (μ_L) as follows:

$$Re = \frac{DU\rho_L}{\mu_L} \qquad \text{I.48}$$

I.3.3 Rheological behaviours

Fluids can exhibit different behaviours according to the way in which the shear stress (τ) evolves with the shear rate ($\dot{\gamma}$). These rheological behaviours are represented in the rheogram or flow curve in Figure I.16 (τ vs. $\dot{\gamma}$).

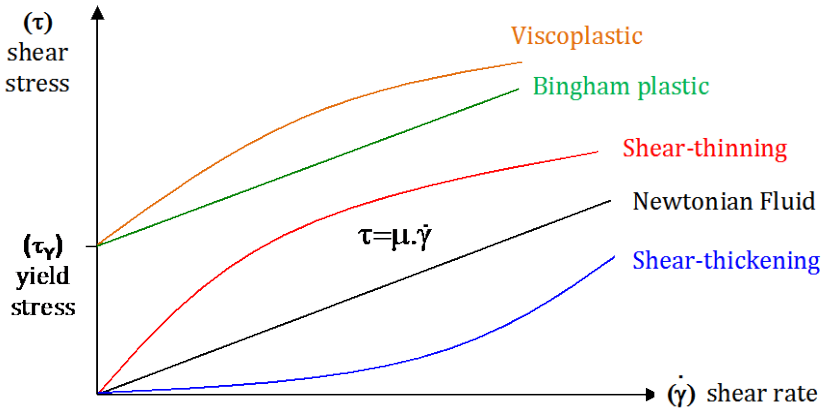

Figure I.16. Representation of different rheological behaviours in a rheogram.

When the correlation between the shear stress and the shear rate is linear, the fluid is said to exhibit a **Newtonian behaviour** which means that the dynamic viscosity, the slope of the flow curve, is independent on the exerted shear rate. Pure liquids such as water, solvents, glycerol, benzene, etc, are generally Newtonian (Dupuis, 2008).

I.3.3.1 Non-Newtonian fluids

For fluids that exhibit a non-Newtonian behaviour, the shear stress does not follow a linear trend in respect to the shear rate. Viscosity is then a function of the exerted shear and the term *apparent viscosity* is introduced to refer to the viscosity of a fluid associated to a given shear rate. The non-Newtonian behaviours are listed in the following paragraphs.

I.3.3.1.1 Shear-thinning

When the increment of the shear rate ($\dot{\gamma}$) leads to a reduction of the apparent viscosity (μ_{app}), the fluid is said to exhibit a *shear-thinning behaviour*. This is generally explained by the fact the structural units composing these fluids (particles, aggregates, etc) are rearranged and stratified in the flow when submitted to a higher shear stress and consequently the fluid circulation is easier. At high shear rates the apparent viscosity becomes almost constant and is no longer dependent on the shear rate; this is called the limit viscosity (μ_{∞}).

I.3.3.1.2 Shear-thickening

When the apparent viscosity (μ_{app}) increases with the increase of shear rate ($\dot{\gamma}$), the fluid is said to exhibit a *shear-thickening behaviour*. This behaviour is rare and occurs in concentrated slurries when the increment of the shear rate leads to the formation of clusters that rigidify the

suspension structure. If the suspension is composed by associative polymers, an increase in shear forces favours the polymer interactions resulting in a more solid structure.

I.3.3.1.3 Viscoplasticity

For some non-Newtonian fluids, generally suspensions having strong interparticle forces (Van-Der-Waals forces), it is necessary to overcome a threshold shear stress in order to disrupt these forces and induce flow. Below this shear stress, referred as yield stress (τ_y), the suspension behaves as a solid and flow does not occur. This initial solid behaviour is commonly explained by the presence of an interconnected three-dimensional network of suspended aggregates (Seyssiecq *et al.,* 2003).

The experimental identification of a shear stress requires the performance of rheological measurements at very low shear rates and with high precision instruments. In the practice it may be difficult to determine the yield stress (τ_y) because it is required to apply a shear stress that increases uniformly and exceeds the yield stress by a small amount. To circumvent this technical barrier, the yield stress is often estimated by extrapolating the experimental rheogram to the ordinate (Seyssiecq *et al.,* 2003) as illustrated in Figure I.17.

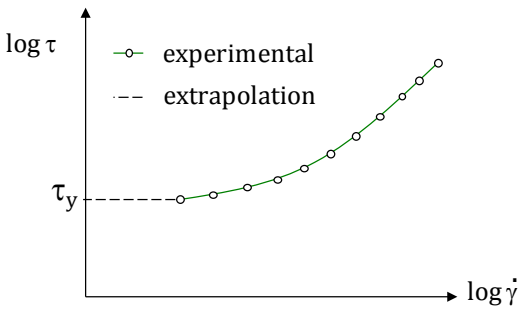

Figure I.17. Typical flow curve of a viscoplastic fluid and estimated yield stress from the extrapolation of experimental data.

I.3.3.1.4 Thixotropy

In addition to the rheological behaviours explained up to this point, some non-Newtonians fluids may exhibit a rheological behaviour that is time-dependant. In fact, different values of shear stress (and viscosity) can be measured under the same exerted shear rate and an undetermined time is required to reach stationary measurements. This phenomenon indicates that the suspension structure continues to change and respond to the exerted shear rate even when the latter has already been modified or stopped (hysteresis). If the apparent viscosity decreases or

increases with the duration of the exerted shear rate, the fluids are either called thixotropic or antithixotropic respectively. After a certain motionless period, suspensions would recover their initial structure (Tixier, 2003; Dupuis, 2008).

Typical identification of this time-dependant behaviour in a flow curve consists first in submitting the suspension to successive increasing levels of shear stress. Subsequently the shear stress is continuously decreased down to the initial point. For a thixotropic fluid the increasing flow curve is over the decreasing rheogram. The Figure I.18 represents the typical thixotropic behaviour in a flow curve.

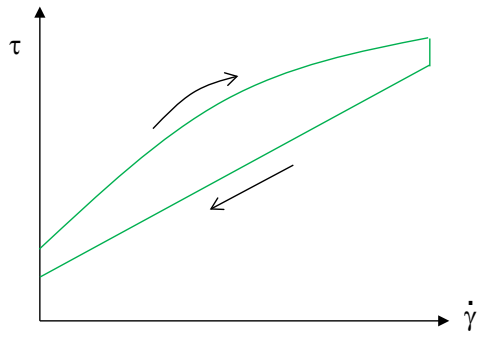

Figure I.18. Representation of a thixotropic behaviour in a rheogram.

I.3.3.1.5 Viscoelasticity

Similarly to thixotropic fluids, viscoelastic fluids exhibit also a time-dependant behaviour. However these suspensions exhibit additionally an elastic behaviour explained by the ability to store part of the mechanical energy supplied to the fluid as elastic energy in inter-particle bonds for instance (Seyssiecq *et al.,* 2003). Consequently when shear stress is reduced to zero, these suspensions retrieve a fraction of the stored energy and a partial elastic recovery is observed. In contrast to this behaviour, for only viscous fluids the deformation energy is entirely dissipated as heat (Dupuis, 2008). For the characterization of viscoelastic fluids, dynamic methods are implemented and other variables such as the storage modulus (G') and loss modulus (G'') associated with the stored energy and the dissipated energy as heat, are introduced. Further details of this more complex characterization can be found in Dupuis (2008).

I.3.4 Activated sludge rheology

Activated sludge suspensions have been largely described as non-Newtonian fluids with a shear-thinning behaviour: their viscosity decreases with an increment of the shear rate (Forster, 1982,

1983; Sutapa, 1996; Rosenberger *et al.,* 2002; Seyssiecq *et al.,* 2003; Tixier *et al.,* 2003; Laera *et al.*, 2007; Seyssiecq *et al.,* 2008; Khongnakorn *et al.*, 2009; Xia *et al.,* 2009; Yang *et al.*, 2009; Ratkovich *et al.*, 2013; Forster, 2002; Jin *et al.*, 2006; Mori *et al.,* 2006). Besides, depending on the suspended solids concentration, activated sludge can exhibit viscoplastic behaviour (presence of a yield stress). According to Forster (2002), the yield stress is negligible for activated sludge with suspended solids concentrations below 11 g L^{-1}.

I.3.4.1 Activated sludge thixotropy

Some activated sludge can exhibit thixotropic behaviour. The study carried out by Tixier *et al.* (2003) showed that this behaviour is associated to the presence of filamentous bacteria. This authors performed rheological measurements with a rotational rheometer and a double gap coaxial cylindrical geometry, on two different activated sludge samples with the same suspended solids concentration (5.5 g L^{-1}) but different in the level of proliferation of filamentous bacteria: "high" versus "low". The resulting rheograms, presented in Figure I.19, show that both activated sludge samples manifested thixotropy, though the sample with high proliferation of filamentous bacteria (F1) showed a more significant hysteresis area.

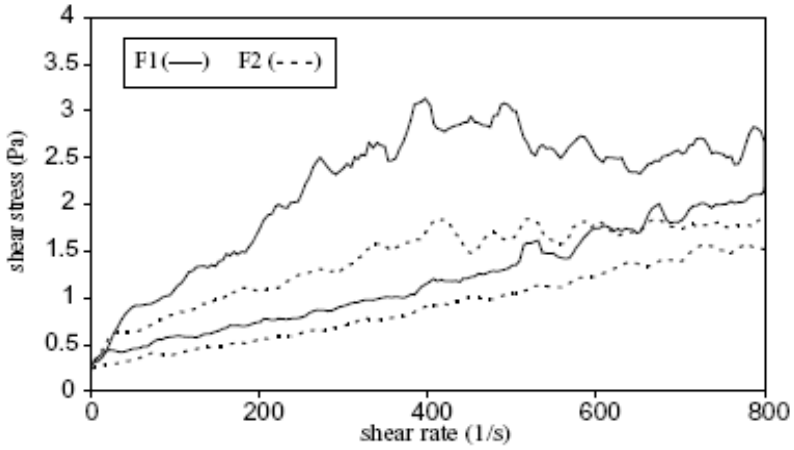

Figure I.19. Flow curve for two types of filamentous activated sludge. F1: Excessive filamentous sludge→significant hysteresis; F2 : Low-filamentous sludge. Rheometer: rotational with double gap coaxial cylindrical geometry. (from Tixier *et al.,* 2003)

Besides, the obtained flow curves, either in the increasing or the decreasing ramp of shear rate, did not exhibit a steady trend, the irregularity being more pronounced for the most filamentous sample.

Since the rheology of these suspensions depends on the previously exerted shear rate, the rheological behaviour of such systems seems difficult to capture. Consequently, when

performing rheological measurements with fluids exhibiting this behaviour, it is recommended to maintain a constant shear until a steady value of apparent viscosity is reached (Forster, 2002). Alternatively, uniform protocols including pre-shear phases at high shear rates are usually implemented. This allows obtaining a similar internal structure before the rheological characterization (Seyssiecq *et al.,* 2003).

I.3.4.2 Activated sludge rheology modelling

The activated sludge rheological behaviour is represented using classical non-Newtonian laws. In the absence of a yield shear stress (non plastic fluids), the rheological behaviour can be modelled using the Ostwald (1925)-de Waele (1923) equation that integrates the consistency index (K) and the flow index (n) to correlate the shear stress (τ) to the shear rate ($\dot{\gamma}$) in a power low as follows:

$$\tau = K\dot{\gamma}^n \qquad \text{I.49}$$

The consistency index (K) is proportional to the sludge apparent viscosity. As activated sludge is a shear-thinning fluid, the index flow (n) should be lower than 1.

The *Sisko* model integrates the infinite shear rate viscosity (μ_∞) which corresponds to the plateau viscosity obtained at very high shear rates. The Sisko model is written as:

$$\tau = \mu_\infty\dot{\gamma} + K\dot{\gamma}^n \qquad \text{I.50}$$

The *viscoplastic* behaviour can be represented with the *Herschel-Bulkley* model which integrates the yield stress (τ_y) to the Ostwald-de Waele equation as follows:

$$\tau = \tau_y + K\dot{\gamma}^n \qquad \text{I.51}$$

If the flow index in the Herschel-Bulkley model (Equation I.51) is equal to the unit (n=1), the model is called the *Bingham* model. Also, the Casson equation is used to represent the activated sludge viscoplastic behaviour as follows:

$$\sqrt{\tau} = \sqrt{\tau_y} + \sqrt{K\dot{\gamma}} \quad \text{I.52}$$

Although the Ostwald-de Waele and the Herschel-Bulkley models seem to be the most commonly used for activated sludge in the literature, Xia *et al.* (2009) showed that the model best fitting the rheological behaviour of activated sludge depends on the range of the considered shear rate. This is in agreement with Baudez *et al.* (2004) who additionally underline that rheological models should be used to represent the sludge behaviour only in the range of the shear rate and shear stress in which rheological measurements have been performed.

In this context, if the rheological measurements are performed in a low range of shear rate and a yield stress (τ_y) is observed, viscoplastic models (Herschel Bulkley, Bingham, Casson) are convenient. Instead, if the applied range of shear rate range is high and the infinite shear rate viscosity (μ_∞) is identified, the Sisko model is more adapted. If the range of the applied shear rate is intermediate and neither the yield stress (τ_y) nor the infinite shear rate viscosity (μ_∞) are determined, the Ostwald-de Waele model seems to be appropriate.

Regarding the modelling practices, Ratkovich *et al.* (2013) highlighted the importance of avoiding model "overparameterization", which refers to models including more rheological parameters than necessary to describe the experimental rheological data. Instead of representing the true underlying relation between the rheological parameters and the rheological behaviour, overparameterization could lead to over fit the data. Consequently some rheological parameters could become "unidentifiable" or in other words they could lose their power of representing the experimental data thus leading to models with less prediction capacity.

Table I.5 and Table I.6 present a summary of the rheological parameters (τ_y, K, n, μ_∞) obtained in literature studies from the modelling of the activated sludge rheological behaviour under different experimental conditions. These tables show that for the same activated sludge sample, the rheological behaviour can be represented with shear-thinning or viscoplastic models and obtain in general satisfactory determination coefficients (R^2>0.95). Comparison between the values of rheological parameters presented in theses tables must consider that the sludge characteristics (MLSS, COD, etc) and measurement conditions and protocols (rheometer geometry, °C, range of shear stress (τ), range of shear rate ($\dot{\gamma}$), …) may determine the rheological results as described in the next paragraphs.

Table I.5. Literature results for the Ostwald-de Waele rheological model parameters (K and n) determined under different conditions: temperature, shear rate, geometry, air flow rate and with activated sludge having different characteristics (MLSS, EPS, SRT, soluble COD)

Author	T (°C)	Studied parameter					Rheological model parameters		
							Ostwald-de Waele or power law		
		MLSS (g L^{-1})	SRT (days)	$\dot{\gamma}$ (s^{-1})	Geometry	Air flow rate(L h^{-1})	K (x 10^{-3}Pa.s)	n	R^2
Laera *et al.* (200L7)	20	3.7	20	0-800	CC	-	7.66	0.856	0.99
		6.1	40				5.81	0.886	0.97
		7.9	60				9.16	0.823	0.95
		9.4	80				5.24	0.782	0.97
		22.9	1200				91.71	0.608	0.99
Seyssiecq *et al.* (2008)	20	10.0		0-200	HRI	0	341	0.154	0.92-0.99
		15.0					2081	0.192	
		18.0					5411	0.142	
		24.0					6432	0.114	
		28.0					11578	0.107	
		35.0					13395	0.114	
Yang *et al.* (2009)	5-35	2.7	30	1-1000	Cone plate	-	9	0.729	0.99
		5.1					34	0.579	0.96
		7.4					57	0.557	0.98
		10.2					150	0.486	0.98
		16.0					1259	0.249	0.89
Rosenberger *et al.* (2002)	21	10-40.0		5-2200	DCC		$K = 1.9e^{(MLSS^{0.43})}$* $n = 1 - 0.22MLSS^{0.37}$		

CC: concentric cylinder; HRI: helicoidal ribbon impeller; DCC: double gap concentric cylinder. *Correlation for domestic activated sludge

Table I.6. Literature results for viscoplastic rheological model parameters (τ_y, K and n) determined from different experimental configurations: temperature, shear rate, geometry and with activated sludge having different characteristics (MLSS, EPS, SRT, soluble COD).

Author	T (°C)	Studied parameter							Parameters for Plastic Fluids rheological models									
									Bingham			Casson			Herschel-Bulkley			
		MLSS (g L^{-1})	EPS (mg $gMLSS^{-1}$)	Soluble COD (mg L^{-1})	Activated sludge age (days)	τ (Pa)	$\dot{\gamma}$ (s^{-1})	Geometry	τ_y (x 10^{-3}Pa)	K (x 10^{-3}Pa.s)	R^2	K (x 10^{-3}Pa.s)	τ_y (Pa)	R^2	τ_y (x 10^{-3}Pa)	K (x 10^{-3}Pa.s)	n	R^2
Laera *et al.* (2007)	20	3.7	-	-	20	-	3-1312	CC	141	2.54	0.98	-	-	-	-	-	-	-
		6.1			40				81	2.39	0.98	-	-	-	-	-	-	-
		7.9			60				125	2.73	0.95	-	-	-	-	-	-	-
		9.4			80				226	3.25	0.95	-	-	-	-	-	-	-
		22.9			1200				737	6.26	0.99	-	-	-	-	-	-	-
Mori *et al.* (2007)	20	43	-	-	-	-	0-1000	CC	-	-	-	-	-	-	12230	1524.6	0.312	n.a
		15							-	-	-	-	-	-	120	163.5	0.525	n.a
		4							-	-	-	-	-	-	50	8.9	0.775	n.a
		43						HRI	-	-	-	-	-	-	35000	593.3	0.598	n.a
		15							-	-	-	-	-	-	1000	8.4	0.966	n.a
		4							-	-	-	-	-	-	90	4.7	0.964	n.a
		15						DCC	-	-	-	-	-	-	310	161.5	0.516	n.a
		4							-	-	-	-	-	-	20	14.1	0.734	n.a
	20	43	1.1	-	-	-	0-1000	CC	-	-	-	-	-	-	12000	1500	0.3	n.a
			0.45*						-	-	-	-	-	-	10000	1300	0.7	n.a
Yang *et al.* (2009)	5-35	2.74	-	-	30	-	1-1000	Cone-plate	89	1.5	0.99	34.7	21.3	0.99	-	1.9	0.97	0.99
		5.08							236	2	0.99	36.7	91.8	0.99	-	2.8	0.951	0.99
		7.43							406	2.7	0.99	42	167	0.99	-	5.2	0.915	0.99
		10.22							887	4	0.99	48.6	433	0.99	-	11.1	0.869	0.99
		16							2096	8.6	0.97	62	1484	0.99	-	108.4	0.62	0.99
Khongnakorn *et al.* (2010)	21.5	4.5-15	-	+/- 120	-	0-185	-	CC	-	-	-	-	-	-	100-700	10-60	1-0.8	n.a
		2.5-6.2	-	550-900	-	-	-		-	-	-	-	-	-	1000-5000	25-150	1-0.8	n.a

CC: concentric cylinder; HRI: Helicoidal Ribbon Impeller; DCC: double gap concentric cylinder. (*measurement of EPS after 4 days of substrate absence).

Conclusions on activated sludge rheological behaviour and modelling

- Activated sludge is a non-Newtonian fluid with a shear-thinning behaviour. A viscoplastic behaviour can be observed for sludge with high MLSS concentrations (*ca.* 11 g L^{-1} according to Forster, 2002).
- Rheological models integrating two or three rheological parameters are proposed in the literature to describe the sludge rheological behaviour. A literature review highlights the importance of avoiding model "overparameterization" in which parameters become unidentifiable and models lose their prediction capability.

I.3.4.3 Sensitivity of activated sludge rheology to measurement conditions

I.3.4.3.1 Influence of temperature on activated sludge apparent viscosity

To express the decrease of activated sludge viscosity with an increase in temperature (T), Yang *et al.* (2009) have obtained the empirical correlation presented in Table I.7 (Equation I.53). This relationship was obtained with suspended solids concentration ranging from 0 to 18.7 g L^{-1}.

For the case of pasty sludge (15% of dry matter) Dieudé-Fauvel *et al.* (2009), modelled the decrease of apparent viscosity with temperature, using a version of the Vogel-Fulcher-Tammann (VTF) correlation, shown in Table I.7 (Equation I.54), with the empirical parameters a=0.95; b=90.6; To=244 K; and c=10.5 (R^2=0.98).

Table I.7. Empirical correlations expressing the decrease of activated sludge apparent viscosity with an increment of temperature.

Correlation		Temperature range (°C)	Solid content	Shear rate (s^{-1})	Rheometer geometry	Author
$\mu_{app} \propto 1.0024\ T^{-0.206}$ with T(°C)	I.53	5 - 35	MLSS between 0 and 18.7 g L^{-1}	100	CC	Yang *et al.* (2009)
$\mu_{app} = a \cdot e^{\left(\frac{b}{T-To}\right)} + c$ with T(K)	I.54	4 - 35	15% dry matter	100	CC	Dieudé-Fauvel *et al.* (2009)

CC: Coaxial cylinders

With the correlation proposed by Yang *et al.* (2009), the sludge apparent viscosity decreases by 13.3% when temperature rises from 10 to 20°C, while with the one proposed by Dieudé-Fauvel *et al.* (2009) the reduction of the apparent viscosity is of 18.0%.

These results indicate a non-negligible influence of temperature on sludge apparent viscosity. Consequently, rheological measurements need to be performed at constant temperature and results need to specify this parameter.

I.3.4.3.2 Influence of rheometer geometry on rheology results

Using three different geometries of rotational rheometers (HRI, CC and DCC) to evaluate the rheology of two sludge samples with 4 and 15 g L^{-1} of MLSS concentration, Mori *et al.* (2007) obtained diverging rheograms. Moreover, using the same rotational rheometer geometry (CC) but different space between cylinders (1 mm and 1.25 mm), Ratkovich *et al.* (2013) presented also diverging rheograms obtained for two sludge samples with 5.93 g L^{-1} and 11.86 g L^{-1} of MLSS concentration (Figure I.20). The authors attributed these disparities to (i) the generation

of different flow patterns that lead to the onset of vortices and turbulence at different shear rates and to (ii) a different shear repartition in the measurement volume (cf. I.3.2.1).

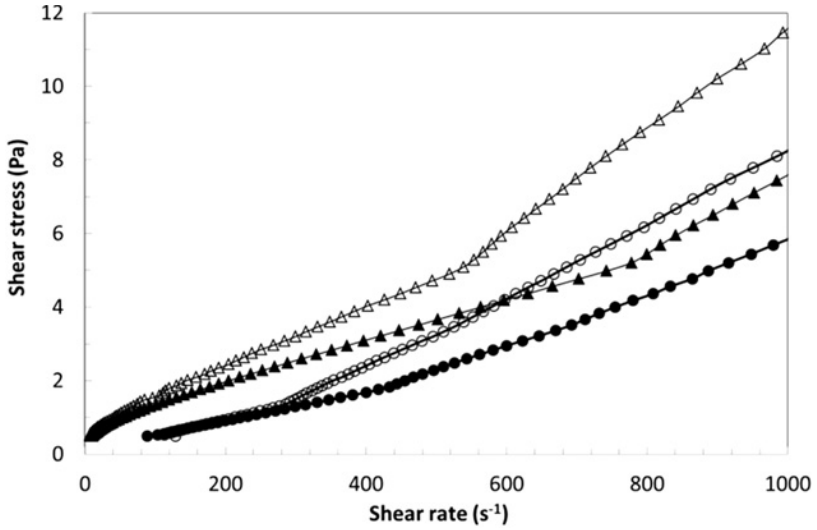

Figure I.20 Comparison between rheograms obtained for two sludge samples (5.93 g L^{-1} and 11.86 g L^{-1} of MLSS concentration) using a rotational rheometer with concentric cylinders (CC) but with different gap size (1 mm and 1.25 mm). Figure from Ratkovich *et al.* (2013).

These results highlight that special attention needs to be paid while performing rheological measurements in order to keep the required laminar conditions. Likewise, they underline the need of an adequate rheometer geometry in order to assure the homogenous distribution of shear in the measurement volume.

Conclusions on sensitivity of sludge rheology results on measurement conditions

- Rheology results are sensitive to temperature, and may diverge with the use of different rheometer geometries. During rheological measurements with activated sludge, it is necessary to keep a constant temperature, to control adequate flow conditions (laminar flow) and to use a suitable rheometer geometry in order to homogenously distribute shear into the measurement volume. Likewise, the rheometer geometry must be adapted to the fluid characteristics such as viscosity, particle size and settleability.

I.3.4.4 Activated sludge properties affecting the rheological behaviour

The viscosity of a suspension depends on the viscosity of the continuous phase, the characteristics of the dispersed phase such as particles shape, size, concentration and interaction between particles as well as on temperature and the exerted shear rate or shear stress (Dupuis, 2008). This is the case for activated sludge; its rheological behaviour results from the impact of multiple constituents that depend not only on the origin of raw wastewater but also on the operating conditions. Several works have tried to identify the link between activated sludge characteristics and its rheological behaviour. The main results found in the literature are analysed in the following paragraphs.

I.3.4.4.1 Solid fraction

For Newtonian fluids with low solids concentration, viscosity (μ) is an increasing function of the volume occupied by the solid fraction, in conformity with the Einstein equation written as follows:

$$\mu = \mu_o(1 + 2.5\emptyset_s) \qquad \text{I.55}$$

with

μ_o fluid viscosity without particles

$\emptyset_s$ solids volumetric fraction

According with this equation, an increment of the solid volume fraction from 0 to 10% implies an increase of 25% in the fluid viscosity fluid. This correlation highlights the importance of the solid fraction on the viscosity of a suspension.

I.3.4.4.1.1 Mixed liquor suspended solids (MLSS)

In activated sludge, several rheology studies have evaluated the impact of the MLSS concentration on the sludge rheological behaviour (Sutapa, 1996; Lotito *et al.,* 1997; Mikkelsen, 2001; Rosenberger *et al.,* 2002; Tixier *et al.,* 2003; Jin *et al.,* 2006; Mori *et al.,* 2006; Seyssiecq *et al.,* 2008; Xia *et al.,* 2009; Yang *et al.,* 2009). It must be highlighted that with the exception of a few studies (Rosenberger *et al.,* 2002; Khongnakorn *et al.,* 2009; Xia *et al.,* 2009) the different MLSS concentrations result from centrifugation, sedimentation or filtration (100 μm) protocols as well as dilution with supernatant. The effect of these procedures on the original sludge nature and the subsequent rheological results is unknown and neglected. However all these

studies have shown an increase of the sludge apparent viscosity as a result of an increment in the MLSS concentration. According to Mikkelsen (2001), with an increment of the solid content, the particle interaction frequency increases rapidly and leads to the formation of a network of particles that opposes to the flow of the suspension. The Figure I.21 represents the results obtained by Yang *et al.* (2009) for the evolution of sludge apparent viscosity with the shear rate for MLSS concentrations comprised between 2.7 and 16.0 g L^{-1}.

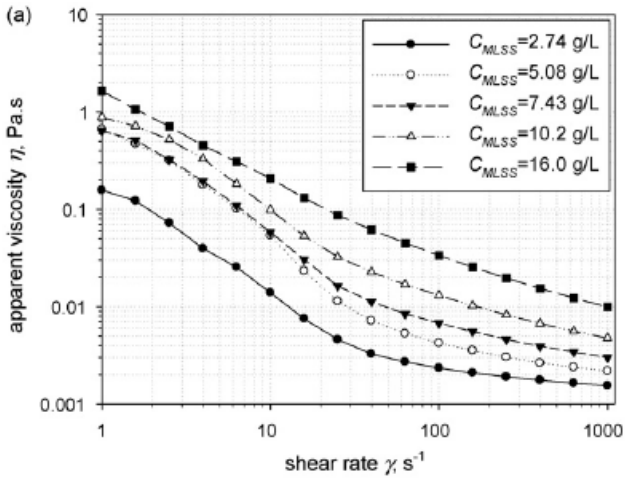

Figure I.21. Sludge apparent viscosity as a function of the shear rate for different MLSS concentrations (between 2.7 and 16.0 g L^{-1}) (log-log scale). Measurements with a rotational rheometer, cone plate geometry. Sludge samples from the same origin and concentrated by settling. Figure from Yang *et al.* (2009).

Tixier *et al.* (2003) conducted rheological measurements varying the MLSS concentration (from 0 to 20 g L^{-1}) for four samples of activated sludge from different WWTPs and investigated the impact of MLSS on the infinite shear rate viscosity (μ_∞), which is the apparent viscosity measured at very high shear rates. The results showed that, the most concentrated sludge did not necessarily exhibit the highest value of limit viscosity (μ_∞). Similar results on apparent viscosity were found Baudez *et al.* (2004) on pasty sewage sludge from different wastewater treatment plants and with solid volume content between 11.0 and 12.6 % (Figure I.22). This suggests that other sludge properties different to MLSS concentration also influence the apparent viscosity and play a role on sludge rheology.

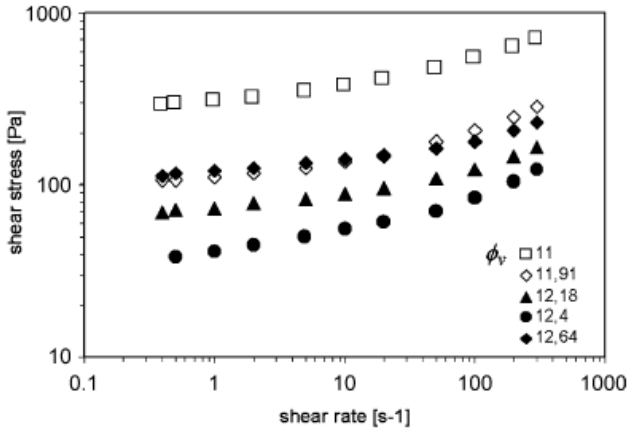

Figure I.22. Rheogram (log-log scale) of pasty sewage sludge from different natures and with solid volume content ($\emptyset_v$) between 11.0 et 12,6%. Measurements with a rotational rheometer and a cylinder concentric geometry. Baudez *et al.* (2004).

I.3.4.4.1.1.1 Correlation between sludge MLSS concentration and rheological parameters

Several authors have evaluated the correlation between the MLSS concentration with the parameters of the rheological shear-thinning models (Table I.5) and viscoplastic models (Table I.6). Most of the data available refers to the Ostwald-de Waele equation and it is thus possible for this model to compare the results between different studies. Figure I.23 illustrates the Ostwald-de Waele rheological parameters (K and n) as a function of the sludge MLSS concentration.

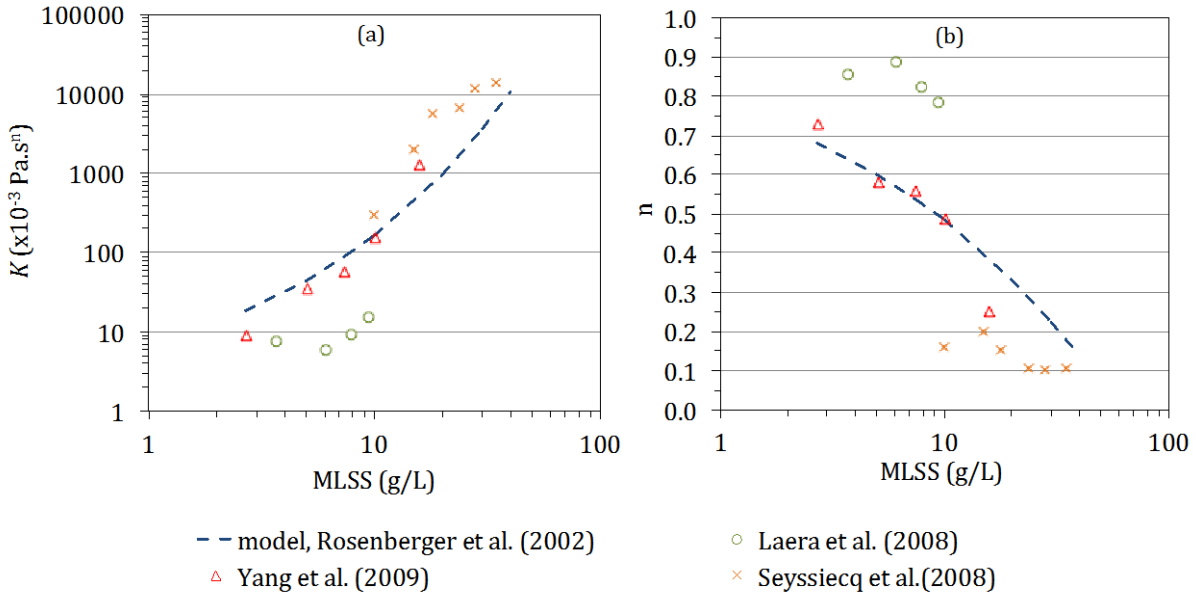

Figure I.23. Ostwald-de Waele rheological parameters as a function of the activated sludge MLSS concentration, obtained by 4 different studies at 20-21°C using different rotational geometries and domestic sludge: (a) consistency index, ***K*** and (b) flow index, ***n***.

Two main general trends can be observed with the increase of the MLSS concentration: an increase of the consistency index (K) and a reduction of the flow index (n). While some data overlap (Rosenberger *et al.,* 2002; Yang *et al.,* 2009), others are more dispersed. Judging only from similar data, the sludge rheological behaviour seems to be strongly defined by the MLSS concentration, regardless of the origin of the sample. However if all data are considered, it seems that the rheological behaviour is also influenced by another activated sludge property related to the origin of the sample. Nevertheless, it should be reminded that some authors have shown that the rheological results can be influenced by the rheometer geometry (cf. I.3.4.3.2). The authors concerned by the comparison presented in Figure I.23, obtained these results using rotational rheometers but with different geometries (CC, HRI, cone plat and DCC; cf. Table I.5). Additionally, it should be noted that the presented data were not obtained within the same range of shear rate and MLSS concentration. It is difficult to establish whether the data scattering observed in Figure I.23 for the various authors, is due to the effect of using distinct geometries, to the different range of shear rate and MLSS concentration in which they were obtained, or to the possibility that MLSS concentration is not the only sludge property characterizing its rheology for activated sludge from different origins.

I.3.4.4.1.2 Effect of the MLSS concentration on the yield stress

Published results on the impact of MLSS on the yield stress (Sutapa, 1996; Forster, 2002; Mori *et al.,* 2007; Khongnakorn *et al.,* 2009; Yang *et al.,* 2009) showed that there is a rapid increase of the yield stress with the suspended solids concentration. This increase is explained by the fact that a higher number of particles present in the suspension require a higher shear stress to disrupt their interaction and to induce flow. Figure I.24 shows the increase of the yield stress with the increase of suspended solids concentration observed in the work of Forster (2002). As previously mentioned, this author states that below a MLSS concentration of 11 g L^{-1}, the yield stress is negligible.

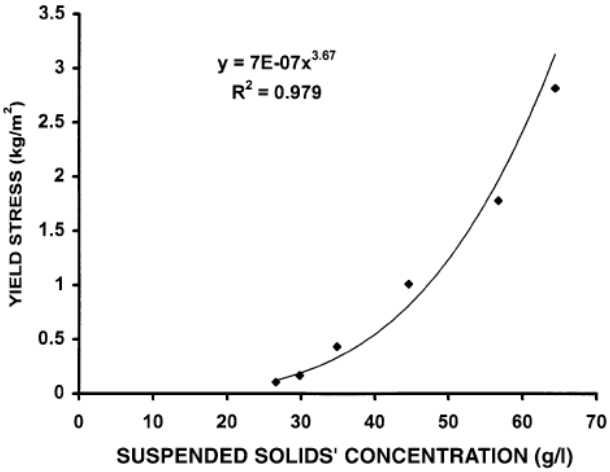

Figure I.24. Yield stress as a function of the MLSS for pasty sewage sludges. Sludge concentrated by centrifugation. Rot*ati*onal rheometer. Forster (2002).

I.3.4.4.2 Extra cellular Polymeric Substances (EPS)

As mentioned in I.2.6.2.1.3 the EPS constitute the major organic fraction of activated sludge. These substances are bound to the biomass in biological flocs and their composition includes proteins, humic acids, polysaccharides, DNA and nucleic acids. They play an important role in the floc structure and contribute to develop a polymeric network through chemical bonds between macromolecular chains (Mikkelsen and Keiding, 2002). Because the EPS partially define the floc structure, some authors have evaluated the impact of these substances on the sludge apparent viscosity.

Rosenberger *et al.* (2002), studied the influence of bound EPS (proteins and polysaccharides, extraction with an ion exchange resin) on the rheology of activated sludge from 9 different MBR (including domestic and industrial sludge). The authors observed that industrial activated sludge had, in average, higher ratio of EPS content to MLVSS content than domestic sludge (*ca.* 145 mg EPS/g MVLSS versus *ca.* 60 mg EPS/g MVLSS respectively). According to these authors, this difference in the EPS content would explain why for a given shear rate and MLSS concentration, the apparent viscosity of industrial sludge was generally higher than the one measured for domestic sludge.

Besides, Mori *et al.* (2007) has assessed the impact of bound EPS on the rheology of pasty sludge with a MLSS concentration of 43 g L^{-1}. The activated sludge was subjected to a period of starvation of 4 days. Before and after this period the ratio of bound EPS content to MLSS content was measured (bound EPS extraction by sonication) and the sludge rheological behaviour was studied. After four days, the ratio of bound EPS/MLSS (mg L^{-1}) was divided by two (bound EPS

released during starvation) and the apparent viscosity decreased (τ_y and K were reduced while n was increased). To explain these results, the authors hypothesized that a reduction of the EPS content induced a reduction of the cohesion forces in the flocs and consequently the structure of the suspension is less rigid and less viscous. It should be noted that in this study, the evolution of the rheological behaviour with the EPS concentration was observed only in two different conditions (before and after the starving period), which is not sufficient to state a conclusive trend between EPS and sludge rheological behaviour.

However, the observations made by these two mentioned studies coincide in affirming that the EPS content has an increasing effect on apparent viscosity.

I.3.4.4.3 Cations

The impact of added cations on sludge rheology was evaluated by Forster (1982). This author measured the apparent viscosity (320 s^{-1}) of several activated sludge samples with different NaCl concentrations (from 0 to 24 g L^{-1}) and the MLSS concentration was kept constant. The results of this study showed that the sludge apparent viscosity decreased and seemed to reach a limit value when the salinity (ionic strength) of the sludge increases. The same author (Forster, 1983) also added copper, zinc and calcium ions (up to 50 mg M^{2+} L^{-1}) to the sludge samples in order to evaluate the impact of other cations on the activated sludge apparent viscosity. He observed a decrease in the sludge apparent viscosity (320 s^{-1}) with the addition of the metal ions to the activated sludge samples.

A similar influence of cations on apparent viscosity was found in the work of Tixier (2003) who added NaCl and $CaCl_2$ (from 0 up to 10 and 20 g L^{-1} respectively) on three activated sludge samples from different wastewater treatment plants and with MLSS concentration of 10 g L^{-1}. Likewise, Dieudé-Fauvel *et al.* (2009) observed that adding KCl (from 0 up to 22% of dry matter) to pasty sludge, led to a reduction of apparent viscosity.

According to these studies, the added cations modify the structure of polymers at the floc surface and lead to the reduction of the sludge viscosity. The phenomenon explanation is given as follows: an increase in the ionic strength modifies the thickness of the double electric layer of sludge aggregates and consequently the biological flocs become more compact and their cross sectional area exposed to the fluid decreases which ends up facilitating the sludge flow and reducing the sludge viscosity.

I.3.4.4.4 Soluble organic matter

Khongnakorn *et al.* (2009) studied the influence of the soluble organic matter, measured as soluble COD (chemical oxygen demand), on the sludge rheology. Activated sludge samples were taken from a 50 L pilot MBR in which the MLSS concentration was stabilized around 6.2 g L^{-1} by means of continuous sludge extraction. The soluble COD evolved from about 500 to 1000 mg L^{-1} thanks to an increase of the feeding synthetic substrate. The experimental rheograms were modeled with the Herschel-Bulkley equation. It was observed that an increase in the soluble COD concentration produces an increase of the apparent viscosity (μ_{app}), the yield stress (τ_y) and the consistency index (K) as well as to a decrease in flow index (n) (Table I.6).

To explain these results the authors argued that the measurement of soluble COD accounts for soluble EPS that are likely to create linkages between the flocs, thus rigidifying the sludge structure.

I.3.4.4.5 Solids Retention Time (SRT)

The impact of the solids residence time on the sludge rheology was studied by Laera *et al.* (2007). The authors conducted rheological tests on sludge samples taken from a pilot membrane bioreactor (6L) at sludge age from 20 to complete retention time (~1200 days) and MLSS concentrations between 3.7 and 22.9 g L^{-1} respectively. The experimental rheograms were modelled with the Ostwald and Bingham equations (Table I.5 and Table I.6). The rheological parameters of these models seemed to follow two different tendencies with the increase of the MLSS concentrations and the SRT. First, from 20 to 40 days, the sludge apparent viscosity decreased and the non-Newtonian character was reduced despite an increase of the MLSS concentration from 3.7 to 6.1 g L^{-1}. Subsequently, from 60 to 1200 days, the apparent viscosity increased and the shear-thinning behaviour was accentuated simultaneously with the increase of the MLSS concentration from 7.9 to 22.9 g L^{-1}.

To explain this double trend, the authors argued that under 40 days, soluble and colloidal substances accumulated in the bioreactor and the observed rheological behaviour results from the influence of both the suspended solids concentration and the highly concentrated soluble substances, the latter leading to the reduction of sludge apparent viscosity. Subsequently, for SRT above 60 days, the biomass concentration increases and because of substrate biocompetition the soluble substances are significantly reduced. Then, the rheological behaviour would be mainly defined by the concentration of suspended solids.

Although soluble and colloidal substances were not characterized in this study, these results suggest that the SRT, associated to the presence of soluble matter and colloids, participates in the definition of the sludge rheological behaviour.

Conclusions on the effect of activated sludge properties on its rheological behaviour

- For activated sludge from the same origin, the rheological behaviour seems to be mainly determined by the MLSS concentration, regardless of the implemented protocol to obtain the different suspended solids concentrations (settling, filtration, dilution, etc). An increase in the MLSS concentration leads to an augmentation of apparent viscosity and yield stress.

- For activated sludge from different origins, results are not conclusive and the rheological behaviour may not only be determined by the MLSS concentration, but other sludge properties associated to the sludge origin may also have an influence on it.

- Results from some studies have shown that for a given MLSS concentration, a higher content of bound EPS, or higher soluble DCO in activated sludge has an increasing effect on the apparent viscosity. Besides, other studies have observed that higher cations concentrations or higher solids retention time (associated to lower soluble DCO concentrations) have a reducing effect on apparent viscosity.

- The effect of mixed liquor volatile suspended solids on the sludge rheology is not specified in the literature since it is evident that this characteristic related to the MLSS concentration is also correlated to the sludge rheology. However, since the volume occupied by the solid fraction seems to have a significant effect on viscosity (Equation I.55) and because the MVLSS concentration appears to have a close correlation with the volume occupied by the biological flocs (HFV, Henkel, 2010), it would be of interest to study the influence of the MLVSS concentration (as well as HFV) on the activated sludge rheological behaviour.
- In the context of activated sludge, no studies have been published concerning the influence of this parameter on rheology. However, since the floc size is related to the volume occupied by the solid fraction, it can be supposed that this sludge characteristic influence the sludge viscosity and it would be of interest to study the effect of floc size on the rheology of activated sludge.

I.3.5 Shear rate in aerated bioreactors

Because activated sludge is a non-Newtonian fluid, its viscosity depends on the exerted shear stress or shear rate. In bioreactors, suspensions are sheared by the swarm of rising fine bubbles and/or by the stirring system. However, the measurement of local shear rate is complex because it is based on the fluid velocity profile throughout the bioreactor (Shi *et al.*, 1990). Several works have established empirical and theoretical correlations to estimate the average shear rate ($\dot{\gamma}_{av}$) in bioreactors with Newtonian and non-Newtonian fluids (Table I.8). In all correlations the average shear rate is an increasing function of the superficial gas velocity (U_G).

Nishikawa *et al.* (1977) proposed an equation deduced from experimental measurements of heat transfer. Since the oxygen transfer takes place through the bubbles interfacial area, some authors deduced a correlation from the measurements of the oxygen transfer coefficient (Henzler, 1980; Schumpe and Deckwer, 1987).

Kawase and Kumagai (1991) and Sanchez Pérez *et al.* (2006) followed a theoretical approach based on the concept of the aeration specific power input and proposed a correlation in which the shear rate depends on the fluid rheological properties (expressed as the Ostwald parameters, K and n).

More recently, Cerri *et al.* (2008) and Thomasi *et al.* (2010) followed the oxygen transfer approach and included also the Ostwald rheological parameters. However this correlation is not applicable for Newtonian fluids (n=1).

For the airlift reactors, the proposed correlations (Chisti and Moo-Young, 1989; Al-Masry, 1999; Shi *et al.*, 1990) may also include geometry factors such as the ratio of the riser section to the downcomer section (A_R/A_D) and of the liquid height (h).

Table I.8. Literature correlations to estimate the average shear rate ($\dot{\gamma}_{av}$) in aerated reactors.

Author	Correlation	Range of superficial gas velocity	Reactor type	Fluid type	Model type
Nishikawa *et al.* (1977)	$\dot{\gamma}_{av} = 5000 U_G$	0.04 <U_G< 0.1 m s^{-1}	BC	N, NN	E
Henzler (1980)	$\dot{\gamma}_{av} = 1500 U_G$	0.040 <U_G< 0.1 m s^{-1} 0.38 <n< 0.82	BC	N, NN	E
Schumpe and Deckwer (1987)	$\dot{\gamma}_{av} = 2800 U_G$	0.02 <U_G< 0.2 m s^{-1}	BC	N, NN	E
Chisti and Moo-Young (1989)	$\dot{\gamma}_{av} = 5000 \left(1 + \frac{A_D}{A_R}\right) U_{GR}$		AL	N, NN	E
Shi *et al*, (1990)	$\dot{\gamma}_{av} = 14800 {U_{GR}}^2 - 351 U_{GR} + 3.26$		AL	N, NN	E
Al-Masry (1999)	$\dot{\gamma}_{av} = 3.36(1 - U_{GR})^{-32.56} \left(1 + \frac{A_D}{A_R}\right)^{0.89} h^{0.44}$	0.0018<U_G<0.07 m s-1 0.11<A_D/A_R<1 1.4<h<6 m	AL		E
Kawase and Kumagai (1991)	$\dot{\gamma}_{av} = (10.3 n^{-0.63})^{1/(n+1)} \left(\frac{U_G \rho_L g}{K}\right)^{1/(n+1)}$		BC	NN	E, T
Henzler and Kauling (1985); Sanchez Pérez *et al.* (2006)	$\dot{\gamma}_{av} = \left(\frac{U_G \rho_L g}{K}\right)^{1/(n+1)}$		BC		T
Cerri *et al.* (2008)	$\dot{\gamma}_{av} = \left(1.641 \times 10^{-3} {U_{GR}}^{-0.386} K^{-0.213}\right)^{1/(n-1)}$	U_{GR}<0.05 m s^{-1}	AL AL	NN	E
	$\dot{\gamma}_{av} = \left(4.495 \times 10^{-2} {U_{GR}}^{0.743} K^{-0.288}\right)^{1/(n-1)}$	U_{GR}>0.05 m s^{-1}			E
Thomasi *et al.* (2010)	$\dot{\gamma}_{av} = \left(7.38 \times 10^{-3} {U_G}^{0.11} K^{-0.389}\right)^{1/(n-1)}$		BC	NN	E

U_{GR} : Superficial gas velocity in the riser section; A_R : riser section ; A_D: downcomer section; h: liquid height, K and n: Ostwald rheological parameters; ρ_L: liquid density. BC: bubble column; AL: Airlift reactor. N: Newtonian Fluid; NN: Non-Newtonian Fluid. T: theoretical Equation; E: Empirical equation.

Using some of the Equations presented in Table I.8, an estimation of the average shear rate at different superficial gas velocities is shown in Figure I.25 for clean water and for an activated sludge at MLSS concentration of 5.0 g L^{-1}. Superficial gas velocities values correspond to the range of applied gas flow rates in aeration basins according to Gillot *et al.* (2005). To consider activated sludge rheology, the Ostwald-de Waele rheological parameters proposed by Yang *et al.* (2009) are used.

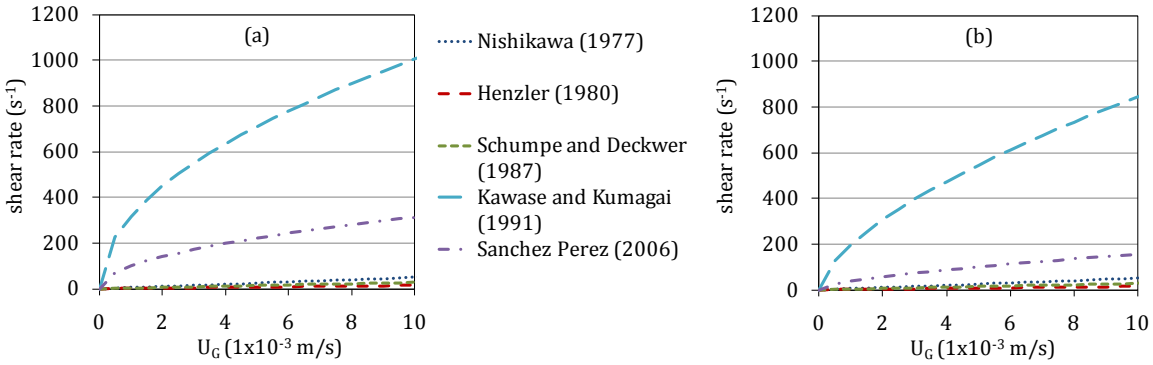

Figure I.25. Estimated average shear rate ($\dot{\gamma}_{av}$) as a function of the superficial gas velocity (U_G) in a bubble column according to some correlations available in the literature in two different aerated media: (a) clean water (**K**=0.001 Pa.s^n, **n**=1) and (b) activated sludge with Ostwald rheological parameters obtained from Yang *et al.* (2009) (**K**=0.034 Pa.s^n, **n**=0.579, MLSS=5.1 g L^{-1}).

As some of the proposed correlations do not consider the fluid viscosity or rheological behaviour, they lead to the estimation of the same average shear rate in water and in activated sludge. For the equations that consider the fluid rheology, the estimated average shear decreases with the increase of viscosity. A significant dispersion is however observed between the estimated shear rate values for a given superficial gas velocity, the values obtained with the equation of Kawase and Kumagai (1991) being particularly isolated.

Conclusions on the estimated shear rate

- Since activated sludge is a non-Newtonian fluid, determining its apparent viscosity in a bioreactor requires the estimation of the average shear rate prevailing in the dispersion. Several empirical and theoretical correlations are available to determine the shear rate. For the simplest equations, it is basically an increasing function of the superficial gas velocity. Other equations include geometrical aspects and some others integrate the fluid rheological behaviour (in the form of the Ostwald-de Waele parameters). For activated sludge with a MLSS concentration of 5.0 g L^{-1}, and in a range of superficial gas velocities up to 10x10^{-3} m s^{-1} the proposed correlations let estimate in a bubble column a range of shear rate between approximately 0 and 1000 s^{-1}.

I.4 Conclusions on the literature review and work positioning

The effect of the MLSS concentration on activated sludge has been widely studied and identified as the main property related to the oxygen transfer depletion in activated sludge in comparison to clean water. However a significant dispersion is observed between the different published results and consequently the MLSS concentration is not sufficient to explain the variability of observed oxygen transfer results in the presence of activated sludge.

Sludge apparent viscosity, floc volume (HFV) and solids retention time (SRT) are suggested to be also associated to the oxygen transfer depletion and some correlations are proposed in order to describe their influence on oxygen transfer. However the proposed correlations in literature do not consider the impact of the activated sludge rheological behaviour on oxygen transfer, thus the effects of activated sludge on the hydrodynamic conditions and the bubble regime are overlooked. In that context, the main purpose of this work is to evaluate the impact of the sludge rheological behaviour and other physicochemical properties on oxygen transfer.

To that aim, an initial objective consists in studying and modelling the activated sludge rheological behaviour and its dependence on sludge properties. Since the rheological models proposed in the literature are not convergent, samples from different wastewater treatment plants will be considered in order to determine if the sludge rheology is only defined by the MLSS concentration or if it also influenced by other more intrinsic sludge characteristics, such as soluble DCO, salts, floc volume and floc size. The performance of the rheological measurements requires the use of a rheometer geometry adapted to the activated sludge characteristics (viscosity, settleability and particle size). Likewise a dedicated experimental protocol needs to be implemented in order to obtain valid rheological measurements.

Subsequently, a second objective consists in assessing the impact of sludge properties on oxygen transfer by means of oxygen transfer tests in clean water and in the presence of activated sludge. Similarly to the rheology study, considering activated sludge from different origins will help to elucidate the role played by MLSS concentration and sludge properties on oxygen transfer. The determination of gas phase characteristics such as bubble size and gas hold-up will contribute to analysis and comprehend the effect of sludge properties on bubble regime.

Finally a third objective consists in correlating the oxygen transfer results to the sludge rheological behaviour. Previously, it will be necessary to estimate the shear rate prevailing in the aerated bioreactor associated to the hydrodynamic conditions.

Chapter II. Materials and Methods

II.1 Oxygen transfer in clean water and with activated sludge

II.1.1 Experimental setup: Bubble column and aeration system

The oxygen transfer measurements were performed in a cylindrical column of 4.5 m height and 0.29 m diameter made of PMMA. A schematic of the bubble column is shown in Figure II.1.

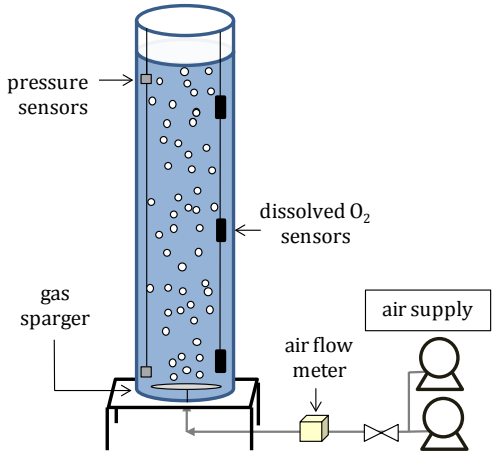

Figure II.1. Schematic of the bubble column used to measure the oxygen transfer in clean water and with activated sludge.

The liquid phase was aerated by means of two rotary vane compressors (BUSCH) supplying air through a gas diffuser installed at the bottom of the column. Two types of diffusers were used:

- Fine bubble diffuser: a flexible fine perforated EPDM membrane with pore sizes of 0.7×10^{-3} m (Figure II.2). The perforated surface is 345.8 cm^2 and the pore density is 20 pores per cm^2.

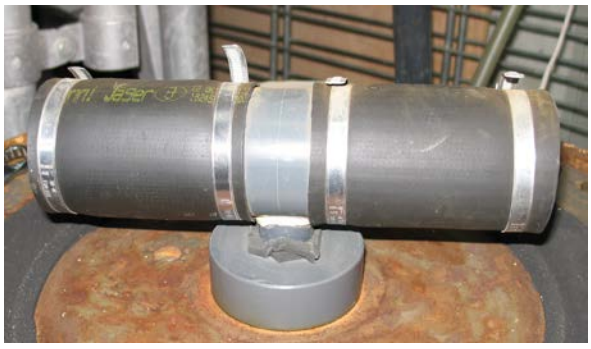

Figure II.2 Fine bubble diffuser used in the oxygen transfer tests

- Coarse bubble diffuser: a PVC elbow with an orifice of 4 mm in diameter (Figure II.3).

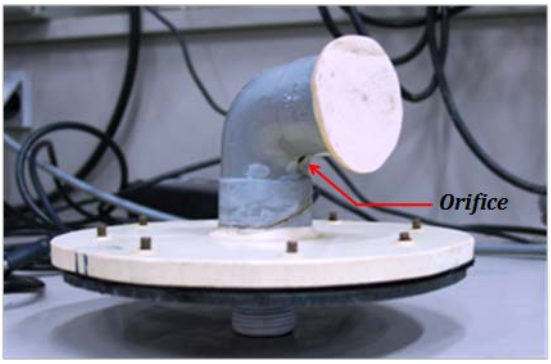

Figure II.3 Coarse bubble diffuser used in the oxygen transfer tests

The injected airflow rate was measured using a volumetric gas meter (Dresser) and a chronometer. Airflow rate measurements consisted of counting up the air volume passing through the gas meter during three minutes. The airflow temperature and pressure were measured using a thermometer and a manometer (KIMO) adapted to the air line. The gas flow rate ($Q_{T,P}$) measured at a given temperature (T) and pressure (P), was reported at normal conditions of temperature and pressure (T_o=0°C and P_o=1013 hPa) using the following equation:

$$Q_{To,Po} = Q_{T,P} \frac{T_o}{T} \frac{P}{P_o} \qquad \text{II.1}$$

where $Q_{To,Po}$ is the air flow rate at standard conditions.

The airflow rate ($Q_{To,Po}$) ranged between 0.13×10^{-3} and 0.36×10^{-3} m^3 s^{-1}. The superficial air velocity (U_G), the ratio of the air flow rate to the column cross-sectional area, ranged between 1.9×10^{-3} and 5.5×10^{-3} m s^{-1} which is an interval of superficial gas velocities found in full scale aeration tanks (Gillot *et al.,* 2005).

II.1.2 Measurements of oxygen transfer coefficient in clean water (k_La)

II.1.2.1 Reoxygenation method - Principles

Oxygen transfer measurements in clean water were performed according to the standard **reoxygenation** method (NF-EN-12255-15, 2004). This method consists of following under stable flow conditions the time evolution of the dissolved oxygen concentration in the liquid media, as it increases from an initial low concentration close to zero up to the saturation concentration.

The time evolution of the dissolved oxygen concentration in the bubble column, considered as a completely mixed reactor, is written according to the 1st Fick's law as follows:

$$\frac{dC}{dt} = k_L a(Cs - C) \qquad \text{II.2}$$

where

t time (h)

C dissolved oxygen concentration at instant t (mg L^{-1})

Cs dissolved oxygen saturation concentration during the aeration test (mg L^{-1})

k_La volumetric oxygen transfer coefficient at the test conditions of temperature and pressure (h^{-1})

The integrated form of Equation II.2 is written as follows:

$$C(t) = \mathrm{Cs} - (\mathrm{Cs} - Co) \cdot e^{-k_L \mathrm{a} \cdot t} \qquad \text{II.3}$$

where,

Co dissolved oxygen concentration at instant t=0 (mg L^{-1})

II.1.2.2 Measurement protocol

The reoxygenation tests were carried out in an experimental hall. The column was first filled with tap water up to a height of 4.42 m above the gas diffuser (fine or coarse bubble). Air was then injected into the column at a constant superficial gas velocity within the specified range during at least 90 minutes in order to obtain the dissolved oxygen saturation concentration. The dissolved oxygen concentration in the liquid media was measured using three stirred electrochemical sensors (YSI) submerged at three different heights in the aerated volume (Figure II.1). These oxygen probes were previously calibrated by following two main steps: (i) adjusting the probes zero concentration value by submerging them in a sodium sulfite concentrated solution and (ii) adjusting the probes saturation concentration value by submerging them in a two-hours previously aerated and stirred tap water volume (50L) at a given liquid temperature and atmospheric pressure.

The temperature and conductivity of the liquid media were measured using a sensor (WTW) submerged at middle height in the column. The dissolved oxygen concentrations, the liquid temperature and conductivity were recorded on a time step of five seconds using a data acquisition system (Yokogawa).

When the dissolved oxygen saturation concentration was reached, the clean water dissolved oxygen concentration was reduced to zero by adding 150 mg of sodium sulfite (Na_2SO_3) and 3 mg of cobalt chloride ($CoCl_2$) per liter. The sodium sulfite reacts with the dissolved oxygen according to:

$$Na_2SO_3 + \frac{1}{2}O_2 \xrightarrow{CoCl_2} Na_2SO_4$$

Figure II.4 illustrates an example of the variation of the dissolved oxygen concentration for the three oxygen probes during a reoxygenation test in the bubble column.

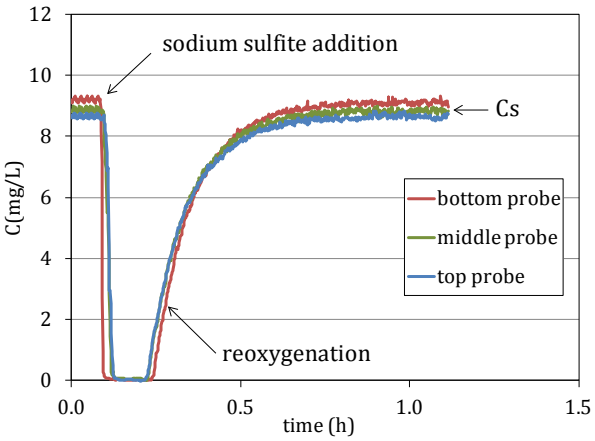

Figure II.4. Dissolved oxygen concentration during a reoxygenation test in the bubble column for the three submerged oxygen probes.

$k_L a$, Cs and Co were estimated by adjusting the model in Equation II.3 to the experimental data using the nonlinear least squares method.

For a given reoxygenation test, the oxygen transfer coefficient ($k_L a$) is the arithmetic average value calculated for the three submerged oxygen probes. The precision of the reoxygenation method is estimated to be 4% (Duchène, 1995).

The volumetric oxygen transfer coefficients measured at the temperature T ($k_L a_T$), are converted to 20°C ($k_L a_{20}$) using the following temperature correction (ASCE, 1996):

$$k_L a_{20} = k_L a_T \cdot \theta^{(20-T)} \text{ with } \theta = 1.024 \qquad \text{II.4}$$

II.1.3 Measurements of oxygen transfer coefficient in activated sludge ($k_L a'$)

II.1.3.1 Off-Gas method - Principles

In activated sludge, the oxygen transfer coefficient was measured according to the **off-gas method** (Redmon *et al.,* 1983; Capela *et al.,* 2004). In this method the mass of transferred oxygen is measured by means of a gas-phase mass balance over the aerated volume and the measurement of the oxygen transfer efficiency (OTE_c).

The mass flow of transferred oxygen is expressed as follows (Figure II.5):

$$F_{O_{2(g)inlet}} - F_{O_{2(g)outlet}} = F_{O_{2(g)transferred}} \quad \text{II.5}$$

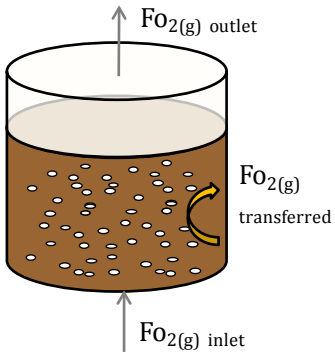

Figure II.5. Schematic of the gas-phase mass balance in the aerated volume

The development of the terms in Equation II.5 gives:

$$Q_i \rho_i y_i - Q_e \rho_e y_e = k_L a'(Cs' - C)V \quad \text{II.6}$$

with

Q_i inlet air flow rate ($m^3\ h^{-1}$)

ρ_i air density at the inlet air flow ($kg\ m^{-3}$)

y_i oxygen volume fraction at the inlet air flow (-)

Q_e outlet air flow rate ($m^3\ h^{-1}$)

ρ_e air density at the outlet air flow ($kg\ m^{-3}$)

y_e oxygen volume fraction at the outlet air flow (-)

$k_L a'$ oxygen transfer coefficient in activated sludge (h^{-1})

Cs' dissolved oxygen saturation concentration in activated sludge ($kg\ m^{-3}$)

C dissolved oxygen concentration in activated sludge ($kg\ m^{-3}$)

V aerated volume (m^3)

The oxygen transfer efficiency at the test conditions (OTE_c) is defined as the ratio of the mass flow of transferred oxygen to the mass flow of injected oxygen:

$$OTE_c = \frac{F_{O_{2(g)inlet}} - F_{O_{2(g)outlet}}}{F_{O_{2(g)\ inlet}}} \quad \text{II.7}$$

The oxygen transfer efficiency (OTE_c) can be expressed in terms of the molar fractions of the different gases contained in the air flow assuming that the inert gases (such as N_2, Ar, Ne, He) do not affect the oxygen transfer and that denitrification is negligible (ASCE, 1996):

$$OTE_c = \frac{\frac{y_i}{1-y_i+y_{CO2,i}+y_{w,i}} - \frac{y_e}{1-y_e+y_{CO2,e}+y_{w,e}}}{\frac{y_i}{1-y_i+y_{CO2,i}+y_{w,i}}} \quad \text{II.8}$$

where

OTE_c oxygen transfer efficiency at the test conditions of temperature T and pressure P (-).

y_i oxygen molar fraction at the inlet air flow (-).

y_e oxygen molar fraction at the outlet air flow (-).

$y_{CO2,i}$ carbon dioxide molar fraction at the inlet air flow (-).

$y_{CO2,e}$ carbon dioxide molar fraction at the outlet air flow (-).

$y_{w,i}$ water vapor molar fraction at the inlet air flow (-).

$y_{w,e}$ water vapor molar fraction at the outlet air flow (-).

The measurement of the oxygen transfer efficiency (OTE_c) is simplified if the water vapor and carbon dioxide are removed from the analysed gas, through an absorption device. The *OTEc* can be expressed as follows:

$$OTE_c = 1 - \frac{y_e'(1-y_i')}{y_i'(1-y_e')} \quad \text{II.9}$$

where

y_i' oxygen molar fraction at the inlet air flow free of water vapor and carbon dioxide (-).

y_e' oxygen molar fraction at the outlet air flow free of water vapor and carbon dioxide (-).

The oxygen transfer efficiency at standard conditions (20°C, 1013 hPa) is written as follows:

$$SOTE_c = OTE_c \cdot \theta^{(20-T)} \frac{Cs', s}{(Cs' - C)} \quad \text{II.10}$$

where

$SOTE_c$ standard oxygen transfer efficiency (-)

θ temperature correction coefficient ($\theta = 1.024$)

Cs', s dissolved oxygen saturation concentration in activated sludge at standard conditions (20°C, 1013 hPa , and hydrostatic overpressure ΔP) (mg L^{-1})

Cs' dissolved oxygen saturation concentration in activated sludge at measurement conditions (liquid temperature T, atmospheric pressure P and hydrostatic overpressure ΔP) (mg L^{-1})

C dissolved oxygen concentration in activated sludge at measurement conditions (mg L^{-1})

The standard oxygen transfer coefficient in activated sludge at 20°C ($k_L a'_{20}$) is deduced from the measured oxygen transfer efficient at standard conditions ($SOTE_c$) and the oxygen mass flow in the supplied air flow ($FO_{2(g)inlet}$).

$$k_L a'_{20} = \frac{SOTE_c \cdot FO_{2(g)inlet}}{Cs's \cdot V} = \frac{SOTE_c \cdot Q_i \rho_{air} y_i}{Cs's \cdot V} \quad \text{II.11}$$

with

$k_L a'_{20}$ oxygen transfer coefficient in activated sludge at 20°C (h^{-1})

$SOTE_c$ standard oxygen transfer efficiency at the standard conditions (20°C, 1013 hPa) (-)

Q_i inlet air flow rate ($m^3\ h^{-1}$)

ρ_i air density at the inlet air flow ($kg\ m^{-3}$)

y_i oxygen molar fraction at the inlet air flow (y_i=0.2095)

Cs', s dissolved oxygen saturation concentration in activated sludge at measurement conditions (liquid temperature T, atmospheric pressure P and hydrostatic overpressure ΔP) (kg m^{-3})

V aerated volume (m^3)

It is recommended to perform the oxygen transfer measurements at dissolved oxygen concentrations 0.5 times lower than the Cs' concentration in order to reduce the experimental error. A dissolved oxygen concentration higher than 1 mg L^{-1} is also advised in order to consider that denitrification is negligible.

II.1.3.2 Experimental setup for oxygen transfer measurements with activated sludge

Oxygen transfer measurements with activated sludge were performed on site. The bubble column was installed in the wastewater treatment plants of two different municipalities located in Ile de France: Marolles/Saint Vrain (conventional activated sludge plant, later called CAS) and Briis-sous-Forges (membrane bioreactor, later called MBR). These facilities are designed to treat the domestic effluents of 22 000 and 17 000 population equivalents (PE), respectively and are operated under extended aeration, food to mass ratio (F/M) < 0.1 kg BOD5 (kg VSS)-1 d-1). The influent load of these wastewater treatment plants during the measurement period (2012 and 2013) is presented in Table II.1. Some of the design characteristics as well as the removal efficiency of these two plants are presented in APPENDIX 1.

Table II.1. Average influent load in the wastewater treatment plants where the oxygen transfer tests were performed with activated sludge in the bubble column.

Influent Load	Units	**CAS** Saint Vrain (2012)	**MBR** Briis-sous-Forges (2013)
Flow rate	m^3/d	2853	2870
Mixed liquor suspended solids (MLSS)	kg/d	793	617
Biochemical oxygen demand (BOD)	kg/d	564	455
Chemical oxygen demand (COD)	kg/d	1490	1175
Total Kjehdal nitrogen TKN	kg/d	165	142.3
Total Phosporus (TP)	kg/d	18	17.5

CAS: Conventional activated sludge; MBR: Membrane bioreactor

Activated sludge was continuously pumped out either from the aeration tank, the sludge recirculation loop or the membrane reactor, using a helical rotor pump (Seepex) and fed into the

column at its bottom (see Figure II.6). The open reactor configuration in respect to the gas and also to the liquid phase, was implemented in order to maintain relatively constant characteristics of the mixed liquor during oxygen transfer measurements. The liquid flow rate was measured at the outlet of the column using a scale and a chronometer. The superficial liquid velocity (U_L) in the column was maintained low and constant for a given aeration test and ranged between 2.7×10^{-3} and 4.5×10^{-3} m s^{-1}. The superficial gas velocity varied in the range previously specified in II.1.1. At a height of 4.42 m above the diffuser, the sludge flow left the column by overflow.

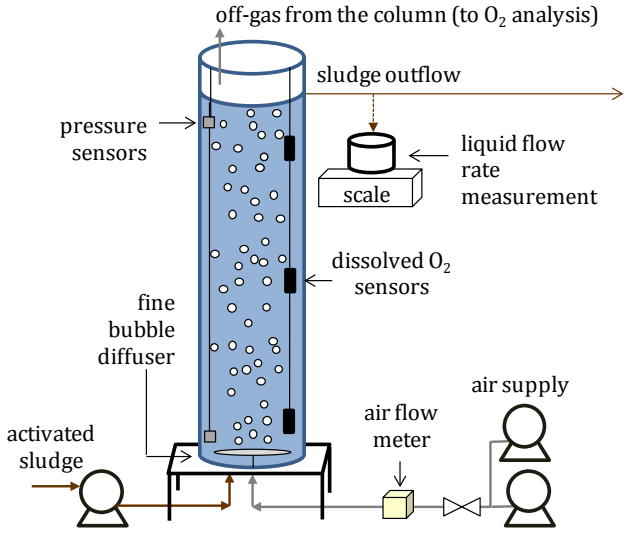

Figure II.6. Schematic of the bubble column installed on site for the oxygen transfer measurements in activated sludge.

Similarly to the oxygen transfer measurements in clean water, the dissolved oxygen concentration in activated sludge was measured using three stirred electrochemical sensors (YSI) previously calibrated and submerged at three different heights in the aerated volume. The temperature and conductivity of the mixed liquor were also measured using a sensor (WTW) submerged at middle height in the column.

II.1.3.2.1 Gas-phase oxygen analysis - OTE_C measurement

The measurement of the oxygen transfer efficiency at the test conditions (OTE_c) is made through the use of a gas-phase oxygen analyser. Oxygen partial pressure is measured in the ambient air (the injected air) and in the off-gas exiting the liquid surface of the column. A plastic

bucket is placed upside down on the liquid surface in order to confine the off-gas on the top of the column and avoid a mixture of the off-gas with the ambient air. Both the confined off-gas and the ambient air are drawn into an oxygen analyser by means of a diaphragm vacuum pump (Cole Parmer).

II.1.3.2.1.1 Gas-phase oxygen analysis instrument

In the gas-phase oxygen analysis unit, the oxygen partial pressure of ambient air and off-gas stream is measured with an electrochemical gas-phase oxygen sensor (Teledyne Analytical Instruments – Class E2). The analyser response for an oxygen flow is a voltage output proportional to the oxygen partial pressure (and concentration), respectively noted I_i and I_e. With a constant air flow pressure in the measurement unit, the oxygen transfer efficiency at the test conditions (OTE_c) can be estimated using the following equation :

$$OTE_c = \frac{I_i - I_e}{I_e - y_i' I_e} \qquad \text{II.12}$$

where

I_i sensor response for the ambient (injected) air flow (mV)

I_e sensor response for the off-gas air flow (mV)

y_i' oxygen molar fraction of the injected air flow free of water vapor and carbon dioxide (y_i'=0.2095)

More specific details of the protocol concerning the OTE_C measurement with the gas-phase analyser instrument are described in **APPENDIX 2**.

II.1.3.2.2 Dissolved oxygen saturation concentration in activated sludge

The dissolved oxygen saturation concentration at the test conditions (Cs') of liquid temperature (T), ambient pressure (P) and hydrostatic overpressure (ΔP) is estimated from the dissolved oxygen saturation concentration at the same test conditions in clean water (Cs) according to:

$$Cs' = \beta \cdot Cs \qquad \text{II.13}$$

Where β is the saturation concentration correction factor (β = 0.99 for domestic wastewater, ASCE, 1996) as previously mentioned in I.2.6.1.

In clean water the dissolved oxygen saturation concentration at the test conditions of liquid temperature (T), ambient pressure (P) and hydrostatic overpressure (ΔP) is deduced from the dissolved oxygen concentration at standard conditions and hydrostatic overpressure (Cs, s) according to the following relation:

$$Cs = Cs_{(P+\Delta P,T)} = Cs, s \cdot \left(\frac{Cs, s_{(P^o,T)}}{Cs, s_{(P^o,T^o)}}\right) \cdot \left(\frac{P}{P^o}\right) \qquad \text{II.14}$$

where

$Cs_{(P+\Delta P,T)}$ dissolved oxygen saturation concentration in clean water at measurement conditions (liquid temperature T, atmospheric pressure P and hydrostatic overpressure (ΔP) (mg L^{-1})

Cs, s dissolved oxygen saturation concentration in clean water at standard conditions 20°C, 1013 hPa , and hydrostatic overpressure (ΔP) (mg L^{-1})

$Cs, s_{(P^o,T)}$ dissolved oxygen saturation concentration in clean water at standard conditions of ambient pressure (P^o=1013 hPa) and test conditions of liquid temperature (T) (mg L^{-1})

$Cs, s_{(P^o,T^o)}$ dissolved oxygen saturation concentration in clean water at standard conditions (20°C, 1013 hPa) (mg L^{-1})

II.1.3.3 Off-gas measurement protocol

Once the bubble column was filled with activated sludge, the superficial gas and liquid velocities were fixed and measurements started under steady state conditions. Dissolved oxygen concentration, liquid temperature as well as the gas-phase oxygen partial pressure were measured and registered continuously with a time step of five seconds using a data acquisition system (Yokogawa). During measurements, the oxygen content in the off-gas stream and the ambient air is analysed sequentially during three minutes and three replicates are made for each flow conditions. The oxygen transfer experiments were performed at different superficial gas velocities, using alternatively the two gas diffusers and for different sludge sampling points

(aeration basin, recirculation loop, membrane reactor) in order to use the full range of MLSS concentration available on each site.

II.1.3.4 Validation of the off-gas method with the reoxygenation method in clean water

In order to validate the off-gas protocol and results, it was decided to perform oxygen transfer tests in the bubble column using clean water and to compare the results with those obtained with the reoxygenation method. The Figure II.7 illustrates the experimental evolutions of oxygen transfer ($k_L a_{20}$) with superficial gas velocity (U_G) obtained with the two methods.

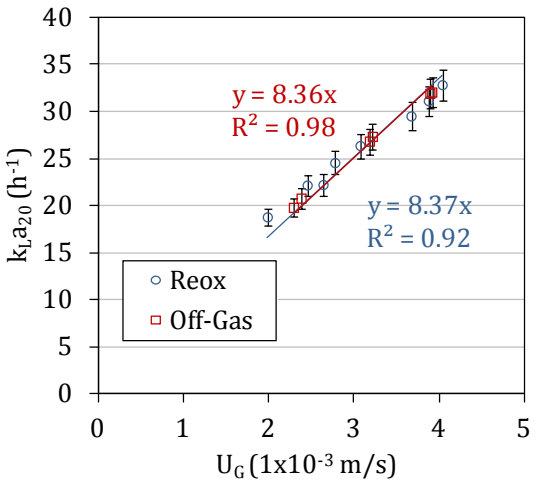

Figure II.7. Results of the oxygen transfer measurements performed in clean water with two different methods: Reoxygenation and Off-gas.

To evaluate whether the oxygen transfer results were dependant on the measuring method (Reoxygenation and Off-gas), an analysis of covariance (ANCOVA) was carried out using the open source statistics software *R* according to the method proposed by Cornillon *et al.* (2012). The method consisted in evaluating if the slope of the function $k_La_{20}=f(U_G)$ was dependant on the implemented configurations. The details of the method are described in **APPENDIX 3**.

With a significance level of 5% ($p<0.05$), the results showed that the slope of the function $k_La_{20}=f(U_G)$ is independent on the measuring method (**APPENDIX 3**.).

II.1.4 Hydrodynamic characterization of the bubble column

Hydrodynamic characteristics of the gas-liquid dispersion in the bubble column such as the overall gas hold-up and the bubble size as well as the residence time distribution were determined. The followed methods are described in the next paragraphs.

II.1.4.1 Measurements of the overall gas hold-up (ε_G)

The overall gas hold-up in the bubble column was measured in clean water and in activated sludge simultaneously with the oxygen transfer measurements. The measurements consisted in determining the ratio of the column height occupied by the gas volume to the one occupied by the gas-liquid mixture. These heights were indirectly determined through the measurement of the hydrostatic pressure at two different liquid heights in the bubble column under aerated and non aerated conditions.

Two hydrostatic pressure sensors (Endress Hauser) were submerged in the aerated volume at constant depths of 0 and 4.1 m above the gas sparger (Figure II.1) and connected to a data acquisition system. When the column was filled with activated sludge or with clean water, the pressure difference between the two sensors was measured and recorded with air supply (during the oxygen transfer tests) and without air supply. Pressure values were averaged simultaneously with the oxygen transfer measurements.

As $\rho_{air} \ll \rho_{eau} \approx \rho_{sludge}$, the overall gas hold-up can be estimated using the following equation:

$$\varepsilon_G\ (\%) = \left(1 - \frac{\Delta P_{with\ air}}{\Delta P_{without\ air}}\right) \times 100 \qquad \text{II.15}$$

The derivation of Equation II.15 is presented in **APPENDIX 4**.

II.1.4.1.1.1 Relative error of the gas hold-up measurement

The measurement of the overall gas hold-up by means of the hydrostatic pressure has been validated by comparison to results obtained by the level difference method performed with a float level sensor (Endress Hauser) which provides an absolute measurement uncertainty of ±0.04% (Fayolle, 2006). Table II.2 and Figure II.8 present the results of this comparison.

Table II.2. Relative error of the overall gas hold-up measurements obtained with the pressure probes compared to the one obtained with the float level sensor.

Overall gas hold-up (ε_G)		Relative difference (%)
Pressure probes (%)	Float sensor (%)	
0.24	0.21	14.33
0.67	0.65	3.31
1.33	1.25	5.80
2.07	2.02	2.13
4.02	3.86	4.02

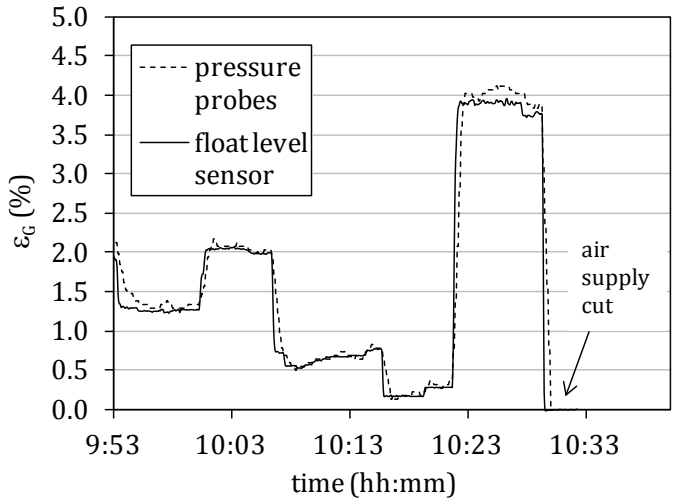

Figure II.8. Comparison of the gas hold-up (ε_G) measured with the float level sensor and pressure probes.

The measurement relative error decreases as the gas hold-up values increases. For low gas hold-up values of about 0.2% the relative error is 14% while for higher values between 0.6 and 4%, the relative error varies between 2 and 6%.

II.1.4.1.1.2 Temperature effect on the overall gas-hold-up

The gas hold-up measurements carried out simultaneously with the oxygen transfer tests, were performed at different temperatures ranging from 9 to 27°C. It was then required to evaluate the temperature effect on the overall gas hold-up in order to correct the results obtained at a temperature T to a standard temperature (e.g. 20°C) at which all results were comparable. To this aim, the effect of temperature on overall gas hold-up was studied by means of aeration test performed in the bubble column with clean water at a mean temperature of 10, 16 and 22°C and using the fine bubble diffuser.

The obtained results and the proposed correction will be presented in Chapter V in the gas hold-up section related to the clean water experiments (IV.2.1).

II.1.4.1.2 Bubble size distribution

To measure the bubble size distribution, photographic images were taken from the outside of the column at a height of 1m above the gas diffuser. The camera was focused on a piece of graph paper fixed on the column wall. This focus allowed seeing clearly the bubbles rising next to the column wall. Two spotlights were placed in the back of the column and white sheets were fixed on the column, in front of the spotlights, in order to uniformly diffuse the light through the column. The inside and outside of bubbles become brighter compared to their contour and bubbles appear as black rings as shown in Figure II.9.

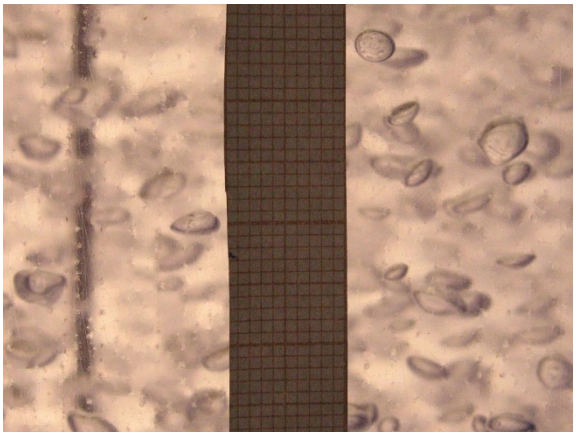

Figure II.9. Photography of fine bubbles captured at the wall of the column

The captured images allowed determining the bubble eccentricity (χ) which is the ratio of the bubble major axe (A) to the minor axe (b). The equivalent diameter of bubbles, defined by the Equation I.21 ($db = (A^2 b)^{1/3}$), was estimated and a histogram of its distribution was obtained. The Sauter diameter (d_{bs}) was deduced from the distribution of the equivalent diameter using (Equation I.20).

The bubble size was determined at three superficial gas velocities within a range from $1x10^{-3}$ to $5x10^{-3}$ m s^{-1}. For a given gas flow rate, the bubble size was determined from at least 100 bubbles. This number is the minimal bubbles quantity that allows measuring the bubbles size with an error lower than 3% in respect to the average Sauter diameter (Fayolle *et al.*, 2010).

The bubbles size and shape were determined only for the fine bubble system, because in the case of bubbles generated with the coarse bubble diffuser, the bubbles rising near to the wall were very different (much smaller) from those rising through the central axis of the column. Consequently, determining the bubble size by means of images of bubbles rising near the wall was not representative of the bubble population and would underestimate the actual mean bubble size.

In activated sludge, because of the opacity of the mixed liquor, only the bubbles rising very close to the wall could be detected and not enough bubbles could be captured to obtain a representative mean value.

The photographic images were takes using a Canon Powershot G6 camera. The captured images were processesed using the ImageJ software. For lighting, 2 spotslights of 1000W were used.

II.1.4.1.3 Residence time distribution in the aerated column

Oxygen transfer tests in activated sludge were performed with liquid co-current circulation through the bubble column. In order to evaluate the flow characteristics in the reactor under this configuration, a study of the reactor's residence time distribution (RTD) was carried out using tap water and the fine bubble diffuser.

The liquid was directed into the column at the bottom with the use of a helical rotor pump and exited the top of the column by overflow (at 4.2 m above the gas diffuser). The estimation of the RTD consisted first in injecting a rapid pulse of a concentrated inert tracer at the nearest point of the liquid inlet and subsequently measuring and recording the concentration of this tracer with time at the reactor's outlet.

The tracer was a saline solution of 260 g NaCl L^{-1} and volume 0.05 L. The evolution of the salt concentration was measured using a conductivity meter installed at the outlet of the column and connected to a data acquisition (Yokogawa). A calibration curve relating the dissolved NaCl concentration with the conductivity had been previously obtained in the laboratory.

The RTD was studied under three different superficial liquid velocities ($0.8\text{x}10^{-3}$ m s^{-1} < U_L <$4.5\text{x}10^{-3}$ m s^{-1}) at a constant superficial gas velocity ($U_G \approx 4.4\text{x}10^{-3}$ m s^{-1}). Three superficial gas velocities ($2.0\text{x}10^{-3}$ m s^{-1} < U_G <$4.3\text{x}10^{-3}$ m s^{-1}) were also tested at a constant liquid flow rate ($U_L \approx 4.5\text{x}10^{-3}$ m s^{-1})

The experimental evolutions of concentration with time are presented in Figure II.10 in terms of the dimensionless residence time distribution, $E(\theta)$, which is the ratio of the salt concentration at an instant t to the initial salt concentration ($E(\theta) = C/Co$), and in terms of the dimensionless time which is the ratio of the time t to the mean residence time ($\theta = t/t_{mean}$).

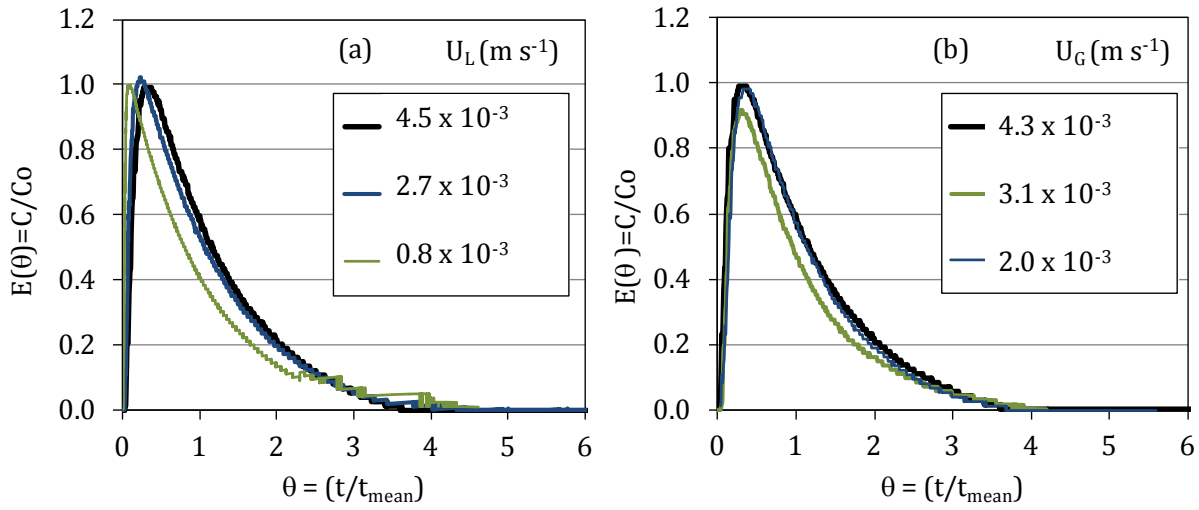

Figure II.10. RTD in the bubble column: Evolution of the normalized concentration $\boldsymbol{E(\theta)}$ with normalized time (θ). (a) $\mathbf{U_G}$ fixed (≈4.4×10^{-3} m s^{-1}) and three liquid superficial velocities (b) $\mathbf{U_L}$ fixed (≈4.5×10^{-3} m s^{-1}) and three superficial gas velocities. C: concentration at a time t. Co: initial concentration. t_{mean}: mean residence time.

The observed concentrations describe a reactor with flow characteristics close to a completely mixed reactor. The dimensionless residence time distribution, $E(\theta)$, was modelled representing the reactor volume (V) as a number of J reactors of volume V/J in cascade. This model is written as follows (Roustan, 2003):

$$E(\theta) = \frac{J^J}{(J-1)}\theta^{(J-1)}e^{-J\theta} \qquad \text{II.16}$$

where

$E(\theta)$ dimensionless residence time distribution

θ dimensionless time (t/t_{mean})

J number of reactors

t_{mean} mean residence time

The obtained results of the tracing experiments are summarized in Table II.3.

Table II.3. Results of the tracing experiments with NaCl in the bubble column at three different gas and liquid superficial velocities.

	U_L ($1x10^{-3}$ m s^{-1})	U_G ($1x10^{-3}$ m s^{-1})	Mean residence time (min)	V/Q (min)	J (reactors)
U_G fixed	0.8	4.2	95.5	93.9	1
	2.7	4.6	24.8	27.9	2
	4.5	4.3	13.1	16.6	2
U_L fixed	4.6	2.0	13.8	16.4	2
	4.5	3.1	15.9	16.7	2
	4.5	4.3	13.2	16.6	2

The number of estimated reactors (J) was in all cases equal or lower than 2. The bubble column with liquid circulation can then be considered as a completely mixed reactor.

Conclusions on the setup of the oxygen transfer measurements

- The oxygen transfer coefficient in clean water and activated sludge is measured in a bubble column using two types of bubble diffusers (FB and CB) in a range of superficial gas velocity between $2x10^{-3}$ and $5x10^{-3}$ m s^{-1}.
- In clean water, the oxygen transfer measurements are carried out by the Reoxygenation method. In activated sludge, the oxygen transfer coefficient is determined by the Off-gas method. The techniques are equivalent in clean water.
- Oxygen transfer measurements with activated sludge are performed on site in two wastewater treatment plants: a conventional activated sludge system (CAS) and a membrane bioreactor process (MBR).
- Simultaneously with the oxygen transfer measurements in clean water and activated sludge, the overall gas hold-up is also measured.
- The bubble size distribution is determined in clean water with the fine bubble aerations system.

II.2 Activated sludge rheological measurements

In order to study the rheological behaviour of activated sludge, a tubular rheometer was designed and constructed. Tubular rheometers are known for being mechanically simple, allowing the application of a wide range of shear stress (between 10^{-2} and $10^{7} s^{-1}$) and the instrument configuration helps to avoid low MLSS concentration samples to settle during the measurements (Dupuis, 2008; Ratkovich *et al.,* 2013).

II.2.1 Construction of a tubular rheometer

II.2.1.1 Rheometer specifications

II.2.1.1.1 Characteristics of the evaluated material

- *Fluid:* Activated sludge (AS)
- *MLSS concentration:* Up to 15 g L^{-1} (in the case of MBR sludge).
- *Apparent viscosity:* Depends on the exerted shear rate. At high shear rates of about 1000 s^{-1}, the apparent viscosity may reach values of up to 1.5mPa.s for a MLSS concentration of 2.7 g L^{-1} and up to approximately 7mPa.s at a MLSS concentration of 15 g L^{-1}. At lower shear rates of about 40 s^{-1}, this value may be up to approximately 50 mPa.s (Rosenberger *et al.,* 2002; Yang *et al.,* 2009).
- *Steady state floc size:* Approximately 100 μm at low shear rates (40 s^{-1}). (Biggs and Lant, 2000).

II.2.1.1.2 Measurement range

- *Exerted shear rate:* Up to 1000 s^{-1} which is the highest estimated average shear rate using the correlations available in the literature (cf. Figure I.25) associated with the superficial gas velocity existing in bioreactors (up to 10×10^{-3} m s^{-1}).
- In agreement with the rheological principles, rheological measurements must be performed in a *laminar (Re<2000) and steady state flow regime*.

II.2.1.1.3 Other specifications

- The instrument must allow monitoring the fluid *temperature*.
- The instrument must be easy to transport in order to perform rheological measurements on site.

II.2.1.2 Principles of a rheological measurement with a tubular rheometer

Before explaining the design work the measurement principles are exposed hereafter. In tubular rheometers, the rheological measurement consists in determining the pressure loss $(\Delta P = P_1 - P_2)$ associated to the liquid flow rate (Q) through a capillary tube of known length (L) and diameter (D=2R). Figure II.11 presents the variables involved in the measurement of a tubular rheometer.

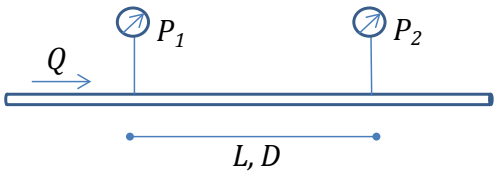

Figure II.11. Schematic of the measurement variables involved in a tubular rheometer.

Since in a capillary tube the velocity profile (and the related shear rate) is a parabolic function of the radial distance to the axe, the apparent viscosity of a non-Newtonian fluid is radius dependant. For that reason it is agreed to calculate the shear rate $(\dot{\gamma})$ and shear stress (τ) at the tube's wall where the shear rate is maximum. For a Newtonian fluid, according to the Poiseuille's law the shear rate and the shear stress in a tube are respectively written as follows (see **APPENDIX 5** for the development of these equations):

$$\dot{\gamma} = \frac{4Q}{\pi R^3} \qquad \text{II.17}$$

$$\tau = \frac{R\Delta P}{2L} \qquad \text{II.18}$$

The velocity profile of a non-Newtonian fluid circulating in a tube is also a function of the non-Newtonian behaviour. Thus, the estimation of the shear rate requires the use of a correction to consider the impact of the sludge non-Newtonian character on the tubular rheological measurement. The corrected shear rate is then calculated by applying the Rabinowitsch-Mooney equation as follows (Dupuis, 2008):

$$\dot{\gamma} = \frac{4Q}{\pi R^3}\left(\frac{3n+1}{4n}\right) \qquad \text{II.19}$$

where n corresponds to the index flow of the Ostwald-de Waele rheological model. It can be deduced from the slope of the experimental flow curves in log-log scale ($\log \tau$ vs. $\log(4Q/\pi R^3)$). (see **APPENDIX 5** for development of Rabinowitsch correction).

II.2.1.3 Design of the tubular rheometer

The constructed measurement device was inspired by the tubular rheometer used by Ndoye *et al.* (2013) for the rheological study of a whey protein suspension. Different tube geometries were implemented in order to have a large range of shear rate. Besides, the use of different geometries allows the verification of the non-slip hypothesis at the tube's wall, verifying that no discrepancy was observed between the flow curves obtained with different diameters (Dubus, 1994).

As can be seen in Equation II.19, a small reduction of the radius (R) implies a significant increase of the exerted shear rate ($\dot{\gamma}$). Thus, for a given applied flow rate (Q), the use of tubes with different radius (R) allows the application of a wide range of shear rate.

Based on the presented equations and the device specifications, the design work consisted in following two main steps:

1. The flow rate (Q) through the capillary tube was defined (with Equation II.19) in relation to the tubes radius (R) in order to achieve the specifications of the range of shear rate ($\dot{\gamma}$) within the limit fluid velocity (Re<2000) and considering the floc size as well as the commercial availability of tubes radius.

2. The tubes length (L) was defined as follows: first, the applied shear stress in the tubes was estimated with the Newton's law in relation to the specifications of the range of viscosity and shear rate ($\mu = \tau/\dot{\gamma}$). Then the tubes length was defined using Equation II.18 based on the measurement range and accuracy of the differential pressure instruments commercially available. It was also considered that the pressure loss measurement in the tube should be placed as far as possible from the tube's edges in

order to avoid extremities convective effects that disrupt the flow development in the measurement length (edge effects, Dupuis, 2008).

II.2.1.4 Description of the constructed tubular rheometer

The rheometer is composed of four PMMA transparent tubes of 4, 7, 12 and 14 mm of diameter. Two piezometric rings, separated by a given length (L = 0.4, 0.8, 1 and 1 m respectively), were located on each tube in order to measure the differential pressure between the two measurement points (ΔP). The piezometric rings are separated from the tubes extremities by a distance of 0.6, 0.4, 0.3 and 0.3 m respectively for the four tubes. The manufacturing of the piezometric rings as well as their adaption to the tubes was carried out by an exterior contractor (s.a.r.l. STIM).

The sludge is pumped into the tubes using a helical rotor pump characterised by a pulseless and low shear flow (PCM – Moineau Technology). The liquid flow rate (Q) in the tubes ranges a value between 5 and 50 L h^{-1} that is measured by weighing the sludge flux at the outlet of the tubes using scales connected to a PC. The pressure loss (ΔP) associated to the flow rate is measured using micromanometers with a piezoresistive sensor (KIMO MP200). These are provided with two interchangeable measurement modules attaining various ranges of differential pressure (up to 500 Pa and 2500 Pa) with different accuracies. Depending on the fluid viscosity and the tubes geometry the modules are used alternatively. The sludge temperature is measured at the tubes outlet using a PT100 thermometer.

Figure II.12 and Figure II.13 show a schematic and a picture of the constructed tubular rheometer.

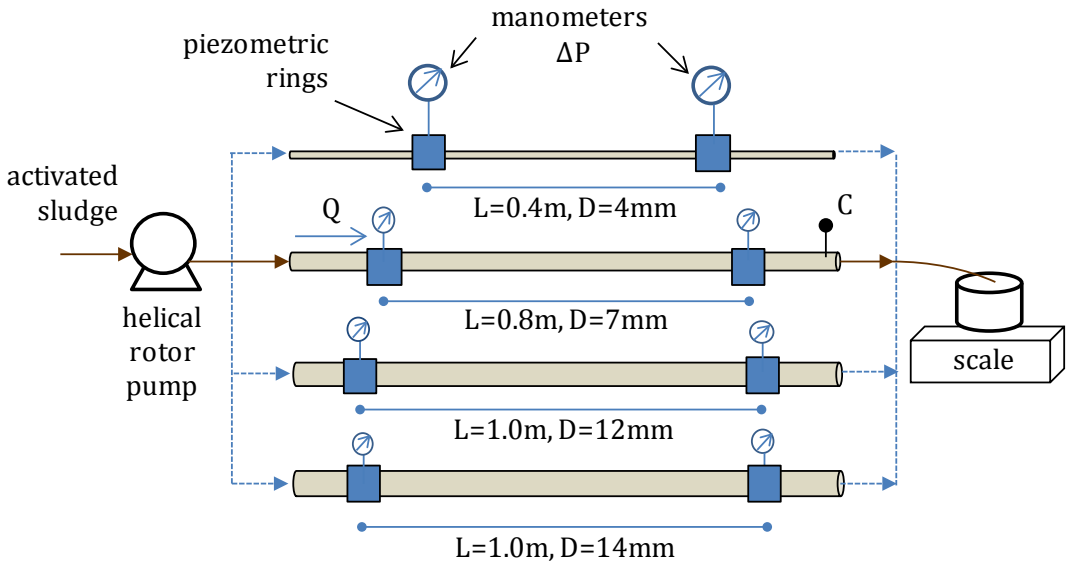

Figure II.12. Schematic of the constructed tubular rheometer.

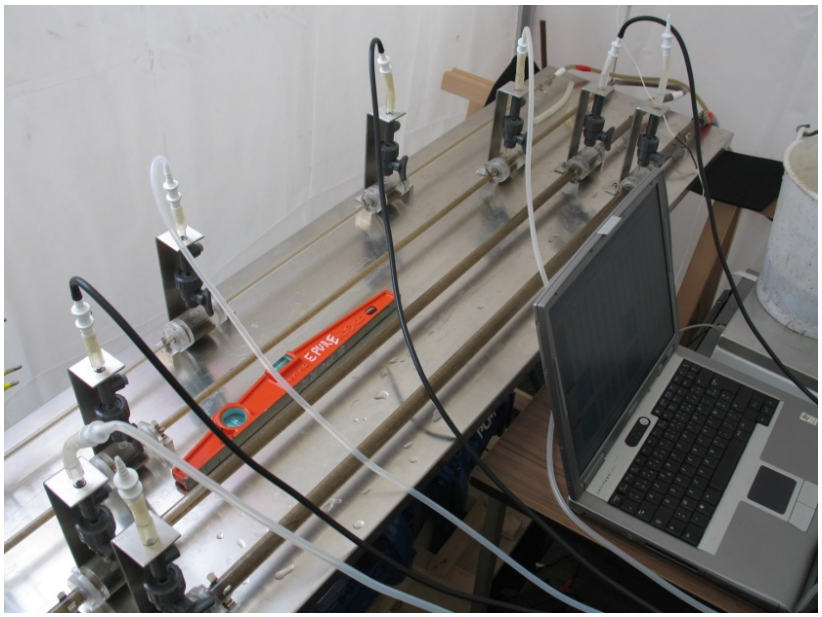

Figure II.13. Picture of the constructed tubular rheometer.

An image of one of the pressure capture points is shown in Figure II.14.

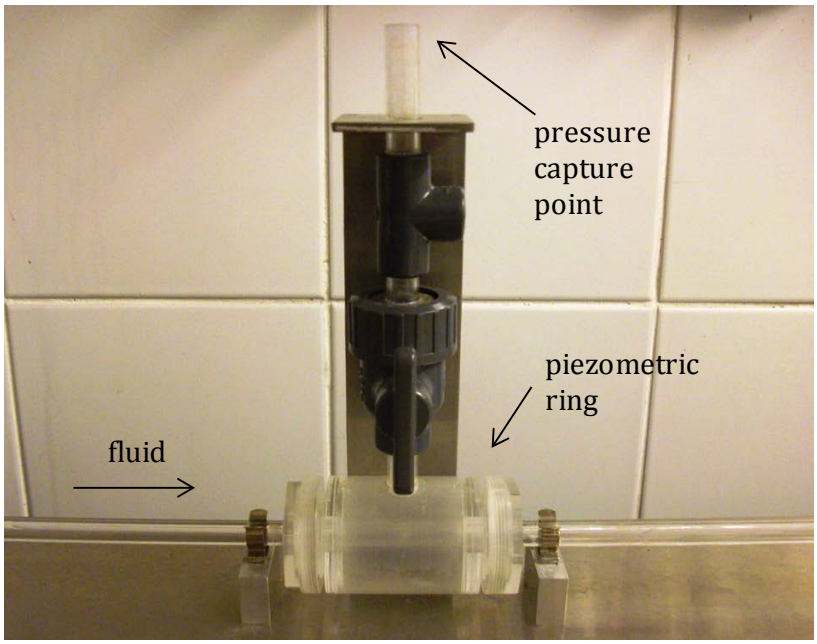

Figure II.14. Illustration of a piezometric ring adapted to one of the rheometer tubes.

The determination of the instrument accuracy and the developed methodology to characterise the rheological behaviour of activated sludge is presented in Chapter III.

Conclusions on the construction of a tubular rheometer for activated sludge

- A tubular rheometer adapted to the sludge characteristics (floc size, settleability, viscosity) has been designed and constructed in order to study the rheological behaviour of AS. Its design with four tube geometries allows applying a shear rate range from approximately 50 up to 1000 s^{-1} which according to the literature review would correspond to the range of shear rate exerted by the bubbles in aerated reactors in accordance to the applied superficial gas velocities (U_G).

II.2.2 Rheological behaviour of activated sludges from different plants

Rheological measurements were performed with activated sludges grab samples taken from the wastewater treatment plants (WWTPs) of five different municipalities located in the Ile de France Region, two of them are membrane bioreactor processes (MBR) and the others are conventional activated sludge (CAS) systems (Table II.4)

Table II.4. Wastewater treatment plants from where the activated sludge was sampled for the study of the rheological behaviour.

WWTP	PE	Activated sludge process
Marolles/Saint Vrain	22 000	CAS
Briis-sous-Forges	20 000	MBR
Etampes	55 000	CAS
Ollainville	66 667	MBR
Etrechy	10 000	CAS

PE: population equivalent; CAS: Conventional activated sludge; MBR: membrane bioreactor.

The sludge was sampled from the aerated bioreactor and/or the recirculation loop and/or the membrane bioreactor in order to obtain different concentrations.

II.2.3 Activated sludge rheology and oxygen transfer measurements on site

Simultaneously to the oxygen transfer measurements in activated sludge previously described in paragraph §II.1.3, some rheological measurements were also performed on site. Basically, the rheological experiments on site were carried out following the same protocol defined in the laboratory but the sludge was pumped into the tubular rheometer from the column outflow without any intermediate stirred reservoir. Hence the sludge temperature in the tubular rheometer corresponded approximately to the temperature in the bubble column and in the aeration basin. The schematic of the experimental setup installed on site that included the oxygen transfer and rheological measurements is presented in Figure II.15.

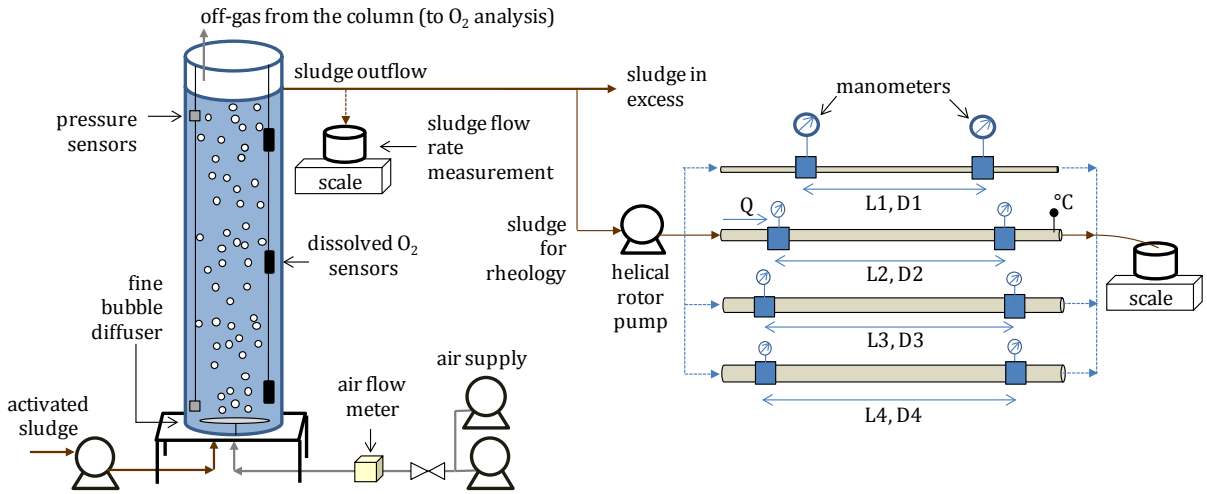

Figure II.15. Representation of the experimental setup installed two wastewater treatment plants: bubble column and tubular rheometer.

II.2.4 Temperature effect on the activated sludge rheological behaviour

Rheological measurements with activated sludge were then performed on two different locations: (i) on the laboratory and (ii) on site. While the rheological measurements performed in the laboratory were carried out at a controlled temperature of 20°C, the on-site measurements were performed without temperature control and the sludge temperature corresponded basically to the mixed liquor temperature in the aeration basin (as described in the paragraph here above). In order to extrapolate the results obtained on site at different temperatures to 20°C, the effect of temperature on activated sludge rheology was evaluated. Rheological measurements were thus performed inside a room with a temperature controlled at three different levels (10, 15 and 20°C) with the same activated sludge. After the sample reception at the laboratory, the volume was divided in three equivalent samples. Before starting the rheological measurements, the resulting three volumes were refrigerated if needed or left in a constant temperature room with gentle stirring and aeration.

The results from this study are presented in the next chapter concerning the setting up of the rheological characterization (cf. III.4).

II.3 Physicochemical characterisation of activated sludge

Table II.5 presents the physicochemical properties of activated sludge that were characterised in relation to the measurements of oxygen transfer coefficient and the study of the sludge rheological behaviour. The median floc diameter (D50), the floc cohesion index (FCi) and the pH, were only evaluated for samples concerning the rheological measurements.

Table II.5. Characterized physicochemical activated sludge properties

Sample	Property	Symbols and units	Method
Activated sludge samples	Mixed liquor suspended solids	MLSS (g L^{-1})	Standard: NF T 90-105-2. 250 mL sample → 15 min centrifugation → drying at 110°C during 12h at least.
	Mixed liquor volatile suspended solids	MLVSS (g L^{-1})	Standard. 250 mL sample → centrifugation → drying at 550°C during 2 h at least.
	Total chemical oxygen demand	Total COD (mg L^{-1})	250 mL sample homogenisation with Ultraturrax (1 minute) → Hach Lange cuvette tests: LCK 514.
	Hydrostatic Floc Volume (Henkel, 2010)	HFV (mL L^{-1})	1L sample → settling in a graduated glass tube at 4°C during 24-48h→reading of settled volume.
	Floc median diameter	D50 (μm)	Granulometrie Mastersizer 3000 (Laser diffraction)
	Floc Cohesion index	FCi (-)	Granulometrie Mastersizer 3000 (Laser diffraction)
	pH	pH	pH probe
	Density	ρ (kg m^{-3})	weighing of a 50 mL graduated flask filled with activated sludge
	Sludge Volume Index	SVI (mL g^{-1})	1L sample → 30 minutes settling in a laboratory tube→ calculation of ratio to the MLSS concentration.
Filtered activated sludge sample (250 mL sample filtration at 2 μm → 100 mL filtration at 0.45 μm)	Soluble chemical oxygen demand	Soluble COD	Hach Lange cuvette tests: LCK 314
	Surfactants (anionic, cationic, non-ionic)	S-A; S-C; S-NI (mg L^{-1})	Hach Lange cuvette tests: LCK 332, LCK 333, LCK 331.
	Static surface tension	σ (mN m^{-1})	Ring tensiometer LAUDA
	Calcium, Magnesium, Sodium, Potasium	Ca^{++}, Mg^{++}, Na^{+}, K^{+} (mg L^{-1})	Ionic chromatography (Dionex)

II.3.1.1.1 Floc mean diameter (D50)

The floc granulometry was studied by means of a particle size analyser that uses the laser diffraction technique (Mastersizer 3000, Malvern) to determine the size distribution in a range of particle size from 0.01 μm up to to 3500 μm.

II.3.1.1.1.1 Measurement principle

The laser diffraction technique consists in the emission of a laser beam through a sample with dispersed particles. Depending on the size on the encountered particle, the incident light scatters at different angles (see Figure II.16.a). Measuring the angular scattered intensity allows the particle size calculation based on the Mie light scattering theory. In the measurement unit, the intensity of the scattered light is measured by means of light detectors located at different angles around the dispersed particles in order to create a pattern of light scattering for the particles. Two laser beams with different wave lengths (blue: 477 nm; red: 633 nm) are sequentially emitted in order to enlarge the range of detected particle size (Figure II.16b).

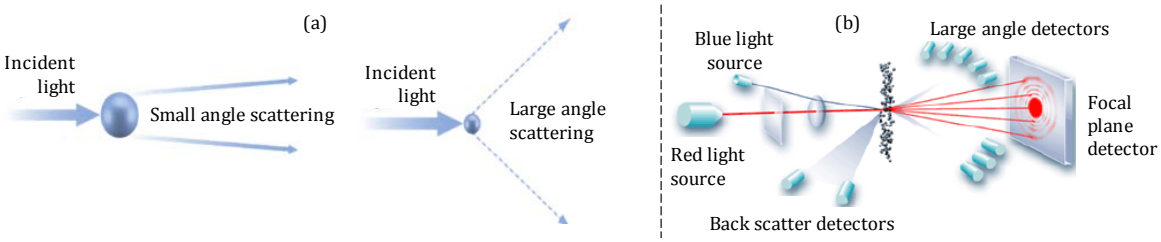

Figure II.16. (a) Incident laser beam on particles with different size and scattering angle. (b) Representation of light detectors and laser beams (blue and red) in the measurement unit. (Images adapted from Malvern).

The light scattering technique assumes the following hypothesis:

- The light is not absorbed by the continuous phase
- Particles concentration is low
- The particles are spherical
- The studied suspension is homogenous

Considering that some particles are non-spherical, an equivalent diameter is calculated. It corresponds to the diameter of a sphere that occupies a volume equivalent to the particle volume.

II.3.1.1.1.2 Protocol description

The particle analyzer is provided with an external stirring module that has two main functions: keeping a homogenous suspension and driving the sample into the measurement area. As activated sludges are shear sensitive, the stirring speed influences the floc granulometry. Hence, to measure the floc size, the stirring speed was fixed to 500 rpm which is the minimum stirring speed provided by the external module. Parallel studies carried out in the laboratory with a standard cuve, not presented in this work, showed that 500 rpm corresponds to a shear rate in an interval between 120 and 300 s^{-1}. The analysed sample corresponded to an activated sludge

sample diluted to approximately 0.1 g L^{-1} of MLSS concentration using sludge supernatant obtained from a filtration step at 2µm. The degree of this dilution is defined in order to carry out the measurements within the range of obscuration of 10-20% recommended by the manufacturer for avoiding particle superposition and ensuring correct results. Before examining the diluted sample, the internal measurement area is rinsed and a "blank" sample of distilled water is analysed in order to set a scattered light pattern of a particle-less media. The activated sludge refraction index was defined as 1.596, according to previous works with this type of material (Stricot, 2008). The experimental setup for the particle size analysis is represented in Figure II.17.

Figure II.17. Schematization of the experimental setup for the particle size analysis using the granulometer.

Connected to a PC, the granulometer provides an instantaneous volume distribution of the floc equivalent diameter which evolves up to the moment when the aggregation-rupture equilibrium is established. Then, the median floc diameter (D50) is obtained from the stable volume size distribution. The mean surface and mean volume diameters, respectively $D_{3/2}$ and $D_{4/3}$, are as well obtained from the stable size distribution.

II.3.1.1.2 Floc Cohesion index (FCi)

The floc cohesion index characterizes the floc resistance to fragmentation when submitted to shearing conditions (Wilen *et al.,* 2003). Its measurement consists in determining the relative variation of the equilibrium median floc size when measured at two different shearing conditions. Therefore, to estimate the floc cohesion index, the same protocol previously described was implemented but the stirring speed in the granulometer external module was set to 2000 rpm after having earlier set it to 500 rpm. The speed of 2000 rpm corresponded to an intermediate stirring speed within the applicable range of the provided external stirring module. This speed corresponds to a shear rate higher than 1000 s^{-1} in accordance to the previously

mentioned parallel study (not shown in this work) carried out in the laboratory with a standard cuve. The floc cohesion index was then calculated as follows:

$$FCi = 1 - \left(\frac{\mathrm{D50}_{500\mathrm{rpm}} - \mathrm{D50}_{2000\mathrm{rpm}}}{\mathrm{D50}_{500\mathrm{rpm}}} \right) \qquad \text{II.20}$$

The more the sludge cohesion index (FCi) is close to 1, the more the sludge floc is resistant to shear. The typical evolution of the median floc diameter under two different shear conditions is presented in Figure II.17a. The change in the volume floc size distribution after two different shear conditions is presented in Figure II.18b.

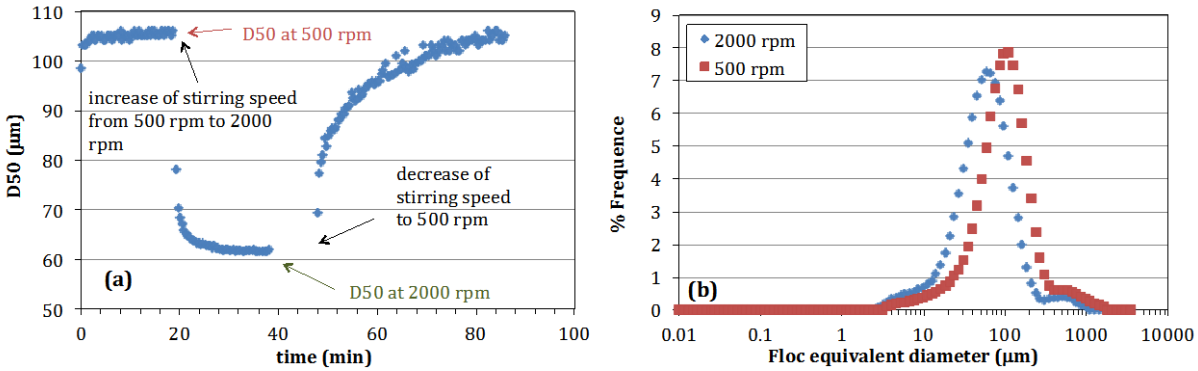

Figure II.18. (a) Median floc diameter under two different shear conditions: 500rpm→ 2000 rpm → 500 rpm. (b) Volume floc size distribution at two different shear conditions: 2000 rpm and 500 rpm.

II.4 Statistical analysis

In order to examine the link between the activated sludge physico-chemical properties, its rheological behaviour (apparent viscosity) and oxygen transfer coefficient ($k_L a$), results were studied by means of an univariate linear regression analysis. Despite the fact that the correlation between some variables may not be linear, this simple method allows identifying major correlations (Wilen *et al.,* 2003; Gardener 2012). The Pearson's linear correlation coefficient (r) was calculated to identify how strongly a given independent variable impacts the standard deviation of the response variable. It ranges between -1 and +1, where -1 indicates a perfect negative correlation, +1 indicates a perfect positive correlation and 0 means the absence of association. Correlations are considered statistically significant if the p-value is lower than 0.001 ($p<0.001$). The statistical computing was performed using the software environment R.

Chapter III. Development of a methodology to characterise the rheological behaviour of activated sludge

In order to study the rheological behaviour of activated sludge, a tubular rheometer adapted to the sludge characteristics (floc size, settleability, viscosity) was designed and constructed. It is composed of four tubes of different diameter (4, 7, 12 and 14 mm) and the applied shear rate can range from approximately 50 up to 1000 s^{-1} (cf. specifications in § II.2.1.4). This chapter develops the methodology to use this apparatus in order to characterize the rheological behaviour of activated sludge. The uncertainty of the measurement is first assessed, and the implementation of the apparatus is described, especially the conditions allowing to reach a given accuracy.

III.1 Rheometer measurement uncertainty

III.1.1 Theoretical measurement uncertainty

The theoretical measurement uncertainty was computed considering the accuracy and tolerance of the involved instruments and tubes using the partial derivatives method. This allowed establishing the measurement conditions ($Q, \dot{\gamma}, R$) in which the tubular rheometer gives results with a sufficient accuracy. The instruments accuracy and the tubes tolerance as well as the procedure for the calculation of uncertainties are presented in APPENDIX 6.

Figure III.1 presents, for a fluid with the same viscosity of water (μ=1 mPa.s), the estimated measurement uncertainty (±%) related to the viscosity of the fluid, as a function of the shear rate for each tube geometry. The different tube geometries are referenced as D4, D7, D12 and D14 in relation to their diameter length (in millimetres). The data presented in these figures are also shown in detail in APPENDIX 6 in a table format.

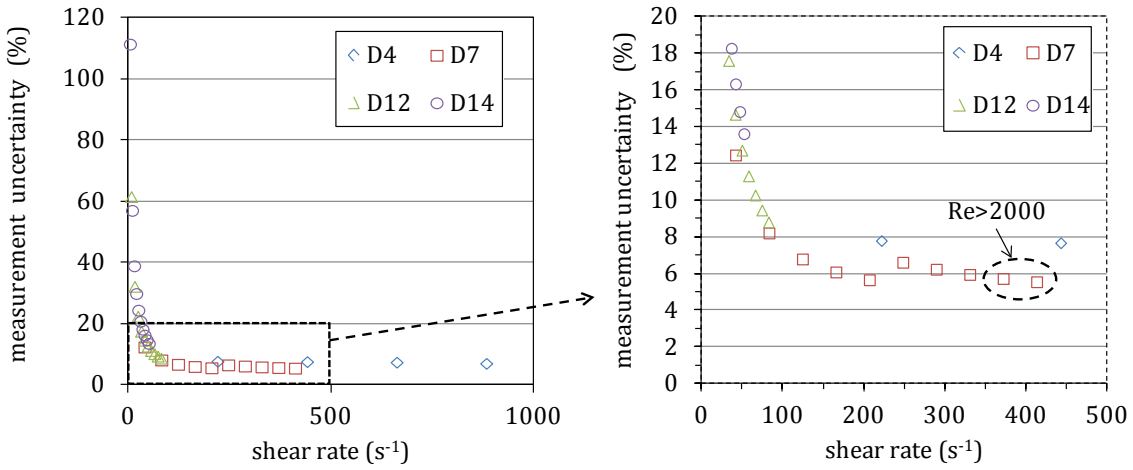

Figure III.1. Estimated measurement uncertainty (±%) related to the viscosity of the fluid as a function of the applied shear rate ($\dot{\gamma}$) for each tube geometry and for a fluid with the same viscosity of clean water (μ=1 mPa.s).

The measurement uncertainty increases with a decrease in the shear rate because the measured differential pressure decreases with the liquid flow rate and approaches the manometers accuracy (~1Pa). At the same time, the manometers provide better accuracy at lower differential pressures (see Appendix table 4). That explains the trend break observed for the geometry D7: the decrease of the shear rate and the pressure loss leads to a reduction of the measurement uncertainty.

According to the estimated uncertainty values, for fluids with the same viscosity as water, rheological measurements must be performed in the tubes referenced as D4, D7 and D12 and above a shear rate of 70 s^{-1}, in order to obtain uncertainties lower than 10%. In order to maintain a laminar flow (Re<2000), high flow rates ($\dot{\gamma}$>370s^{-1}) must be avoided with the tube D7.

Figure III.2 and Figure III.3 present the estimated uncertainties for fluid viscosities 1.5 and 7 times the water viscosity. These values correspond approximately to an average value of the lowest apparent viscosity (limit viscosities) found in the literature (Tixier et *al.*, 2003 and Yang *et al.*, 2009) for activated sludge with MLSS concentrations typical for conventional activated sludge and MBR sludge (between 2 and 15 g L^{-1}).

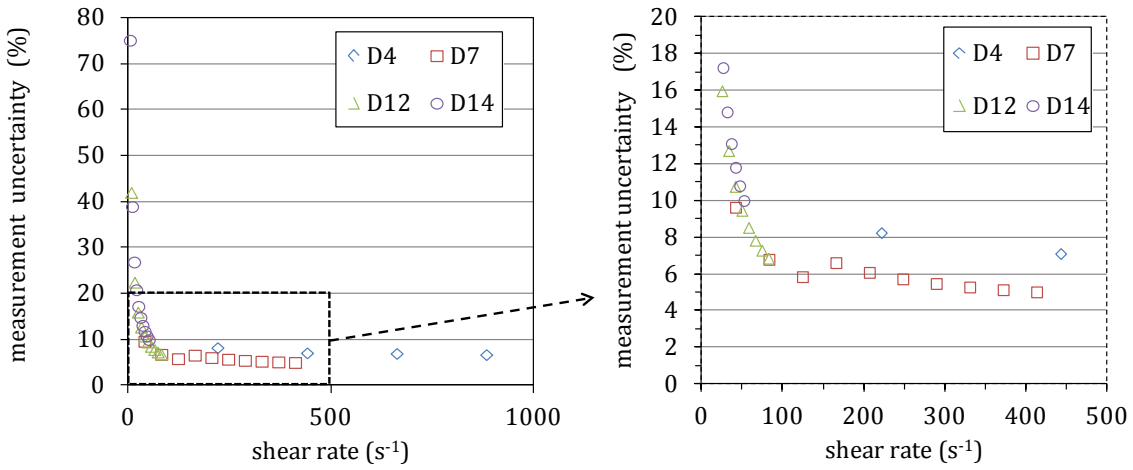

Figure III.2. Estimated measurement uncertainty (±%) related to the viscosity of the fluid as a function of the applied shear rate ($\dot{\gamma}$) for each tube geometry and for a fluid with a viscosity **1.5 times water dynamic viscosity.**

The instrument uncertainty is reduced with the increase of the fluid viscosity because the pressure loss becomes higher in respect to the accuracy provided by the manometers (~1Pa).

For a fluid with a viscosity 1.5 times the water dynamic viscosity the use of the tubes D4, D7 and D12 at shear rates above 50 s^{-1} provides measurement uncertainties lower than 10%.

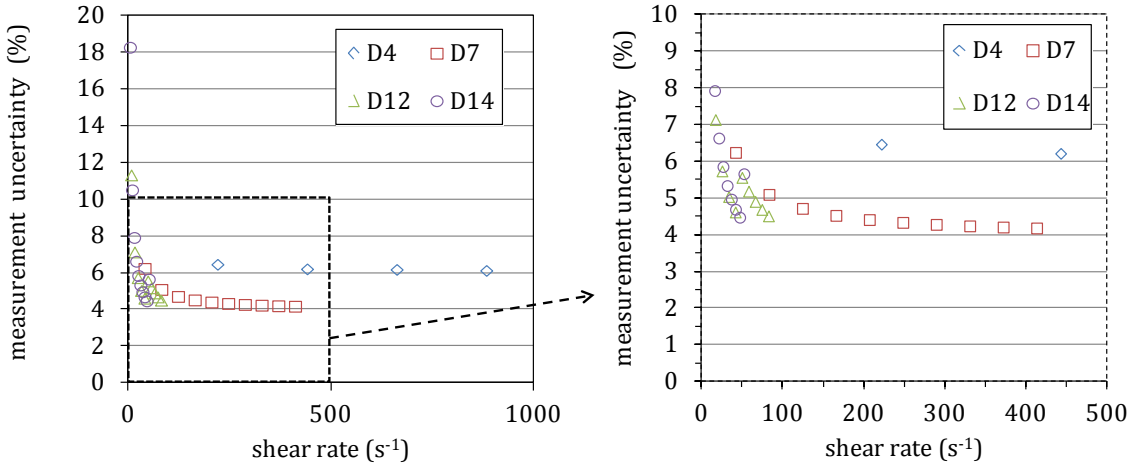

Figure III.3. Estimated measurement uncertainty (±%) related to the viscosity of the fluid as a function of the applied shear rate ($\dot{\gamma}$) for each tube geometry and for a fluid with a **viscosity 7 times the *water dynamic* viscosity**.

The apparatus uncertainty is reduced with the increase of the fluid viscosity because the pressure loss becomes higher in respect to the accuracy provided by the manometers (~1Pa).

For a fluid with a viscosity 1.5 times the water dynamic viscosity the use of the tubes D4, D7 and D12 at shear rates above 50 s^{-1} provides measurement uncertainties lower than 10%.

For fluids with a viscosity 7 times the water dynamic viscosity, the four tubes (D4, D7, D12 and D14) can be used in a wide range of shear rates to reach an uncertainty lower than 10%. At shear rates above 50 s^{-1}, the estimated uncertainty is lower than 6.5%.

III.1.2 Experimental error with tap water

Rheological measurements were carried out with tap water in order to estimate the experimental error with a fluid model which represents the lower viscosity that can be found in activated sludge. Measurements were performed using three diameters (D4, D7, D12) and on the range of flow rates where measurement uncertainties have been estimated to be lower than 10%.

Rheological measurements were performed in five steps as follows:

1. Fixing a flow rate with the pump
2. Waiting 30 seconds to reach a steady state flow
3. Measuring the differential pressure (ΔP), flow rate (Q) and temperature during 2 minutes and computing the average values. Two minutes were fixed as the time assuring to reach a representative average value.
4. Stopping the fluid flow
5. Measuring the differential pressure in motionless conditions (ΔP_o) during 1.5 minutes and computing the average values.

As shown in Table III.1, the experimental relative error is lower than ±10% with an average of 5% by comparison with the dynamic viscosity of water at the measurement temperature (Kestin *et al.,* 1978).

Table III.1. Experimental error on tap water dynamic viscosity obtained with three diameters (D4, D7, D12).

Tube	T (°C)	Shear stress τ (Pa)	Shear rate $\dot{\gamma}$ (s^{-1})	Experimental viscosity μ (Pa.s)	Theoretical viscosity* (Pa.s)	Relative error (%)	Reynolds number
D4	19	1.1	1000.8	1.1E-03	1.0E-03	-3.7	1946
	21	0.9	910.2	1.0E-03	9.9E-04	-4.0	1834
	19	0.9	871.2	1.1E-03	1.0E-03	-1.8	1685
	21	0.8	798.7	1.0E-03	9.9E-04	-3.1	1612
	19	0.8	794.7	1.0E-03	1.0E-03	-1.1	1537
	20	0.8	778.3	1.1E-03	9.9E-04	-8.7	1564
	20	0.6	563.6	1.0E-03	1.0E-03	-1.9	1130
	20	0.3	361.5	9.4E-04	1.0E-03	5.5	723
	20	0.3	293.9	9.5E-04	1.0E-03	4.7	588
D7	21	0.2	241.5	1.0E-03	9.9E-04	-1.2	1490
	21	0.2	218.4	1.0E-03	9.8E-04	-2.6	1356
	21	0.2	196.6	9.5E-04	9.9E-04	3.7	1220
	21	0.2	172.0	9.4E-04	9.9E-04	4.6	1062
	21	0.1	151.9	9.4E-04	9.9E-04	4.8	940
	20	0.1	110.1	1.1E-03	1.0E-03	-6.8	676
	21	0.1	72.8	1.0E-03	9.9E-04	-4.0	450
	21	0.1	57.8	1.1E-03	9.8E-04	-7.0	360
D12	20	0.1	80.4	1.0E-03	1.0E-03	-2.3	1432
	20	0.1	73.3	1.1E-03	1.0E-03	-9.8	1433
	21	0.07	80.17	9.1E-04	9.85E-04	8.0	1321

* Kestin *et al.* (1978).

The experimental flow curves obtained for tap water with the tubes D4, D7 and D12 are presented in Figure III.4.

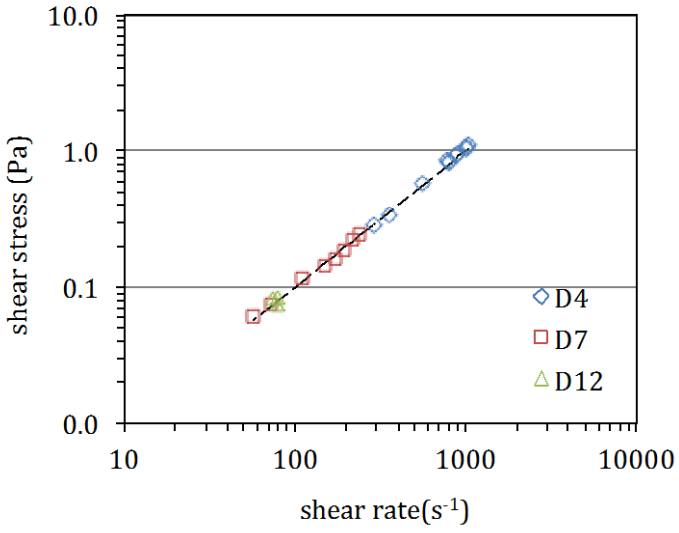

Figure III.4. Experimental rheograms obtained for tap water at an average temperature of 20°C. Dotted line: theoretical values at 20°C.

The obtained rheograms with the three different tubes overlap which indicates that no corrections related to wall slip or convective effects at the tube's ends are required, even if the Reynolds numbers are relatively high questioning the fact that the flow is laminar.

Conclusions on the constructed rheometer

- The constructed tubular rheometer to study the rheological behaviour of activated sludge within a shear rate range of approximately 50 up to 1000 s^{-1}.

- The measurement uncertainty has been determined by means of the partial derivative method considering the accuracy of the involved instruments. These results allowed establishing an abacus that presents the measurement relative uncertainty as a function of the viscosity of the fluid, the tube geometry and the flow rate (hence shear rate). The measurement uncertainty is reduced as: (i) the fluid viscosity is increased, (ii) the flow rate is increased and (iii) the tube diameter is reduced.

- Using tap water in the adequate conditions (shear rate, laminar regime and tube geometry), the experimental relative error on water dynamic viscosity provided by the tubular rheometer is estimated to be lower than ±10% with an average of 5%. As showed in the established abacus, the use of a more viscous fluid leads to a reduction of the measurement uncertainty.

III.2 Rheological measurements with activated sludge

III.2.1 Setting up a rheological measurement with activated sludge

With activated sludge, rheological measurements in the laboratory were performed under the configuration shown in Figure III.5.

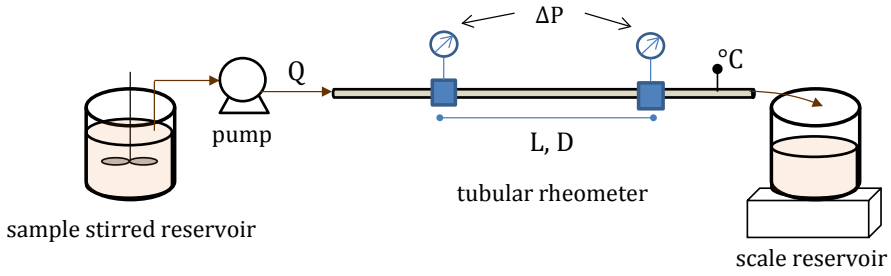

Figure III.5. Laboratory configuration for the rheological measurements with activated sludge.

Defining a measurement protocol for studying the rheological behaviour of activated sludge in the laboratory consisted in answering the following questions:

- What volume of activated sludge is necessary to perform a rheological measurement?
- What is the impact on the rheological behaviour of recycling the same sample of activated sludge several times in the rheometer? This question arises in relation to the thixotropic behaviour of some activated sludge reported in the literature (Seyssiecq *et al.,* 2003; Tixier, 2003). Since the rheological behaviour of a thixotropic sample is a function of the shear previously exerted on the suspension, an extended shearing of a thixotropic sample will result in a different flow curve compared to the one obtained with a less sheared sample.
- What is the impact of the stirring speed in the feeding reservoir on the measurement results?
- What is the impact of storage on rheology results?

The measurements performed in order to answer these questions and the related results are presented in the following paragraphs. These tests were carried out with activated sludge sampled from the aerated bioreactor (or the recirculation loop) of the Marolles/Saint Vrain wastewater treatment plant (see Table II.4 and APPENDIX 1 for characteristics of the Saint Vrain wastewater treatment plant). Samples transportation time was about 1h and the rheological measurements were performed within 10h after sampling. At reception in the laboratory,

samples were slightly aerated and gently stirred and introduced in the measurement room controlled at a temperature of 20°C. Measurements started when the activated sludge sample reached a constant temperature.

To evaluate the impact of the system configuration on the obtained rheograms, a covariance analysis (ANCOVA) was performed according to the method proposed by Cornillon *et al.* (2012) using the statistics software R. The method, described in detail in APPENDIX II.3, consisted in evaluating if the slopes and intercepts of the obtained flow curves were dependent on the implemented configurations.

III.2.1.1 Sample volume

Two modes to introduce the activated sludge into the apparatus were tested:

(i) The sample passed through the system only once. A volume of 40 L was necessary.

(ii) A smaller sample of 10 L was recycled several times in the system.

The obtained flow curves for the same activated sludge sample are shown in Figure III.6.

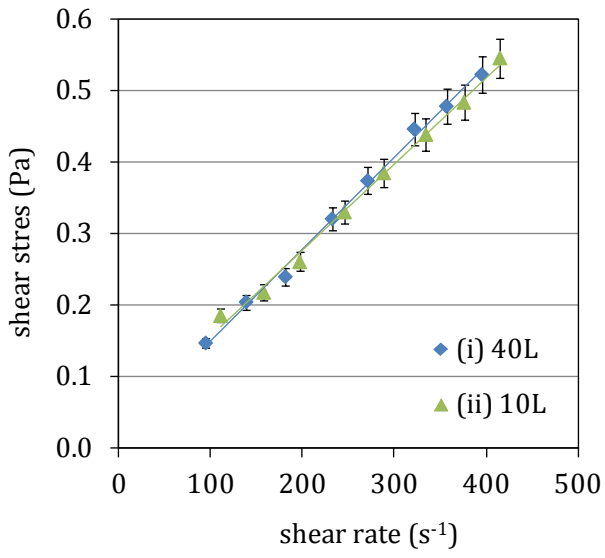

Figure III.6. Rheograms obtained with the same activated sludge sample under two different feeding modes (i) one only passage through the system and (ii) recycled sludge through the system. Bars of error represent ± 5%. Tube geometry: D7. MLSS concentration: 3.4 g L^{-1}.

With a significance level of 5% ($p<0.05$), the results of the ANCOVA analysis, showed that the resulting rheogram is statistically independent of the mode of supplying the activated sludge to the apparatus. Thus several passages through the system (4 times) do not impact the observed

rheological behaviour compared to only one passage through the system. The configuration using a recirculation of the sample is retained since it is simpler on a logistic point of view.

Besides, no thixotropic behaviour was observed, although it was not possible to differentiate whether the absence of a thixotropic behaviour is related to the instrument configuration or to the properties of the sample itself.

III.2.1.2 Stirring speed in the feeding reservoir

Three flow curves were obtained consecutively with the same activated sludge sample but different stirring speeds in the feeding tank: 40, 80, 120 rpm (Figure III.7). The lowest speed (40 rpm) corresponds to the minimum speed required to avoid settling and to maintain a homogenous sample. Above 120 rpm the formation of a vortex was observed.

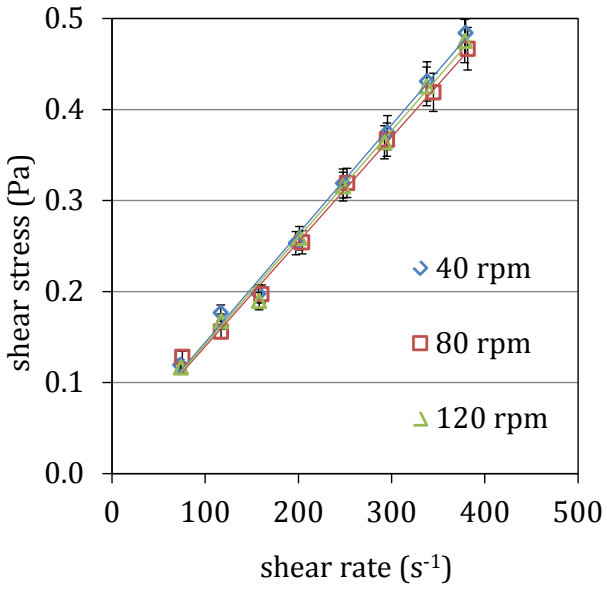

Figure III.7. Rheograms obtained with the same activated sludge sample and three different stirring speeds in the feeding reservoir. Bars of error correspond to ± 5%. Tube geometry: D7.

With a significance level of 5% ($p<0.05$), the results of the ANCOVA analysis showed that the resulting rheograms are statistically independent of the stirring speed in the feeding tank. An intermediate speed of 80 rpm was therefore adopted.

III.2.1.3 Sample storage

Rheological measurements were performed during three consecutive days with the same activated sludge. At reception in the laboratory, the sample was divided into three equivalent volumes, one was used for the first rheological measurement on the sampling day (Day zero). The remaining two volumes were stored in a refrigerated room at 4°C with gentle stirring and aeration. These two samples were used to carry out rheological measurements a day after sampling (D+1) and two days after sampling (D+2). The obtained rheograms are presented in Figure III.8.

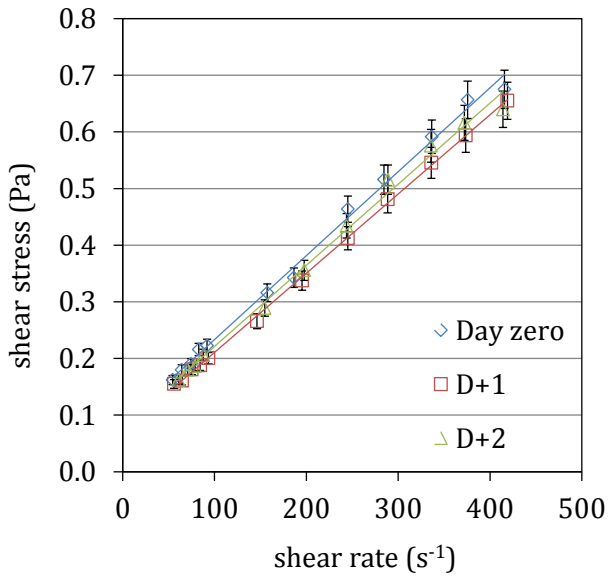

Figure III.8. Rheograms obtained for the same activated sludge with different storage time after sampling. Bars of error represent ±5%. Tube geometry: D7. MLSS concentration: 4.3 g L^{-1}.

With a significance level of 5% ($p<0.05$), the results of the ANCOVA analysis, showed that the resulting rheograms are statistically not affected by the sample storage time within Day zero and D+2. Though in this study the rheological measurements were performed on the same sampling day, this information is useful for upcoming studies.

Conclusions on the setup of rheological measurement with activated sludge

- The volume of sludge sample in the feeding reservoir is defined to 10L. The sample passes through the measurement system approximately 4 times.
- The stirring speed in the feeding reservoir is fixed to an intermediate value of 80 rpm; this stirring speed maintains a homogenous sample and avoid settling.
- Rheological measurements could be performed within two days after collection.

III.2.2 Applying the Rabinowitsch-Mooney correction

In order to consider the impact of the non-Newtonian character on the rheological measurements performed with the tubular rheometer, the Rabinowitsch-Mooney equation was applied to correct the experimental shear rate at the wall according to Equation III.1 (referenced in APPENDIX II.5).

$$\dot{\gamma} = \frac{4Q}{\pi R^3}\left(\frac{3n+1}{4n}\right) \qquad \text{III.1}$$

The correction factor $\left(\frac{3n+1}{4n}\right)$ becomes more significant as the shear-thinning behaviour accentuates and n decreases from 1 (Figure III.9a). For n values between 1 and 0.82, the impact of the rheological behaviour on the shear rate can be considered as negligible (<5%). On the contrary, for suspensions with a more pronounced shear-thinning behaviour, for instance n=0.5, the use of this correction avoid underestimating the applied shear rate by 25%. A visual example of how the Rabinowitsch correction impacts the experimental flow curves obtained with activated sludge with two different MLSS concentrations (4.0 and 7.9 g L^{-1}) is shown in Figure III.9b. It can be observed that the correction is more significant for the flow curve with the lowest flow index (n=0.49).

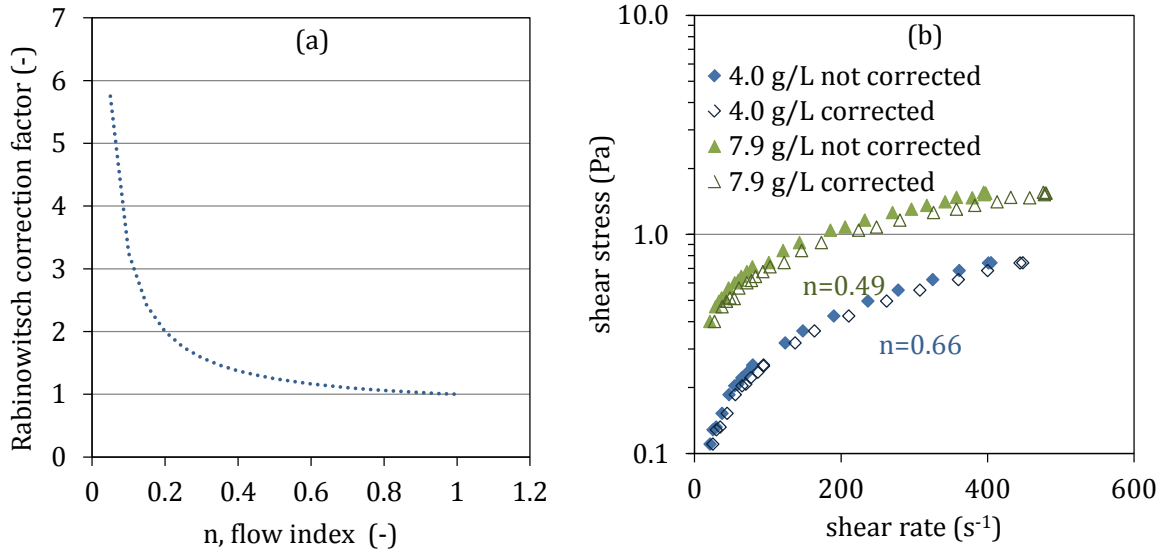

Figure III.9. (a) Evolution of the Rabinowitsch-Mooney correction factor with n (flow index in the Ostwald equation). (b) Experimental and corrected flow curves obtained for activated sludge with two different MLSS concentrations (4.0 and 7.9 g L^{-1}). Results at 20°C.Tube geometries: D7 and D12.

The Rabinowitsch-Mooney correction was applied to all experimental flow curves obtained independently of the estimated value of the flow index (n).

III.3 Comparing the flow curves obtained with the tubes of different diameter

In the present study, the rheological behaviour of activated sludge was studied in a range of shear rate between 50 and 400 s^{-1}. This range of shear rate was defined according to the shear rate values estimated using the equations presented in Table I.8 and the superficial gas velocities applied in the bubble column implemented to perform the measurements of the oxygen transfer coefficient (cf. II.1.1). To attain this measurement range, two tube geometries were used: D7 and D12.

Rheological measurements performed with activated sludge using the different tubes showed that the obtained rheograms overlapped (Figure III.10). The applied correction (Rabinowitsch-Mooney equation) for non-Newtonian fluids is adequate and no other corrections seem to be required in relation to wall-slip or convective effects at the tube's extremities.

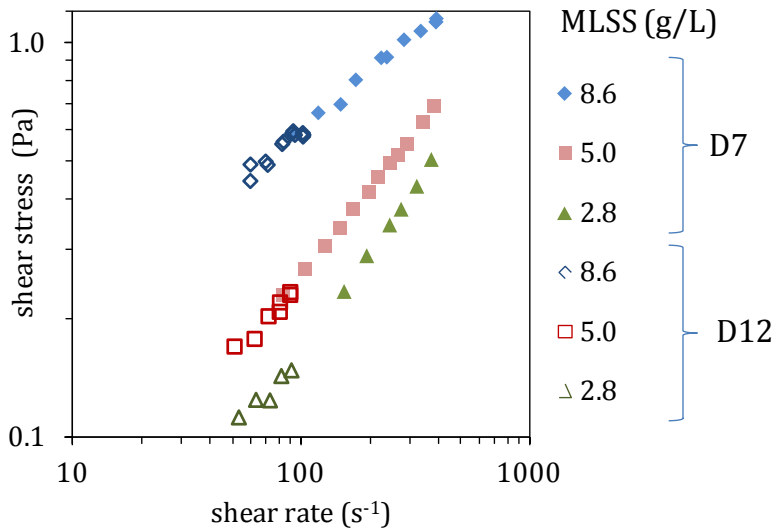

Figure III.10. Experimental rheograms for AS with different MLSS concentrations and obtained with different tubes diameters (D7 and D12). Results at 20°C.

III.4 Temperature effect on the rheological behaviour of activated sludge

The influence of temperature on sludge rheological behaviour was evaluated according to the protocol mentioned in the previous chapter in paragraph § II.2.7.

Figure III.11 shows the obtained rheograms and the evolution of the apparent viscosity with the shear rate at three different temperatures (10, 15 and 20°C) for an activated sludge sample from Saint Vrain WWTP and with MLSS concentration of 5.3 g L^{-1}.

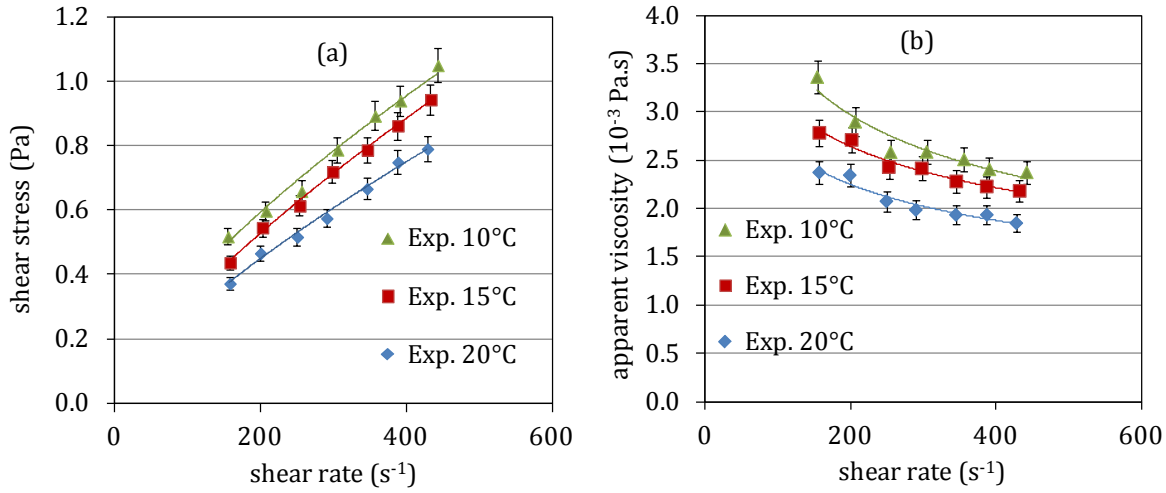

Figure III.11. (a) Experimental rheograms and (b) apparent viscosity evolution with the applied shear rate obtained for the same activated sludge at 10, 15 and 20°C. Tube geometry: D7. MLSS concentration: 5.3 g L^{-1}.

The apparent viscosity, the slope of flow curves (shear stress vs. shear rate), decreases with the increase of temperature. When the temperature rises from 10 to 20°C, the apparent viscosity at a given shear rate is reduced by 24.5% on average which is close to the decrease of water dynamic viscosity (23.3%) within the same range of temperature (Kestin *et al.*, 1978).

From the observed rheograms, an empirical correlation to extrapolate the activated sludge flow curves to a temperature of 20°C was obtained. In analogy to the Arrhenius equation, the correlation is written as:

$$\frac{\mu_{app-AS(20°C)}}{\mu_{app-AS(T°C)}} = A\ exp^{\left(\frac{B}{T+273.15}\right)} \qquad \text{III.2}$$

where A and B are empirical coefficients. Their values (A=169.6 and B=-1531.4 K^{-1}) were deduced by minimizing the sum of squared residuals between the experimental values and the estimated values using Equation III.2. In Figure III.12, the experimental rheogram and apparent viscosity obtained at 20°C are compared to the rheograms and apparent viscosity obtained at 10°C and 15°C converted to 20°C using Equation III.2.

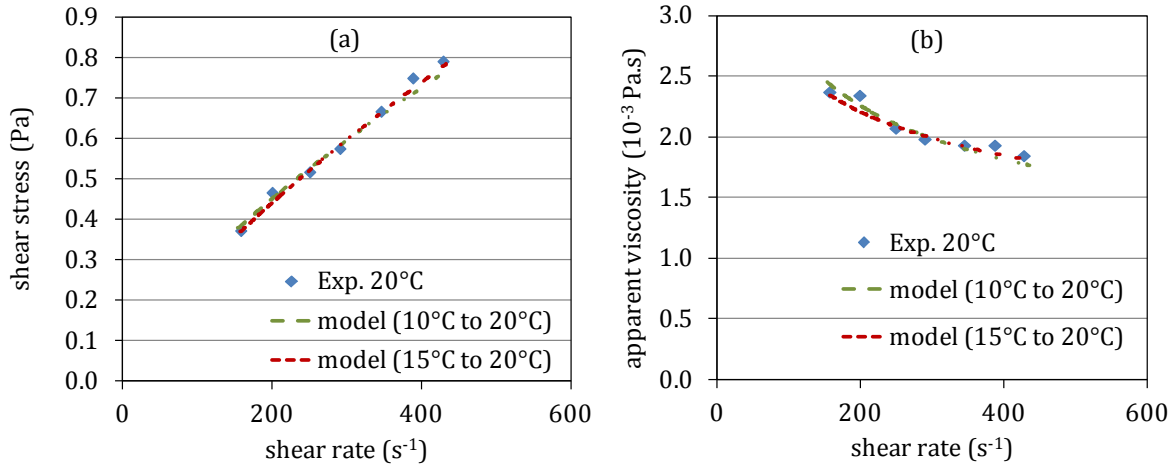

Figure III.12. (a) Experimental rheogram and (b) apparent viscosity at 20°C compared with results obtained at 10°C and 15°C converted to 20°C using Equation III.2.

The effect of temperature on sludge apparent viscosity estimated with the proposed correlation is higher than the one reported by Yang *et al.* (2009) for activated sludge with MLSS concentrations up to 18.7 g L-1 and Dieudé-Fauvel *et al.* (2009) for pasty sludge with 15 % of dry matter. From their proposed correlations, a temperature increase from 10 to 20°C leads to a decrease of apparent viscosity of 13.3% and 18.0% respectively. Instead, similarly to the present work, the study from Lopez *et al.* (2015), using industrial and domestic MBR AS with MLSS concentrations between 5 and 20 g L^{-1}, showed a decrease of 22.6% in sludge apparent viscosity when the temperature rises from 10 to 20°C.

In the present work, the sludge MLSS concentration ranges from 2.3 up to 10.2 g L^{-1} which corresponds to a minimum water content of 98.9 w%. Given that the temperature effect observed on sludge apparent viscosity is similar to the one of temperature on water dynamic viscosity, it is assumed that the proposed correlation is also valid for all the activated sludge samples examined in this study.

The use of this correlation allowed extrapolating the rheological results obtained on site at a given ambient temperature T (between 9 and 27°C) to a temperature of 20°C.

Conclusions on the setup of rheological measurement with activated sludge

- The experimental rheograms of activated sludge are corrected using the Rabinowitsch – Mooney equation which considered the impact of the sludge non-Newtonian character on the shear rate.

- The rheograms obtained using two different tube geometries showed that the rheograms overlapped suggesting that other corrections related to wall-slip or convective effects at the tube's extremities were not necessary.

- The impact of temperature on activated sludge appeared to be similar to the one on water dynamic viscosity. In order to account for this impact, a correlation was proposed and assumed to be valid in the range of the studied MLSS concentrations (from 2.3 up to 10.2 g L^{-1}) to correct the results to 20°C.

Chapter IV. Rheological behaviour of activated sludge from different origins

This chapter presents the results of experiments performed to investigate the rheology of activated sludge (AS) samples issued from five wastewater treatment plants (WWTPs). The AS rheological behaviour is first evaluated by analysing the obtained rheograms. In order to better interpret the results, some physicochemical properties of the different activated sludge samples are analysed and their correlation to the activated sludge rheology is studied. The physicochemical measurements characterise the particulate fraction (MLSS, MLVSS, HFV), the soluble fraction (soluble COD, surfactants and cations concentrations, surface tension) and other properties such as pH, SVI, floc size and floc cohesion index (FCi). Subsequently, the ability of some rheological models to describe each of the experimental rheograms is evaluated and analysed. Finally, based on the set of experimental data and the sludge properties that define its rheological behaviour, a rheological model is proposed and validated.

IV.1 Experimental conditions

All experiments were performed with the tubular rheometer presented in the second chapter in § II.2.1.4. The shear stress was examined in the shear rate range from 50 to 400 s^{-1}. The activated sludge samples were collected from five wastewater treatments plants with a sludge retention time between 10 and 20 day (see table II.5 for WWTP characteristics). For each studied wastewater treatment plant, the sludge was sampled either from the aeration tank and the recirculation loop or from the membrane reactor (in the case of membrane bioreactors). The measurements were performed in two different conditions as previously mentioned in paragraph II.2.6 and II.2.7: (i) in the laboratory at a controlled temperature (20 °C) and (ii) on site at the temperature of the sampled sludge. The physicochemical properties of studied sludge samples were determined on the day of sampling. The samples were analysed without dilution or dewatering in order to avoid modifications of their physicochemical characteristics. Laboratory measurements were completed within 6 hours after sampling.

Table IV.1 and Table IV.2 present the two measurement series as well as some of their general characteristics: origin, operating conditions, sampling point and MLSS concentration.

Table IV.1. Origin, operating conditions, sampling point and MLSS concentration of sludge samples used for the experimental rheological study ***in the laboratory*** (T=20°C).

WWTP	Type	Sampling point	[MLSS] (g/L)
Saint Vrain	CAS	AR	2.8
		RL	4.6
Briis-sous-Forges	MBR	AR	4.0
		MR	7.9
		MR	10.2
Etrechy	CAS	AR	2.3
		RL	4.6
Etampes	CAS	AR	5.5
		RL	8.0
Ollainville	MBR	MR	2.7
		AR	6.2

Where: CAS: Conventional Activated sludge; MBR: membrane bioreactor; AR: Aerated reactor; RL: Recirculation loop; MR: membrane reactor.

On site measurements were performed on two different WWTPs: Saint Vrain and Briis-sous-Forges.

Table IV.2. Origin, operating conditions, sampling point and MLSS concentration of activated sludge used for the experimental rheological study ***on site*** at temperature T.

WWTP	Type	Sampling point	[MLSS] (g/L)	T (°C)
Saint Vrain	CAS	AR	3.0	13
		AR	4.5	9
		AR	5.0	11
		RL	8.5	10
		RL	8.6	11
Briis-sous Forges	MBR	AR	6.1	25
		MR	6.4	24

Where: CAS: Conventional Activated sludge; MBR: membrane bioreactor; AR: Aerated reactor; RL: Recirculation loop; MR: membrane reactor.

IV.2 Characterisation of the rheological behaviour

The rheograms and the apparent viscosity versus the shear rate obtained in the laboratory with the activated sludge samples from five different municipal wastewater treatment plants (cf. Table IV.1) are presented in Figure IV.1. During these experiments, MLSS concentrations ranged from 2.3 to 10.2 g L^{-1}.

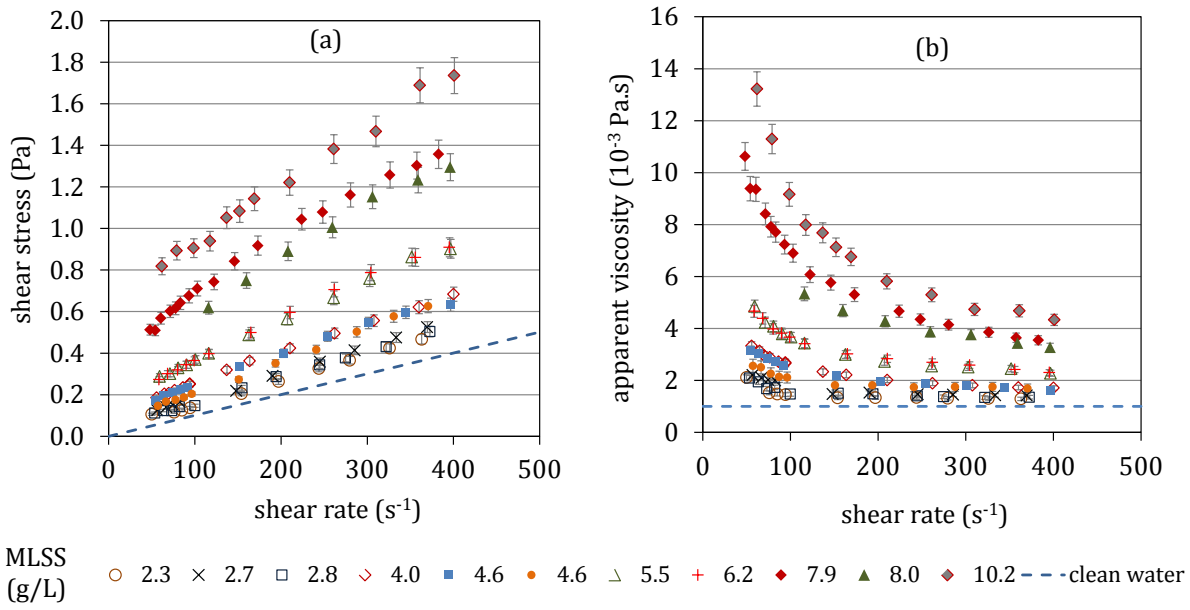

Figure IV.1 (a) Rheograms and (b) apparent viscosity versus shear rate for activated sludge from 5 different wastewater treatment plants at different MLSS concentrations. Etrechy (circles), Briis-sous-Forges (diamonds), Etampes (triangles), Saint Vrain (squares), Ollainville (x,+). Measurements performed *in the laboratory* (T=20°C). (Error bars=±5%, cf. III.1.2)

In contrast to clean water, the slope of the rheograms (Figure IV.1 a), which corresponds to the apparent viscosity, is a function of the applied shear rate. Figure IV.1 b shows that the sludge apparent viscosity is reduced as the shear rate increases. The slope reduction with the increase of the shear rate is higher as the MLSS concentration increases.

For each rheogram, the apparent viscosity of a given sample depends on the applied shear rate (in the range of 50 to 400 s^{-1}) and on the MLSS concentration. At the highest applied shear rate (400 s^{-1}), the apparent viscosity equals 1.3 mPa.s for the sample with 2.3 g L^{-1} of MLSS concentration and is up to 3.4 times higher (4.4 mPa.s) for the sample with 10.2 g L^{-1} of MLSS concentration. These viscosity values are higher than clear water dynamic viscosity. At the lowest applied shear rate (50 s^{-1}), the effect of MLSS concentration on apparent viscosity is more pronounced: the apparent viscosity of the sample with 10.2 g L^{-1} of MLSS is up to 9.5 times higher (15.7 mPa.s) the apparent viscosity of the sample with 2.3 g L^{-1} (1.7 mPa.s).

Figure IV.2 presents the rheograms and the apparent viscosity versus shear rate obtained during the on-site measurements. Results are expressed at 20 °C using Equation III.2.

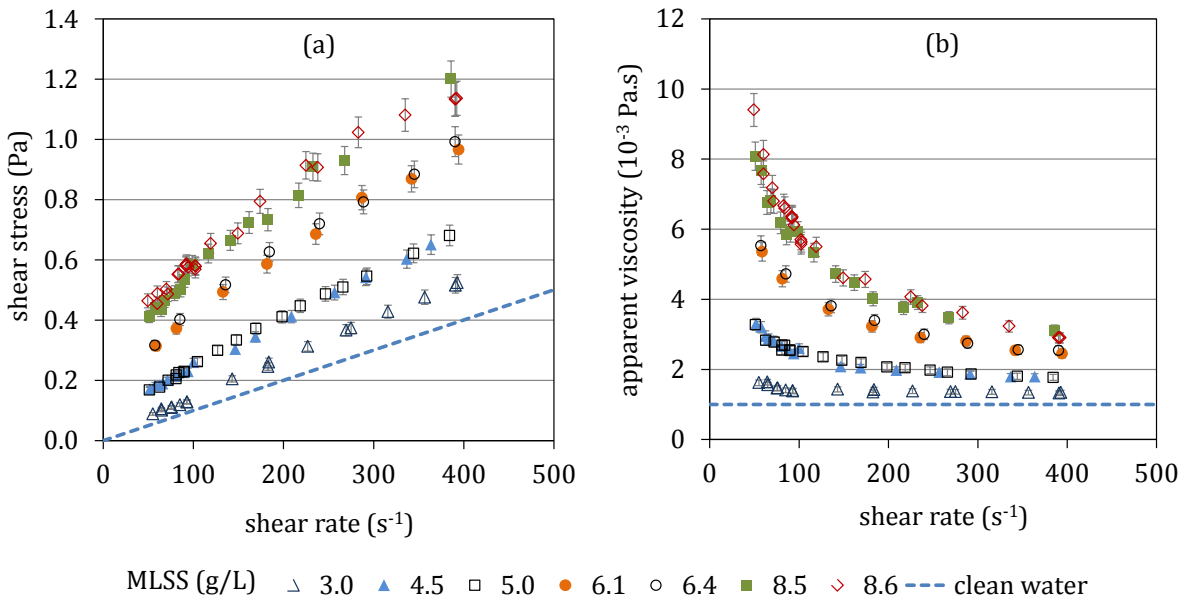

Figure IV.2 (a) Rheograms and (b) apparent viscosity versus shear rate for activated sludge from 2 different the wastewater treatment plants at different MLSS concentrations. Briis-sous-Forges (circles), Saint Vrain (other marks). Measurements performed *on site* at temperature T and corrected to 20°C. (Error bars=±5%, cf. III.1.2)

Sludge samples from the same plant and showing similar MLSS concentrations give similar rheograms. For instance, overlapping trends are observed for the MLSS concentrations at 4.5 and 5.0 g L^{-1}, 8.5 and 8.6 g L^{-1} for samples from Saint Vrain, and at MLSS concentrations of 6.1 and 6.4 g L^{-1} for samples from Briis-sous-Forges.

When considering activated sludge samples from different origins, the correlation between MLSS concentration and sludge rheological behaviour shows more dispersion. In fact, in that case, some samples exhibit similar trends despite their different MLSS concentration. For example, in Figure IV.1, rheograms obtained with sludge at 5.5 and 6.2 g MLSS L^{-1} (from Etampes and Ollainville respectively) present similar trends. Other sludge samples with similar MLSS concentrations do not exhibit exactly the same trend. For instance rheograms obtained with sludge at 7.9 and 8.0 g MLSS L^{-1} (from Briis and Etampes respectively) present slightly different rheograms (beyond the error bars).

Analysis

The observed effect of the shear rate on the activated sludge apparent viscosity is representative of a non-Newtonian fluid and confirms the shear-thinning behaviour reported in the literature by several authors (Seyssiecq *et al.,* 2003; Mori *et al.*, 2006; Yang *et al.,* 2009; Ratkovich *et al.,* 2013). According to Dupuis (2012), the shear-thinning behaviour is typical of suspensions with deformable particles (such as activated sludge flocs) which could be explained by the fact that these tend to line up on the streamlines when the shear rate is increased thus resulting in lower resistance to flow (hence reduction of apparent viscosity). Biological flocs arrangement in the streamlines would occur rapidly under the application of the lowest shear rates and further increments in shear would barely continue to modify the sludge flow structure and have a decreasing influence on apparent viscosity. It is interesting to note that even though the studied activated sludge samples are mainly composed of water (from 98.98 to 99.77 w%), the activated sludge apparent viscosity can be at least 30% higher and up to 4.4 times higher than the water dynamic viscosity, even at the highest applied shear rates. This underlines the potential that the MLSS fraction has to impact the activated sludge apparent viscosity.

The observed relationship between apparent viscosity and MLSS concentration at a given shear rate and for a given sample origin, also previously underlined by various authors (cf. §I.3.4.4.1.1), can be explained by the fact that interactions between particles are intensified when the MLSS concentration increases and this would tend to create a cluster of particles that opposes the suspension's flow (Mikkelsen, 2001). When rheograms of samples from different origins are compared and some disparities appear, concerning the correlation between MLSS content and sludge rheology, it can be suggested that in fact, the organisation of the particles network is not only defined or controlled by shear rate and MLSS content, but other properties, specific of the sludge origin, have an impact and therefore modify the sludge rheological behaviour. In addition to the contribution of MLSS, the effect of the different activated sludge components and properties on the observed rheological behaviours will be further investigated in paragraph IV.3.

Conclusions on the rheological behaviour of the studied activated sludge samples

- A tubular rheometer was used to experimentally study the rheological behaviour of activated sludge from five different WWTPs and with MLSS concentrations comprised between 2.3 and 10.2 g L^{-1}.
- The sludge apparent viscosity depends on the applied shear rate and the MLSS concentration. In addition to the contribution of MLSS, other sludge properties seem to influence the observed rheograms.

IV.3 Impact of activated sludge physicochemical properties on rheological behaviour

The values of apparent viscosity (μ_{app}) at shear rates of 50 and 400 s^{-1} (the lowest and upper limits of the applied shear rates) and the related measured activated sludge properties, are presented in Table IV.3 organized by increasing value of MLSS concentration for the five different sludge origins (laboratory and on-site samples). For each MLSS concentration, the apparent viscosities values were calculated using the rheological model that best reproduced the corresponding experimental rheogram in terms of the lowest RSS value according to the results presented in the Table IV.8 in the following section (IV.4.1)[2].

Linear correlation coefficients (Pearson coefficients, r) between the apparent viscosity at shear rate of 50 and 400 s^{-1} and the different sludge properties are shown respectively in Table IV.4 and

[2] Due to experimental issues, the shear rate range for Etampes WWTP and MLSS = 8.0 g L^{-1} was [120 – 400] s^{-1} and the apparent viscosity at shear rate of 50 s^{-1} was not determined for this condition.

Table IV.5. It must be highlighted that the Pearson coefficients assume a linear correlation between the studied variables and consequently other types of relationship remained unobserved. Consequently, they must be regarded as a tool for identifying a link between two variables but further explorations must be carried out in order to determine the type of the relationship. All samples were collected on WWTPs with a sludge age comprised between 10 and 20 days.

Table IV.3. Characteristics of activated sludge sampled from different wastewater treatment plants and used in the rheological study.

MLSS	g/L	2.3	2.7	2.8	3.0	4.0	4.5	4.6	4.6	5.0	5.5	6.1	6.2	6.4	7.9	8.0	8.5	8.6	10.2
μ_{app} 50 s^{-1}	mPa.s	1.7	2.4	2.0	1.6	3.5	3.4	2.6	3.2	3.1	5.3	5.8	5.0	6.0	10.2	nd	8.2	8.6	15.7
μ_{app} 400 s^{-1}	mPa.s	1.3	1.4	1.3	1.3	1.7	1.8	1.7	1.6	1.7	2.3	2.4	2.3	2.5	3.5	3.3	3.1	2.9	4.4
MLVSS	g/L	1.6	1.8	1.8	2.2	2.6	3.1	2.9	3.2	3.3	3.8	4.1	nd	4.4	5.3	5.6	5.7	5.9	7.1
HFV	mL/L	145	180	175	180	240	280	230	265	285	295	nd	300	465	420	485	400	400	690
CODt	mg/L	2400	3020	2480	3588	4400	4340	4970	6440	5464	5253	6200	5540	6730	8500	7653	8350	8820	12110
SVI	mL/g	100	110	109	94	162*	101	102	115	147	136	165*	139	133*	177*	147	104	117	145*
CODs	mg/L	31.8	22.9	19.9	24.2	25.8	25.4	31.2	27.0	29.3	28.1	35.3	23.5	32.3	29.3	31.6	26.0	22.4	nd
S.an	mg/L	0.7	0.5	0.6	0.4	1.0	0.9	0.4	0.3	0.9	0.4	0.5	0.4	1.3	0.8	0.4	0.8	0.9	1.7
S.cat	mg/L	2.0	<0.2	<0.2	<0.2	0.2	0.2	0.5	<0.2	<0.2	<0.2	<0.2	<0.2	<0.2	0.4	0.2	0.3	0.3	0.3
S.ni	mg/L	0.2	0.3	<0.2	<0.2	<0.2	<0.2	<0.2	0.5	<0.2	<0.2	0.3	0.2	0.4	1.2	0.3	<0.2	<0.2	1.1
surfactants	mg/L	2.9	0.7	0.6	0.4	1.3	1.2	0.9	0.8	0.9	0.4	0.8	0.6	1.8	2.4	1.0	1.1	1.2	3.1
Surface tension (20°C)	mN/m	72.2	73.0	72.1	72.6	71.8	72.2	72.1	72.5	72.5	72.7	72.5	72.7	72.4	72.5	72.3	72.4	72.2	68.8
pH	(-)	8.1	7.8	8.2	nd	nd	nd	7.8	8.0	nd	7.7	nd	7.9	nd	nd	7.8	nd	nd	7.9
AS Density	kg/m3	nd	nd	997	999	999	1000	nd	nd	1003	1000	991	nd	999	1000	1000	1001	1002	1000
Na^{+}	mg/L	99.2	84.5	59.4	nd	54.1	47.2	94.2	74.6	34.8	83.0	12.8	86.3	60.2	10.3	83.2	68.0	37.4	70.0
K^{+}	mg/L	28.8	24.7	20.2	nd	17.4	13.8	30.2	24.2	10.5	21.4	4.5	23.8	22.0	3.9	25.5	22.2	11.9	33.6
Ca^{++}	mg/L	116.9	136.1	177.0	nd	103.4	144.1	108.8	154.6	83.3	124.5	28.1	138.6	124.3	19.0	129.6	152.0	97.0	135.1
Mg^{++}	mg/L	13.4	11.5	19.7	nd	7.6	17.3	14.1	18.0	10.7	6.9	1.7	11.0	8.7	1.5	7.3	23.6	12.3	12.3
cations	mg/L	258.2	256.8	276.3	nd	182.5	222.4	247.3	271.4	139.4	235.8	47.1	259.7	215.2	34.7	245.6	265.9	158.6	251.0
$D50_{500}$	µm	101.0	*111.0*	*119.0*	nd	nd	nd	*82.6*	118.0	nd	*92.2*	nd	106.0	nd	86.6	89.7	nd	nd	*80.5*
$D50_{2000}$	µm	56.5	*66.1*	*101.0*	nd	nd	nd	*54.9*	92.5	nd	*57.8*	nd	61.4	nd	40.1	49.6	nd	nd	*35.2*
FCi	(-)	0.55	*0.60*	*0.85*	nd	nd	nd	*0.66*	0.78	nd	*0.63*	nd	0.58	nd	0.48	0.55	nd	nd	*0.44*
WWTP		Etrec.	Ollainv.	Saint V.	Saint V.	Briis	Saint V.	Etrec.	Saint V.	Saint V.	Etamp.	Briis	Ollainv.	Briis	Briis	Etamp.	Saint V.	Saint V.	Briis
Sampled from		AR	MR	AR	AR	AR	AR	RL	RL	AR	AR	AR	AR	AR	MR	RL	RL	RL	MR
Date	dd/mm/yy	6/8/13	5/8/13	26/6/13	16/11/12	14/8/13	13/2/13	8/8/13	12/7/13	6/2/13	10/7/13	19/7/13	15/7/13	18/7/13	16/8/13	11/7/13	8/2/13	15/2/13	9/7/13
Performed at		LAB	LAB	LAB	ON SITE	LAB	ON SITE	LAB	LAB	ON SITE	LAB	ON SITE	LAB	ON SITE	LAB	LAB	ON SITE	ON SITE	LAB

Results at 20°C / AR=aerated reactor; RL= recycling loop; MR=membrane reactor / nd : not determined / *Floating aggregates observed / Values of D50 and FCi indicated in *italic type* are only estimated values (due to unsteadiness of D50). These values will not be considered in the following.

Table IV.4 Correlation Pearson coefficients (r) between the activated sludge characteristics including the apparent viscosity (μ_{app}) estimated at a shear rates of 50 s^{-1}.

	μ_{app} 50 s^{-1}	p-value	MLSS	MLVSS	HFV	CODt	SVI	CODs	S.an	S.cat	S.ni	surfact.	σ @ 20°C	pH	AS Density	Na^+	K^+	Ca^{++}	Mg^{++}	cations	D50.500	D50.2000	Fci
μ_{app} 50 s^{-1}	1.00																						
MLSS	0.93	4E-08	1.00																				
MLVSS	0.94	4E-08	1.00	1.00																			
HFV	0.95	2E-08	0.93	0.94	1.00																		
CODt	0.94	1E-08	0.96	0.97	0.94	1.00																	
SVI	0.47	0.0598	0.45	0.43	0.50	0.44	1.00																
CODs	0.13	0.6373	0.21	0.24	0.36	0.24	0.40	1.00															
S.an	0.67	0.0035	0.47	0.49	0.65	0.53	0.24	0.07	1.00														
S.cat	-0.07	0.8002	-0.17	-0.16	-0.17	-0.16	-0.24	0.30	0.08	1.00													
S.ni	0.69	0.0022	0.49	0.50	0.62	0.61	0.51	0.31	0.40	0.06	1.00												
surfact.	0.57	0.0167	0.35	0.37	0.49	0.43	0.22	0.40	0.70	0.64	0.66	1.00											
σ@(20°C)	-0.68	0.0029	-0.47	-0.49	-0.64	-0.58	-0.15	-0.05	-0.73	-0.13	-0.48	-0.63	1.00										
pH	-0.23	0.5822	-0.41	-0.40	-0.31	-0.33	-0.45	-0.34	0.14	0.35	0.00	0.29	-0.10	1.00									
AS Density	0.15	0.6371	0.24	0.25	0.26	0.25	-0.24	-0.37	0.28	0.38	-0.06	0.18	-0.07	-0.93	1.00								
Na^+	-0.31	0.2428	-0.29	-0.29	-0.25	-0.28	-0.57	-0.10	-0.27	0.32	-0.24	-0.05	-0.05	-0.37	0.31	1.00							
K^+	-0.02	0.9429	-0.08	-0.06	0.08	-0.02	-0.50	-0.08	0.04	0.28	0.00	0.18	-0.40	-0.12	0.26	0.92	1.00						
Ca^{++}	-0.24	0.3809	-0.22	-0.21	-0.15	-0.22	-0.69	-0.55	-0.04	-0.08	-0.34	-0.22	-0.13	0.61	0.29	0.69	0.70	1.00					
Mg^{++}	-0.20	0.4560	-0.17	-0.17	-0.24	-0.15	-0.83	-0.52	-0.01	0.09	-0.38	-0.13	-0.09	0.80	0.34	0.41	0.45	0.79	1.00				
cations	-0.26	0.3332	-0.25	-0.24	-0.19	-0.24	-0.71	-0.40	-0.11	0.11	-0.31	-0.13	-0.14	0.85	0.32	0.88	0.87	0.95	0.72	1.00			
D50-500	-0.73	0.2685	-0.60	-0.64	-0.64	-0.41	-0.70	-0.55	-0.64	-0.14	-0.44	-0.45	0.31	0.50	-	0.49	0.53	0.73	0.93	0.67	1.00		
D50-2000	-0.62	0.3808	-0.48	-0.47	-0.46	-0.22	-0.63	-0.42	-0.71	-0.26	-0.34	-0.51	0.22	0.35	-	0.40	0.48	0.72	0.90	0.63	0.96	1.00	
Fci	-0.55	0.4526	-0.38	-0.36	-0.34	-0.10	-0.56	-0.37	-0.75	-0.33	-0.28	-0.55	0.20	0.23	-	0.35	0.44	0.70	0.85	0.59	0.90	0.99	1.00

σ@(20°C) : static surface tension at 20°C

Table IV.5 Correlation Pearson coefficients (r) and corresponding p-value between apparent viscosity estimated (μ_{app}) at a shear rate of 400 s^{-1} and activated sludge characteristics.

	μ_{app} 400 s^{-1}	p-value
μ_{app} 400 s^{-1}	1.00	
MLSS	0.96	3E-10
MLVSS	0.96	5E-10
HFV	0.95	6E-9
CODt	0.94	9E-9
SVI	0.51	0.0315
CODs	0.27	0.2922
S.an	0.52	0.0277
S.cat	-0.08	0.7511
S.ni	0.64	0.0041
surfact.	0.49	0.0393
σ@(20°C)	-0.56	0.0155
pH	-0.37	0.3247
AS Density	0.16	0.5947
Na^+	-0.25	0.3365
K^+	-0.01	0.9640
Ca^{++}	-0.24	0.3512
Mg^{++}	-0.27	0.3037
cations	-0.25	0.3424
D50-500	-0.80	0.1033
D50-2000	-0.68	0.2019
Fci	-0.59	0.2943

IV.3.1 Correlation between physicochemical characteristics of interstitial liquid and apparent viscosity

Regarding the soluble fraction, the soluble COD concentration varied between 19.9 and 35.3 mg L^{-1} with an average value of 27 mg L^{-1} for the different MLSS concentrations. The highest total surfactant concentration was 3.1 mg L^{-1}, being in general the anionic type the most concentrated surfactant (<1.7 mg L^{-1}). The surface tensions were very close to the values of clean water except for one sample that exhibited a surface tension of 68 mN m^{-1} which is also the sample with the highest surfactants concentration and highest MLSS concentration (10.2 g L^{-1}). The most concentrated cations were sodium and calcium (in average 99.2 and 177 mg L^{-1}, respectively) and in average, AS from all WWTPs presented similar concentrations of analysed cations (from 222 up to 253 mg L^{-1}) except for the AS from Briis-sous-Forges that presented an average of analysed of 146 mg L^{-1} (due to low concentrations measured for two samples [MLSS = 6.1 and 7.9 g.L^{-1}], the average for the three others samples is 216 mg.L^{-1}). The measured sludge density and pH values remained quite constant for the different samples with average values of 999 kg m^{-3} and 7.9 respectively.

For these mentioned concentrations and properties, no correlation was observed with respect to the apparent viscosity despite the fact that some Pearson correlation coefficients (r) showed some significance (in respect to μ_{app} at 50s^{-1}), such as non-ionic surfactants concentration and surface tension (respectively r=0.69 and r=-0.68 with p-values ~0.002).

IV.3.2 Correlation between physicochemical characteristics of particulate phase and the sludge apparent viscosity

IV.3.2.1 Impact of mixed liquor suspended solid concentration on apparent viscosity

Figure IV.3 presents the correlation between the MLSS concentration and the apparent viscosity at shear rates of 50 and 400s^{-1} for AS samples from all five wastewater treatment plants (Etampes, Olainville, Etrechy, Saint Vrain and Briis-sous-Forges) and obtained at the laboratory and on site. The error bars consider an error of 10% based on the experimental and the modelling error.

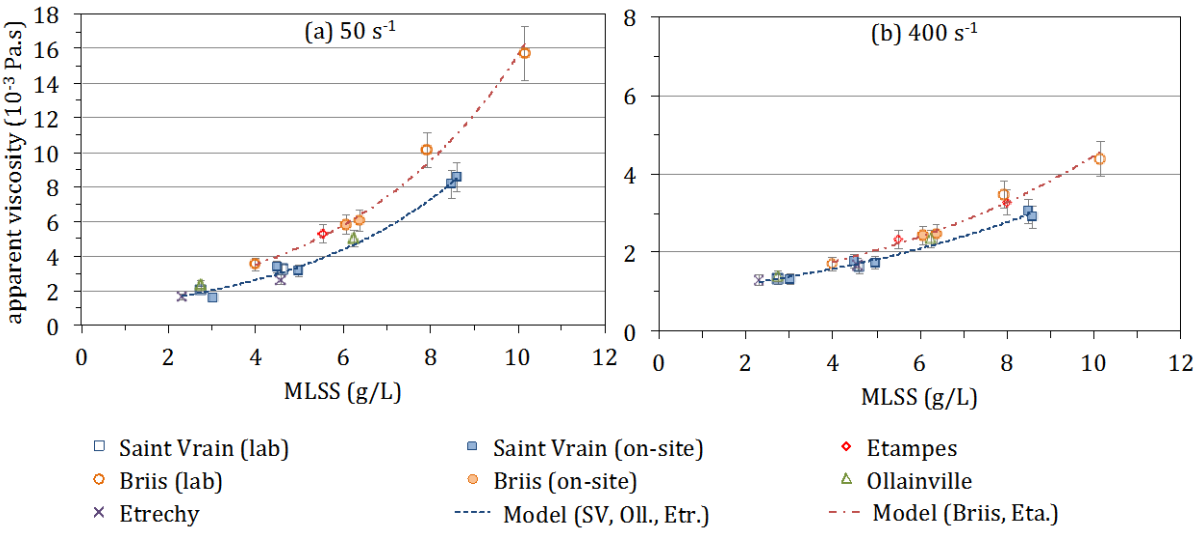

Figure IV.3. Apparent viscosity of municipal activated sludge from different wastewater treatment plants at shear rates of (a) 50 and (b) 400 s^{-1} versus the MLSS concentration. Laboratory and on-site results reported at **20°C**. Error bars=±10%.

For Briis and Saint Vrain WWTPs, for which measurements were performed in laboratory and on-site, no difference is observed between laboratory and on-site results. Therefore, in the following, these will not be distinguished.

For each studied WWTP, the apparent viscosity follows an exponential curve with an increment in the MLSS concentration. Even though the activated sludge samples come from different WWTPs, the sludge apparent viscosity appears to be significantly determined by the MLSS content. These tendencies confirm the observation of paragraph IV.2 on the impact of the MLSS concentration on AS rheology. This dependency is confirmed by the statistical analysis (cf. Table IV.4 and Table IV.5) where apparent viscosity exhibited a strong correlation with the MLSS concentration with Pearson correlation coefficients of r=0.93 and r=0.96 for μ_{app} at 50 and 400 s^{-1} respectively (p-values << 0.001).

Although the apparent viscosity is mainly controlled by MLSS concentration, some data dispersion is observed, highlighting that other sludge properties, intrinsic to the sludge origin, may have an incidence when defining the AS rheology. For the two represented shear rates (50 and 400 s^{-1}), the results of the sludge samples from the Briis-sous-Forges and Etampes WWTPs are systematically above the overall trend obtained for the three other sludge origins. The average difference between these two trends is +32% and +15% for shear rate of 50 and 400 s^{-1} respectively.

Different sludge properties closely correlated to the MLSS concentration such as the MLVSS concentration, the hydrostatic floc fraction (HFV)[3] and the total COD concentration, exhibit also a strong linear correlation with the apparent viscosity ($r=0.95$, p-value<0.001). Since the rheology of suspensions is conventionally referred as a function of the solids volumetric fraction (Baudez et al., 2004, Dupuis, 2102), it is of particular interest to evaluate the correlation between the apparent viscosity and the hydrostatic floc volume (HFV), which is a direct measurement of the volume occupied by the compressed solids. Because of the simple measurement protocol (cf. II.3) and the close relation that exhibits with the apparent viscosity ($r=0.95$), the hydrostatic floc volume (HFV) appears as an interesting property to evaluate the sludge apparent viscosity. It must be however highlighted that this characteristic could not systematically be estimated thoroughly because in some cases, not all flocs settled but remained floating due to degasification in the samples which implied a lack of accuracy in determining the volume occupied by the flocs. Moreover, the methodology employed for HFV determination could be criticized because of its measurement protocol in static operating conditions while HFV must be considered as shear rate dependant as developed in the following.

IV.3.2.2 Impact of other physicochemical characteristics of the particulate phase on apparent viscosity: Introducing the floc structure as an impacting parameter

Apart from the sludge properties related to the suspended solids, the other evaluated sludge characteristics showed less significant linear correlations with the apparent viscosity ($r<0.80$). In general, all samples exhibited adequate settling properties except for the sludge from Briis-sous-Forges which exhibited poor settling properties (SVI>155 mg L^{-1}) and floating aggregates.

IV.3.2.2.1 Introducing the floc structure to explain rheological data dispersion

The median floc size determined at 500 rpm ($D_{50\text{-}500rpm}$) and at 2000 rpm ($D_{50\text{-}2000}$ rpm) as well as the Floc cohesion index exhibit slight correlations with the apparent viscosity ($0.55<r<0.80$). However, the particle size is not sufficient to relate physical characteristics of the floc to the rheological behaviour of the sludge. Table IV.6 presents some information about the particle size but also the characteristics of the size distribution of the studied sludge sample.

[3] The hydrostatic floc volume (HFV) corresponds to the settled volume of an activated sludge sample (1L) in a graduated glass tube of 1 L after 24/48 hours of settling (Henkel 2010).

The D_{10}, D_{50} and D_{90} are presented in Table IV.6 to provide some characteristics of the floc size distribution for each sludge sample. For all studied sludge, these three parameters decrease with an increase in the stirring speed of the experimental apparatus showing the shear dependence of the floc size. The distribution's width ($\frac{D_{90}-D_{10}}{D_{50}}$) increases with an increment in the stirring speed. This increase is higher for Briis-sous-Forges, Etampes and Etrechy WWTPs than for other sludge origin, highlighting a heterogeneous break-up of the floc, due to a heterogeneous floc structure, with an increase in average shear rate.

Table IV.6 Characteristics of the floc size distribution for the studied WWTPs. The values indicated in the table correspond to the retained samples indicated in Table IV.3.

WWTP	Stirring speed (rpm)	D_{10} (µm)	D_{50} (µm)	D_{90} (µm)	$\frac{D_{90}-D_{10}}{D_{50}}$ (-)	$D_{3/2}$ (µm)	$D_{4/3}$ (µm)	$FCi_{D4/3}$ (-)
Saint Vrain	500	43.1	118	281	2.02	73.2	147	0.80
	2000	30.4	92.5	224	2.09	55	118	
Ollainville	500	37.1	106	246	1.97	63.6	133	0.82
	2000	20.8	61.4	148	2.07	28.9	109	
Etrechy	500	32.5	101	235	2.00	60.9	129	0.75
	2000	17.4	56.5	165	2.61	36.4	96.4	
Etampes	500	25.3	89.7	219	2.16	50.2	115	0.60
	2000	14.6	49.6	136	2.45	29.6	69.4	
Briis	500	23.3	86.6	229	2.38	49.6	118	0.53
	2000	13.5	40.1	133	2.98	26.9	62.6	

D50 is the diameter below which lies half of the population (the median). Similarly, 90 percent of the distribution lies below diameter D90, and 10 percent of the population lies below diameter D10. D3/2 and D4/3 are respectively the surface and volume mean diameters of the flocs. FCiD4/3 is the floc cohesion index calculated using D4/3 values.

The mean volume diameter ($D_{4/3}$) is determined using the floc size distribution for all studied sludge. This mean volume is characteristic of the floc size constituting the bulk of the sludge sample and of the mean volume occupied by the floc.

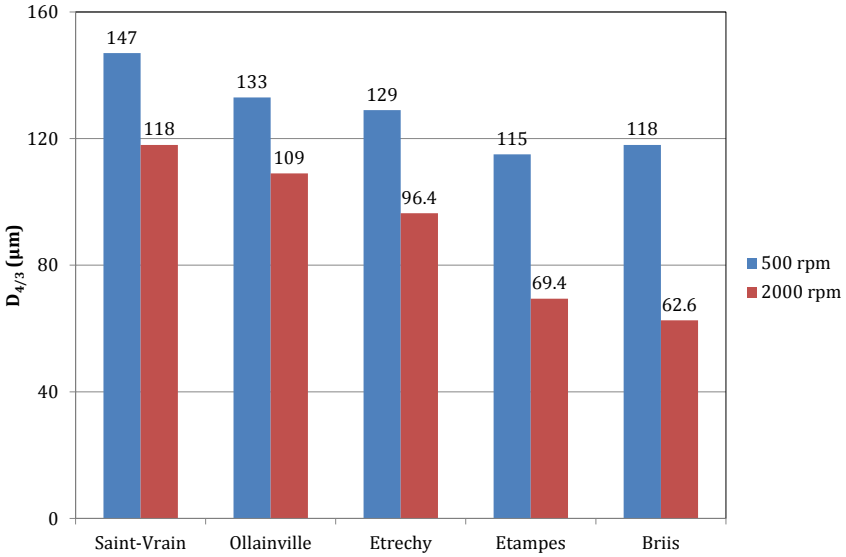

Figure IV.4. Mean volume floc diameter ($D_{4/3}$) for each studied sludge and stirring speed.

The mean volume floc diameter ranges within 115 and 147 µm for a stirring speed of 500 rpm and ranges from 63 to 118 µm for a stirring speed 2000 rpm. For a fixed stirring speed, the volume mean diameter is dependant of the sludge origin. The highest mean volume floc diameters are measured for Saint Vrain WWTP sample, and the lowest ones are obtained for Etampes and Briis-sous-Forges (Figure IV.4).

The floc cohesion index based on the mean volume diameter is presented in Table IV.6. The Floc cohesion index ($Fci_{D4/3}$) varies between 0.53 and 0.82, being the highest values for AS from Ollainville and the lower values for the AS from Briis-sous-Forges. After intensive shearing conditions (2000 rpm), the floc diameter of the sludge from Briis-sous-Forges is reduced by more than 50% in relation to the diameter measured at lower shear conditions (500 rpm). Activated sludge from different origins would have distinct floc cohesion indexes because different operating conditions (organic load, dissolved oxygen, sludge retention time) induce the production of different EPS concentrations and types by the microorganisms (Mikkelsen and Keiding, 2002; Jin *et al.,* 2003; Wilen *et al.,* 2003).

This floc cohesion index provides some indication about the complex floc structure and the internal connection (strong and loose bonds) within the floc. The biological flocs have a multi-scale structure, with a loosely packed global structure and a compactly packed local structure (Chu and Lee, 2004). When the flocs are submitted to an increment in shear rate, some of the loose bonds are broken, inducing a decrease in mean volume floc size. The strength of the loosely bonds depends on the sludge origin and the conditions in which the floc have been constituted.

In parallel to the present study, microscopic observations of activated sludge samples from four out five WWTPs (Saint-Vrain, Ollainville, Briis-sous-Forges and Etampes) were performed with the aim of evaluating the flocs structure. The obtained images show that the flocs structure from Saint Vrain and Ollainville is irregular, compact and dense (Figure IV.5) and those from Briis-sous-Forges and Etampes are irregular, diffuse and loose (Figure IV.6). These two results could characterize the floc structure and its density.

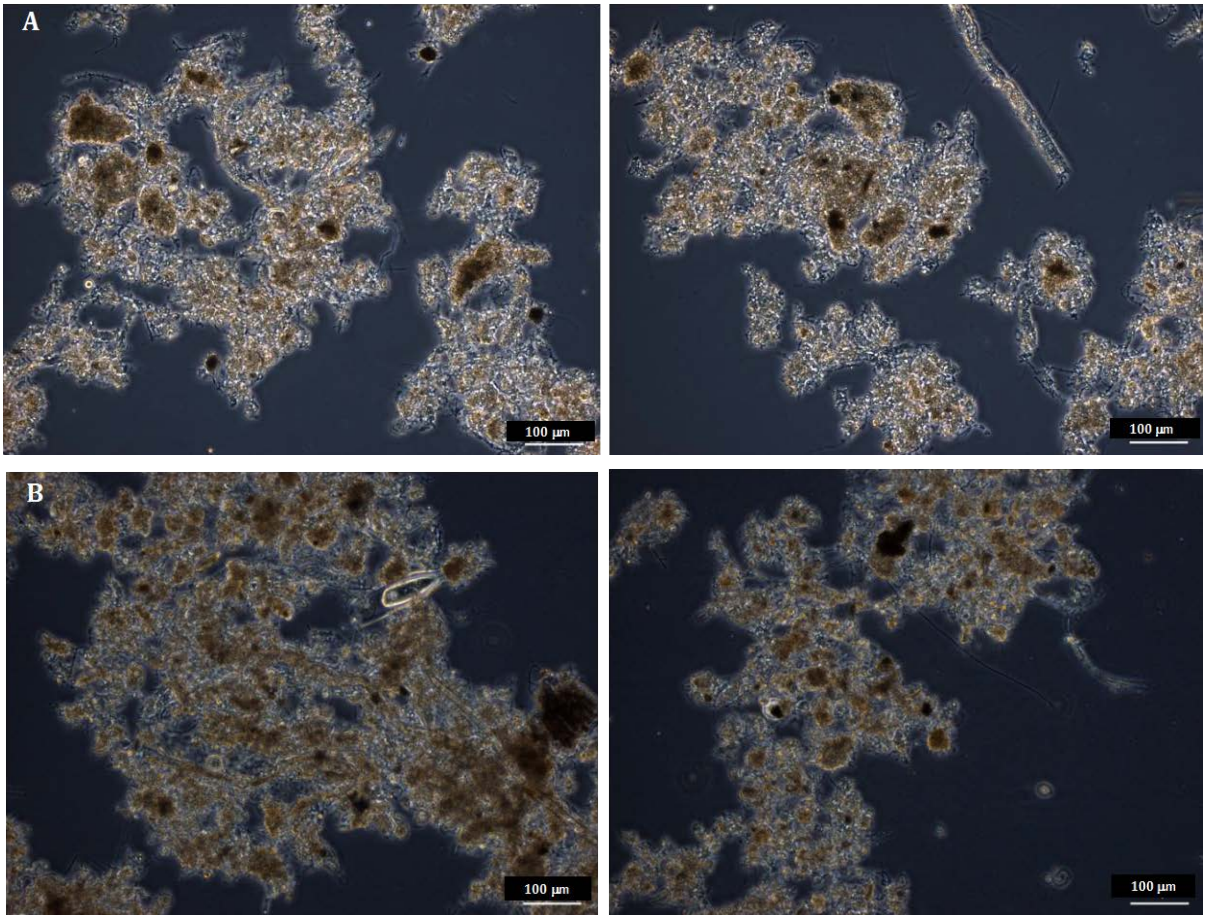

Figure IV.5. Microscopic images of activated sludge flocs from Saint Vrain (A) and Ollainville (B)

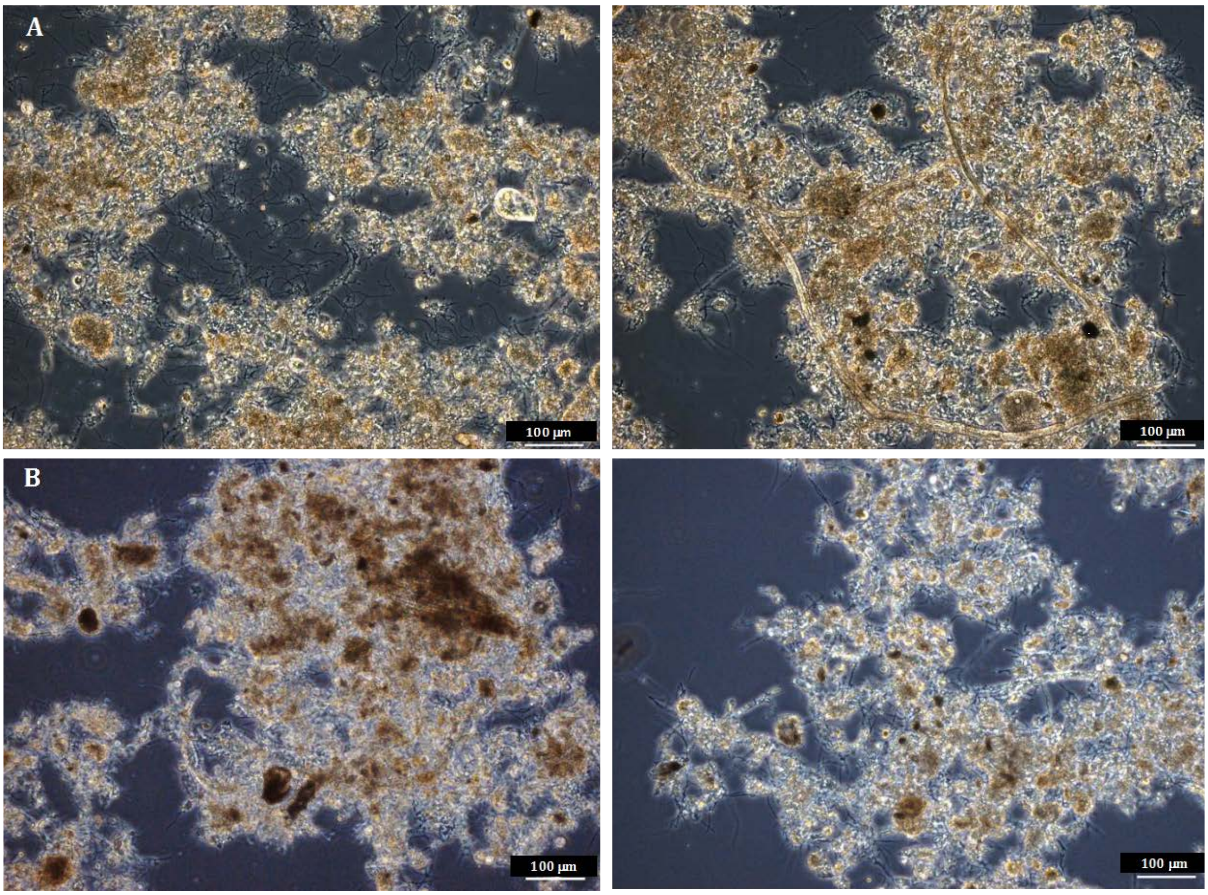

Figure IV.6. Microscopic images of activated sludge flocs from Briis-sous-Forges (A) and Etampes (B).

As highlighted by the microscopic observation, the AS having exhibited the highest floc cohesion index, Saint-Vrain or Ollainville, have also a denser floc structure. On the contrary, AS from Briis-sous-Forges and Etampes contain loose flocs with an easily breakable internal connection, which is linked to the obtained low floc cohesion index.

Analysis

According to these results, the floc structure is heterogeneous and depends on the sludge origin. This difference in floc structure could have an impact on the rheological characteristics of the sludge.

For a given MLSS concentration, the floc size and density define the total volume occupied by the floc. For a same quantity of material, looser flocs (*i.e.* with a lower density) will induce a higher total volume of the solid phase at the micro-scale. As the total volume occupied by the solid phase increases, the floc interaction frequency (by collision or friction) increases too, inducing higher viscosity at the meso-scale.

This hypothesis could explain the different apparent viscosity trends observed for Briis-sous-Forges/Etampes and other sludge origins (Figure IV.3). Etampes and Briis-sous-Forges sludge structure is close in terms of mean volume floc diameter (respectively 115 and 118µm for 500 rpm and 69.4 and 62.6µm for 2000 rpm) and floc cohesion index (0.60 and 0.53). For the two different stirring velocities, the mean volume floc diameter and floc cohesiveness measured for these two sludge samples is lower than for sludge from Saint Vrain/Ollainville/Etrechy ($D_{4/3[500\ rpm]}$ from 129 to 148 µm; $D_{4/3\_[2000\ rpm]}$ from 96.4 to 118 µm; $FCi_{D[4/3]}$ from 0.75 to 0.82), traducing denser structures for these latter samples, confirmed by microscopic observation. This difference in floc structure between these two groups of samples is translated in terms of apparent viscosity, with higher viscosity for looser floc structure as observed in (Figure IV.3).

Denser floc with higher cohesiveness such as for Saint-Vrain/Etrechy/Ollainville WWTPs could have a different response under shearing conditions due to higher particle deformability. The more cohesive flocs would modify their shape under shearing instead of breaking up and reducing the floc diameter (the more cohesive flocs are in fact the ones with the larger diameters). According to Dupuis (2012), the shear-thinning character of suspensions is accentuated as the rigidity of the particles is reduced and particles deformability increases: deformable (and cohesive) particles tend to line up on the streamlines with an increment of the shear rate as previously mentioned which leads to lower resistance to flow and reduce viscosity in consequence (shear-thinning behaviour).

Finally, the release of EPS and SMP (soluble microbial products) from the flocs to the interstitial liquid during floc breakage induced by a shear rate increase could have an impact on the apparent viscosity of the sludge sample. However, the order of magnitude of the impact of such substances on the sludge rheology evolution at the meso-scale needs to be evaluated.

Considering the impact of these sludge characteristics on rheological behaviour, in addition to the MLSS concentration, could improve the understanding as well as the prediction tools developed in respect to activated sludge rheology. However, a better evaluation of the floc density and the parameters affecting it is needed to link the apparent viscosity to the floc structure.

IV.3.2.2.2 Critical consideration with regards to rheological experiments for AS and its impact on floc structure

The concept of the influence of floc structure on the sludge rheological behaviour, discussed in the previous paragraphs, could be very useful in order to define good experimental practice for rheological characterisation of activated sludge.

Figure IV.7, presented by Ratkovich *et al.* (2013), compares the evolution of apparent viscosity obtained with a given activated sludge sample (MLSS = 5.7 g L^{-1}) under two different experimental procedures (two different shear rate ramps): (i) from 1 s^{-1} to 1000 s^{-1} and back to 1 s^{-1} and (ii) from 1 s^{-1} to 100 s^{-1} and back to 1 s^{-1}. For these two sequences, the apparent viscosity decreases with increasing shear rate and increases when shear rate is back to 1 s^{-1}. However, a different hysteresis is observed for each of the two sequences, with lower values of apparent viscosity obtained when shear rate decreased than when shear rate was incremented. Moreover, while the apparent viscosity values obtained with the increasing shear rate ramps overlap, those obtained with the decreasing shear rate ramps are not equivalent.

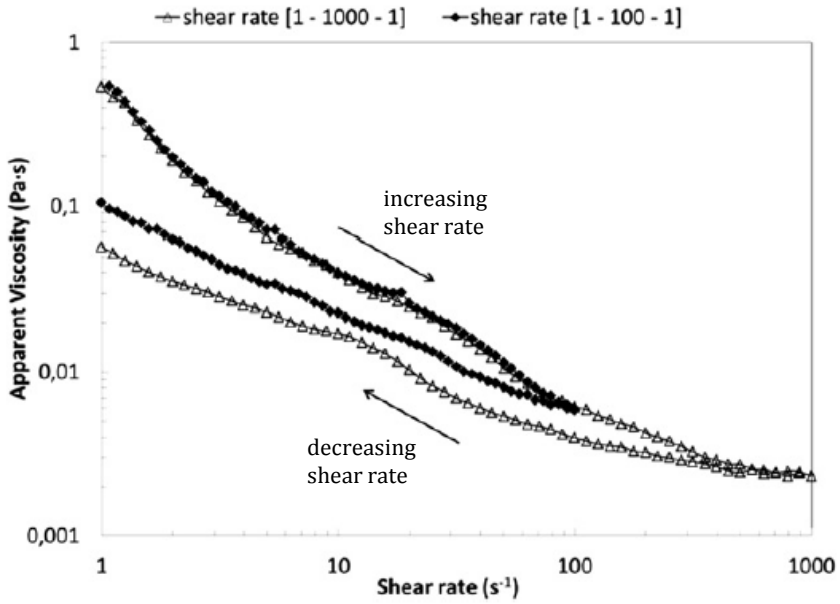

Figure IV.7. Apparent viscosity measured under two different shear rate ramps (i) 1→1000→1 s^{-1} and (ii) 1→100→1 s^{-1}) with the same MBR AS sample (MLSS 5.7 g L^{-1}) and same rotational rheometer (Anton Paar rheometer type MCR101 with double gap cylinder (0.5 mm gap size) and air bearing) (Data: Osnabrück University of Applied Sciences) – Extracted from Ratkovich *et al.* (2013).

Analysis

As observed on Figure IV.8, the floc size is shear rate dependent. A rapid decrease in the floc size is observed for an increase in the shear rate (related to the stirring speed). On the contrary, flocculation is a longer process; a period of about 30 minutes is required to reach the floc initial size after reducing the shear rate.

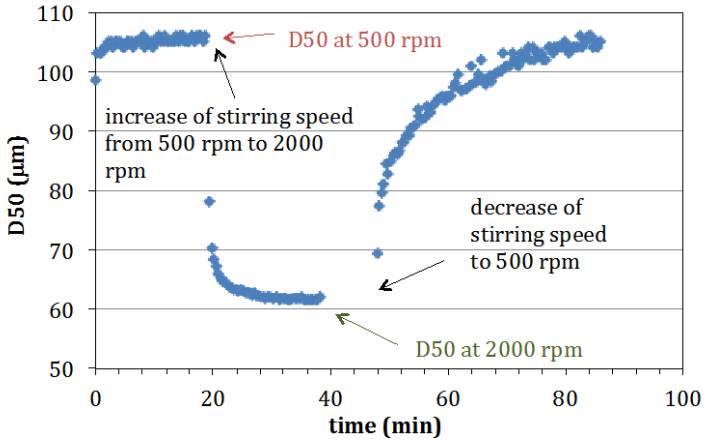

Figure IV.8. Median floc equivalent diameter under two different shear conditions: 500rpm→ 2000 rpm → 500 rpm.

The hysteresis phenomenon observed in Figure IV.7 indicates that the history of experienced shear has an impact on activated sludge apparent viscosity. Since the impact of increasing shear rate on floc size reduction is almost immediate, each measurement point obtained during the increasing ramp could be considered as adequate because the AS floc structure reaches rapidly steady state conditions. That explains why both trends obtained under the two increasing shear rate ramps are similar: the AS has the same MLSS concentration and has attained the same stable floc structure (linked to a same shear rate).

On the contrary, when the shear rate is reduced, the obtained trend is different compared to the other shear rate decreasing ramp and compared to the increasing shear rate ramp. Considering the impact of shear on the floc structure and the time lapse of the floc aggregation/breakage dynamics, these different trends could be attributed to the difference in the floc structuration at the micro-scale. Between the two shear decreasing ramps, the main difference is the shear rate applied initially (respectively 1000 and 100 s^{-1}). As the floc aggregation is a slow process, the floc size is different between the two rheograms during the increasing shear rate ramp. For a same shear rate, the floc size is lower when the initial shear rate is 1000 s^{-1} instead of 100 s^{-1}. Since the floc structure is heterogeneous, it could be considered that the loose bonds are first impacted during the floc breakage, inducing an overall denser floc structure in the sample. Thereby, the total volume occupied by the floc decreases. Moreover, for a given sludge type, lower floc size could induce a better floc arrangement in the streamlines resulting in lower resistance to flow and a decrease in apparent viscosity at the meso-scale.

Such experimental observation could be explained by determining the "granulometric signature" of the activated sludge (by measuring the floc size evolution for a shear rate range) with an appropriate methodology. Introducing such floc size characteristics, and its shear rate

dependence, would lead to a dynamic model of the activated sludge rheology with variable apparent viscosity for a shear rate, related to the historic shear rate of the sludge.

In the context of good experimental practice, rheological measurements must be performed with increasing shear rate ramps to measure the apparent viscosity of the activated sludge with the "real" floc structure linked to the shear rate. In addition, pre-treatment of the sample must be performed carefully in order to avoid an impact on the floc structure that could induce experimental errors.

Conclusions on the impact of sludge properties on its rheological behaviour

- The rheological behaviour of activated sludge is strongly determined by the sludge MLSS concentration, even for sludge samples that have different origins.

- However the correlation between sludge MLSS concentration and apparent viscosity exhibits some data dispersion beyond the estimated uncertainty (±10%) in particular at low shear rates (50 s^{-1}). Specially, AS from Briis-sous-Forges and Etampes, exhibited systematically higher values of apparent viscosity compared to AS from the other three WWTPs. It is suggested that other sludge property contributes, together with MLSS concentration, to define the sludge rheological behaviour.

- The sludge properties closely related to the MLSS concentration such as MVLSS, total COD, hydrostatic floc volume (HFV) showed a strong correlation with the sludge apparent viscosity. Among these, the MLSS concentration exhibited the best correlation with apparent viscosity following an exponential curve.

- The AS rheological behaviour is also defined by floc characteristics such as size, cohesiveness and density. These properties, related to the sludge origin and history, could explain the different trends of apparent viscosity as a function of the MLSS concentration for sludge from different WWTPs. Related to the floc size and density for a given MLSS concentration, the floc structuring and the total volume occupied by the solid phase have an impact on the flocs interaction hence differentiating the AS rheological characteristics. This AS rheology dependence on physical characteristics of the floc is also useful to explain the rheogram dependence to measurement conditions, as observed in literature, related to the shear dependence of the floc size.

IV.4 Modelling the rheological behaviour of activated sludge

IV.4.1 Evaluation of existing models

Several models have been proposed in literature to represent AS rheology. The main ones, described in § I.3.4.2 and represented in Figure I.16, are reported in Table IV.7.

Table IV.7. Rheological equations mainly used in literature to represent AS rheological behaviour.

Model	Expression	Number of parameters
Ostwald-de Waele	$\tau = K \cdot \dot{\gamma}^n$	2
Bingham	$\tau = \tau_y + K \cdot \dot{\gamma}$	2
Casson	$\sqrt{\tau} = \sqrt{\tau_y} + \sqrt{\mu_\infty \dot{\gamma}}$	2
Herschel-Bulkley	$\tau = \tau_y + K \cdot \dot{\gamma}^n$	3
Sisko	$\tau = K \cdot \dot{\gamma}^n + \mu_\infty \dot{\gamma}$	3

Each of these models was adjusted to the experimental rheograms by minimizing the sum of squared residuals (RSS) between the experimental data and the modelled data. A colour-based evaluation was used to depict the results (Table IV.8) in terms of sum of squared residuals per number of experimental points per rheogram (RSS/N). For each rheogram, underlined and **bold type** values indicate the model providing the less adequate and the best adjustments respectively. The bottom line in Table IV.8 corresponds to the sum of the RSS for the five different models.

Table IV.8. Residual sum of squares (RSS) obtained after adjusting the rheological models to the each one of the experimental rheograms.

WWTP	MLSS (g/L)	Ostwald	Bingham	Casson	Herschel-Bulkey	Sisko
Etrechy	2.3	*1.73E-05*	**8.12E-06**	1.16E-05	**8.12E-06**	**8.12E-06**
Ollainville	2.7	*8.03E-05*	**1.23E-05**	3.48E-05	**1.23E-05**	5.43E-05
Saint Vrain	2.8	*5.09E-05*	**2.33E-05**	3.07E-05	**2.33E-05**	**2.33E-05**
Saint Vrain	3.0	*2.20E-05*	2.14E-05	2.10E-05	**2.06E-05**	2.10E-05
Briis	4.0	4.00E-05	*1.11E-04*	**7.94E-06**	8.47E-06	1.69E-05
Saint Vrain	4.5	*1.41E-04*	**3.58E-05**	6.44E-05	**3.58E-05**	**3.58E-05**
Saint Vrain	4.6	5.05E-05	*1.65E-04*	7.56E-05	**4.87E-05**	5.01E-05
Etrechy	4.6	*1.48E-04*	**5.30E-05**	9.15E-05	**5.30E-05**	6.04E-05
Saint Vrain	5.0	2.52E-05	*7.56E-05*	2.71E-05	**1.96E-05**	2.02E-05
Etampes	5.5	*2.56E-04*	**1.10E-04**	1.18E-04	**1.10E-04**	**1.10E-04**
Briis	6.1	1.28E-04	*2.91E-04*	9.77E-05	**8.07E-05**	8.26E-05
Ollainville	6.2	1.03E-04	*2.20E-04*	**9.97E-05**	1.03E-04	1.03E-04
Briis	6.4	1.66E-04	*3.88E-04*	1.53E-04	1.33E-04	**1.22E-04**
Briis	7.9	1.36E-04	*9.38E-04*	2.55E-04	**1.05E-04**	1.16E-04
Etampes*	8.0	**2.78E-05**	*3.41E-04*	1.23E-04	**2.78E-05**	**2.78E-05**
Saint Vrain	8.5	5.26E-04	*5.55E-04*	3.45E-04	3.52E-04	**3.40E-04**
Saint Vrain	8.6	4.31E-04	*1.17E-03*	6.28E-04	**4.29E-04**	4.31E-04
Briis	10.2	2.08E-03	6.24E-04	*2.76E-03*	**6.20E-04**	6.21E-04
Σ RSS/N		4.42E-03	5.15E-03	4.95E-03	**2.19E-03**	2.24E-03

* For this sample, rheological measurements were performed in a shear rate range between 120 and 400 s^{-1}.

Independently on the MLSS concentration, the Herschel-Bulkley and Sisko models provide more frequently than the two-parameter models the best adjustment to the experimental rheograms. The lowest values of the Σ RSS/N are in fact obtained with the use of these two equations.

Obviously, models with two theological parameters (Ostwald-de Waele, Bingham and Casson) provide higher RSS values than 3-parameter models. Among these 2-parameter models, the Ostwald model provides the best adjustment considering the group of rheograms (lowest Σ RSS/N), though it is only once the best fit and seven times the poorest adjustment for each of the flow curves (mostly MLSS < 5.0 g L^{-1}). On the contrary, the Bingham model proposes the best fits for six rheograms (all with MLSS < 5.5 g L^{-1}) and is mainly the poorest fit for rheograms obtained for sludge with MLSS > 5.5 g L^{-1}. Besides, the Casson model provides twice the best fit, and only once the poorest adjustment.

In addition, model fits seem to be generally better when the MLSS concentrations are below 5.0 g L^{-1}.

Table IV.9 presents the minimal and maximal relative error as well as the average relative error obtained after adjusting each of the mentioned rheological models to each of the experimental flow curves.

Table IV.9. Interval of relative error (%) and average error (%) obtained after adjusting the rheological models to the each of the experimental rheograms. Samples are listed according to a MLSS concentration increasing order.

WWTP	MLSS (g/l)	Ostwald			Bingham			Casson			Herschel - Bulkley			Sisko		
		Min	Max	Avg.	Min	Max	Avg.	Min	Max	Avg.	Min	Max	Avg.	Min	Max	Avg.
Etrechy	2.3	0.1	7.4	1.8	0.1	3.6	1.1	0.0	5.4	1.4	0.1	3.6	1.1	0.1	3.6	1.1
Ollainville	2.7	0.5	5.6	3.3	0.0	3.1	1.1	0.3	3.3	1.9	0.0	3.1	1.2	0.4	4.1	**2.6**
Saint Vrain	2.8	0.1	**11.7**	3.3	0.0	6.3	2.2	0.2	7.9	2.7	0.0	6.3	2.2	0.0	6.3	2.2
Saint Vrain	3	0.1	9.1	2.5	0.1	6.9	2.4	0.2	7.9	2.5	0.2	**7.7**	2.5	0.2	7.7	2.5
Briis	4	0.3	5.0	1.6	0.5	5.0	2.8	0.1	1.8	0.7	0.0	1.6	0.7	0.0	2.7	1.1
Saint Vrain	4.5	0.3	9.3	3.5	0.0	6.1	1.4	0.1	6.1	2.2	0.0	6.1	1.4	0.0	6.1	1.4
Saint Vrain	4.6	0.1	2.9	1.6	0.4	7.7	2.7	0.0	3.3	1.5	0.2	2.5	1.4	0.2	2.7	1.5
Etrechy	4.6	0.0	10.8	**3.9**	0.2	5.9	2.0	0.2	8.2	2.9	0.2	5.9	2.0	0.1	6.4	2.2
Saint Vrain	5	0.0	8.1	1.4	0.3	7.4	2.5	0.0	5.6	1.6	0.2	5.2	1.4	0.3	5.8	1.4
Etampes	5.5	0.0	9.3	2.6	0.1	3.1	1.2	0.4	4.5	1.6	0.1	3.1	1.2	0.2	3.2	1.2
Briis	6.1	0.4	3.8	1.8	1.1	7.1	2.8	0.1	0.0	1.1	0.1	2.5	0.8	0.0	2.6	0.9
Ollainville	6.2	0.0	5.1	1.9	0.1	4.3	1.9	0.0	2.5	1.2	0.1	5.1	1.9	0.0	5.1	1.9
Briis	6.4	0.4	2.6	1.4	0.1	10.5	3.1	0.4	4.9	1.8	0.0	2.1	1.4	0.1	2.1	1.3
Briis	7.9	0.1	4.2	1.2	0.2	**11.1**	3.1	0.2	6.9	1.6	0.0	3.7	1.1	0.1	3.8	1.1
Etampes	8	0.3	0.8	0.5	0.0	4.1	1.8	0.3	2.3	1.1	0.3	0.8	0.5	0.3	0.9	0.5
Saint Vrain	8.5	0.5	5.9	2.9	1.4	7.4	3.4	0.3	5.4	2.3	0.2	5.5	2.4	0.3	5.3	2.3
Saint Vrain	8.6	0.2	8.2	2.6	0.1	10.9	**3.8**	0.3	7.0	2.9	0.3	**7.7**	**2.6**	0.2	**8.2**	**2.6**
Briis	10.2	0.5	9.0	3.5	0.7	4.1	1.9	0.2	**9.4**	**3.8**	0.2	4.1	1.8	0.1	4.2	1.8

For a given rheogram, the maximal relative error obtained with the models that generally provided the best adjustment to the experimental rheograms, the Herschel-Bulkley and Sisko equations, can reach 7.7% and 8.2%, respectively, and the average relative error provided by these two models is in all cases lower than 2.6%. Concerning the Ostwald-de Waele, Bingham and Casson models, their adjustement to a given rheogram results in a maximal relative error of 11.7%, 11.1% and 9.4% respectively, and the obtained average error is always lower than 3.9%.

Analysis

The Herschel-Bulkley and Sisko equations are the models that best reproduce each of experimental rheograms which is logical as they integrate three parameters and provide therefore more degrees of freedom than the two-parameter models. However, for some experimental rheograms, the RSS value obtained with a two-parameter model is sometimes not different from the RSS value obtained with a three-parameter model. On the one hand, when the RSS value estimated using the Herschel-Bulkley equation equals the RSS value of the Bingham equation, the value of the Flow index (n) integrated by the Herschel-Bulkley models equals one and the two models become identical. On the other hand, when the RSS value obtained using the Sisko model equals the RSS value of the Ostwald model, the value of the Limit viscosity (μ_∞) integrated by the Sisko model, is close to zero and the equations are no longer different. Same observations can be made when the Herschel-Bulkley and the Ostwald models are concerned by an equal RSS value; the value of the Yield stress (τ_y) introduced by the Herschel-Bukley is zero

and consequently converts to the Ostwald model. In these cases, only two rheological parameters appear to be necessary to model the experimental flow curves, 3-parameter models are over parameterized as stated by Ratkovich *et al.* (2013). This will be further analysed in the following section (IV.4.1.1).

Besides, the capacity of the Ostwald-de Waele and the Bingham models to represent each of the experimental rheograms appears to be related to the sludge MLSS concentration. While the Ostwald model reproduce generally better the rheograms obtained with sludge at MLSS concentrations above 5.0 g L^{-1}, the Bingham model reproduce generally better the experimental flow curves obtained with sludge at lower MLSS concentrations. This alternated better adjustment can be explained as follows: the Flow index (n) in the Ostwald equation allows the model to freely reproduce the curvature obtained in the experimental rheograms, which is especially pronounced for those obtained with sludge at MLSS concentration above 5.0 g L^{-1}. Instead, the Bingham equation does not have the capacity to reproduce the observed curvature and the modelled rheograms separate from the experimental flow curves. At lower MLSS concentrations, the Ostwald equation forces the modelled rheograms to start at the origin since it does not integrate a Yield stress (τ_y), which results in deviating its trend from the experimental rheogram. Instead, because the Bingham model integrates this rheological parameter (τ_y), the modelled rheogram is able to follow more accurately the trend of the experimental rheogram. Additionally, the experimental rheograms obtained with sludge at MLSS concentrations below 5.0 g L^{-1} presented trends that appear more like straight lines which is convenient for the Bingham equation to reproduce them suitably.

If the Casson model provides rarely either the best or the poorest fit to the experimental data, this appears to be reasonable as in fact this equation allows reproducing the main characteristics observed in the experimental rheograms presented above. First, it integrates the Yield stress (τ_y), which avoids introducing errors by forcing the model to initiate at the origin instead of starting from the abscissa when required. Second, the equation allows the modelled rheograms to reproduce the curvature observed specially for flow curves obtained at MLSS concentrations above 5.0 g L^{-1}, even though the model fixes the curvature by integrating a constant exponent.

Conclusions

- The ability of five different rheological equations to reproduce each of 18 experimental rheograms of activated sludge from five different WWTPs and with MLSS concentrations between 2.3 and 10.2 g L^{-1} was evaluated.
- Logically, the three-parameter models provided generally a better adjustment to the experimental rheograms than the two-parameter models, although similar fits were occasionally obtained with the two types of model.
- The suitability of the Ostwald and Bingham equations to model each of the experimental rheograms appears to be related to the MLSS concentration. The Ostwald equation is more adequate to reproduce the rheograms obtained with sludge at MLSS concentrations higher than 5.0 g L^{-1}, the Bingham model is more suitable to reproduce the flow curves obtained with sludge at lower MLSS concentrations.

IV.4.1.1 Correlation between rheological parameters and MLSS concentration

Figure IV.9 presents the rheological parameters of the Ostwald-de Waele, Bingham, Casson, Herschel Bulkley and Sisko models, as a function of the MLSS concentration. These were obtained by adjusting each rheological equation to the 18 different experimental flow curves.

For the Ostwald-de Waele and Bingham models (Figure IV.9 a and b respectively), the Consistency index (K) increases exponentially with the MLSS concentration. Similarly to the increase of the sludge apparent viscosity with an increment in the MLSS concentration, this trend is usually explained by an increase in the number of interaction between particles that consequently move less freely and exert more resistance to flow. Although the Consistency index (K) has the same physical meaning for both models, it is noted that their order of magnitude is not in the same range. The Flow index (n) of the Ostwald-de Waele equation is reduced exponentially as the MLSS content increases, thereby accentuating the shear-thinning character of the activated sludge. Concerning the Yield stress (τ_y) of the Bingham model, it increases in a power law trend with the MLSS concentration. This trend is explained by an augmentation in the particle interaction "at rest" (Baudez *et al.,* 2004) with the increase in the particle content. Since the lowest applied shear rate in this study was 50 s^{-1}, this rheological parameter, was not

measured experimentally. Hence, the mentioned Yield stress (τ_y) consists of an estimated value issued from the adjustment of the rheological equation to the experimental flow curves.

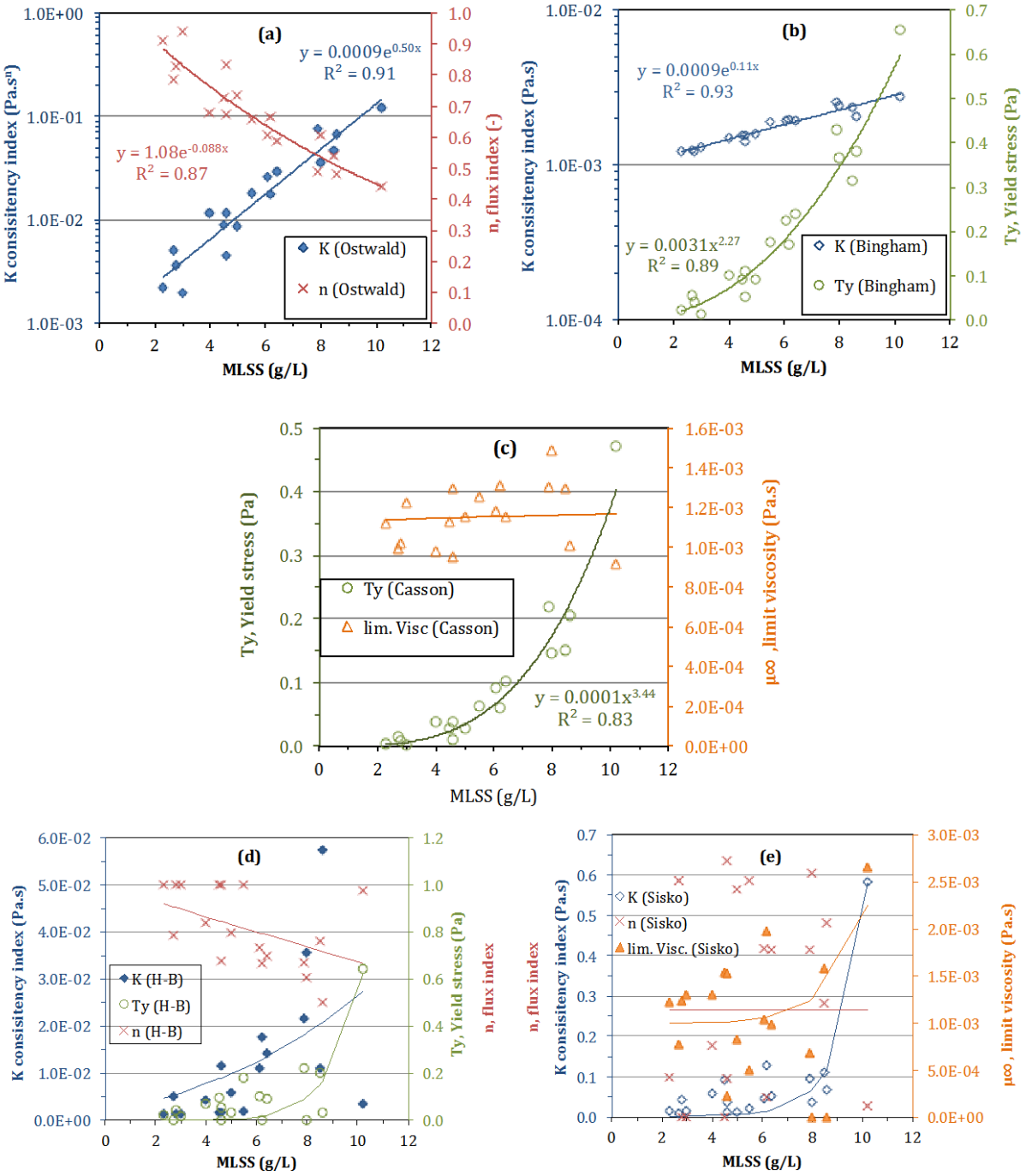

Figure IV.9. Rheological parameters versus activated sludge MLSS concentration for the rheological equations of (a) Ostwald-de Waele, (b) Bingham, (c) Casson, (d) Herschel Bulkley and (e) Sisko.

Although the rheological parameters from the Ostwald-de Waele and the Bingham models exhibit a close correlation with the sludge MLSS concentration, those from the Ostwald-de Waele model show slightly more dispersion.

Concerning the rheological parameters of the Casson model (Figure IV.9 c), the Yield stress (τ_y) presents a good correlation with the MLSS concentration. Similarly to the Yield stress of the Bingham model, it increases with the MLSS content following a power trend. On the contrary, the Limit viscosity (μ_∞) exhibits a poor correlation with the sludge MLSS concentration and it is difficult to determine the parameter trend, putting into question a potential problem of identifiability.

Concerning the Herschel-Bulkley and Sisko equations, their parameters appear to be weakly correlated to the sludge MLSS concentrations. It is evident in these figures that considering a third parameter to reproduce the group of experimental results led to a significant increase of data scattering. A similar increase of data dispersion using the Herschel Bulkley equation was observed in the modelling work of activated sludge rheology presented by Rosenberger *et al.* (2006). As later stated by Ratkovich *et al.* (2013), this model over parameterization leads to hide the true underlying relation between the rheological parameters and the sludge properties. Indeed, the use of such over parameterized equations results in unidentifiable parameters since multiple sets of parameters may provide a suitable fit to the experimental data.

In order to reduce the data dispersion of the Herschel-Bulkley rheological parameters observed in Figure IV.9 (d), a similar analysis to the one proposed by Baudez *et al.* (2004) was applied. The authors used the Herschel-Bulkley model to represent the rheological behaviour of sewage sludge, but fixed the Flow index (n) to a constant value. For 48 sewage sludge samples from 6 different wastewater treatment plants the authors estimated n to be around 0.45.

In the present work, the Flow index (n) was then kept constant and the Herschel-Bulkley model was adjusted to each of the 18 experimental rheograms and the rheological parameters τ_y and K were obtained. Parameter estimation led to a Flow index value of 0.96 to get the most significant reduction of the observed data scattering. The correlation between the rheological parameters of the Herschel-Bulkley model with a fixed Flow index (n=0.96) and the MLSS concentration is presented in Figure IV.10.

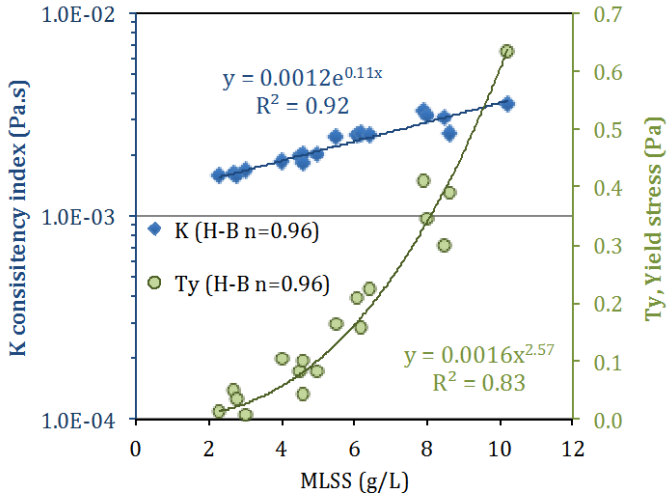

Figure IV.10. Rheological parameters of the Herschel-Bulkley equation (τ_y, K) versus activated sludge MLSS concentration. The Flow index (n) is a fixed valued (n=0.96).

Keeping a constant Flow index (n), independent on the MLSS concentration in the Herschel-Bulkley model, reduces significantly the data scattering observed in Figure IV.9 (d). However the obtained model is not significantly different from the Bingham model and therefore the latter, with only two rheological parameters, is preferred.

Conclusions

- The rheological parameters of the Ostwald-de Waele and Bingham are significantly governed by the MLSS concentration. Concerning the Casson model, only the Yield stress was closely correlated to the MLSS concentration. Instead, no clear trend was observed for the Limit viscosity and multiple values could correspond to a given MLSS concentration. The Herschel-Bulkley and Sisko parameters presented a significant data scattering when expressed as a function of MLSS. This data dispersion indicated over-parameterized models that could be unable to reproduce experimental rheograms.

IV.4.1.2 Modelling experimental rheograms with MLSS concentration

With the aim of obtaining a rheological model for the set of collected data, this section presents an evaluation of the Ostwald-de Waele and Bingham rheological equations in terms of their capacity to model a group of flow curves instead of each of the rheograms individually. These two models have been selected since they did not exhibit over-parameterization issues.

The experimental flow curves of activated sludge samples studied in this work have been divided in two groups of rheograms in consistency to observations made in section IV.3.2.1 where two diverging trends of apparent viscosity were observed for (i) Saint Vrain, Ollainville, Etrechy and (ii) Briis-sous-Forges, Etampes. The parameters of the Ostwald-de Waele and the Bingham equations were modeled as a function of the MLSS concentration for these two groups of rheograms. Different equations were tried. The selected ones are presented in Table IV.10.

Table IV.10. Rheological parameters of the Ostwald-de Waele and the Bingham models as a function of the AS MLSS concentration considering two different sets of experimental rheograms : (i) Saint Vrain, Ollainville, Etrechy and (ii) Briis-sous-Forges and Etampes.

		WWTP					
		Saint Vrain, Ollainville, Etrechy		Briis-sous-Forges, Etampes			
Model	Equation form	A	B	A	B	Eq. number (i)	Eq. number (ii)
Ostwald-de Waele	$K(Pa.s^n) = \exp(A \cdot MLSS^B) \times 10^{-3}$	0.38	1.11	0.85	0.75	IV.1	IV.2
	$n = 1 - A \cdot MLSS^B$	0.05	1.12	0.13	0.63	IV.3	IV.4
Bingham	$\tau_y(Pa) = A \times 10^{-4} \cdot (MLSS^B)$	28.0	2.25	51.8	2.09	IV.5	IV.6
	$K(Pa.s) = \exp(A \cdot MLSS^B) \times 10^{-3}$	0.09	1.04	0.14	0.85	IV.7	IV.8

The form of these equations has been guided by a suitable fit to the experimental data as well as to allow the calculation of dynamic water viscosity at 20°C (10^{-3} Pa.s) when the MLSS concentration is equal to zero. The form of the equations concerning the Ostwald-de Waele model, is also proposed by Rosenberger *et al.* (2002).

To evaluate the fit of the proposed equations to the experimental data, the experimental rheograms were modelled using the Equations IV.1 to IV.8. Table IV.11 presents the values of the residual sum of squares per number of experimental points per rheogram (RSS/N) obtained for each flow curve (ordered by sludge MLSS concentration) and for the Ostwald-de Waele and Bingham equations. Values in **bold type** highlight the lowest RSS values. Also Table IV.12 presents, the obtained minimal, maximal and average error of the modeled data in respect to the experimental rheograms.

Table IV.11. Residual sum of squares per number of experimental points (RSS/N) obtained with the equations of the modeled parameters (Equations **IV.1** to **IV.8**) to estimate the two experimental sets of flow curves (i) and (ii). Samples are listed according to a MLSS concentration increasing order.

(i) Saint Vrain, Ollainville, Etrechy			
WWTP	MLSS (g/L)	Ostwald	Bingham
Etrechy	2.3	5.04E-05	**2.42E-05**
Ollainville	2.7	**4.03E-04**	7.08E-04
Saint Vrain	2.8	1.19E-04	**6.66E-05**
Saint Vrain	3.0	8.09E-04	**4.36E-04**
Saint Vrain	4.5	2.83E-04	**2.10E-04**
Saint Vrain	4.6	**2.58E-04**	3.90E-04
Etrechy	4.6	1.06E-03	**8.48E-04**
Saint Vrain	5.0	**2.27E-04**	2.82E-04
Ollainville	6.2	2.88E-03	**1.83E-03**
Saint Vrain	8.5	1.06E-03	**7.87E-04**
Saint Vrain	8.6	**5.28E-04**	1.67E-03
Σ RSS/N		7.67E-03	**7.25E-03**

(ii) Briis-sous-Forges, Etampes			
WWTP	MLSS (g/L)	Ostwald	Bingham
Briis	4.0	**4.06E-04**	4.76E-04
Etampes	5.5	3.06E-04	**1.26E-04**
Briis	6.1	4.19E-04	**3.90E-04**
Briis	6.4	1.70E-03	**1.30E-03**
Briis	7.9	**5.69E-03**	7.93E-03
Etampes	8.0	2.81E-03	**6.37E-04**
Briis	10.2	1.50E-02	**1.32E-03**
Σ RSS/N		2.64E-02	**1.22E-02**

For the two groups of flow curves, the proposed Bingham model provides more often than the Ostwald-de Waele model the lowest RSS value and consequently the lowest sum of RSS/N values in both cases. In contrast to what had been previously observed in Table IV.8 in section IV.4.1, the adjustment quality obtained with the Ostwald-de Waele and the Bingham models do not seem to be dependent on the sludge MLSS concentrations.

Table IV.12. Minimum, maximum and average error (%) obtained with the equations of the modeled rheological parameters (**Table IV.10**) to estimate the two sets of experimental flow curves: (i) Saint Vrain, Ollainville, Etrechy and (ii) Briis-sous-Forges, Etampes. Samples are listed according to a MLSS concentration increasing order.

Saint Vrain (S.V), Ollainville (Oll.), Etrechy (Etr)							
WWTP	MLSS (g/L)	Ostwald			Bingham		
		Min	Max	Avg.	Min	Max	Avg.
Etr.	2.3	0.3	7.7	2.9	0.7	6.9	2.3
Oll.	2.7	1.9	19.5	9.3	5.0	21.4	12.4
SV	2.8	0.7	12.1	4.5	0.1	12.9	3.8
SV	3.0	4.0	27.6	15.0	4.2	21.0	11.3
SV	4.5	0.2	14.6	5.7	0.3	10.4	4.4
SV	4.6	0.4	10.1	4.5	0.0	9.0	3.8
Etr.	4.6	1.6	20.6	11.0	2.1	18.5	11.3
S.V	5.0	1.4	10.3	4.6	0.0	14.5	5.1
Oll.	6.2	4.4	11.4	8.1	0.2	10.2	5.7
SV	8.5	0.1	7.9	3.5	0.2	11.9	4.4
SV	8.6	0.0	8.5	2.8	0.1	8.2	3.7
All rheogr.		0.0	27.6	6.4	0.0	21.4	6.0

Briis-sous-Forges (BsF), Etampes (Eta.)							
WWTP	MLSS (g/L)	Ostwald			Bingham		
		Min	Max	Avg.	Min	Max	Avg.
BsF	4.0	0.9	6.7	3.9	0.7	7.9	3.2
Eta.	5.5	0.3	6.0	2.8	0.0	4.2	1.4
BsF	6.1	0.4	4.8	2.6	0.4	8.3	2.9
BsF	6.4	3.0	8.0	5.2	0.8	15.0	5.0
BsF	7.9	5.1	17.8	9.8	0.4	14.1	9.1
Eta.	8.0	2.1	11.4	6.0	0.1	7.9	2.4
BsF	10.2	0.2	14.0	9.0	0.1	5.7	2.3
All rheogr.		0.2	17.8	6.0	0.0	15.0	4.2

The maximal experimental error with respect to the experimental rheograms was 27.6%, and was obtained with the Ostwald-de Waele equation. For this model, the average error with respect to a given flow curve varied from 2.8 to 15%. For the Bingham model the obtained relative error was generally lower, the maximal obtained error being 21.4% and the average error for a given rheogram varying between 1.4 and 12.4%. For the two sets of rheograms, (i) and (ii), the Ostwald-de Waele model provided an average error of 6.4 and 6.0% respectively, while the Bingham model provided an average error of 6.0 and 4.2% respectively.

Figure IV.11 depicts the adjustment for six of the flow curves for which the highest errors were obtained (in red type in Table IV.12).

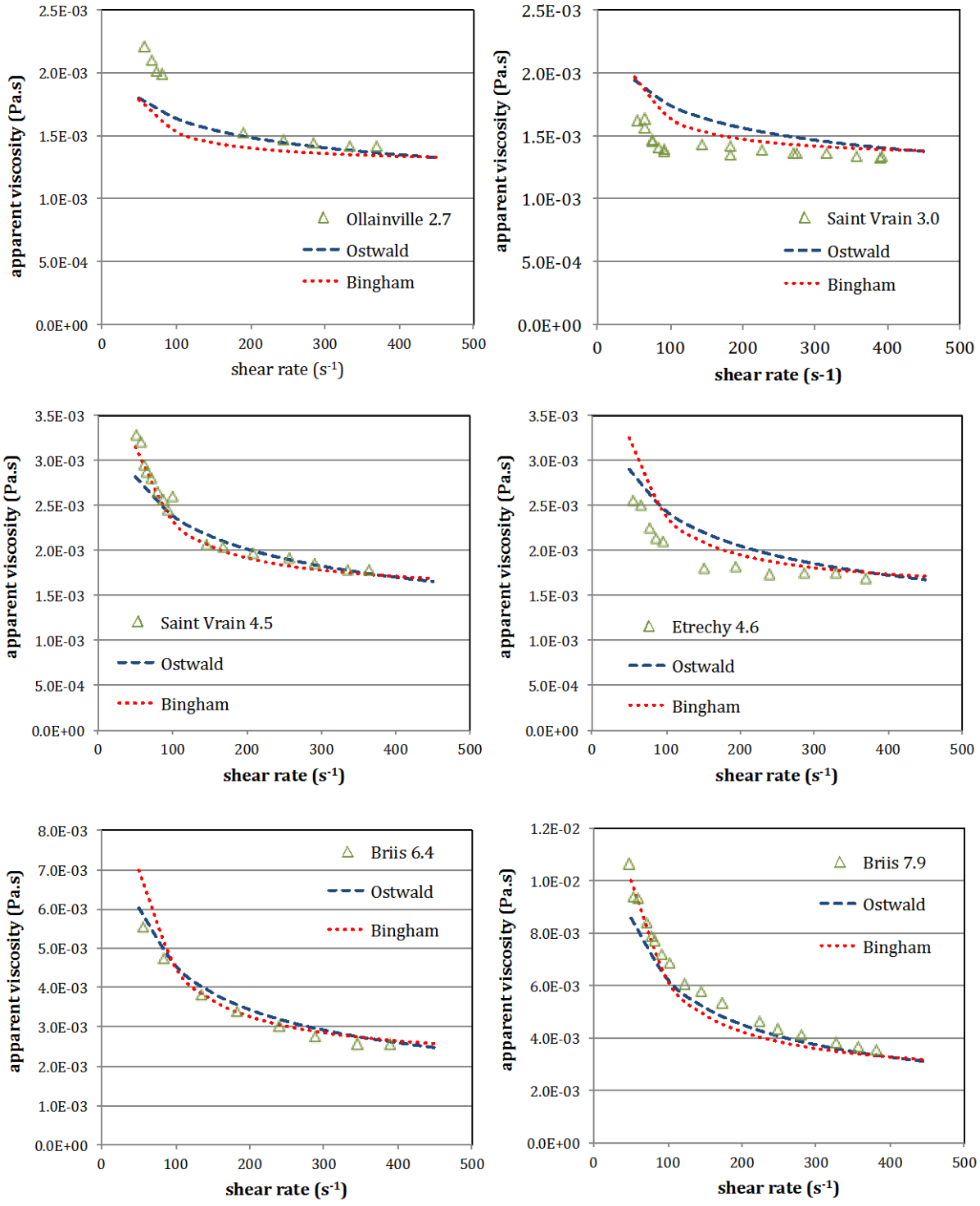

Figure IV.11. Experimental and predicted apparent viscosity as a function of the shear rate for the rheograms with the poorest fit in terms of relative error according to Table IV.12. Viscosity values are predicted with Ostwald-de Waele and Bingham models using Equations IV.1 to IV.8.

The Figure IV.12 presents a comparison between the predicted values of apparent viscosity (at 50 and 400 s^{-1}) versus MLSS concentration using the proposed models of the Ostwald-de Waele and Bingham equations for the two sets of flow curves, (i) and (ii).

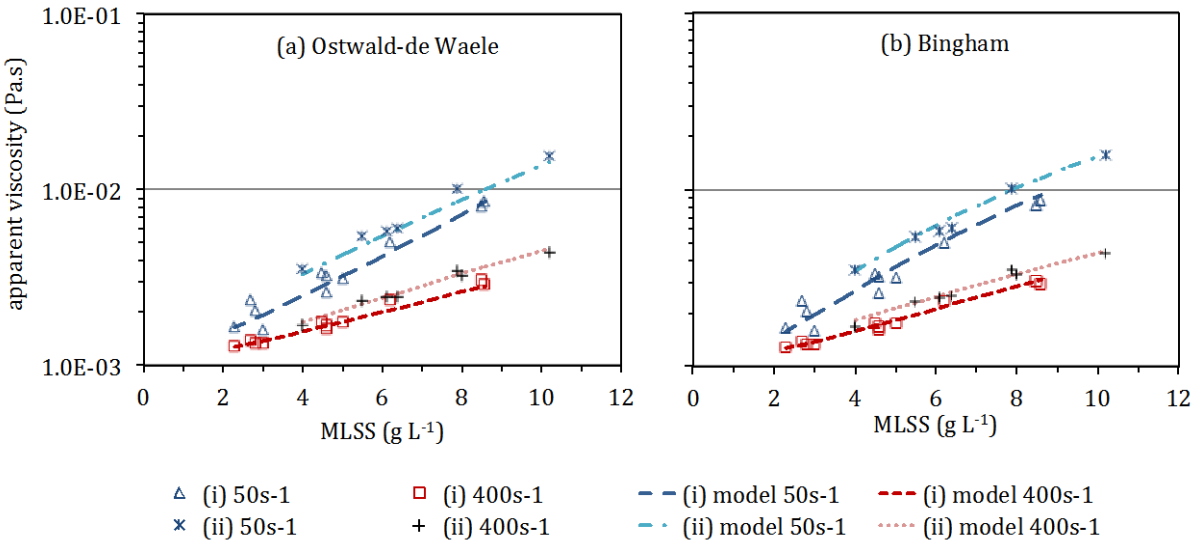

Figure IV.12. Experimental and predicted values of apparent viscosity (at 50 and 400 s^{-1}) versus MLSS concentrations for the two sets of experimental rheograms, (i) SV, Oll. and Etr. and (ii) Briis and Eta., using the rheological models of (a) Ostwald-de Waele and (b) Bingham (using Equations **IV.1** to **IV.8**).

Visually both obtained models reproduce suitably the increase of the apparent viscosity with the MLSS concentration for the two sets of experimental rheograms, (i) and (ii). For the two models, a good agreement is observed between the modeled and the experimental data.

The predicted values of shear stress estimated using the proposed models of the Ostwald-de Waele, and Bingham equations (Equations IV.1 to IV.8.) are compared in Figure IV.13 to the shear stress values issued from the experimental flow curves. No trend for under or overestimating the experimental values is observed.

Although both models provide similar prediction of the experimental values, the Bingham equation appears to be slightly more suitable to reproduce the apparent viscosity of the studied activated sludge from the five different municipal wastewater treatment plants (lowest RSS/N, lowest average relative error and lowest maximal error).

(i) Comparison for the first set of experimental rheograms (Saint Vrain, Ollainville, Etrechy)

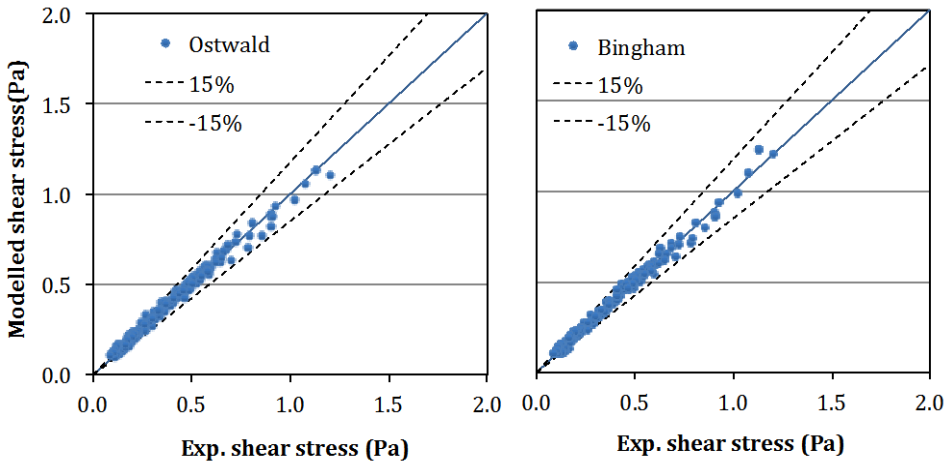

(ii) Comparison for the second set of experimental rheograms (Briis-sous-Forges, Etampes)

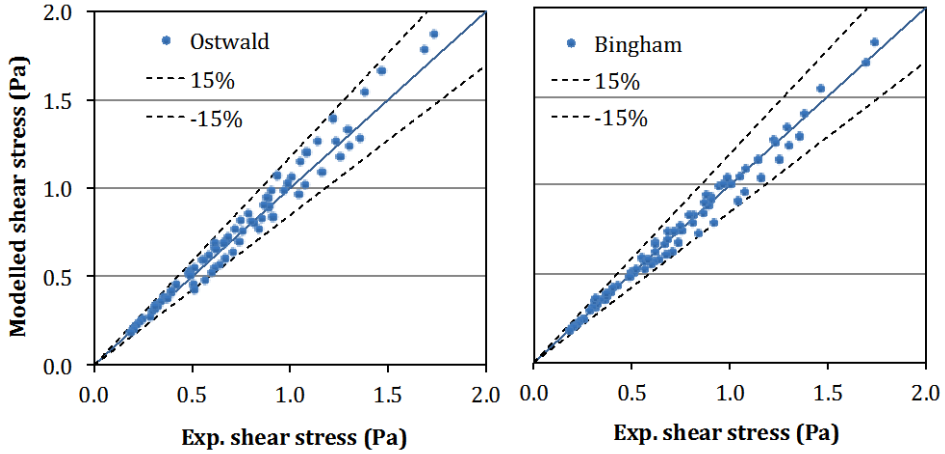

Figure IV.13. Comparison between experimental and predicted values of shear stress using the rheological models of Ostwald-de Waele and Bingham for the two sets of experimental rheograms, (i) and (ii), (using Equations **IV.1** to **IV.8** presented in Table IV.10).

IV.4.1.3 Comparison of the developed model with other studies

Figure IV.14 presents the apparent viscosity of municipal activated sludge at three different shear rates (50, 200 and 400 s^{-1}) according to the modeling results obtained in this work with the Bingham model, which provided the best fit to the experimental data for the two groups of experimental rheograms [(i) Eqs. IV.5 and IV.7; (ii) Eqs. IV.6 and IV.8], and different authors.

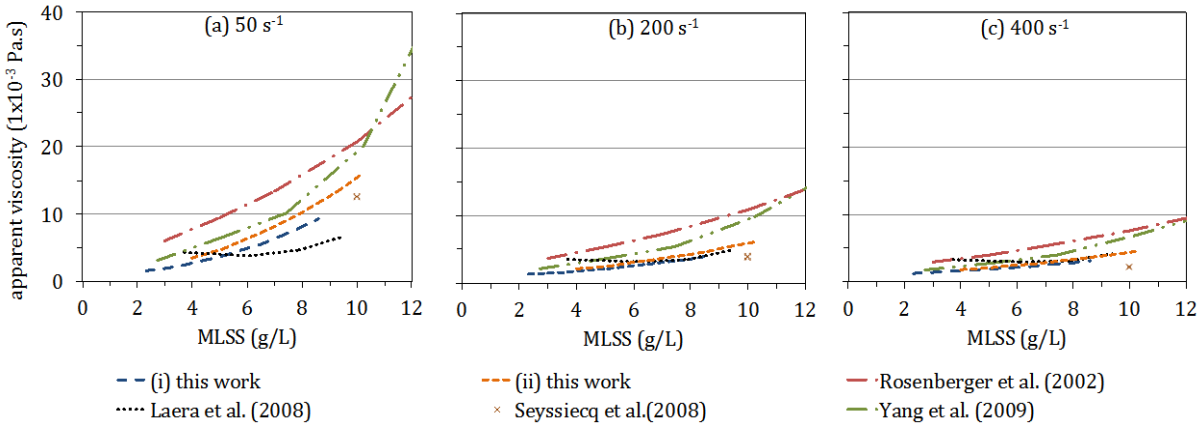

Figure IV.14.Apparent viscosity as a function of MLSS concentration at different shear rates (a) 50 s^{-1}, (b) 200 s^{-1} and (c) 400 s^{-1} for best fit in this work ((i) Eqs. **IV.5** and **IV.7**; (ii) Eqs. **IV.6** and **IV.8**) and other studies.

A significant dispersion between the different results is observed at the lowest shear rate (50 s^{-1}) while at higher shear rates the difference between models is reduced and the results from different authors converge towards similar values. The data dispersion at low shear rates may have different explanations. First, the use of different rheometer geometries that induce different flow patterns leading to the onset of turbulence at distincts shear rates (cf. I.3.4.3.2). Also, at lower velocity gradients the instruments precision might be reduced due to a heterogeneous shear repartition in the sample volume due to sample settling during the measurements. Also at low shear rates the rheometers uncertainty is probably higher because the values of the measured variables approach the components accuracy. Finally, the influence on rheology of some sludge properties that structurally differentiate the sludge origin can be reduced with the increase of the shear rate.

Conclusions

- The rheological parameters of the Ostwald-de Waele and Bingham equations were modelled as a function of the MLSS concentration based on the 18 experimental flow curves. Since the group of experimental rheograms had previously exhibited diverging trends of apparent viscosity at a given shear rate for different MLSS concentrations, two groups of data were differentiated to perform this modelling work.
- The issued models allow to estimate the experimental rheograms with similar quality. However the Bingham equation provided a slight better fit than the Ostwald-de Waele model (lowest RSS/N, lowest average error and lowest maximal relative error). The models goodness-of-fit did not appear to be related to the MLSS concentration.

IV.5 Conclusions

Rheological measurements were performed with AS within the shear rates of 50 s^{-1} and 400 s^{-1} using a tubular rheometer, designed and constructed in this work. The studied AS was sampled from five different wastewater treatment plants and MLSS concentrations varied between 2.3 and 10.2 g L^{-1}. First of all, evaluating and analysing the 18 obtained experimental rheograms allowed to:

- Confirm the non-Newtonian fluid shear thinning behaviour of AS mentioned in the literature: Its apparent viscosity decreases with an increment of the shear rate. In this work, for AS with the highest evaluated MLSS concentration (10.2 g L^{-1}), the apparent viscosity decreased from $15.7x10^{-3}$ to $4.4x10^{-3}$ Pa.s when the shear rate increased from 50 to 400 s^{-1}. For AS with the lowest studied MLSS concentration (2.3 g L^{-1}), the apparent viscosity decreased from $1.7x10^{-3}$ to $1.3x10^{-3}$ Pa.s within the same shear rate interval.

- Confirm that AS rheological behaviour is significantly determined by the MLSS concentration, as showed by other literature results, the apparent viscosity increasing exponentially with an increment of the MLSS concentration. In this study, the apparent viscosity at a shear rate of 50 s^{-1} can increase from $1.7x10^{-3}$ Pa.s up to $15.7x10^{-3}$ Pa.s when MLSS increases from 2.3 to 10.2 g L^{-1}.

Subsequently, other AS properties were also determined in order to evaluate if besides the MLSS concentration, the AS rheological behaviour is influenced by other AS properties. This evaluation of other AS properties showed that physical characteristics regarding the biological flocs such as size, cohesiveness, density and overall structure could explain why two AS samples having similar MLSS concentration but different origins exhibit different values of apparent viscosity.

Concerning the modelling of the experimental rheograms, the ability of five known rheological models to describe each of the experimental rheograms was evaluated. Logically, three-parameter models (Sisko and Herschel Bulkley) provided generally a better fit to the experimental flow curves than the two-parameters models (Ostwald-de Waele, Bingham, Casson). It was however highlighted that for some rheograms, only two rheological parameters were needed to describe with an equivalent suitability the experimental data. Moreover, representing the rheological parameters of the different studied rheological equations as a function of the MLSS concentration, highlighted that some parameters, in particular those integrating the 3-parameter models, as well as the Limit viscosity in the Casson model, lacked of identifiability. As a consequence, in order to avoid over-parameterised models with low

prediction capacity, the two-parameter models, in particular the Ostwald-de Waele and the Bingham equations, were preferred to continue the modelling work.

The rheological parameters of the Ostwald-de Waele and the Bingham equations were modelled as a function of the MLSS concentration. To this aim, the group of experimental data was divided in two groups of flow curves in view of the two diverging trends observed when representing the AS apparent viscosity at a given shear rate for different MLSS concentrations. For the two groups of rheograms, the two models provided similar adjustments to the experimental rheograms, although the Bingham equation provided slightly better results (lowest RSS/N, lowest average error, lowest maximal error).

The apparent viscosity calculated with the Bingham models obtained in this work was different in comparison to other values predicted by different models available in the literature. This discrepancy, specially pronounced at low shear rates could be attributed to the use of different rheometer geometries, to sample settleability during measurements, to the reduction of the instruments accuracy and to the impact on rheology of some sludge properties that structurally differentiate the sludge origin and that can be reduced with the increase of the shear rate.

Chapter V. Measurement and interpretation of oxygen transfer parameters in a bubble column located on site

In this chapter, experimental results of oxygen transfer measurements performed in a bubble column are presented and analysed. The main objective of this section was to precise the impact of the gas diffuser type (fine bubble, coarse bubble) and activated sludge properties on mass transfer, both in clean water and in activated sludge conditions.

The column (Dc=0.29 m, Hc = 4.4 m) was therefore equipped alternatively with a fine bubble and a coarse bubble diffuser. Clean water experiments were performed in the Irstea laboratory, whereas the experimental set-up was mounted on two full-scale plants - a conventional activated sludge system (CAS) and a membrane bioreactor (MBR) - for mixed liquor experiments. In parallel to the oxygen transfer measurements, activated sludge properties were characterised.

V.1 Experimental conditions

All experiments were performed at a liquid level of 4.4 m in the column presented in paragraph II.1. Measurements consisted in clean water and sludge determination of the volumetric oxygen transfer coefficients and the gas hold-ups for different air flow rates, corresponding to superficial gas velocities comprised between 1.9 and 5.5 x 10^{-3} m s^{-1}. Additionally, bubble size was determined in clean water for the fine bubble diffuser.

To perform the on-site experiments with mixed liquor, measurements were carried out in an open reactor co-current configuration with respect to the gas and to the liquid phases. The superficial liquid velocity was kept low and constant for a given measurement and ranged between 2.5 x 10^{-3} and 4.6 x 10^{-3} m s^{-1}. Within the range of measured overall gas hold-up in this study (ε_G<1.6%), the interval of superficial liquid velocity corresponds to an average liquid velocity comprised between 0.003 m s^{-1} to 0.005 m s^{-1} ($U_l = U_L/(1-\varepsilon_G)$). These values are very low compared to the measured average bubble rise velocity (U_b > 0.29 m s^{-1}). Consequently it is considered that bubble rise velocity and overall gas hold-up are not significantly affected by the liquid velocity. This assumption is supported by the study presented by Moustiri *et al.* (2009) in a bubble column with clean water and a wider and higher range of gas and liquid flow rates (31.9 x 10^{-3} m s^{-1} < U_G < 56.7 x 10^{-3} m s^{-1} ; 6.2 x 10^{-3} m s^{-1} < U_L < 18.6 x 10^{-3} m s^{-1}). Their results showed a negligible effect of liquid velocity on gas hold-up, bubble slip velocity and bubble size.

During mixed liquor experiments, sludge was withdrawn from the aeration tank of the plant under study, or from the return sludge line, or from the membrane reactor, in order to investigate the impact of MLSS concentration on oxygen transfer parameters.

Experimental conditions during the measurements performed in the bubble column are summarized in Table V.1.

Table V.1. Conditions during the experiments performed in the bubble column.

Diffuser	Sludge origin	Liquid conditions	MLSS (g/L)	Temperature (°C)	U_G (10^{-3} m/s)	U_L (10^{-3} m/s)	Measurements		
							k_La	ε_G	d_b
FB		Clean Water	-	19.5 - 24.1	2.0 – 4.4	0	X	X	X
CB		Clean Water	-	21.6 - 27.0	2.2 – 4.3	0	X	X	
FB	CAS	ML from AT	2.8 – 3.2	14.1 - 17.9	2.3 – 4.4	3.0 – 4.5	X	X	
		ML from RL	5.2 – 5.4	14.2 – 14.7	2.8 - 5.5	4.5	X	X	
		ML from RL	8.6	9.8 – 10.8	2.0 – 4.4	3.0	X	X	
	MBR	ML from AT	6.1	20.3 - 20.8	2.0 – 4.8	4.1	X	X	
		ML from AT	6.8	19.8 – 19.9	2.2 – 4.0	4.0	X		
		ML from MR	8.8 – 9.0	19.7 – 23.8	1.9 – 4.7	4.1	X		
		ML from MR	9.9	22.2 – 22.8	2.3 – 4.5	3.1	X	X	
CB	CAS	ML from AT	5.5	11.6 – 11.8	2.3 – 3.5	3.0 – 4.6	X		
		ML from RL	8.5	10.1 - 10.2	2.5 – 3.1	3.1	X		
		ML from RL	9.1 – 9.5	8.9 – 9.3	2.0 – 4.3	2.7 – 2.9	X	X	
	MBR	ML from AT	6.4	20.3 - 20.4	2.2 - 4.4	4.0	X	X	
		ML from MR	8.6	20.2 - 22.0	2.2 - 4.3	2.5	X	X	
		ML from MR	10.4	20.6 – 20.8	2.1 – 4.3	3.8	X	X	

ML: Mixed liquor; AT: Aeration tank; RL: Recirculation loop; MR: membrane reactor; k_La: Oxygen transfer coefficient; ε_G: Overall gas hold-up; d_b: Bubble size

V.2 Preliminary measurements in clean water at different temperatures

As seen in Table V.1, measurements have been performed within a temperature range from 8.9°C to 27°C. If the impact of temperature on the oxygen transfer coefficient is well documented (cf. Equation II.4), this is not the case for its impact on the gas hold-up. A series of experiments was therefore performed in the bubble column in clean water in order to study the effect of temperature on the overall gas hold-up.

V.2.1 Temperature effect on the overall gas hold-up

V.2.1.1 Experimental results

The overall gas hold-up (ε_G) obtained in the bubble column with clean water at a mean temperature of 10, 16 and 22°C using the fine bubble diffuser (FB) are presented in Figure V.1a.

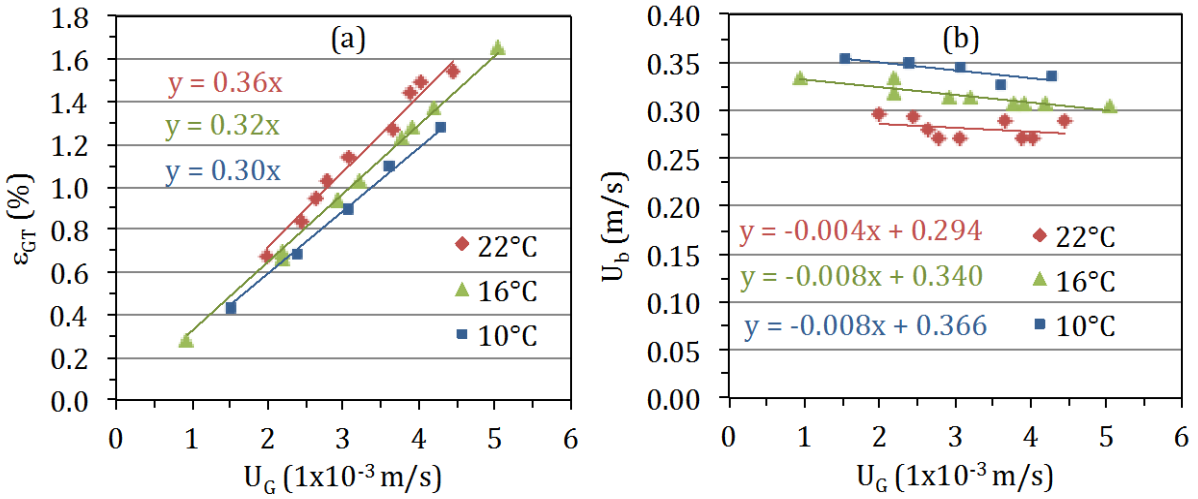

Figure V.1. (a) Overall gas hold-up and (b) average bubble rise velocity ($\mathbf{U_b}$) obtained at a temperature of 10, 16 and 22°C in clean water in the bubble column at different superficial gas velocities ($\mathbf{U_G}$) - FB diffuser.

At a given superficial gas velocity, the gas hold-up is reduced with a decrease in the liquid temperature by a factor of 17% comparing 22 and 10°C. This gas hold-up reduction may be due to the effect of temperature on the bubble rise velocity (U_b), related to the influence of temperature on the liquid properties. To evaluate the impact of temperature on U_b, the average bubble rise velocity was determined from the experimental data of gas gold-up (ε_G) and superficial gas velocities (U_G) using Eq. I.27 ($U_b = U_G/\varepsilon_G$), as shown in Figure V.1b.

When the water temperature is reduced from 22 down to 10°C, the bubble rise velocity is increased by 21%. For instance, at $U_G \approx 3x10^{-3}$ m s^{-1}, U_b increases from 0.28 m s^{-1} up to 0.34 m s^{-1}.

The available literature data related to the effect of temperature on bubble rise velocity in clean water are scarce. In agreement with the present work, though for *isolated* bubbles, the work carried out by Leifer *et al.* (2000) in clean water showed that the rise velocity of bubbles with diameters comprised between 2.0 and 6.9 mm, increased with a temperature reduction within the studied range (0-40°C). The observed increment of the rise velocity became less significant as the bubble size increased. For bubbles with a diameter of 2 mm, the bubble rise velocity increased by approximately 26% (from 0.27 up to 0.34 m s^{-1}) while for bubbles with a diameter of 4 mm the bubble rise velocity increased by approximately 10% (from 24.0 up to 26.5 m s^{-1}). By means of video images, the authors noted that the impact of temperature on bubble rise velocity relates to the bubble size and oscillating rising trajectory. It was observed that for a given bubble size (d_b>2mm), the temperature reduction promotes the bubble horizontal oscillations. However the reasons at the origin of this impact remained unclear.

V.2.1.2 Influence of temperature on gas hold-up: potential mechanisms

When the temperature changes, the water viscosity, density and surface tension are affected. The ways these properties may influence the bubble rise velocity and consequently the gas hold-up, are exposed in the next paragraphs in an attempt to identify the phenomena at the origin of the temperature impact on the gas hold-up.

Viscosity: A temperature decrease from 22 to 10°C increases the water dynamic viscosity by approximately 38% (Kestin *et al.* 1978). Three overlapping phenomena then impact the overall gas hold-up:

(i) at a given gas flow rate, the bubble coalescence is promoted and the bubble size increases. In tap water, an increase in the bubble diameter leads to a slight increase in the bubble rise velocity as shown by Sardeing *et al.* (2006). Even in the homogenous regime (ε_G<20%, U_G<40x10^{-3} m s^{-1}) in which bubbles interactions are considered to be not significant, Zahradnik *et al.* (1997) showed that an increment in viscosity, from 1mPa s to 3mPa s, leads to the reduction of the overall gas hold-up due to the existence of drag forces that promote the bubble coalescence in the diffuser region.

(ii) at a given gas flow rate, the bubble formation time is extended and consequently larger bubble are formed (Gaddis and Vogelpohl, 1986; Jamialahmadi *et al.,* 2001; Kulkarni and Joshi, 2005). As a result, bubbles rise faster and the gas hold up is reduced.

(iii) at a given bubble size, the bubble drag coefficient increases with an increase of the liquid viscosity, which leads to a reduction of the bubble rise velocities and enhances the overall gas hold-up.

Density: On the other hand, when the water temperature drops from 22°C down to 10°C, the liquid density increases slightly by 0.2% (Lide, 2004). An increase in water density leads to an augmentation of buoyance forces and consequently of bubble rise velocity.

Surface tension: When the temperature is reduced from 22 to 10°C the water surface tension is increased by 2.4% (Mezger, 1946). An increment in surface tension may lead to the following effects on bubble rise velocity:

(i) At a given gas flow rate, the bubble size increases with an increment in surface tension (Kulkarni and Joshi, 2005; Gaddis and Vogelpohl, 1986). Consequently bubbles would rise faster thus reducing the gas hold-up.

(ii) For a given bubble size, the bubble eccentricity is increased with an increment in surface tension (Jimenez, 2013). According to Maldonado *et al.* (2013) and Quinn *et al.* (2014) when the bubble eccentricity is increased, bubbles exhibit more horizontal oscillations and rise faster than spherical bubbles. It is difficult to estimate how much an increase in surface tension affects the bubble eccentricity and thus the bubble rise velocity. However the link established by Maldonado *et al.* (2013) and Quinn *et al.* (2014) between the bubble eccentricity, horizontal oscillations of the rising bubbles and bubble rise velocity joins the results by Leifer *et al.* (2000) mentioned above, who observed that bubble rise velocity is positively correlated with bubble horizontal movements.

Using the correlation proposed by Gaddis and Vogelpohl (1986) to predict the bubble size at formation from the liquid properties (cf. I.2.34), the impact of viscosity, density and surface tension on bubble size, associated to a temperature reduction, can be approximated. With a temperature drop from 22 to 10°C, the bubble diameter[4] would be reduced by approximately 0.1% (from 3.154 to 3.151 mm), the bubble size change due to the temperature increment can thus be considered to be negligible. As the temperature effect on liquid density and surface tension could be considered as negligible (respectively +0.2% and +2.4% for a temperature reduction from 22 to 10°C), the decrease in the overall gas hold-up could be attributed to the increase in dynamic liquid viscosity and associated impact on bubble coalescence and drag forces.

[4] Estimated at a superficial gas velocity per nozzle section (U_{gn}) of 0.104 m s^{-1}, which corresponds to $4.2x10^{-3}$ m s^{-1} of superficial gas velocity (U_G) using the fine bubble diffuser.

V.2.1.3 Conclusion on the effect of temperature on the overall gas hold-up

- Several simultaneous counterbalancing effects take place behind the observed increase of the bubble rise velocity with the temperature reduction and the associated decrease of the overall gas hold-up. A global analysis of the mentioned mechanisms show that the prevailing phenomenon explaining the reduction of the overall gas hold-up with a temperature decrease is bubble coalescence promoted by the increase of the liquid viscosity associated to an increase of the interfacial drag forces between bubbles and the liquid phase.
- In the present work, bubble size and eccentricity were determined only at 20°C and additional experiments at different temperatures are necessary to confirm the further evaluate the involved phenomena that could be at the origin of the increment of bubble rise velocity and gas hold-up reduction with a temperature decrease. Such experiments could help to understand the impact of viscosity change on gas phase characteristics and dynamics.

V.2.2 Overall gas hold-up temperature correction

A temperature correction equation has been computed using the results of aeration tests performed in the bubble column with clean water at a mean temperature of 9.9, 15.3 and 21.6°C and presented in Figure V.1a. The form of this equation has been chosen by analogy to the temperature correction formula used for the estimation of the $k_L a$ coefficient at 20°C (ASCE, 1996).

The empirical correlation for estimating the gas hold-up at 20°C with clean water in the bubble column is written as follows:

$$\varepsilon_{G_{20}} = \varepsilon_{G_T} \cdot \theta'^{(20-T)} \qquad \text{V.1}$$

Where

$\varepsilon_{G_{20}}$ estimated gas hold-up at 20°C (%)

ε_{G_T} gas hold-up measured at a temperature T (%)

θ' temperature correction factor for the overall gas hold-up ($\theta' = 1.015$)

The correction factor ($\theta' = 1.015$) was estimated by means of the least squares method and using the experimental data. Figure V.2 shows the overall gas hold-up obtained at 10.9, 15.3 and 21.6°C (presented in Figure V.1a) and corrected to 20°C using Equation V.1.

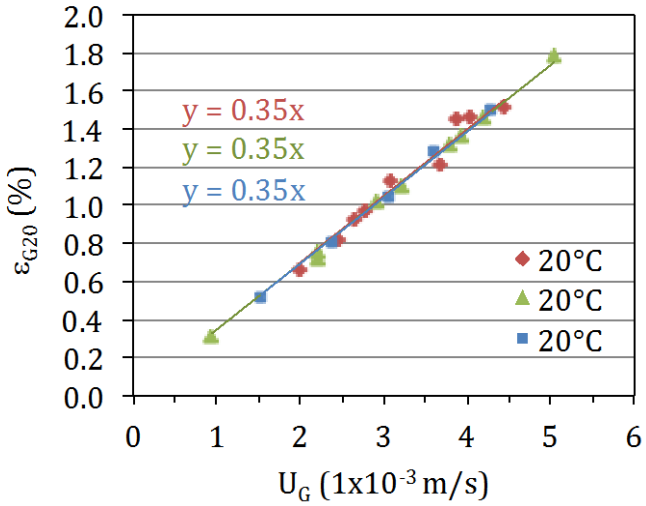

Figure V.2. Overall gas hold-up in clean water using the fine bubbles diffuser (FB) at different superficial gas velocities. Experimental data at 10, 16 and 22°C from Figure V.1a corrected to 20°C using Equation V.1.

Assuming that temperature similarly affects the rise velocity of the coarse bubbles and fine bubbles, the presented temperature correction (Equation V.1) was also applied to convert the overall gas hold-up results obtained with the coarse bubble diffuser. As the effect of temperature on mixed liquor viscosity is similar to water, as observed in paragraph III.4, the same temperature correction was also applied to the overall gas hold-ups obtained in activated sludge with both types of diffusers.

V.3 Impact of diffuser type of on oxygen transfer in clean water

V.3.1 Oxygen transfer volumetric coefficients

Volumetric oxygen transfer coefficients in clean water at 20°C ($k_L a_{20}$) obtained at different superficial gas velocities (U_G), using the fine bubble (FB) or the coarse bubble (CB) diffusers, are presented in Figure V.3.

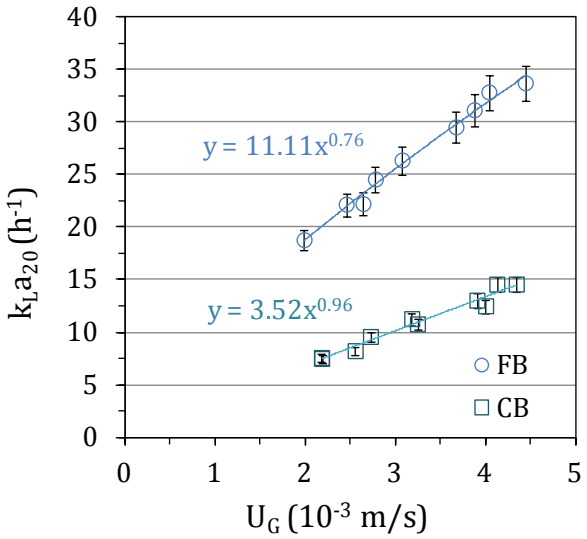

Figure V.3. Oxygen transfer coefficient at 20°C ($\boldsymbol{k_L a_{20}}$) at different superficial gas velocities ($\boldsymbol{U_G}$) in clean water obtained with two different gas diffusers: fine bubble (FB) and coarse bubble (CB).

For both types of diffusers the oxygen transfer coefficient increases with an augmentation of the superficial gas velocities. At a given gas flow rate, the oxygen transfer coefficient is higher in the fine bubble system than in the coarse bubble system by at least a factor of 2.3. These evolutions are explained by the modification in characteristics of the gas/liquid dispersion as presented in the following.

V.3.2 Characteristics of the gas/liquid dispersion

V.3.2.1 Overall gas hold-up

The gas hold-up (ε_G) at 20°C in clean water for the fine bubble (FB) and coarse bubble (CB) diffusers is presented in Figure V.4 at different superficial gas velocities (U_G). For both types of diffusers, the gas hold-up increases with the increase in the superficial gas velocity.

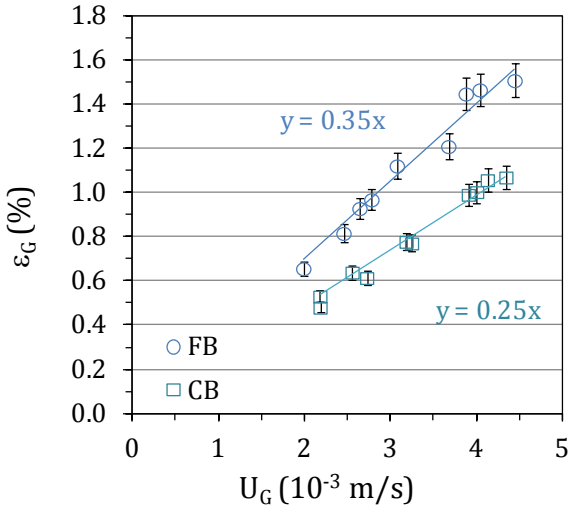

Figure V.4. Gas hold-up ($\boldsymbol{\varepsilon_G}$) at 20°C in clean water obtained with two different gas diffusers (FB and CB) at different superficial gas velocities ($\boldsymbol{U_G}$).

Within the range of applied gas flow rate, the observed gas hold-up increases linearly with U_G from 0.7 to 1.5% for the fine bubble aeration system and from 0.5 to 1.1% for the coarse bubble diffuser. At a given superficial gas velocity, the gas hold-up obtained with the fine bubble diffuser is about 1.4 times higher than the one obtained with the coarse bubbles diffuser. This difference is explained by the difference in mean bubble size, which induces a higher bubble rise velocity for coarse bubble aeration than for fine bubble aeration.

V.3.2.2 Bubble size, interfacial area and liquid-side volumetric coefficient

The bubble size (in terms of the Sauter diameter, d_{bS}) and bubble eccentricity obtained with the fine bubble diffuser at different superficial gas velocities are presented in Figure V.5.

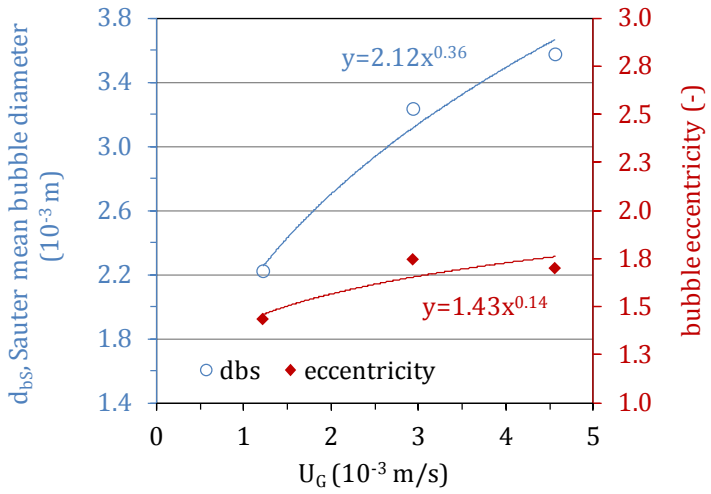

Figure V.5. Bubbles Sauter mean diameter (d_{bS}) and bubble eccentricity in clean water using the fine bubble (FB) diffuser at different superficial gas velocities.

The bubble size increases from 2.2 to 3.6 mm with an increase in the superficial gas velocity (U_G) from 1.2 to 4.6 m s^{-1}. The effect of the airflow rate on bubble size is more significant at lower superficial gas velocities because the membrane stretches and the pore's size become larger under the effect of the pressure associated to the airflow rate. Concerning the bubble's shape, their eccentricity slightly increases from 1.4 up to 1.7 with the increase of the superficial gas velocity.

Knowing the overall gas hold-up (ε_G) and the bubble Sauter diameter (d_{bS}), the interfacial area (a) was calculated for the fine bubble diffuser using Equation I.23. The calculated interfacial area is presented in Figure V.6. From the results of the oxygen transfer coefficient (Figure V.3) and the calculated interfacial area (a), an estimate of the liquid-side mass transfer coefficient (k_L) was computed as follows: $k_L = k_L a/a$ (see Figure V.6).

As mentioned in Chapter II, the size and shape of bubbles generated by the coarse bubble diffuser could not be determined in this study because bubbles rising near the wall were not representative of the bubble population rising through the column. However, the liquid-side oxygen transfer coefficient (k_L) could be estimated using the empirical correlation proposed by Calderbank and Moo-Young (1961) for a mobile interface (Equation I.16). Subsequently, the interfacial area (a) in the coarse bubble system was determined from $k_L a$ results and the estimated k_L values using Equation I.16 ($a = k_L a/k_L$). Results are also reported on Figure V.6.

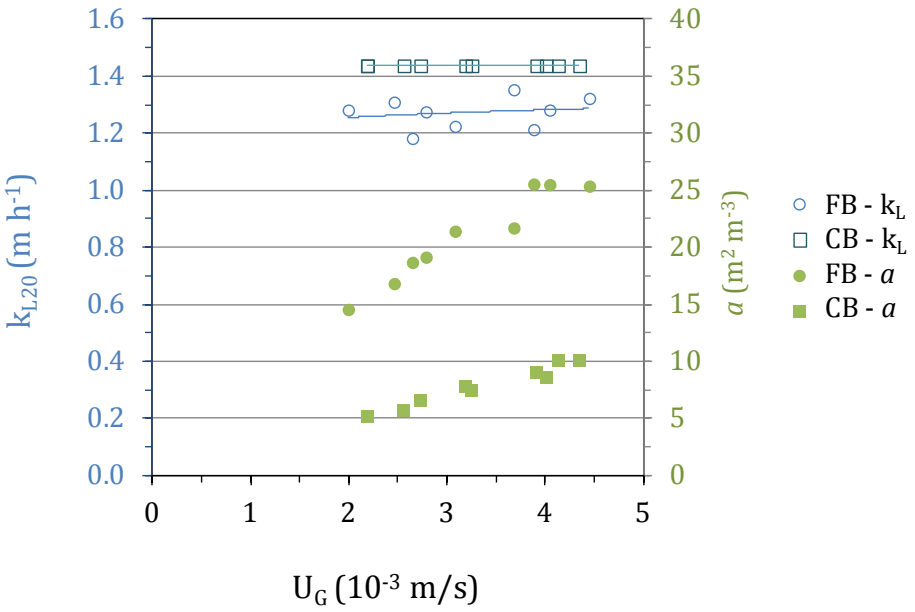

Figure V.6. Estimated liquid-side oxygen transfer coefficient ($\boldsymbol{k_L}$) and interfacial area (a) as a function of the superficial gas velocity ($\mathbf{U_G}$) in clean water for the two diffusers (FB and CB).

Within the range of the gas superficial velocity studied (1.9 – 4.5 x 10^{-3} m s^{-1}), the liquid-side oxygen transfer coefficient (k_L) for the fine bubble diffuser is almost constant. The power-law relationship between $k_L a_{20}$ and U_G (Figure IV.3) is therefore due to the increase of the interfacial area (a) with U_G following also a power law.

The coarse bubble aeration system induces a lower interfacial area, explained by the fact that coarse bubbles have higher rising velocities than fine bubbles because of their significantly larger size; consequently their residence time in the bubble column is shorter.

V.3.3 Transfer number in clear water

Transfer numbers (N_T) are given as a function of the Reynolds numbers of the column ($Re_{column}= \frac{\rho_L U_G D_{column}}{\mu_L}$) in Figure V.7. This dimensionless group ($N_T = \frac{k_L a_{20}}{U_G}\left(\frac{{\mu_L}^2}{{\rho_L}^2 g}\right)^{1/3}$) defined by Zlokarnik (1979) and Roustan (1996) has the same physical meaning as the specific standard oxygen transfer efficiency (SOTE in %) per meter of diffuser submergence for clean water operating conditions (Gillot *et al.* 2005).

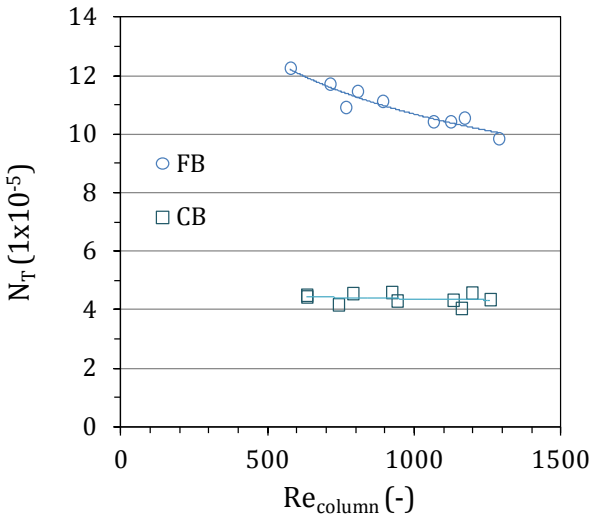

Figure V.7. Transfer number at different column Reynolds number in clean water obtained with the two different gas diffusers (FB and CB)

For a given Reynolds number, the transfer number is at least 2.3 times higher with fine bubbles than with coarse bubbles. Using a coarse bubble diffuser, the transfer numbers are independent of Re, which traduces the linear dependency of the oxygen transfer coefficient and the superficial gas velocity, as depicted in Figure V.3. For the fine bubble diffuser, N_T is a decreasing function of Re, with a power law coefficient of -0.24. This evolution is related to the dependency of the bubble Sauter mean diameter to the superficial gas velocity, as depicted in Figure V.5

In order to highlight this dependency, transfer numbers are reported in Figure V.8 as a function of the Sauter diameter. For coarse bubble, Sauter diameters have been estimated using the calculated interfacial area (a) as $d_{bS} = \frac{6\,\varepsilon_G}{(1-\varepsilon_G)a}$. Results obtained in a different bubble column equipped with a fine bubble diffuser synthesised by Gillot (2010) are also reported in this figure. Low d_{bS} values in these results were obtained adding sodium sulfite to tap water. Other oxygen transfer results reported in this figure have been obtained for fine bubble systems by Fayolle *et al.* (2010, 2011) in full-scale stirred reactors. Reactors configurations and measurement conditions corresponding to those results are presented in Table V.2.

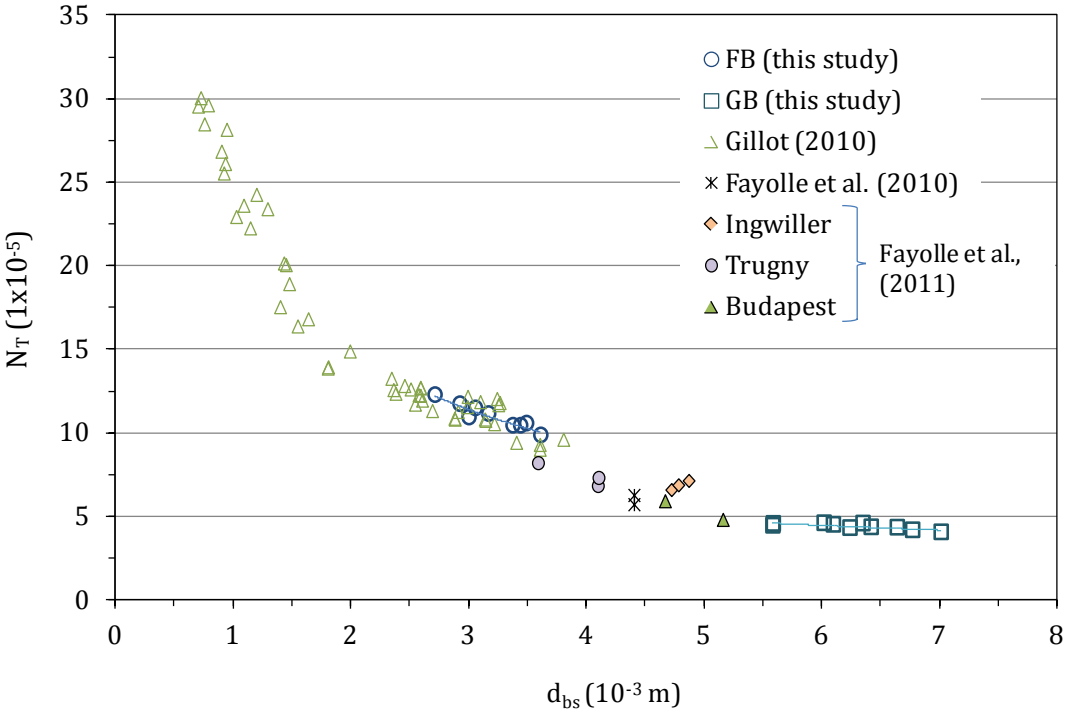

Figure V.8. Transfer number ($\boldsymbol{N_T}$) as a function of bubble Sauter diameter ($\boldsymbol{d_{bs}}$). Results obtained in this study with fine and coarse bubbles and compared to previous works.

Table V.2. Configuration of the reactors and measurement conditions for the results obtained with fine bubble diffusers and presented in Figure V.8.

	Reactor characteristics	U_G (10^{-3} m/s)	Nb. of stirrers	FB gas diffuser type	Variable conditions
Gillot *et al.* (2010)	Bubble column; D = 0.39m, H = 2.6 m.	1.6 – 7.6	-	Disc; (S=0.05 m^2)	U_G and concentration of sodium sulfite (0.2 – 17.3 g L^{-1})
Fayolle *et al.* (2010)	Annular loop reactor; Vol=1546 m^3; H=5.91 m	1.35	2	Tube	-
	Annular loop reactor; Vol=1493 m^3; H=5.45 m	1.58	1		
Fayolle *et al.* (2011)	(*Ingwiller*) Annular, Vol=2835 m^3; H=5.4 m	0.95 - 0.97	2	Tube	U_G and number of operating aeration grids
	(*Trugny*) Annular; Vol=1569 m^3; H=5.5 m	0.35 – 0.86	2	Tube	
	(*Budapest*) Folded plug flow; Vol=8368 m^3; H=8.0 m	1.18, 2.27	6	Disc	U_G

In clean water, in water with electrolytes and for reactors with different configurations (from pilot scale to full scale reactors), the transfer number (N_T) seems to be determined by the Sauter diameter that fixes the surface mobility (and therefore k_L) and the interfacial area, by

controlling the overall gas hold-up. With an increase of the bubble Sauter diameter, the transfer number is reduced with a power law coefficient of -0.88. Results also clearly demonstrate the fact that the Transfer Number is an adequate scale-up factor for systems equipped with fine bubble diffusers.

V.3.4 Conclusions

- The diffuser type (FB or CB) induces different bubble diameters that explain the higher oxygen transfer coefficients obtained with fine bubbles in comparison to coarse bubble. The transfer number is moreover an adequate scale-up factor to represent the relationship between oxygen transfer parameters and the bubble Sauter diameter.

V.4 Oxygen transfer in activated sludge

V.4.1 Oxygen transfer coefficients (FB and CB diffusers)

The evolution of the oxygen transfer coefficient at 20°C with the superficial gas velocity (U_G) for CAS (conventional activated sludge) and MBR (membrane bioreactor) mixed liquor at different MLSS concentrations is shown in Figure V.9 and Figure V.10 for the fine and the coarse bubble diffusers respectively.

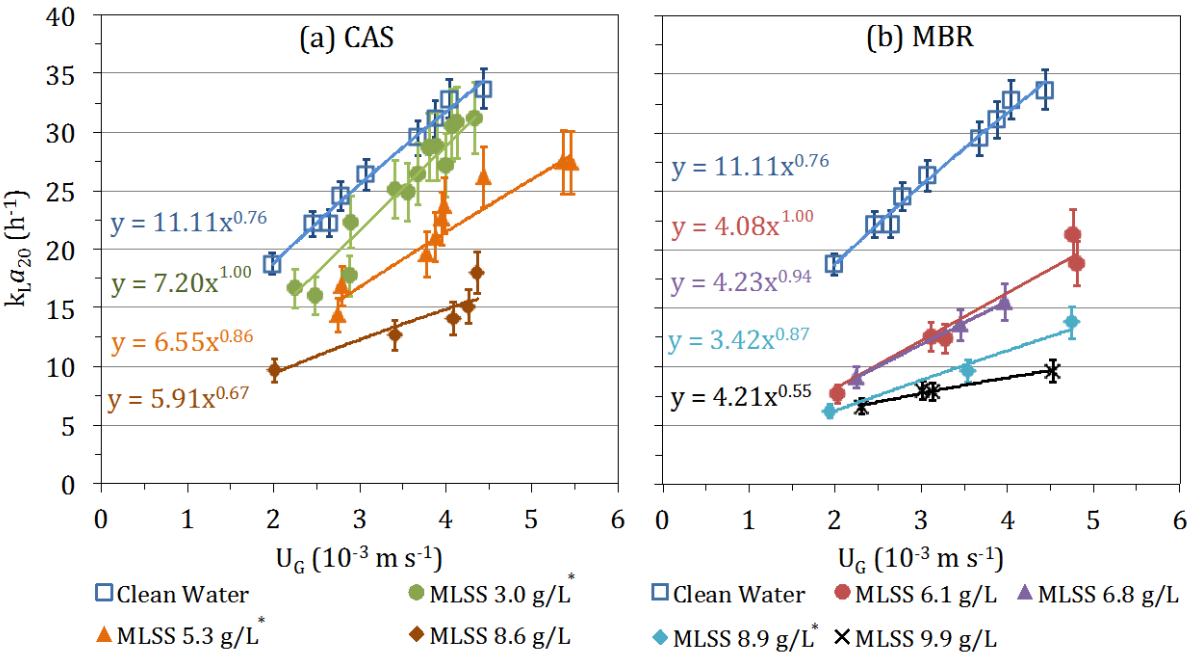

Figure V.9. Oxygen transfer coefficient at 20°C ($k_L a_{20}$) versus superficial gas velocity (U_G) in clean water and (a) CAS and (b) MBR sludge at different MLSS concentrations with the fine bubble diffuser (FB).*Averaged MLSS concentration.

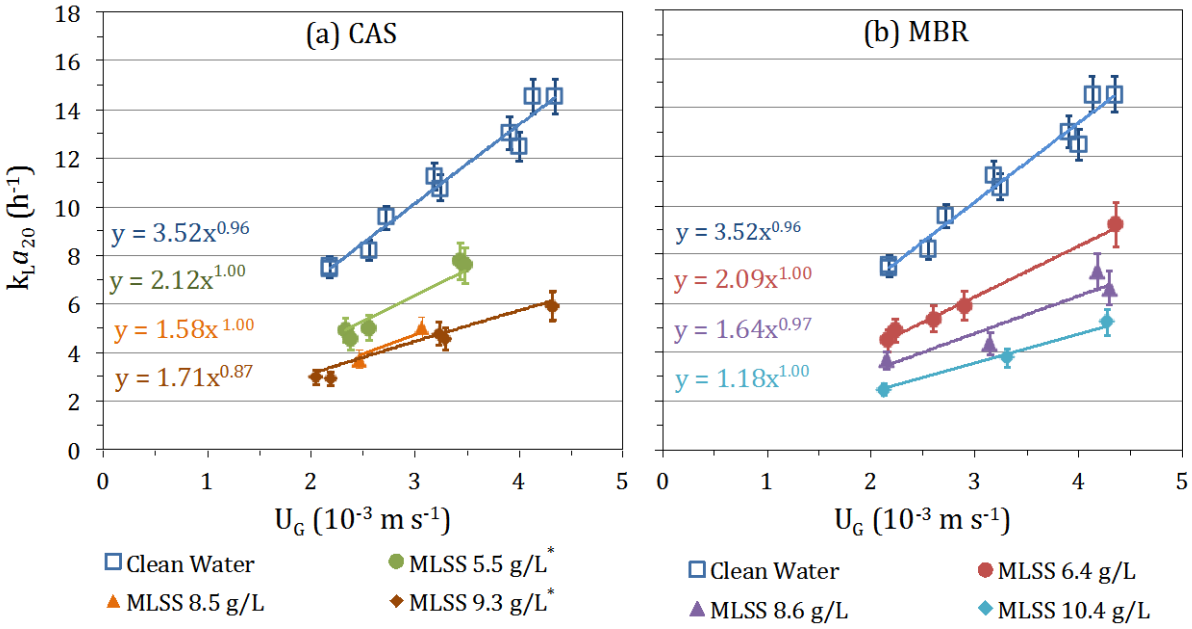

Figure V.10. Oxygen transfer coefficient at 20°C (k_La_{20}) versus superficial gas velocity (U_G) in clean water and (a) CAS and (b) MBR sludge at different MLSS concentrations with the coarse bubble diffuser (CB). *Averaged MLSS concentration.

Similarly to results in clean water, the oxygen transfer coefficient is an increasing function of the superficial gas velocity, with both diffusers (FB and CB). For a given superficial gas velocity (U_G), an increase in the MLSS concentration induces a decrease in k_La_{20} such as well described in literature data. This impact is similar whatever the origin of the sludge (CAS or MBR).

V.4.1.1 Characteristics of the gas/liquid dispersion: overall Gas hold-up (FB and CB diffusers)

The overall gas hold-up (ε_G) in clean water, CAS and MBR mixed liquor at different MLSS concentrations is shown in Figure V.11 for the two bubble diffusers.

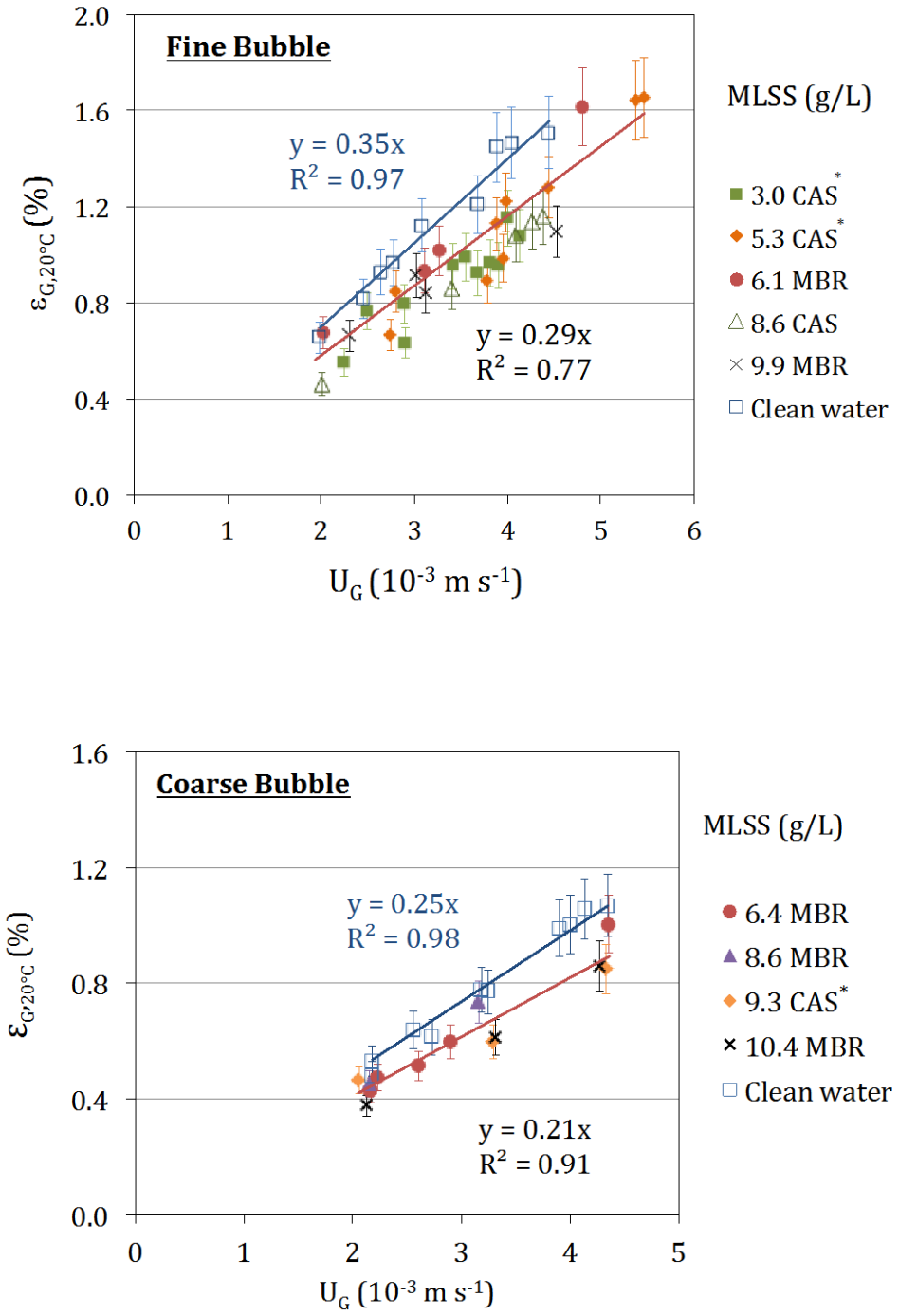

Figure V.11. Overall gas hold-up (ε_G) at 20°C versus superficial gas velocity (U_G) in clean water, CAS and MBR sludge at different MLSS concentrations. Results obtained with the fine bubble diffuser (FB) and the coarse bubble diffuser (CB). *Averaged MLSS concentration.

For both systems, the overall gas hold-up in clean water and in mixed liquor increases linearly with the superficial gas velocity.

At a given superficial gas velocity, the overall gas hold-up is higher in clean water compared to activated sludge. The order of magnitude of the gas hold-up reduction in activated sludge is

similar for both aeration systems (respectively 17% and 16% in average). This impact is equivalent within the studied ranges of the MLSS concentration ([3.0 – 9.9] g/L and [6.4 – 10.4] g/L for FB and CB respectively).

From the results, the average rise velocity (U_b) in clean water and activated sludge can be estimated for the fine bubble and the coarse bubble diffusers using Equation I.27, despite the heterogeneous characteristics of the gas phase in terms of bubble size (confirmed by visual observations). In general, the estimated values, shown in Table V.3, suggest that bubbles rise faster in activated sludge than in clean water, which explains the gas hold-up reduction and partially the k_La depletion in activated sludge.

Table V.3. Estimated average bubble rise velocity (U_b) in the bubble column for clean water and the two types of activated sludge (CAS and MBR) at 20°C using the fine bubble (FB) and the coarse bubble (CB) diffuser. ($\boldsymbol{U_b = U_G/\varepsilon_G}$)

	Fine Bubble diffuser	
	MLSS (g/L)	**U_b (m/s)**
Clean water	-	0.29
CAS	3.0	0.38
	5.3	0.35
	8.6	0.38
MBR	6.1	0.32
	9.9	0.38

	Coarse Bubble diffuser	
	MLSS (g/L)	**U_b (m/s)**
Clean water	-	0.41
CAS	9.3	0.50
MBR	6.4	0.48
	8.6	0.45
	10.4	0.53

The reduction of overall gas hold-up in the presence of activated sludge has also been reported by other authors in different operating conditions. Within a similar range of superficial gas velocity and gas hold-up comparable to the present work ($0.6\text{x}10^{-3}$ m s^{-1} < U_G < $3.2\text{x}10^{-3}$ m s^{-1}; 0.5% < ε_G < 2%), Mineta *et al.* (2011) observed the reduction of gas holdup in batch oxygenation tests performed in a bubble column filled with AS at MLSS concentrations ranging from 2 to 8 g L^{-1} and gas hold-up between 0.5 and 2%. Additionally this author observed a decrease in the gas fraction with the increase in the MLSS concentration more important than in the present study. Besides, within a higher and a wider range of superficial gas velocity and gas hold-up compared to this study ($15\text{x}10^{-3}$ m s^{-1} < U_G < $150\text{x}10^{-3}$ m s^{-1}; 2% < ε_G < 15%), Jin et al. (2006) observed in two configurations of airlift reactors (internal and external loop), that an increment of MLSS concentration from 2.0 up to 4.0 g L^{-1} resulted in a gas hold-up reduction. Fransolet *et al.* (2005) also observed a gas holdup decrease with an increment of xanthan concentration in non-Newtonian shear-thinning xanthan aqueous solutions with concentrations from 1 to 5 g L^{-1} and

superficial gas velocities (U_G) between 20x10^{-3} and 150x10^{-3} m s^{-1}. However the effect on gas hold-up was less pronounced at higher xanthan concentrations (4 and 5 g L^{-1}).

The experimental evolutions measured during this study follow trends similar to literature data. These results highlight an impact of the non-Newtonian fluid, such as activated sludge, on the characteristics of the gas phase, resulting in an increase in the bubble rise velocity. Moreover, in the present study, an increase in the MLSS concentration does not induce a further impact on the overall gas hold-up in the bubble column, whatever the installed aeration system (FB or CB). This impact of sludge properties, such as the MLSS concentration, on oxygen transfer coefficient and gas hold-up are discussed in the following paragraphs.

V.4.2 Impact of sludge properties on oxygen transfer parameters

V.4.2.1 Statistical analysis of sludge properties on oxygen transfer

Table V.4 and Table V.5 present some activated sludge properties that have been characterized in parallel to the oxygen transfer measurements with the FB and CB diffusers respectively. In order to establish the individual effect of sludge physicochemical properties on oxygen transfer coefficient, Table V.6 and Table V.7 present the Pearson linear correlation coefficients (r) between these properties and k_La_{20} (U_G = 3x10^{-3} m s^{-1}) determined with the FB and CB diffusers as well as the corresponding p-values resulting from the statistical analysis. These latter two tables also present the Pearson coefficient between the sludge physiochemical properties to show their interdependency.

V.4.2.1.1 Impact of the interstitial liquid characteristics on oxygen transfer

It is known that the dissolved substances such as surfactants can also participate to the depletion of the oxygen transfer coefficient (k_La) by accumulating at the gas-liquid interface, (i) reducing the bubbles rise velocity (Alves *et al.* 2005; Sardeing *et al.* 2006) and/or (ii) hindering the oxygen diffusivity into the liquid (Rosso *et al.* 2006; Hebrard *et al.* 2009; Jamnongwong *et al.* 2010) and consequently reducing the liquid-side oxygen transfer coefficient (k_L). However, most of the properties and characteristics of the soluble phase determined in this study were poorly correlated with the k_La coefficient, except for the experiments performed with the FB diffuser only, for which some properties such as the content of non-ionic surfactant or analysed cations presented significant Pearson coefficients and p-values (r>0.8; p-values<0.001).

The soluble COD concentration varied between 14.5 and 48.2 mg L^{-1} with a mean value of 25.5 mg L^{-1} for CAS and 36.7 for MBR sludge. Sodium and calcium were the most concentrated cations with average values of 27.8 and 54.3 mg L^{-1} respectively.

The sum of surfactant concentrations, always lower than 3.6 mg L^{-1}, was in average higher for the MBR sludge than for CAS (1.8 vs. 0.9 mg L^{-1} respectively) and the most concentrated surfactant type was the anionic surfactant (2.9 g L^{-1}). These low values could be related to the characteristics of studied wastewater treatment plants (extended aeration, low F/M ratio, SRT > 15d) which enhance the biodegradation and adsorption of surfactants.

The impact of anionic surfactant addition to clean water on oxygen transfer has been observed by different authors (Painmanakul *et al.*, 2005; Rosso *et al.*, 2006) but for significantly higher concentrations (from 50 mg L^{-1}) than those encountered in activated sludge reactors. Wagner and Popel (1996), Gillot *et al.* (2000) and Capela *et al.* (2002) measured the impact of different surfactant types and concentrations (from 1 to 7.5 mg L^{-1}) on clean water oxygen transfer characteristic parameters. These studies highlight that for such concentrations, oxygen transfer is reduced by non-ionic surfactant addition (detected in the present study mostly in MBR sludge with three of the samples having a concentration higher than 1 mg L^{-1} and a maximal value of 1.9 mg L^{-1}) and is less or not influenced by anionic surfactant addition (which is the most concentrated surfactant type in the present study). According to our results, the concentration of non-ionic surfactant seems to have an impact on oxygen transfer coefficient for fine bubble aeration, as highlighted by the good correlation presented in Table V.6 (r=-0.8, p-value<0.001). On the contrary, no impact of any surfactant type has been detected on oxygen transfer coefficient for coarse bubble aeration (Table V.7; r=-0.47, p-value=0.2). This is attributable to the difference in gas-liquid interface characteristics between the bubbles generated by each aeration system: compared to fine bubbles, coarse bubbles generate higher interfacial velocities and higher renewal rates.

Concerning the supernatant surface tension, a slight variation is observed for the different studied samples, with similar values to clean water ones (71.5 mN m^{-1}<σ<72.5 mN m^{-1}).

In collaboration with the present work, Jimenez (2013) measured the liquid-side transfer coefficient (k_L) of isolated bubbles (d_b≈1.2 mm) rising in filtered interstitial water sampled from the aeration basin and the recirculation loop of the Saint Vrain wastewater treatment plant (CAS) where some of the k_La measurements of the present study were carried out. By means of planar laser-induced fluorescence (PLIF, Dietrich et al. (2015), Jimenez (2013) scrutinized the oxygen concentration in the wake of rising bubbles and observed that the liquid-side transfer coefficient in activated sludge interstitial water was almost 50% of the one measured in pure

water. In parallel, the author noted that the k_L reduction was accompanied with a decrease of the bubble rise velocity (U_b) and bubble eccentricity (χ) while the oxygen diffusivity coefficient remained equivalent to the one measured in clean water (1.85 – 2.02 x 10-9 m^2 s^{-1} in AS interstitial liquid and 1.95 – 2.00 x 10-9 m^2 s^{-1} in clean water). Given that these results were obtained with interstitial waters with similar qualities as the ones presented in the present work (Table V.4 and Table V.5), the study of Jimenez (2013) supposes that despite of the low concentrations of soluble substances measured in this study, their presence can lead to significant reductions of liquid-side transfer coefficients. However, it is not easy to extrapolate the mentioned results to those obtained in the present work, since under different hydrodynamic regimes, with the presence of a bubble swarm of fine bubbles ($d_b \approx 3mm$) or coarse bubbles and suspended solids inducing distinct shear conditions at the bubble interface, the liquid-side transfer coefficient may be affected differently.

Table V.4. Physicochemical characteristics of activated sludge samples (CAS and MBR) related to the oxygen transfer measurements performed with the **fine bubble diffuser**

Diffuser type→		Fine bubbles (FB)												
	WWRF→	**CAS (Saint Vrain)**								**MBR (Briis)**				
MLSS	g/L	3.1	3.2	2.8	3.0	5.4	5.2	5.3	8.6	6.1	6.8	8.8	9.0	9.9
MLVSS	g/L	2.2	2.3	2	2.1	3.9	3.7	3.7	5.9	4.1	4.6	6.0	6.1	6.7
HFV	mL/L	195	185	180	180	nd	250	240	400	nd	600*	800*	800*	745*
CODt	mg/L	3900	3468	3592	4138	5884	nd	5540	8820	6200	5310	8130	7890	9810
SVI	mL/g	94	93	97	94	93	100	95	117	165*	120	nd	102*	161*
CODs	mg/L	19.4	25.1	34.8	48.2	17.7	17.5	21.2	22.4	35.3	32	31.8	38	40.1
S-A	mg/L	0.4	0.4	0.5	0.5	0.4	0.3	0.4	0.9	0.5	1	0.5	1	0.8
S-C	mg/L	<0.2	<0.2	<0.2	<0.2	<0.2	<0.2	0.3	0.3	<0.2	0.3	0.4	<0.2	<0.2
S-NI	mg/L	<0.2	<0.2	<0.2	<0.2	0.2	<0.2	<0.2	<0.2	0.3	0.3	<0.2	1.5	1.4
Surfactants	mg/L	0.4	0.4	0.5	0.5	0.6	0.3	0.7	1.2	0.8	1.6	0.9	2.5	2.2
Surface tension (20°C)	mN/m	72.2	72.3	72.3	72.1	72.2	72.3	72.4	72.2	72.5	72.2	72.1	71.9	72.5
AS Density	kg/m^3	1000	998	995	997	1000	996	1000	1002	1001	988	nd	985	1000
Na^+	mg/L	nd	4	6.2	7.7	5.3	7.0	5.7	37.4	12.8	11.6	57.7	68.8	58.7
K^+	mg/L	nd	1.9	2.9	2.3	1.9	2.7	2.2	11.9	4.5	3.9	19.6	21.6	20.7
Ca^{++}	mg/L	nd	3.8	6.3	8.8	6.5	10.2	7.7	97	28.1	21.7	120.8	130.5	123.8
Mg^{++}	mg/L	nd	0.4	0.6	0.8	0.4	0.6	0.5	12.3	1.7	1.3	8.3	8.2	8.4
Analysed cations	mg/L	nd	10	15.9	19.7	11.8	17.2	16	158.6	47.1	33.3	178.5	199.3	211.6
Date	dd/mm/yy	18/10/12	19/10/12	30/10/12	15/11/12	20/11/12	21/11/12	21/11/12	15/02/13	19/07/13	10/07/13	22/07/13	11/07/13	01/08/13
Liquid from		AT	AT	AT	AT	RL	RL	RL	RL	AT	AT	MR	MR	MR

AT=aeration tank; RL= recycling loop; MR=membrane reactor. nd : not determined.*Floating aggregates observed. WRRF: Water resource recovery facility or WWTP.

Table V.5. Physicochemical characteristics of activated sludge (CAS and MBR) related to the oxygen transfer measurements performed with the **coarse bubble diffuser**

Diffuser type →		Coarse bubbles								
	WRRF →	**Saint Vrain (CAS)**						**MBR (Briis)**		
MLSS	g/L	5.5	5.5	5.5	8.5	9.1	9.5	6.4	8.6	10.4
MLVSS	g/L	3.7	3.7	3.7	5.7	6.4	6.8	4.4	5.8	7
HFV	mL/L	315	290	310	400	410	450	465	420*	465*
CODt	mg/L	5964	6252	6732	8350	8970	9184	6730	9620	10940
SVI	mL/g	109	103	100	104	105	105	133*	122*	144*
CODs	mg/L	14.5	23.3	22.3	26	34	30	32.3	38.4	45.5
S-A	mg/L	<0.2	0.3	0.4	0.8	1.8	2.9	1.3	1.5	0.4
S-C	mg/L	<0.2	0.3	<0.2	0.3	0.3	<0.2	<0.2	0.2	<0.2
S-NI	mg/L	<0.2	<0.2	<0.2	<0.2	0.3	<0.2	0.4	1.9	0.4
surfactants	mg/L	0.0	0.6	0.4	1.1	2.4	2.9	1.8	3.6	0.8
Surface tension (20°C)	mN/m	72.3	72.0	72.3	72.4	71.9	71.5	72.4	72.1	72.3
AS Density	kg/m³	1002	999	1000	1001	999	1004	999	989	1020
Na^+	mg/L	9.3	5.6	4.8	68	5	5.6	60.2	65.9	76
K^+	mg/L	3.1	2.1	1.8	22.2	1.5	1.4	22	22.8	23.5
Ca^{++}	mg/L	17.3	9	0.7	152	5.7	3.9	124.3	129.3	132.5
Mg^{++}	mg/L	1.5	0.9	7.3	23.6	0.6	0.5	8.7	8.6	8.5
Analysed cations	mg/L	31.2	17.6	14.6	265.8	12.9	11.4	215.2	226.5	240.5
Date	dd/mm/yy	09/01/13	10/01/13	11/01/13	08/02/13	24/01/13	23/01/13	18/07/13	12/07/13	16/07/13
Mixed liquor from		AT	AT	AT	RL	RL	RL	AT	AR	MR

AT=aeration tank; RL= recycling loop; MR=membrane reactor. nd : not determined.*Floating aggregates observed. WRRF: Water resource recovery facility or WWTP.

Table V.6. Pearson linear correlation coefficients (r) and p-value between k_La_{20} (U_G=3x10^{-3} m s^{-1}) obtained with **FB diffuser** and the activated sludge physicochemical properties. The right side of the table presents the Pearson coefficients between the sludge properties to show their interdependency.

	r	p-value	r															
	k_La_{20}*		MLSS	MLVSS	HFV	CODt	SVI	AS Density	CODs	S-A	S-C	S-NI	surfactants	Surface tension (20°C)	Na^+	K^+	Ca^{++}	Mg^{++}	Analysed cations
k_La_{20}*	1.00																		
MLSS	-0.97	2E-08	1.00																
MLVSS	-0.97	7E-08	1.00	1.00															
HFV	-0.95	1E-05	0.90	0.89	1.00														
CODt	-0.90	6E-05	0.96	0.97	0.81	1.00													
SVI	-0.69	0.0122	0.60	0.58	0.70	0.60	1.00												
AS Density	-0.24	0.4395	0.17	0.14	0.36	0.13	0.38	1.00											
CODs	-0.65	0.0157	0.67	0.66	0.68	0.57	0.36	0.41	1.00										
S-A	-0.40	0.1758	0.42	0.42	0.34	0.33	0.00	-0.16	0.28	1.00									
S-C	-0.65	0.0162	0.64	0.63	0.71	0.60	0.46	0.45	0.63	-0.28	1.00								
S-NI	-0.80	0.001	0.81	0.79	0.84	0.73	0.46	0.44	0.88	0.11	0.90	1.00							
surfactants	0.04	0.8876	-0.09	-0.10	-0.30	0.00	0.59	-0.13	-0.32	-0.13	-0.10	-0.22	1.00						
Surface tension (20°C)	0.27	0.3983	-0.19	-0.18	-0.53	0.03	0.19	-0.34	-0.55	-0.03	-0.44	-0.52	0.64	1.00					
Na^+	-0.82	0.001	0.87	0.86	0.90	0.85	0.39	0.34	0.60	0.20	0.71	0.80	-0.36	-0.31	1.00				
K^+	-0.82	0.001	0.87	0.86	0.90	0.85	0.43	0.34	0.58	0.20	0.71	0.79	-0.31	-0.28	1.00	1.00			
Ca^{++}	-0.84	0.0006	0.90	0.90	0.87	0.90	0.45	0.30	0.62	0.26	0.66	0.77	-0.31	-0.21	0.99	0.99	1.00		
Mg^{++}	-0.73	0.0073	0.84	0.84	0.68	0.88	0.37	0.15	0.63	0.37	0.45	0.64	-0.27	0.00	0.87	0.86	0.93	1.00	
Analysed cations	-0.83	0.0008	0.90	0.89	0.85	0.91	0.47	0.31	0.63	0.23	0.68	0.78	-0.26	-0.16	0.98	0.98	1.00	0.93	1.00

*k_La_{20} at a superficial gas velocity of 3x10^{-3} m s^{-1}.

Table V.7. Pearson linear correlation coefficients (r) and p-value between k_La_{20} (U_G=3x10^{-3} m s^{-1}) obtained with **GB diffuser** and the activated sludge physicochemical properties. The right side of the table presents the Pearson coefficients between the sludge properties to show their interdependency.

	r	p-value	r															
	k_La_{20}*		MLSS	MLVSS	HFV	CODt	SVI	AS Density	CODs	S-A	S-C	S-NI	surfactants	Surface tension (20°C)	Na^+	K^+	Ca^{++}	Mg^{++}	Analysed cations
k_La_{20}*	1.00																		
MLSS	-0.99	5E-07	1.00																
MLVSS	-0.97	9E-06	1.00	1.00															
HFV	-0.70	4E-02	0.78	0.79	1.00														
CODt	-0.97	2E-05	0.96	0.94	0.72	1.00													
SVI	-0.37	0.3288	0.39	0.34	0.66	0.47	1.00												
AS Density	-0.77	0.0142	0.79	0.77	0.79	0.87	0.73	1.00											
CODs	-0.44	0.236	0.55	0.62	0.61	0.44	-0.08	0.36	1.00										
S-A	-0.18	0.6477	0.15	0.13	-0.15	0.10	-0.38	0.04	0.06	1.00									
S-C	-0.27	0.4772	0.29	0.26	0.35	0.44	0.42	0.56	0.21	0.17	1.00								
S-NI	-0.47	0.2009	0.56	0.60	0.62	0.55	0.12	0.55	0.86	0.24	0.67	1.00							
surfactants	0.31	0.4245	-0.35	-0.43	-0.13	-0.27	0.36	-0.09	-0.76	-0.09	0.03	-0.56	1.00						
Surface tension (20°C)	-0.45	0.2248	0.40	0.38	0.28	0.38	0.46	0.31	-0.22	-0.43	-0.45	-0.44	0.10	1.00					
Na^+	-0.43	0.243	0.44	0.37	0.62	0.51	0.75	0.63	-0.10	0.04	0.50	0.19	0.54	0.19	1.00				
K^+	-0.37	0.3253	0.39	0.32	0.61	0.45	0.74	0.60	-0.08	0.04	0.53	0.21	0.55	0.12	1.00	1.00			
Ca^{++}	-0.38	0.3196	0.39	0.32	0.58	0.43	0.67	0.55	-0.09	0.11	0.48	0.19	0.56	0.11	0.99	0.99	1.00		
Mg^{++}	-0.19	0.6214	0.18	0.12	0.23	0.18	0.15	0.13	-0.20	0.26	0.09	-0.07	0.61	0.01	0.72	0.72	0.78	1.00	
Analysed cations	-0.39	0.3048	0.40	0.33	0.58	0.45	0.68	0.56	-0.10	0.09	0.47	0.18	0.56	0.13	0.99	0.99	1.00	0.79	1.00

*k_La_{20} at a superficial gas velocity of 3x10^{-3} m s^{-1}.

V.4.2.1.2 Impact of the solid phase characteristics on oxygen transfer

According to Henkel (2010), the occupied volume of solid phase would represent an obstacle for the gas-liquid oxygen transfer and this impact would be characterized by the hydrostatic floc volume (HFV) and the mixed liquor suspended solids (MLVSS) (cf. I.2.6.2.1.1).

The hydrostatic floc volume (HFV), closely related to the MLSS content (r>0.78), exhibited a significant linear correlation with $k_L a_{20}$ using the fine bubble system (r=-0.95, p-value<0.001). The correlation is less significant (r=-0.70, p-value<0.001) for the $k_L a_{20}$ values determined using the coarse bubble system. It must be noted that the measurement of this characteristic was occasionally less accurate since not all flocs settled but remained floating especially for the MBR sludge (Briis-sous-Forges) as previously commented in Chapter IV. In fact, the two types of studied sludge (CAS and MBR) differentiated on their settling properties, the MBR sludge (Briis-sous-Forges) presenting almost systematically higher SVI (sludge volume index) values than the CAS (Saint Vrain).

Other sludge properties closely related to the MLSS concentration, such as MLVSS and CODt, show a statistically significant impact on the oxygen transfer coefficient (r>0.90, p-value<0.001). For both aeration systems, the oxygen transfer coefficient ($k_L a_{20}$) in activated sludge increases with the superficial gas velocity (U_G), which can be explained by an increment in the gas-hold up (Figure V.11) and therefore a larger specific interfacial area ($a = 6\varepsilon_G/d_b$). At a given superficial gas velocity, $k_L a$ is reduced with an increase in the MLSS concentration. These results confirm other literature data (Cornel *et al.,* 2003; Krampe and Krauth, 2003; Jin *et al.,* 2006; Germain *et al.,* 2007; Henkel *et al.,* 2009; Mineta *et al.,* 2011; Racault *et al.* 2011).

Moreover, similarly to the mentioned studies, it is also observed that the slopes characterizing the evolution of the $k_L a$ coefficient with the superficial gas velocity (U_G), evolve with the sludge MLSS concentration, being lower for higher MLSS concentrations. In addition, the MLSS concentration effect on the $k_L a$ coefficient seems to be amplified in comparison to the effect on the gas hold-up.

Three overlapping effects help to explain the observed impact of MLSS concentration on the overall gas hold-up and partially on oxygen transfer:

(i) As the solid fraction rises, the activated sludge becomes more viscous and consequently the bubble coalescence is favoured which leads to an increase of bubble size and bubble rising velocity (Mena *et al.* 2005)

(ii) At the bubble formation stage in a non-Newtonian fluid, the bubble growth time is extended with the increasing solids concentration due to higher viscoelastic stresses

exerted on the bubble and consequently bubble size is increased (Kulkarni and Joshi, 2005).

(iii) At a given bubble size, the velocity of the rising bubbles is reduced in viscous liquids due to a higher bubbles drag coefficient (Mena *et al.* 2005).

As depicted on Figure V.11, the overall gas hold-up is impacted by the presence of sludge but not by its MLSS concentration in the range from 3.0 to 10.4 g L^{-1}, despite the fact that viscosity is significantly increasing within this range (as highlighted in chapter IV). As viscosity increases, larger bubbles can be generated but may not necessarily rise faster because an increment in the bubble drag coefficient, associated to the increase in liquid viscosity, would actually extend the bubbles residence time in the liquid.

As oxygen diffusivity and gas hold-ups in AS are not affected by the sludge physicochemical characteristics, the MLSS effect on oxygen transfer could be attributed to bubble size variations due to increase in bubble growth time and coalescence, inducing a decrease in interfacial area (a) and/or to a decrease in k_L due to transport limitation, associated to the increase in liquid viscosity.

V.4.3 Alpha factor

From the oxygen transfer results in clean water and activated sludge (CAS and MBR) with the two types of diffusers (FB and CB), the alpha factors have been determined ($\alpha = k_L a_{sludge}/k_L a_{water}$). They are presented in Figure V.12 (FB) and Figure V.13 (CB) as a function of the superficial gas velocity for different MLSS concentrations.

V.4.3.1 Impact of operating conditions on alpha factor

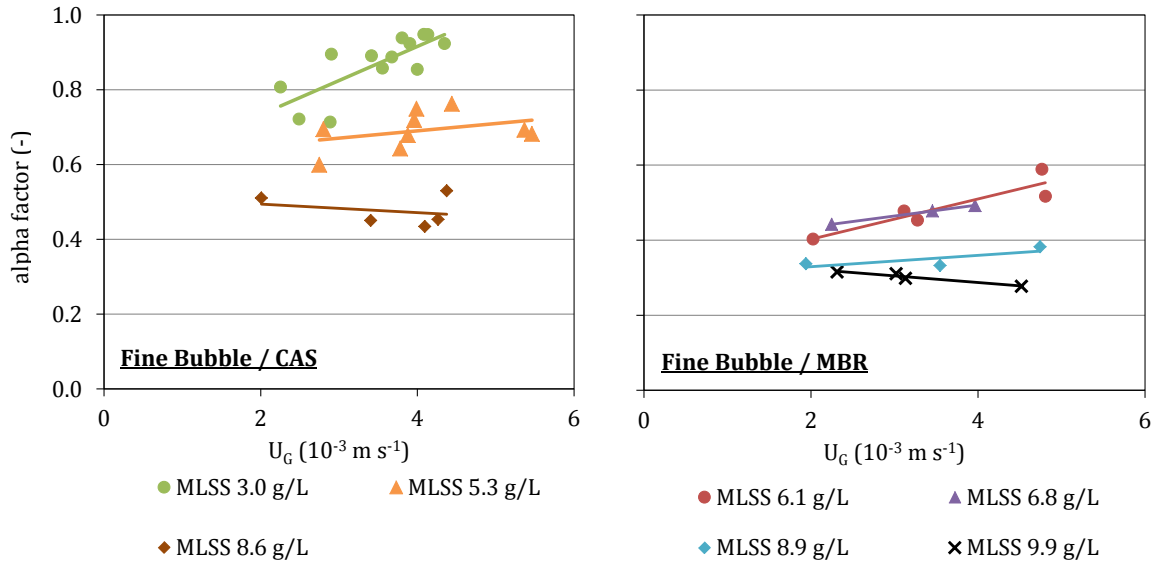

Figure V.12. Alpha factor versus superficial gas velocity (U_G) obtained with activated sludge from CAS and MBR with different MLSS concentrations and using the fine bubble diffuser (FB).

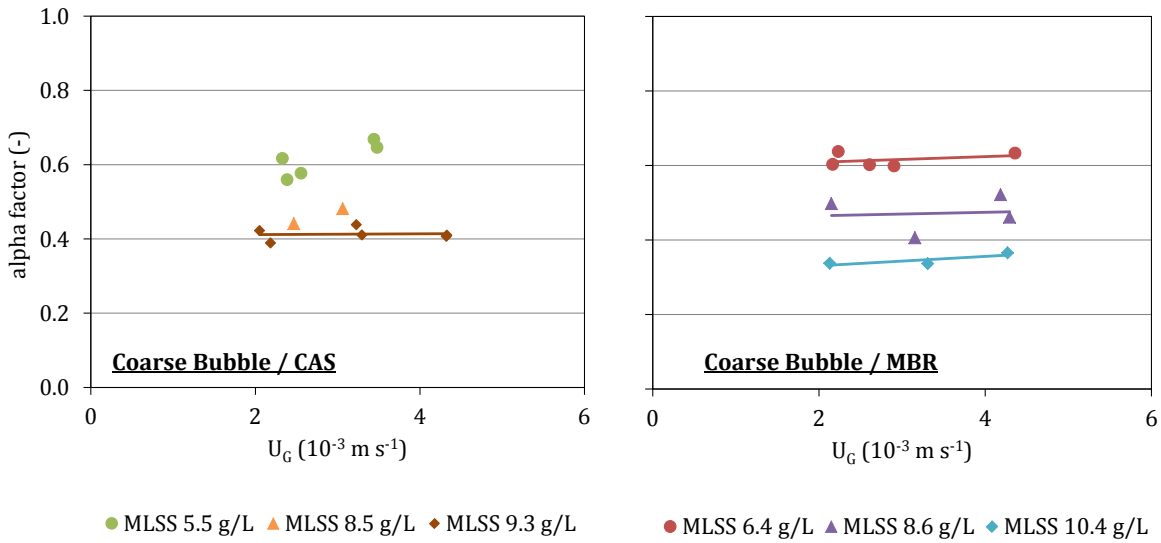

Figure V.13. Alpha factor versus superficial gas velocity (U_G) obtained with activated sludge from CAS and MBR with different MLSS concentrations and using the coarse bubble diffuser (CB)

The determined alpha factor ranges from 0.28 to 0.95, depending on the aeration system, the superficial gas velocity, MLSS concentrations and the sludge origin.

V.4.3.1.1 MLSS concentration

Similarly to the results obtained for $k_L a$, the alpha factor is reduced with an increase in the MLSS concentration. However, different trends are observed for fine and coarse bubble aeration, in particular for the effect of the superficial air velocity on alpha factor.

V.4.3.1.2 Superficial air flow rate

According to the Higbie model (cf. Equation I.13 in Table I.1) and the expression of the interfacial area (cf. I.2.3), the oxygen transfer coefficient for a single bubble can be expressed as:

$$k_L a = 2\sqrt{\frac{D_{O_2}.U_b}{\pi.d_b}}\ \frac{6.\varepsilon_G}{d_b.(1-\varepsilon_G)} \qquad \text{V.2}$$

Where D_{O_2} is the oxygen diffusion coefficient.

By using the equation V.2, the alpha factor could be expressed as:

$$\alpha = \frac{k_L a_{AS}}{k_L a_{CW}} = A.\sqrt{\frac{U_{b,AS}}{U_{b,CW}}\frac{d_{b,CW}}{d_{b,AS}}}\ \frac{\varepsilon_{G,AS}}{\varepsilon_{G,CW}}\frac{d_{b,CW}}{d_{b,AS}}\frac{(1-\varepsilon_{G,CW})}{(1-\varepsilon_{G,AS})} \qquad \text{V.3}$$

Where AS and CW refer to activated sludge and clean water and A is a constant.

For a fixed MLSS concentration, the bubble rise velocity (U_b) and the ratio ($\frac{\varepsilon_{G,AS}}{\varepsilon_{G,CW}}$) can be considered as independent of the superficial air velocity (as previously discussed in V.4.1.1). For such conditions and low overall gas hold-up ($\varepsilon_G << 1$), the alpha factor evolution with superficial air velocity is proportional to the ratio of average bubble size in clean water to average bubble size in activated sludge conditions, as expressed in equation V.4:

$$\text{alpha factor} = \frac{k_L a_{AS}}{k_L a_{CW}} \propto \left(\frac{d_{b,CW}}{d_{b,AS}}\right)^{3/2} \qquad \text{V.4}$$

This equation helps understanding the experimental variation of the alpha factor with the superficial air velocity for the different operation conditions.

For coarse bubble aeration and a fixed MLSS concentration, the alpha factor remains constant independently of the superficial air velocity. As expressed in equation V.4, this may be linked to the equivalent relative evolution of average bubble size for clean water and activated sludge with the superficial air velocity, whatever the MLSS concentration.

For fine bubble aeration, the variation of the alpha factor with the superficial gas velocity seems to depend on the MLSS content: for low MLSS concentration (MLSS < 6.1 g/L^{-1}), the alpha factor increases with an augmentation in the superficial air flow rate which could be explained by a reduction of the coalescence phenomena for activated sludge in comparison to clean water. Such reduction could be associated to the characteristics of the liquid phase able to induce a contamination of the gas-liquid interface. On the contrary, for higher MLSS concentration (MLSS > 6.8 g/L^{-1}), the alpha factor remains constant or could decrease with an augmentation of the superficial air velocity. This decrease could be related to a higher increase in the average bubble size with superficial air velocity in presence of activated sludge than in clean water operating conditions. Such a higher increase could be explained by more important viscous effects that promote bubble coalescence.

V.4.3.1.3 Sludge origin

For bubble aeration, the sludge origin seems to have an impact on the order of magnitude of the alpha factor. Independently of the airflow rate and considering the same order of magnitude of MLSS concentration, the alpha factor for CAS is higher than for MBR. According to the measured physico-chemical characteristics and the previously presented statistical analysis, this difference could be mainly linked to the difference in the interstitial liquid characteristics in terms of non-ionic surfactant concentration. Such difference is not observed for coarse bubble aeration system as highlighted in Figure V.14, with similar trends for CAS and MBR, indicating that the alpha factor for coarse bubble is not affected by the surfactant concentration, in the applied range of this study. Besides, Figure V.14 also indicates that the order of magnitude of the alpha factor and its variation with MLSS concentration is similar for fine and coarse bubble aeration for CAS sludge origin (with very low concentration of non-ionic surfactant).

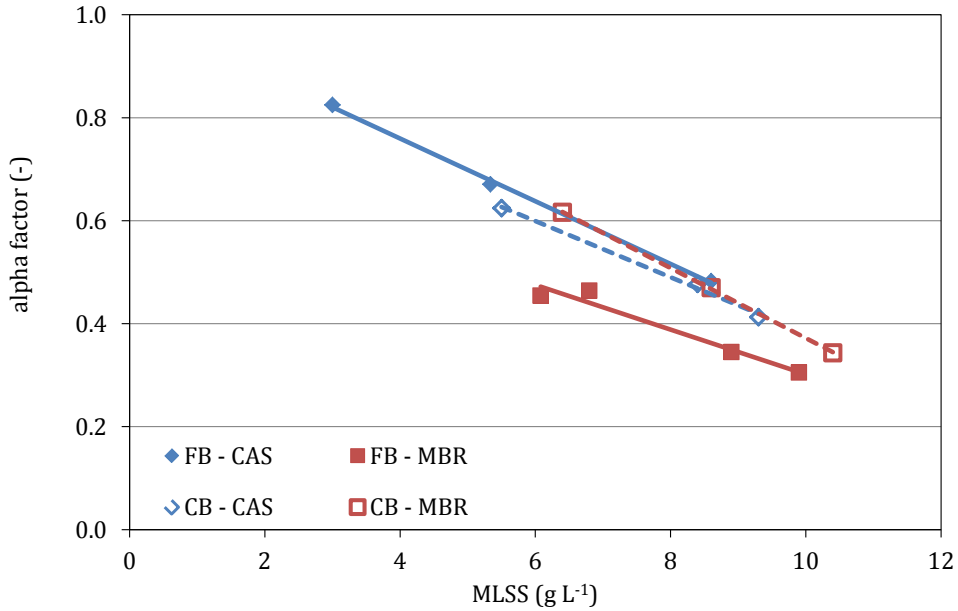

Figure V.14. Alpha factor as a function of the MLSS concentration obtained with activated sludge from CAS and MBR and using the fine and the coarse bubbles diffuser, (FB) and (CB). Results at $\boldsymbol{U_G}$ = 3.0 m s^{-1}

However it is commonly accepted that coarse bubble systems present higher alpha factors than fine bubble systems (Rosso *et al.,* 2006) because the first generate turbulent regimes where bubbles have higher interfacial velocities and higher renewal rates that hinder surfactant accumulation at the bubble interface and are consequently less affected by soluble substances such as surfactants or organic soluble matter. On the opposite, fine bubbles have lower interfacial renewal rates and longer residence times in the liquid media which expose them to an extended accumulation of substances affecting oxygen transfer. Nevertheless, the literature related to this difference due to the aeration system refers to clean water with added substances usually highly concentrated (Rosso *et al.,* 2005). In the present work, the concentration of non-ionic surfactants in the interstitial liquid in CAS is very low to evaluate a different impact between the homogenous and turbulent heterogeneous regimes on the alpha factor. On the contrary, the non-ionic surfactants is repeatedly detected in MBR sludge, which explains the higher values of alpha factor for coarse bubble aeration than for fine bubble aeration for this sludge origin.

V.4.3.2 MLSS concentration: A key parameter for alpha factor modelling?

The MLSS concentration is usually the reference parameter to predict the alpha factor in the literature and identified as a key parameter governing the oxygen transfer coefficient in the present study. Figure V.15 presents the reduction of the alpha factor with the MLSS

concentration obtained by different authors and in this study; operating conditions for literature data are summarized in Table V.8.

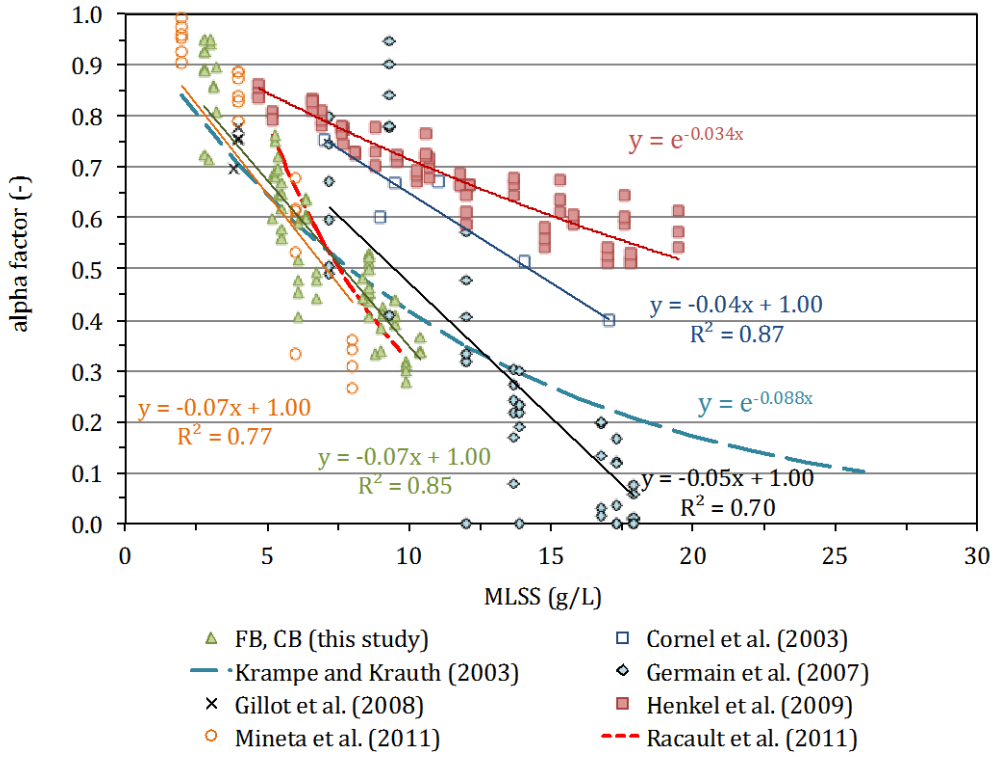

Figure V.15. Alpha factor as a function of the MLSS concentration for different types of activated sludge systems.

While the results obtained in this work (CAS and BRM) follow similar trends compared to those obtained by Gillot *et al.* (2008) in municipal full-scale CAS, Mineta *et al.* (2011) with synthetically fed sludge samples, Racault *et al.* (2011) in municipal full-scale MBR and Krampe and Krauth (2003) with grab sludge samples from CAS, they also diverge from those obtained by Cornel *et al.* (2003) in municipal full-scale MBR, Germain *et al.* (2007) with grab samples from municipal and industrial MBR and Henkel (2011) with synthetically fed greywater MBR sludge. A significant data scattering is observed and it is evident that for sludge from different origins, the oxygen transfer depletion is not only defined by the MLSS concentration.

Table V.8. Configuration of the reactors and operating conditions for previous works with fine bubble diffusers and presented in Figure V.8.

	Mixed liquor type	Reactor characteristics and aeration system	k_La Determination method	U_G ($1x10^{-3}$ m s^{-1})
Cornel *et al.* (2003)	Municipal activated sludge	Two full-scale MBR: Submerged (CB+FB) and external (FB).	Absorption; Off-gas	-
Krampe and Krouth (2003)	Diluted grab samples from different WWTPs	Round container (H_L=3 m, D=0.8, V_L=1.4 m^3); FB and Injector	Absorption	-
Germain *et al.* 2007	Grab samples from 7 MBR (domestic, industrial)	Bubble column (H_L=2.5 m, D=0.1 m, V_L=0.02 m^3); FB.	Non-steady state. Batch tests configuration in respect to liquid.	$0.48 < U_G < 4.17$
Gillot *et al.* (2008)	Municipal activated sludge	Different full-scale CAS. V_L =250 - 10200 m^3. FB diffusers.	CW: Absorption AS: Off-gas; Desorption (H_2O_2)	$1.5 < U_G < 6.4$
Henkel *et al.* (2009)	Synthetic Greywater Influent	Airlift MBR (H_L=2.5 m, V_L=2.6 m^3; FB, CB); MBR (H_L=1.25 m, V_L=3.15 m^3; FB, FB+CB).	Desorption. Batch tests configuration in respect to liquid.	$0.55 < U_G < 8.26$
Mineta *et al.* (2011)	Synthetic influent.	Bubble column (V_L= 6L; D=0.096 m). FB diffuser	Non-steady state. Batch tests configuration in respect to liquid.	$0.64 < U_G < 3.2$
Racault *et al.* (2011)	Domestic Sludge	Full-scale MBR (H_L=7 m, V_L=1000 m^3) FB diffuser	Mass Balance	$8.15 < U_G < 9.26$

V.5 Conclusions

- The oxygen transfer tests in the bubble column (with a liquid depth representative of full-scale aeration tanks and fed continuously) showed that for a given superficial gas velocity, the gas hold-up (ε_G) and oxygen transfer coefficient ($k_L a$) are reduced in activated sludge compared to clean water. A further depletion of the $k_L a$ coefficient was observed with an increase in the MLSS concentration and the magnitude of this impact was higher for the more concentrated sludge.

- Since the decrease in the oxygen transfer coefficient with the increase in the MLSS concentration is more pronounced that the one observed for the overall gas hold-up, it is deduced that there are other mechanisms through which the suspended solids affect the oxygen transfer. It is suggested that the increase in apparent viscosity, associated to the solids concentration would promote the production of larger bubbles at the formation stage an through coalescence hence leading to a reduction of the specific interfacial area (a). The experimental validation of this hypothesis for AS sludge operating conditions would be of great interest.

- According to the statistical analysis, the oxygen transfer coefficient measured under fine bubble aeration is also influenced by the concentration of non-ionic surfactant, mainly detected in the MBR sludge. On the contrary, under coarse bubble aeration, the properties of interstitial liquid such as the concentration of soluble organic matter, surfactants and cations are not significantly correlated to the oxygen transfer.

- Finally, the alpha factor varied between 0.28 and 0.95 depending on the MLSS concentration, the sludge origin, the superficial gas velocity and the diffuser type associated to the presence of non-ionic surfactant in the sludge interstitial liquid.

- From the comparison of the obtained alpha factors to literature data, it is evident that the MLSS concentration is not the only sludge property defining its value.

Chapter VI. Contribution of rheological measurements to interpret gas/liquid oxygen transfer

In this last chapter, the variations of the oxygen transfer parameters are further interpreted with the help of the obtained rheological results. First, an estimation of the average shear rate and apparent viscosity in the bubble column is presented, considering the operating conditions (hydrodynamics and sludge properties) during the oxygen transfer tests. The relationship between the apparent viscosity and oxygen transfer parameters is then analysed. The obtained results in the bubble column, in terms of alpha factors, are finally compared to on-site data.

VI.1 Apparent viscosity for the conditions prevailing in the bubble column

VI.1.1 Rheological models

The rheological study showed that the apparent viscosity (μ_{app}) of activated sludge can be modelled adequately using the Bingham equation written as follows:

$$\mu_{app} = \frac{\tau}{\dot{\gamma}} = \frac{\tau_y}{\dot{\gamma}} + K \qquad \text{VI.1}$$

where the apparent viscosity is a function of shear rate ($\dot{\gamma}$) and the Bingham rheological parameters τ_y, the yield stress and K, the consistency index.

These two parameters can be estimated as a function of the MLSS concentration (in g L^{-1}) according to Equations VI.2 and VI.3:

$$\tau_y\ (Pa) = A \times 10^{-4} \cdot (MLSS^B) \qquad \text{VI.2}$$

$$K(Pa.s) = \exp(C \cdot MLSS^D) \times 10^{-3} \qquad \text{VI.3}$$

As concluded in chapter IV, the sludge MLSS concentration determines significantly the sludge rheological behaviour but other sludge properties, linked to the sludge origin (operating conditions, airflow rates, inflow quality, etc.) can have an effect on its rheology. In order to estimate the apparent viscosity of the sludge from each of the two studied sites for the operating conditions in the bubble column and to remove sources of error associated to viscosity modelling, a set of empirical constants A, B, C and D associated to Equations VI.2 and VI.3, is proposed for each of studied treatment plants (Briis-sous-Forges and Saint-Vrain). These sets are presented in Table VI.1.

Table VI.1. Empirical constants associated to the Bingham rheological parameters (τ_y and K) for the CAS and MBR sludge using Equations VI.3 and VI.2.

WWTP	A	B	C	D
CAS (Saint Vrain)	31.8	2.19	0.07	1.11
MBR (Briis-sous-Forges)	59.2	2.03	0.14	0.87

VI.1.2 Estimation of the average shear rate in the bubble column for the operating conditions

Metz et al. (1979) defined the specific energy dissipation rate (P/V) necessary to maintain the flow of a viscous fluid as follows:

$$\frac{P}{V}=\tau\cdot\dot{\gamma} \qquad \text{VI.4}$$

According to Whalley and Davidson (1974), the specific energy in a bubble column, functioning in co-current configuration, results from the gas and the liquid phases. Assuming that the loss of kinetic energy due to the gas leaving the column and the gas friction at the column walls can be neglected, the specific energy can be expressed as follows:

$$\frac{P}{V}=(U_G+U_L)\cdot(\rho_L-\rho_G)\cdot(1-\varepsilon_G)\cdot g \qquad \text{VI.5}$$

where U_G is the superficial gas velocity (m s^{-1}), U_L the superficial liquid velocity (m s^{-1}), ρ_L the liquid density (kg m^{-3}), ρ_G the gas density (kg m^{-3}), ε_G the overall gas hold-up (-) and g the standard gravity constant (m s^{-2}).

The specific dissipation rate defined in Equation VI.5 could be influenced by the gas diffuser type (fine or coarse bubbles) by considering the associated overall gas hold-up. However, for low gas hold-up such as in the experiments performed (ε_G << 1%), the specific dissipation rate is independent of the diffuser. This expression (Eq. VI.5) is equivalent to the one proposed by Henzler *et al.,* (1985) and Sanchez-Perez *et al.* (2006) for no liquid circulation and low overall gas hold-up.

Reorganizing Equations VI.1, VI.4 and VI.5 gives:

$$K\cdot\dot{\gamma}^2+\tau_y\cdot\dot{\gamma}-(U_G+U_L)\cdot(\rho_L-\rho_G)\cdot(1-\varepsilon_G)\cdot g=0 \qquad \text{VI.6}$$

Solving this quadratic function allows estimating the mean shear rate ($\dot{\gamma}$) prevailing in the bubble column as a function of the sludge rheological properties (defined by the Bingham

parameters τ_y and K), the gas and liquid superficial velocities (U_G, U_L) and the gas hold-up (ε_G) as follows:

$$\dot{\gamma}=\frac{-\tau_y+\sqrt{\tau_y^2+4\cdot K\cdot(U_G+U_L)\cdot(\rho_L-\rho_G)\cdot(1-\varepsilon_G)\cdot g}}{2\cdot K} \qquad \text{VI.7}$$

Figure VI.1 and Figure VI.2 show the estimated average shear rate within the range of applied superficial gas velocities and AS MLSS concentrations studied in the bubble column using the fine and coarse bubble diffusers, respectively.

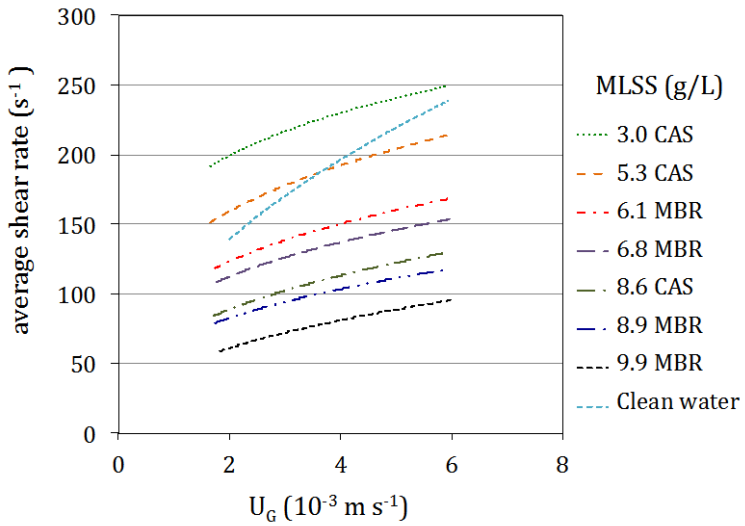

Figure VI.1. Estimated average shear rate prevailing in the bubble column as a function of the superficial gas velocity and the MLSS concentration using the **fine bubble diffuser.**

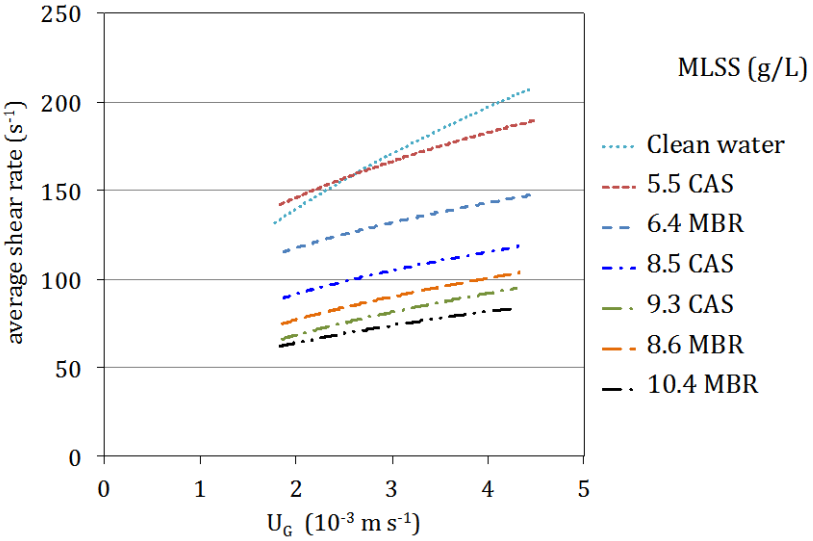

Figure VI.2. Estimated average shear rate prevailing in the bubble column as a function of the superficial gas velocity and the MLSS concentration using the **coarse bubble diffusers**.

For FB bubble aeration, a superficial gas velocity range of 1.9 x 10^{-3} m s^{-1} <U_G< 5.5 x 10^{-3} m s^{-1} and MLSS concentrations up to 10 g L^{-1}, the estimated average shear rate ranges from 65 to 243 s^{-1}. For clean water and activated sludge, the estimated shear rate increases with the superficial gas velocity. It also tends to decrease with an augmentation of the MLSS concentration. However, the estimated shear rate is also an increasing function of the superficial liquid velocity (U_L), as defined in equation VI.7. That explains why the highest mean exerted shear rate in the bubble column occurred for CAS at 3.0 g MLSS L^{-1} since experiments with this sludge were performed at the highest superficial liquid viscosity (in average U_L=4.1x10^{-3} m s^{-1}). The shear rate trend estimated for clean water exhibits a different curvature compared to those estimated in the presence of activated sludge. This is explained by the fact that experiments in clean water were performed in batch configuration with respect to the liquid phase.

The estimated average shear rates for the CB aeration system range from 65 to 205 s-1, which corresponds to the same order of magnitude of the estimated values for the FB system (Figure VI.1). Although the overall gas holdup obtained with the FB system is higher than the one obtained with the CB system, these overall gas holdup values are too small (ε_G < 1.6%) to have a significant impact on the estimated average shear rate.

VI.1.3 Impact of the activated sludge apparent viscosity on the oxygen transfer coefficient

Knowing the mean shear stress exerted by the air bubbles and the liquid velocity allows calculating the apparent viscosity of the mixed liquor in the bubble column associated to the measured superficial gas and liquid velocity (U_G and U_L), the gas hold-up (ε_G) and MLSS concentrations by using the Bingham model (Equation II.3) as well as the rheology experimental results (Equations VI.3 and VI.2).

Figure VI.3 and Figure VI.14 show the variation of $k_L a_{20}$ with the apparent viscosity for the different MLSS concentrations and the two types of sludge and aeration systems in the bubble column.

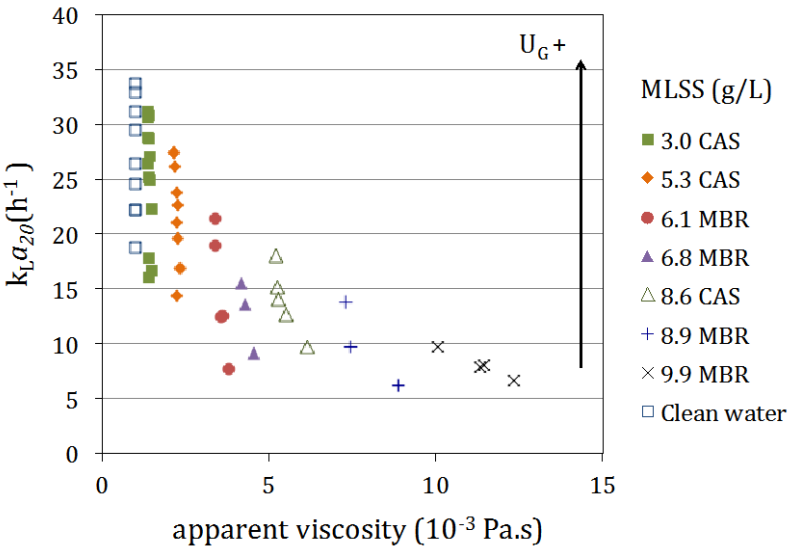

Figure VI.3. Coefficient $k_L a_{20}$ vs. calculated apparent viscosity in the bubble column for different MLSS concentrations and two types of activated sludge - **Fine bubble (FB) diffuser.**

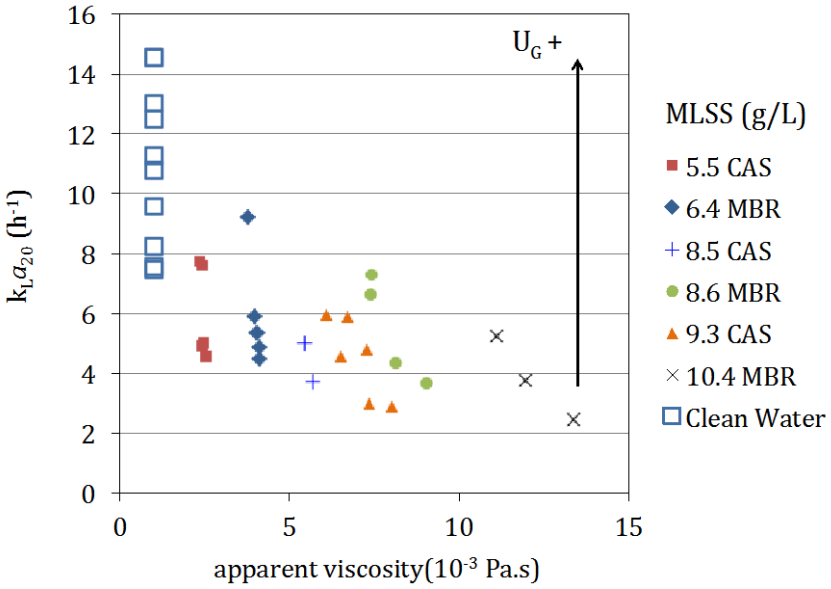

Figure VI.4. Coefficient $k_L a_{20}$ vs. calculated apparent viscosity in the bubble column for different MLSS concentrations and two types of activated sludge - **Coarse bubble (CB) diffuser.**

For the highest MLSS concentration and the lowest superficial gas velocity, the highest values of apparent viscosity are obtained, up to 13 times the water dynamic viscosity. Since for a given MLSS concentration different superficial gas velocities have been applied, different values of apparent viscosity are obtained.

VI.1.4 Modelling the oxygen transfer coefficient in AS considering its non-Newtonian behaviour

In order to improve the estimation of the oxygen transfer coefficient, empirical correlations based on key parameters and properties have been proposed. For the activated sludge process, these correlations consider for instance the coupled effect of solid retention time (SRT) and surface flow rate (Rosso *et al.* 2005), SRT and the bubbles contact time in the liquid phase (Gillot and Héduit 2008), SRT and the MLVSS concentration (Henkel 2010) or viscosity for a fixed applied shear rate (Wagner *et al.*, 2002; Pittoors *et al.*, 2014). Although these correlations clarify the influence of specific parameters on oxygen transfer, they do not take into account the shear-thinning behaviour of the mixed liquor and the fact that the apparent viscosity is a function of experimental conditions (U_G, U_L, MLSS concentration). From the rheology and oxygen transfer experimental results obtained in this study, an empirical model that relates hydrodynamics, rheology (by considering the apparent viscosity and its dependence to the shear rate) and oxygen transfer in the bubble column was thus developed based on dimensional analysis.

VI.1.4.1 Model development

The chosen dimensionless numbers are the transfer number (N_T), previously defined as a scale-up factor for oxygen transfer (Capela *et al.*, 2001; Gillot *et al.*, 2005) and the column Reynolds number (Re_C, ratio of inertial forces to viscous forces). The transfer number compares mass transfer through the gas/liquid interface to inertial forces, but also considers viscous and gravitational forces, which are the main variables of the studied system. These dimensionless numbers are defined as follows:

$$N_T = \frac{k_L a_{20}}{U_G} \left(\frac{\mu_{app,ML}^2}{\rho_{ML}^2 \, g} \right)^{1/3} \quad \text{VI.8}$$

$$Re_C = \frac{U_G D_c \rho_{ML}}{\mu_{app,\,ML}} \quad \text{VI.9}$$

where U_G is the superficial gas velocity (m s^{-1}), $\mu_{app,ML}$ is the mixed liquor apparent viscosity in the bubble column (Pa.s), ρ_{ML} is the density of the mixed liquor (kg m^{-3}) and D_c is the column diameter (m).

The transfer number is expressed as a function of the column Reynolds number as follows:

$$N_T = K_1 . Re_{Column}^{K_2} \quad \text{VI.10}$$

where K_1 and K_2 are numerical constants.

The oxygen transfer coefficient can be written using Equations VI.8 to VI.10, which corresponds to the formalism proposed in the oxygen transfer review by Garcia-Ochoa and Gomez (2009):

$$k_L a_{20} = K'_1 . U_G^{(1+K_2)} . \mu_{app,ML}^{-K_2 - \frac{2}{3}} \quad \text{VI.11}$$

However, in the present work, due to the model construction, the constant exponents associated to the variables U_G and $\mu_{app,\,ML}$ are both interrelated through the empirical constant value K_2.

In Equation VI.11, K'_1 represents all aspects related to the reactor configuration (geometry, diffuser type and distribution, etc) as well as the characteristics of the sludge properties impacting $k_L a_{20}$ that were not measured in these experiments. This correlation reflects that, for a given system, $k_L a_{20}$ is only controlled by the gas superficial velocity and the rheological properties of the AS. The derivation of the K_1 and K_2 is summarized in Figure VI.5 and described thereafter.

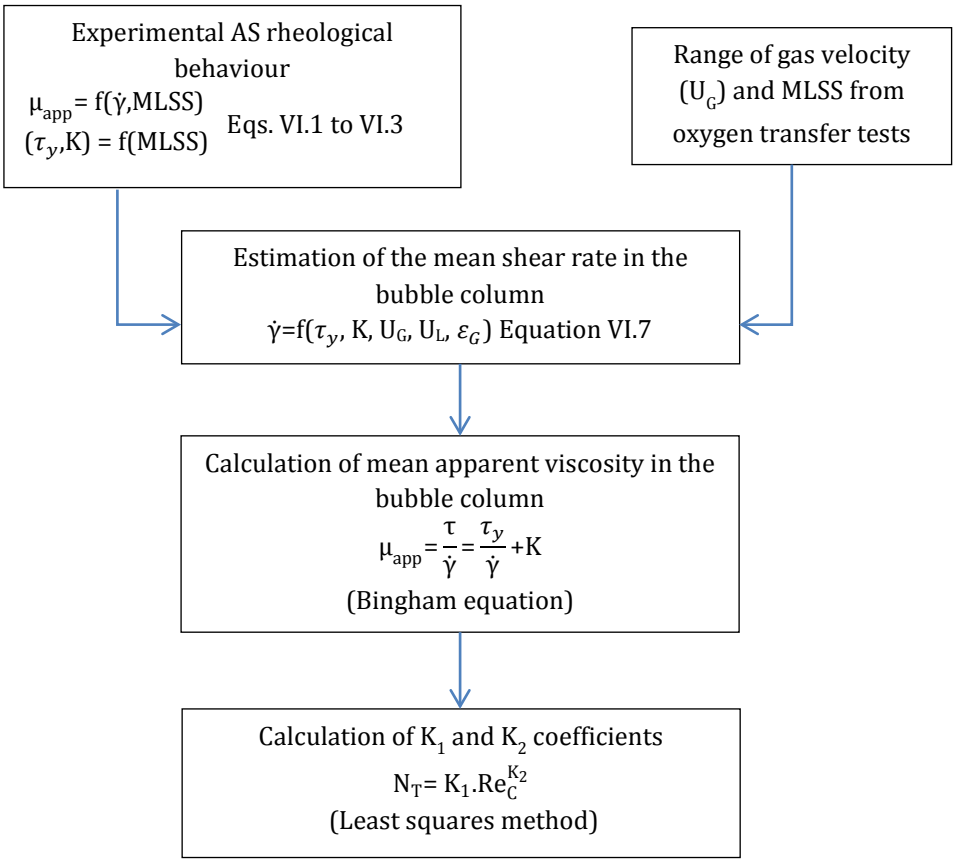

Figure VI.5. Derivation of the empirical coefficients K_1 and K_2 in Equation VI.10.

VI.1.4.2 Transfer number and oxygen transfer coefficient models for fine and coarse bubble aeration

Having estimated the mean apparent viscosity of the mixed liquor in the bubble column for the different oxygen transfer tests, the empirical constants K_1 and K_2 are computed by minimizing the weighted sum of squared residuals between the modelled transfer number and the one obtained using experimental data at a given superficial gas velocity (U_G) and MLSS concentration for the two aeration systems. The resulting models are presented in Table VI.2.

Table VI.2. Obtained models for Transfer number (N_T) and oxygen transfer coefficient (k_La_{20}). Fine and coarse bubble aeration.

Fine bubble		Coarse bubble	
$N_T = 38.0 \times 10^{-5}.Re_C^{-0.19}$	VI.12	$N_T = 22.0 \times 10^{-5}.Re_C^{-0.24}$	VI.13
$k_La_{20} = 2.8 \times 10^{-2}.U_G^{0.81}.\mu_{app,ML}^{-0.48}$	VI.14	$k_La_{20} = 1.2 \times 10^{-2}.U_G^{0.76}.\mu_{app,ML}^{-0.43}$	VI.15

With the coarse bubble diffuser, the impact of superficial gas velocity and apparent viscosity on k_La_{20} is slightly lower compared to the observed effect with the FB aeration system.

For both aeration systems, a good agreement is observed between experimental and modelled transfer numbers and oxygen transfer coefficients (models allow to predict the values with a precision of +/- 15% in most cases) as presented in Figure VI.6 and Figure VI.7.

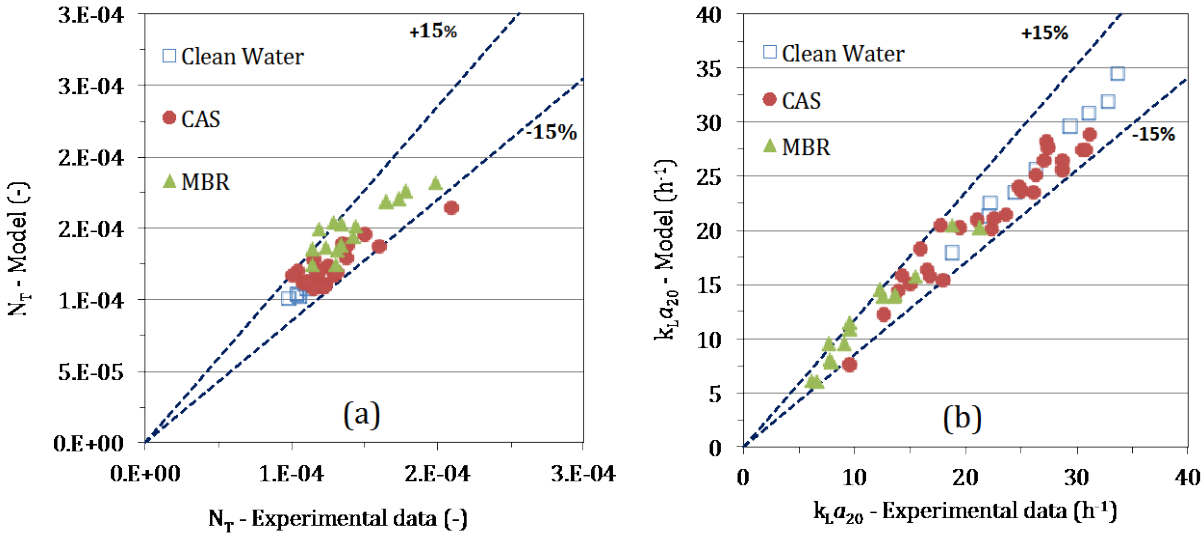

Figure VI.6. Agreement between experimental and modelled transfer number, N_T (a) and between experimental and modelled mass transfer coefficient (b) for the fine bubble diffuser (FB).

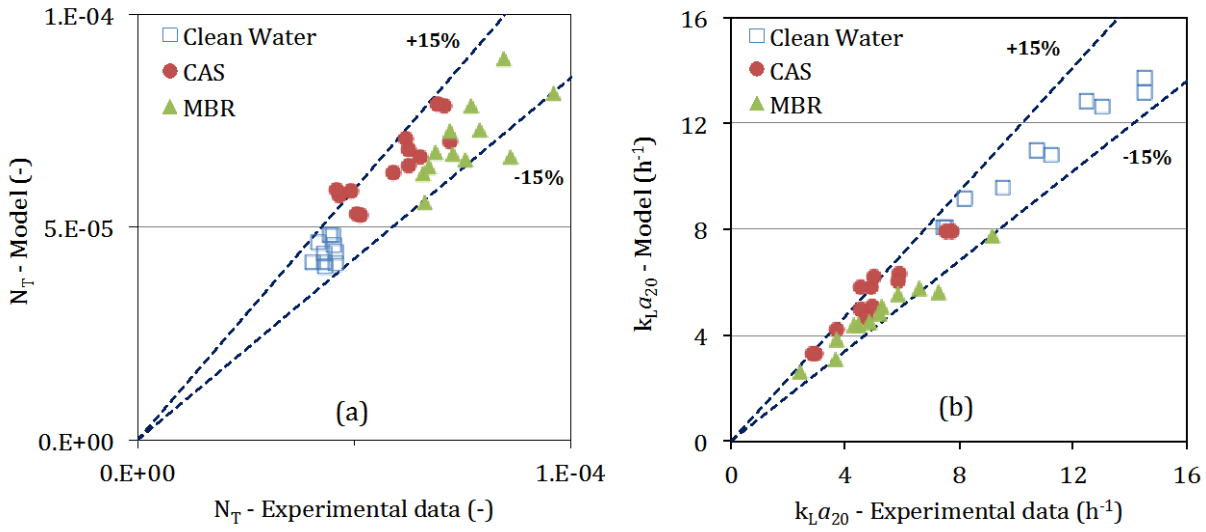

Figure VI.7. Agreement between experimental and modelled transfer number, N_T (a) and between experimental and modelled mass transfer coefficient (b) for the coarse bubble diffuser (CB).

For both aeration systems, the transfer number decreases with an increase in the column Reynolds number (Figure VI.8 and Figure VI.9).

For fine bubble aeration, the experimental transfer number values are in the range 9.9 – 26.3 x 10^{-5} and seem to increase with an increase in the MLSS concentration. The minimal values are obtained for clean water results (9.9 – 12.3 x 10^{-5}) and are in the same order of magnitude than previous results obtained on full-scale aeration tanks with total floor coverage (Capela et al., 2001; Gillot et al., 2005).

For the CB aeration system, the transfer number ranges from 4.0 x10^{-5} to 10x10^{-5}. The order of magnitude of these values is lower than those obtained with FB aeration, highlighting the higher aeration efficiency. Similarly to FB aeration, the lower values are obtained for clean water results.

Integrating inertial forces and physicochemical parameters of the liquid phase including viscous forces, the transfer number (N_T) is an adequate scale-up factor and a tool for oxygen transfer modelling in aerated tanks. However, for various MLSS concentrations, the physical significance of this dimensionless number must not be considered as equivalent to transfer efficiency as for clean water conditions, because it lumps viscosity and velocity impacts. The use of other dimensionless number (mass transfer Stanton number) in the following helps to further analyse and interpret the effect of viscous forces on oxygen transfer efficiency.

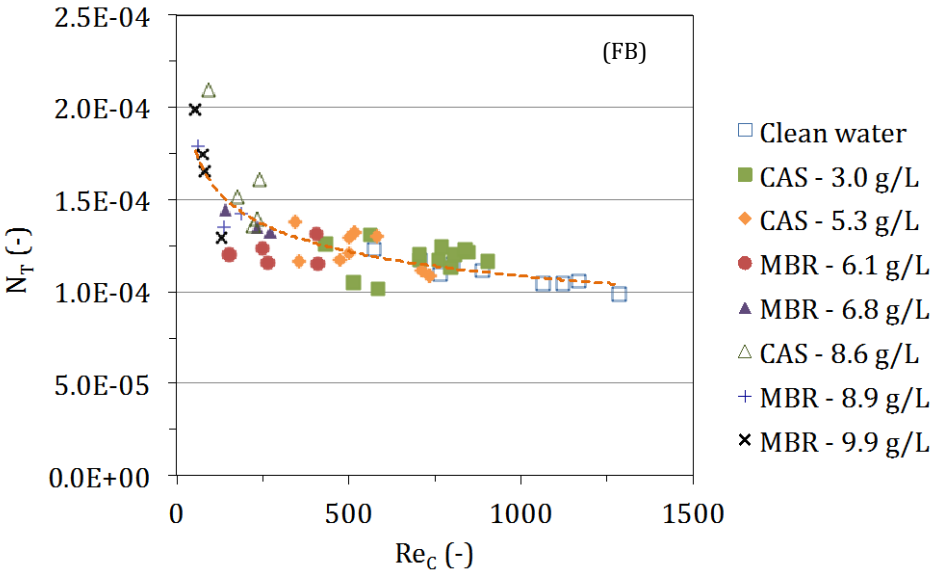

Figure VI.8. Transfer number (N_T) at different column Reynolds number (Re_c) in clean water and activated sludge (CAS and MBR) obtained with the fine bubble diffuser (FB).

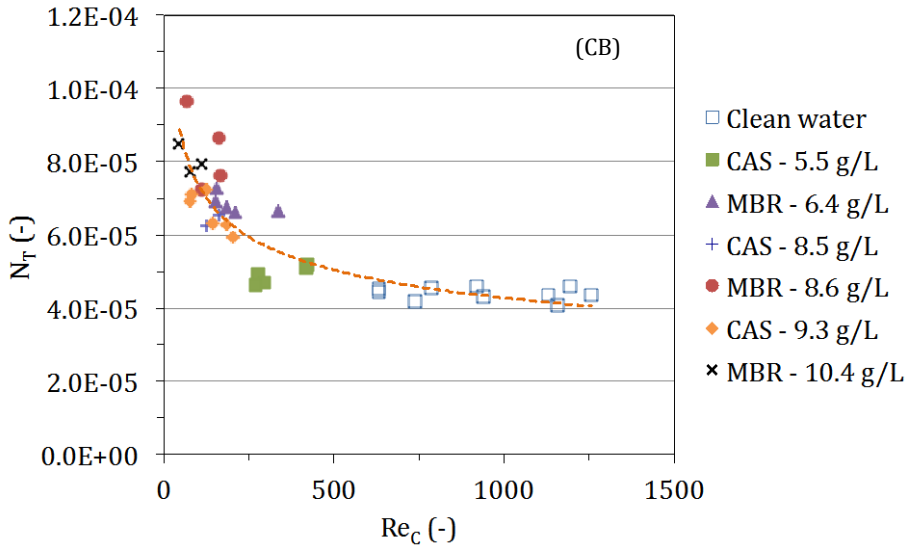

Figure VI.9. Transfer number (N_T) at different column Reynolds number (Re_c) in clean water and activated sludge (CAS and MBR) obtained with the coarse bubble diffuser (CB).

VI.1.5 Interpreting oxygen transfer results with the help of the apparent viscosity

The modelled k_La variations (Eq. VI.14) with the superficial gas velocity for the different MLSS concentrations were drawn and compared to the experimental data. Figure VI.10 shows the agreement between the experimental and the fitted data for CAS and MBR, respectively (fine bubble aeration system). The same representation is given in Figure VI.11 for coarse bubble aeration.

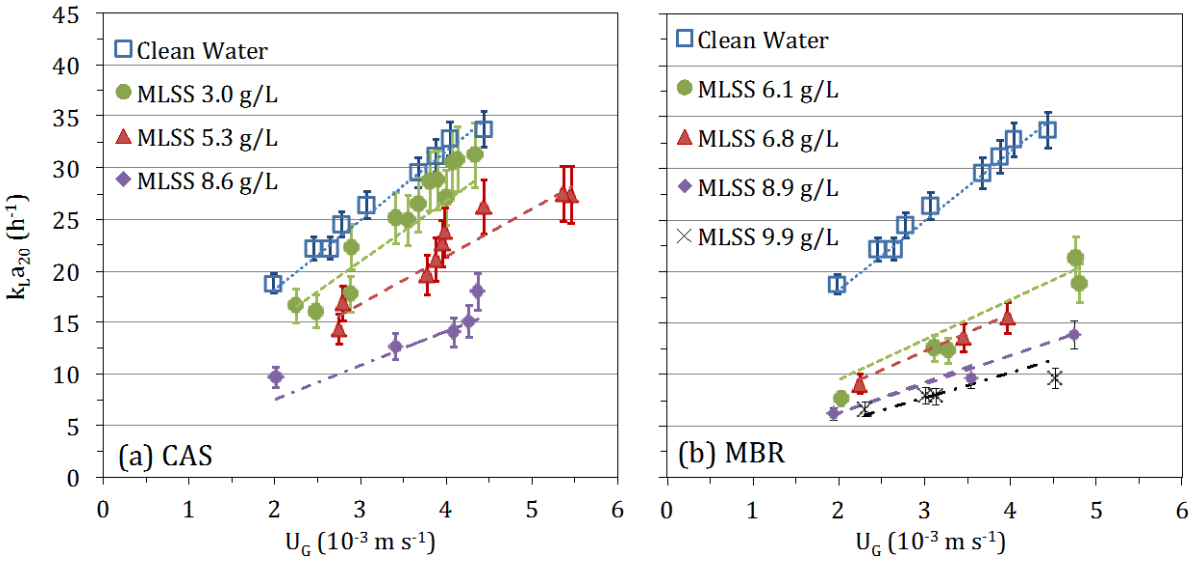

Figure VI.10. Measured and calculated oxygen transfer coefficient (k_La_{20}) as a function of the superficial gas velocity (U_G) for (a) CAS and (b) MBR at different MLSS concentrations using the **fine bubble diffuser (FB)**. Calculated k_La_{20} coefficients (in dotted lines) are estimated by using Equation **VI.14**.

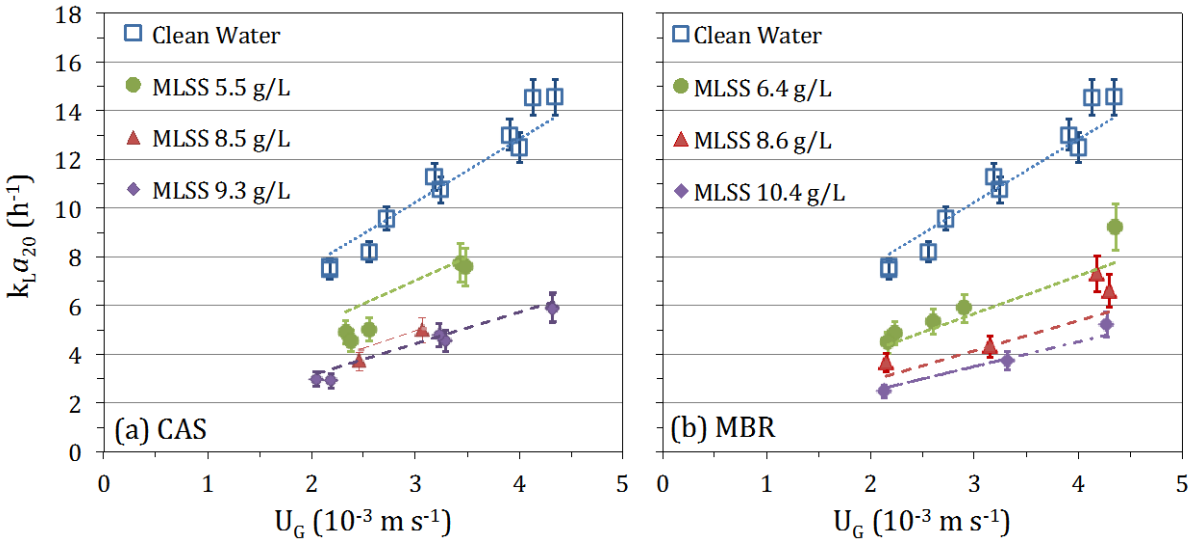

Figure VI.11. Measured and calculated oxygen transfer coefficient (k_La_{20}) as a function of the superficial gas velocity (U_G) for (a) CAS and (b) MBR at different MLSS concentrations using the **coarse bubble diffuser (CB)**. Calculated k_La_{20} coefficients (in dotted lines) are estimated by using Equation **VI.15**.

The impact of MLSS concentration on oxygen transfer is mainly controlled by its effect on the mixed liquor apparent viscosity, considering the sludge shear-thinning behaviour and its variation with the aeration intensity (in relation to the exerted mean shear rate). Taking the effect into account allows to integrate the variations of gas-liquid flow characteristics with MLSS concentration in a mass transfer model. No extra parameter is needed to represent the variations of the mass transfer coefficient despite two origins of activated sludge (CAS and MBR,

with a low F/M ratio and SRT > 15 d) and resulted differences in physicochemical characteristics of the sludge.

The transfer number (N_T) can also be expressed as a combination of mass transfer Stanton number (St_M, ratio of total mass transfer rate to inertia forces which could be considered as equivalent to oxygen transfer efficiency) and Galileo number (Ga, ratio of gravity forces to viscous forces) as presented here below in Equations VI.16 to VI.18.

$$N_T = St_M.Ga^{-1/3} \quad \text{VI.16}$$

$$St_M = \frac{k_L a_{20.} D_c}{U_G} \quad \text{VI.17}$$

$$Ga = \frac{g.D_C^3.\rho_{ML}^2}{\mu_{app,ML}^2} \quad \text{VI.18}$$

The physical significance of Stanton number allows to dissociate mass transfer efficiency from viscous effect and physicochemical characteristics of the liquid phase and is preferred to transfer number for interpretation of AS rheology effect on gas-liquid mass transfer as previously discussed. The Froude number (Fr, ratio of inertial forces to gravitational forces) is also introduced for this interpretation (Equation VI.19).

$$Fr = \frac{U_G^2}{g.D_C} \quad \text{VI.19}$$

where g is the standard gravity constant (m s^{-2}).

For interpreting the impact of AS sludge rheology on gas-liquid mass transfer, the Stanton number is presented as a function of the Galileo number in Figure VI.12 (a) and Figure VI.13(a) for FB and CB aeration systems, respectively.

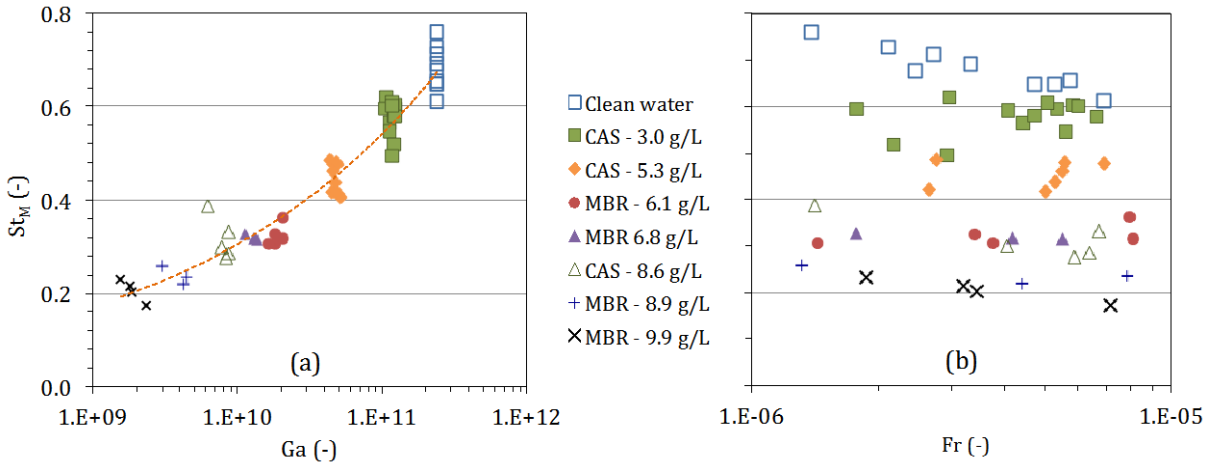

Figure VI.12. Mass transfer Stanton number (St_M) versus Galileo number, Ga (a) and Froude number, Fr (b) for clean water, CAS and MBR – **Fine bubble aeration**.

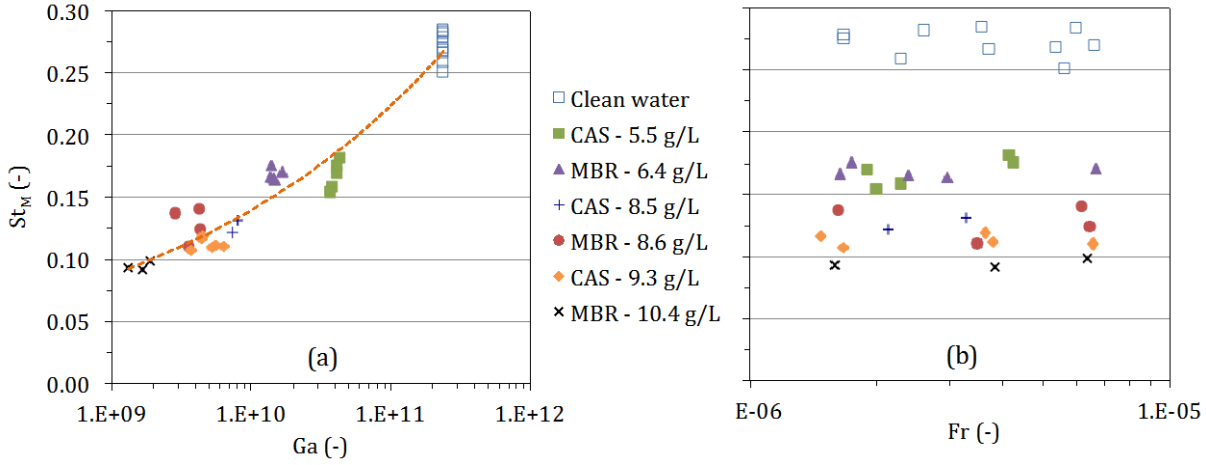

Figure VI.13. Mass transfer Stanton number (St_M) versus Galileo number, Ga (a) and Froude number, Fr (b) for clean water, CAS and MBR – **Coarse bubble aeration**.

For fine bubble aeration system, the Stanton number is comprised between 0.17 and 0.76 with maximum values for clean water operating conditions (from 0.61 to 0.76) and minimum values for maximal MLSS concentration (from 0.17 to 0.23 for a MLSS concentration of 10 g L^{-1}).

For the coarse bubble aeration system, the Stanton number is comprised between 0.09 and 0.28 with maximum values for clean water operating conditions (from 0.25 to 0.28) and minimum values for maximal MLSS concentration (from 0.091 to 0.098 for a MLSS concentration of 10.4 g L^{-1}).

For both aeration systems, the Stanton number is strongly correlated to the Galileo number highlighting that the oxygen transfer efficiency is mainly governed by the AS viscous effects on gas-liquid dynamics in the bubble column, by controlling bubble size (at bubble formation but

also its evolution during bubble rise, due to coalescence and break-up) and rising velocity (in relation to drag forces). It also highlights that the apparent viscosity could be considered as the key parameter to interpret MLSS impact on oxygen transfer efficiency, by integrating the sludge shear-thinning behaviour.

On Figure VI.12 (b) and Figure VI.13 (b), the Stanton number is also presented as a function of the Froude number, in order to compare the impact of the inertial forces (related to gas superficial velocity) to the impact of MLSS concentration (related to viscous forces evolution) on the mass transfer efficiency. As previously discussed, the mass transfer efficiency is mainly controlled by viscous effects (correlated to MLSS concentration and shear rate).

For the fine bubble aeration, the Stanton number also appears to slightly decrease with an increase in the Froude number due to an increase in superficial gas velocity, which is more pronounced for clean water than for AS conditions. In clean water, this impact is mainly due to an increase in bubble size and related rising velocity. For AS operating conditions, the shear-thinning behaviour induces a decrease of the mixed liquor apparent viscosity with an increase in gas superficial velocity, which could counterbalance the effect of superficial air velocity on bubble size in the bubble column filled with AS sludge. It could also explain the slighter impact (or the absence of impact in some cases) of superficial air velocity on oxygen transfer efficiency in AS operating conditions.

On the contrary to results obtained with the FB system, the Stanton number for CB system, clean water and the different MLSS concentrations is independent on the Froude number which shows that the aeration efficiency for the coarse bubble system is not a function of the superficial gas velocity.

VI.1.6 Alpha factor

The impact of MLSS concentration on the alpha factor has been largely commented in the literature (Cornel *et al.,* 2003; Jin *et al.,* 2006; Germain *et al.,* 2007; Gillot and Heduit 2008; Henkel *et al.,* 2009; Mineta *et al.,* 2011; Racault *et al.,* 2011), although MLSS does not allow to explain the entire variability of α-values in all cases.

The alpha factor calculated from the measurements performed in the bubble column on the two sites (CAS and MBR) is shown in Figure VI.14 as a function of the sludge apparent viscosity and for the two aeration systems (FB and CB).

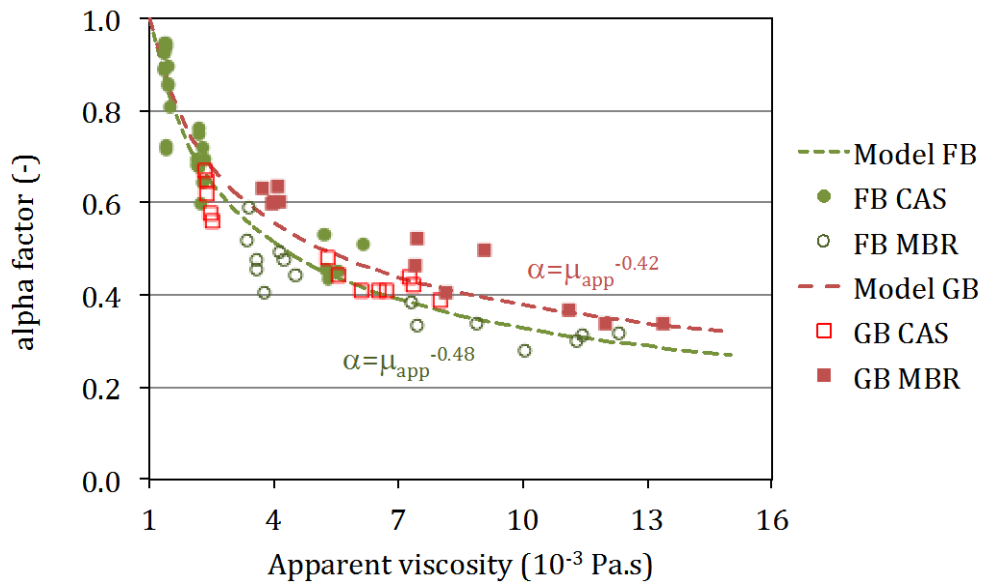

Figure VI.14. Alpha factor as a function of the apparent viscosity. Results and correlations obtained on site (CAS and MBR plants) and the fine and coarse bubbles diffusers.

The observed alpha factor values are highly correlated to the apparent viscosity. α-values obtained with CB aeration are slightly higher than the one obtained with FB aeration. The apparent viscosity has a similar impact on hydrodynamics of the gas phase in the bubble column; however the slight difference could be attributed to impact of physico-chemical characteristics of the interstitial liquid (including surfactant and/or dissolved salt concentration). In the present study, low loaded activated sludge systems have been studied (SRT > 15 d). Therefore the degree of treatment of the interstitial water is high. The differences in CB and FB bubble aeration system, in terms of surface renewal rate linked to the bubble size, do not seem to highly impact oxygen transfer results. This could be completely different if the component in the interstitial water were less degraded.

For the FB aeration system, results are compared with other literature studies having determined the alpha factor with sludge of similar characteristics (domestic sludge from full-scale plants, CAS, MBR). Since the mentioned studies have not evaluated the AS rheological behaviour, the AS apparent viscosity was estimated using a Bingham rheological model issued from the group of rheolological data obtained for the five treatment plants studied in Chapter IV[5]. Literature results have been obtained for full coverage aeration systems, in order to be able to calculate the shear rate in the aeration tanks using Equation VI.7. Figure VI.15 presents the alpha values as a function of the apparent viscosity.

[5] $\tau_y(\text{Pa}) = A \times 10^{-4} \cdot (\text{MLSS}^B)$ with A=29.8, B=2.3 and $K(\text{Pa.s}) = \exp(C \cdot \text{MLSS}^D) \times 10^{-3}$ with C=0.1, D=1.01.

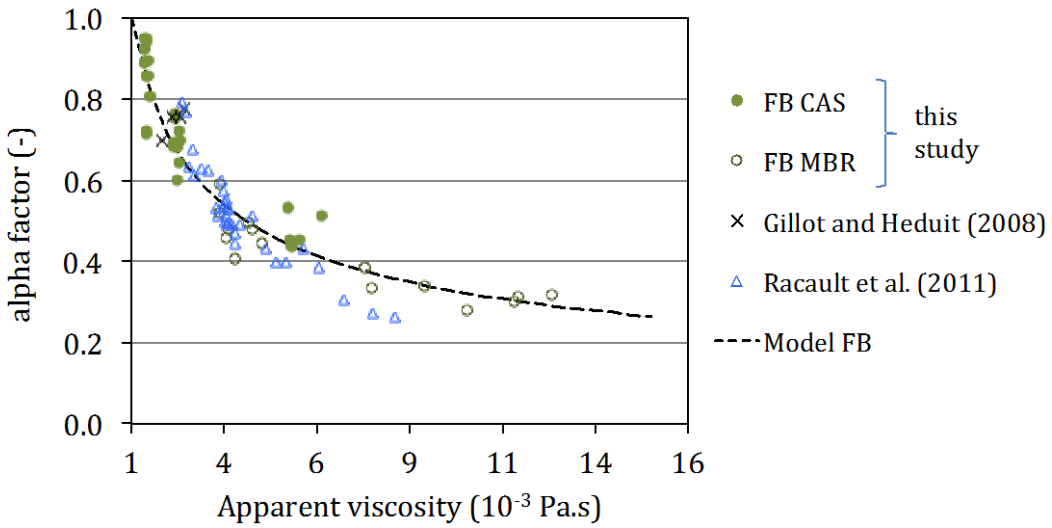

Figure VI.15. Alpha factor as a function of the apparent viscosity. Results and correlation obtained in this study compared to other works performed in full-scale bioreactors.

Despite a data scattering that could be due to the assumed rheological models and to the lack of information concerning the characteristics of the interstitial liquid, the apparent viscosity allows to express the impact of the MLSS concentration on the alpha factor, by integrating the shear-thinning behaviour of the activated sludge together with the impact of the shear rate on oxygen transfer.

Alpha factors obtained for fine bubble aeration systems installed in low loaded activated sludge plants can be estimated from the apparent sludge viscosity as follows:

$$alpha\ factor = {\mu_{app}}^{-0.49} \quad (R^2=0.89) \qquad \text{VI.20}$$

VI.2 Conclusions

- From the rheological experiments and the oxygen transfer coefficient measurements with the FB and the CB diffusers, a powerful model was developed, correlating $k_L a$ to the superficial gas velocity (U_G) and the apparent viscosity, integrating the shear-thinning rheological behaviour of AS. The originality of this correlation lies in the consideration of the impact of rheology and superficial gas velocity on the mean shear stress in the bubble column. This allowed a more accurate representation of the hydrodynamics in the bubble column and hence an adequate reproduction of the experimental oxygen transfer results for activated sludge.
- The apparent viscosity, integrating the shear-thinning behaviour of activated sludge rheology, is the key parameter to interpret the impact of operating conditions (as MLSS concentration and superficial gas velocity) on oxygen transfer efficiency in the bubble column.

Conclusions and Perspectives

Aeration can represent up to 70% of the total electrical consumption in biological wastewater treatment plants. Optimising aeration systems is therefore required to reduce the energy expenditure, in addition to ensure a high level of treatment.

Sludge rheology has been recognised for a long time as a factor that governs bubble size and thus oxygen transfer in subsurface aeration systems, although rheological parameters have not been taken into account directly in aeration models used to design and optimise aeration systems. The main purpose of this study was therefore to evaluate simultaneously the impact of activated sludge (AS) properties and superficial gas velocity on AS **rheological behaviour**, **hydrodynamics** and **oxygen transfer**, in order to propose aeration models that take into account those parameters. To this aim, measurements were performed with activated sludge samples from five full-scale wastewater plants treating domestic effluents.

Rheological behaviour of activated sludge

To characterise the rheological behaviour of activated sludge, a tubular rheometer was specifically designed and constructed in this work taking into account activated sludge characteristics (floc size, settleability, viscosity). The apparatus consists of 4 tubes with diameters comprised between 4 and 14 mm, that allow to impose a shear rate between 50 and 400 s^{-1}. Preliminary tests performed with tap water gave a relative error lower than ±10%, with an average value of 5%. A temperature correction was also developed and validated to compare results obtained on site under different temperature conditions (from 9°C to 27°C).

Experimental rheograms obtained with activated sludge confirmed literature results:

- Activated sludge is a non-Newtonian fluid exhibiting a shear thinning behaviour: the apparent viscosity is reduced with an increase in the shear rate.
- Activated sludge rheological behaviour is significantly determined by the MLSS concentration, the apparent viscosity increasing exponentially with an increase in the MLSS concentration.

In parallel to rheological measurements, AS properties comprising floc size, floc cohesiveness, soluble COD, surfactants and cations concentrations, surface tension and sludge volume index were determined in order to investigate their impact on the rheological behaviour. The obtained results showed that:

- Viscosity not only depends on MLSS concentration, but also on the physical characteristics of the flocs (their size but also their structure defined by cohesiveness

and density). This may explain the difference in sludge rheological behaviour obtained with the different activated sludge samples in this study. For a given MLSS concentration, the floc structure and the total volume occupied by the solid phase (related to the floc size and density) have an impact on the floc interaction (collision or friction) in the dispersion, consequently differentiating the rheological characteristics.

- Other AS properties related to the sludge interstitial water such as soluble COD, surfactants and cations concentrations or static surface tension were not shown to have an effect on AS rheological behaviour, in the range of concentrations measured in this study.

Modelling experimental rheograms

Measurements performed with an MLSS concentration comprised between 2.3 and 10.2 $g.L^{-1}$ show that:

- Models with three parameters (Sisko and Herschel Bulkley) provide in general a better adjustment to individual experimental rheograms than two-parameter models (Ostwald-de Waele, Bingham, Casson). However, for some rheograms, two-parameter models give similar goodness-of-fit as three-parameter models. Representing the different rheological parameters as a function of the MLSS concentration in addition highlights a potential lack of identifiability for the parameters of the Sisko, Herschel Bulkley and Casson equations. Consequently, to model the group of experimental rheograms, the two-parameter models, especially the Ostwald-de Waele and the Bingham equation, were preferred in order to avoid over-parameterisation that may lead to models with low prediction capacity.
- When modelling the group of rheograms with one equation, experimental data was divided in two sets according to their different trends of apparent viscosity as a function of the MLSS concentration, which was related to the difference in floc characteristics (diameter, floc, structure). For the two sets of rheograms, the Bingham equation represents slightly better the experimental curves (lowest RSS/N, lowest average relative error).
- Different aspects may explain the observed discrepancy between some rheological models proposed in the literature and the correlations proposed in this study as a function of the MLSS concentration, in particular at low shear rates. These are the use of different rheometer geometries more or less adapted to the sample characteristics (sludge settleability), the reduction of the instrument accuracy at low shear rates and the

influence of other AS properties on sludge rheology, different to MLSS concentration, that can be reduced with the increase of the shear rate.

Oxygen transfer in a bubble column located on site

In parallel to rheological measurements, the impact of superficial gas velocity (U_G within 1.9x10^{-3} and 5.5 x10^{-3} m s^{-1}), gas diffuser type (FB and CB) and AS properties on oxygen transfer and overall gas hold-up was studied in the bubble column (Dc=0.29 m, Hc=4.4 m). The experimental set-up was installed on two wastewater treatment plants: a conventional AS plant (CAS) and a membrane bioreactor (MBR) treating domestic wastewater. The MLSS concentrations varied from 3.0 to 10.4 g L^{-1} thanks to different sludge sampling locations (aeration tank, recirculation loop, membrane reactor).

Experimental results in clean water showed that:

- The overall gas hold-up (ε_G) and the oxygen transfer coefficient ($k_L a_{20}$) increase with an increase in the superficial gas velocity. Since the estimated liquid-side transfer coefficienf (k_L) appeared to be independent on the superficial gas velocity, the increase in $k_L a_{20}$ is attributed to the enhancement of the interfacial area (a). For a given airflow rate, the oxygen transfer coefficient was higher for the FB aeration system compared to the CB aeration system by at least a factor 2.3. This is attributed to the smaller bubble size obtained with the FB diffuser that results in higher overall gas hold-up (e.g. 1.6% versus 1.1% at U_G=4.5x10^{-3} m s^{-1}) and interfacial area.
- Expressing the results with dimensionless numbers such as the Transfer number (N_T) and the column Reynolds number (Re_{column}) showed that for CB aeration, the aeration efficiency was independent on the superficial gas velocity traducing a linear dependence between the oxygen transfer coefficient and the airflow rate. For FB aeration, the aeration efficiency decreased in a power law trend with an increase in the superficial gas velocity. For this type of diffuser, this trend is related to the power law dependency of bubble size on superficial gas velocity.
- Comparing the results with full-scale measurements clearly shows that the bubble Sauter diameter is the key parameter governing the transfer number in clean water.

Measurements performed on site, while continuously feeding the column with activated sludge showed that:

- For both aeration systems, the overall-gas hold-up and the oxygen transfer coefficient in AS increased with an increase in the superficial gas velocity. $k_L a_{20}$ values were however

lower compared to those obtained in clean water. For a given superficial gas velocity, the oxygen transfer coefficient decreases as the MLSS concentration increases. This reduction in oxygen transfer is partially attributed to the observed decrease in the overall gas hold-up in activated sludge compared to clean water conditions. The impact of suspended solids on the overall gas hold-up was explained by three counterbalancing phenomena induced by the increase of apparent viscosity: (i) promoted bubble coalescence, (ii) extended time of bubble formation and (iii) higher bubble drag coefficient. Increasing the MLSS concentration led to an augmentation of the apparent viscosity and larger bubbles may be generated but may not necessarily rise faster because the bubble drag coefficient is also higher.

- Among the evaluated activated sludge characteristics, the concentration of non-ionic surfactants in the interstitial water, detected in AS from the MBR, was shown to be significantly correlated with the oxygen transfer coefficient in the case of fine bubble aeration and low MLSS concentration. This is explained by the different regimes generated by the fine (FB) and the coarse bubbles (CB), the latter having higher surface renewal rates and consequently reducing the impact of bubble contamination at the g/L interface.
- Since the oxygen diffusivity and the overall gas hold-up in AS are not significantly impacted by the sludge properties, it is argued that the further impact of MLSS concentration on oxygen transfer coefficient is due to (i) variations in bubble size related to extended bubble growth time and promoted coalescence that induce a reduction of the interfacial area and/or (ii) to a decrease in the liquid-side transfer coefficient due to transport limitation.
- For a given superficial gas velocity and diffuser type, the alpha factor is a decreasing function of the MLSS concentration. For the coarse bubble aeration, alpha factors appeared to be independent on the superficial gas velocity. For fine bubble aeration, the alpha factor trend with superficial gas velocity appeared to be a function of the MLSS content: for AS with low MLSS concentration (<6.1 g L^{-1}), alpha factor increases with an augmentation of the superficial gas velocity and for higher MLSS concentrations, the alpha factor remained constant or was reduced with an increase in the superficial gas velocity. These different trends were attributed to the competitive effect of surfactants and MLSS concentration on bubble size evolution which depends on the aeration system.
- For a given superficial gas velocity and MLSS concentration, the alpha factor values obtained for **CAS** with FB aeration were slightly lower than those obtained with CB aeration. This difference was attributed to the detected concentrations of non-ionic

surfactants and the fact that under CB aeration, the effect of bubble contamination at the g/L interface is reduced due to the previously mentioned higher surface renewal rates.

Interpreting oxygen transfer parameters with the help of rheology

The impact of AS properties and superficial gas velocity on the oxygen transfer parameters was finally further analysed with the help of rheological results. The apparent viscosity in the bubble column was therefore evaluated. To that aim, the average shear rate prevailing in the bubble column was first theoretically estimated considering the applied values of superficial gas and liquid velocities, the overall gas hold-up and the AS rheological behaviour (function of the MLSS concentration). For the studied operating conditions, the estimated shear rate ranged from 65 to 243 s^{-1}. An empirical model linking the measured oxygen transfer coefficient to the apparent viscosity was developed:

$$k_L a_{20} = \mathrm{A}\ \ {U_G}^{B}\ {\mu_{app,ML}}^{C} \quad \text{with}$$

Diffuser type	A	B	C
FB	2.84×10^{-2}	0.81	-0.48
CB	1.24×10^{-2}	0.76	-0.43

This formula traduces that the oxygen transfer coefficient ($k_L a_{20}$) is only determined by the superficial gas velocity (U_G), the apparent viscosity of the mixed liquor ($\mu_{app,ML}$) and the aeration system. The impact of the superficial gas velocity and the apparent viscosity on $k_L a$ is more significant for FB aeration than for CB aeration.

The proposed correlation was also represented in terms of the dimensionless transfer number (N_T) and column Reynolds number (Re_{column}) and further interpretation of the obtained variations was made by means of the Stanton transfer number (St_M), the Galileo number (Ga) and the Froude number (Fr). This representation highlights that for the fine and the coarse bubble aeration systems, the aeration efficiency increases with a reduction of the sludge apparent viscosity. Also it showed that with CB aeration and for a given MLSS concentration, the aeration efficiency is independent on the superficial gas velocity, which traduces the linear dependency of oxygen transfer on the airflow rate. With FB aeration, the aeration efficiency for a given MLSS concentration appeared to decrease with an increase in the superficial gas velocity which relates to the effect of airflow rate on bubble diameter.

Finally, correlating the alpha factor with the apparent viscosity, and its dependence to the shear rate, reduced data scattering compared to the correlation between alpha factor and MLSS concentrations. For results obtained in the present study, alpha factor is a decreasing function of apparent viscosity with a power law coefficient of -0.48 and -0.42 for fine and coarse bubble aeration respectively.

Perspectives

The following perspectives have been identified to improve the understanding and the modelling of the rheological behaviour of activated sludge and the oxygen transfer in full-scale aeration tank:

- Impact of solid phase characteristics on sludge rheology: Rheological measurements with AS from different origins and with equivalent MLSS concentration as well as simultaneous AS characterization including SVI and flocs properties (diameter, cohesiveness, structure) would help to confirm the significance of the these floc properties in defining the rheological behaviour of AS. Also, data about the floc density and size and its dependence on influent characteristics and process operating conditions (mixing, pumping, aeration, sludge age) would contribute to develop predictive models.
- Estimation of average shear rate in aerated tanks: The average shear rate prevailing in the bubble column have to be evaluated experimentally under fine and coarse bubble aeration and confronted with the theoretically estimated average shear rate in the present work. It would be interesting to also experimentally determine the average shear rate in full-scale aerated bioreactors where shear is exerted by the rising bubbles and the stirring system.
- Impact of non-Newtonian fluid on local characteristics of the gas phase in the bubble column: Characterising oxygen transfer parameters such as bubble size, bubble rise velocity and overall gas hold-up in a model translucent viscous media whose rheological behaviour is also evaluated would help to confront hypothesis made in the present work associated to the impact of apparent viscosity, in particular concerning an enhanced coalescence phenomena, an extended bubble growth time at formation stage and the increment of the bubble drag coefficient.
- To integrate physicochemical characteristics of the liquid and solid phase of activated sludge in a same oxygen transfer model, a further evaluation of the impact of soluble substances on oxygen transfer coefficient in particular for the interest of treatment plants where the concentration of soluble substances in the aeration tank can reach

higher values than those measured in the present study. This could be performed by installing the experimental set-up near to a full-scale reactor with plug flow configuration and by performing oxygen transfer tests with AS alternatively sampled at different points along the reactor. Such experiments will help to evaluate the relative effect of viscosity and surfactants on oxygen transfer.

Bibliography

Al-Masry W. A. 1999. Effect of scale-up on average shear rates for aerated non-Newtonian liquids in external loop airlift reactors. Biotechnology and Bioengineering. 62. (4). pp. 494-498.

Al-Masry W. A. and Chetty M. 1996. On the estimation of effective shear rate in external loop airlift reactors: non-Newtonian fluids. Resources, Conservation and Recycling. 18. (1-4). pp. 11-24.

Alves S. S., Maia C. I. and Vasconcelos J. M. T. 2004. Gas-liquid mass transfer coefficient in stirred tanks interpreted through bubble contamination kinetics. Chemical Engineering and Processing: Process Intensification. 43. (7). pp. 823-830.

Alves S. S., Orvalho S. P. and Vasconcelos J. M. T. 2005. Effect of bubble contamination on rise velocity and mass transfer. Chemical Engineering Science. 60. (1). pp. 1-9.

Alves S. S., Vasconcelos J. M. T. and Orvalho S. P. 2006. Mass transfer to clean bubbles at low turbulent energy dissipation. Chemical Engineering Science. 61. (4). pp. 1334-1337.

ASCE 1992. Standard Measurement of Oxygen Transfer in Clean Water. American Society of Civil Engineers

ASCE 1996. Standard Guidelines for In-Process Oxygen Transfer Testing. American Society of Civil Engineers.

Banisi S., Finch J. A., Laplante A. R. and Weber M. E. 1995. Effect of solid particles on gas holdup in flotation columns--II. Investigation of mechanisms of gas holdup reduction in presence of solids. Chemical Engineering Science. 50. (14). pp. 2335-2342.

Baudez J.-C. (2008). La gestion des boues résiduaires: de l'étude de la matière molle à la valorisation de la matière organique. Montoldre.

Baudez J.-C., Ayol A. and Coussot P. 2004. Practical determination of the rheological behavior of pasty biosolids. Journal of Environmental Management. 72. (3). pp. 181-188.

Biggs C. A. and Lant P. A. 2000. Activated sludge flocculation: on-line determination of floc size and the effect of shear. Water Research. 34. (9). pp. 2542-2550.

Bouaifi M., Hebrard G., Bastoul D. and Roustan M. 2001. A comparative study of gas hold-up, bubble size, interfacial area and mass transfer coefficients in stirred gas–liquid reactors and bubble columns. Chemical Engineering and Processing: Process Intensification. 40. (2). pp. 97-111.

Bouche E., Roig V., Risso F. and Billet A.-M. 2012. Homogeneous swarm of high-Reynolds-number bubbles rising within a thin gap. Part 1. Bubble dynamics. Journal of Fluid Mechanics. 704. pp. 211-231.

Bouyer D., Coufort C., Liné A. and Do-Quang Z. 2005. Experimental analysis of floc size distributions in a 1-L jar under different hydrodynamics and physicochemical conditions. Journal of Colloid and Interface Science. 292. (2). pp. 413-428.

Bouyer D., Line A., Cockx A. and Do-quang Z. 2001. Experimental Analysis of Floc Size Distribution and Hydrodynamics in a Jar-Test. Chemical Engineering Research and Design. 79. (8). pp. 1017-1024.

Calderbank P. H. and Moo-Young M. B. 1961. The continuous phase heat and mass-transfer properties of dispersions. Chemical Engineering Science. 16. (1–2). pp. 39-54.

Capela S. 1999.Influence des facteurs de conception et des conditions de fonctionnement des stations d'épuration en boues activées sur le transfert d'oxygène. Thèse de Doctorat, Université Paris XII - Val de Marne, 158 p + annexes.

Capela S., Gillot S. and Héduit A. 2004. Comparison of Oxygen-Transfer Measurement Methods Under Process Conditions. Water Environment Research. 76. (2). pp. 183-188.

Cerecero Enriquez R. 2003.Etude des écoulements et des transferts thermiques lors de la fabrication d'un sorbet à l'échelle du pilote et du laboratoire. INA P-G, 161 p. + annexes.

Cerri M. O., Futiwaki L., Jesus C. D. F., Cruz A. J. G. and Badino A. C. 2008. Average shear rate for non-Newtonian fluids in a concentric-tube airlift bioreactor. Biochemical Engineering Journal. 39. (1). pp. 51-57.

Chisti Y. and Moo-Young M. 1989. On the calculation of shear rate and apparent viscosity in airlift and bubble column bioreactors. Biotechnology and Bioengineering. 34. (11). pp. 1391-1392.

Chu C.P., Lee D.J. 2004. Multiscale structures of biological flocs. Chemical Engineering Science. 59. (8–9) pp. 1875-1883.

Clift R., Grace J. and Weber M. E. 1978. Bubbles, drops and particles. Academic Press, New York.

Cockx A. 1997. Modélisation de contacteurs gaz/liquide : Application de la mécanique des fluides numériques aux airlifts. Thèse de Doctorat, INSA Tolouse, 165 p. + annexes.

Cockx A., Do-Quang Z., Audic J. M., Liné A. and Roustan M. 2001. Global and local mass transfer coefficients in waste water treatment process by computational fluid dynamics. Chemical Engineering and Processing. 40. (2). pp. 187-194.

Colombet D., Legendre D., Cockx A., Guiraud P., Risso F., Daniel C. and Galinat S. 2011. Experimental study of mass transfer in a dense bubble swarm. Chemical Engineering Science. 66. (14). pp. 3432-3440.

Cornel P., Wagner M. and Krause S. 2003. Investigation of oxygen transfer rates in full scale membrane bioreactors. Water Science and Technology. 47. (11). pp. 313-319.

Cornillon P.-A., Guyader A., Husson F., Jégou N., Josse J., Kloareg M., Matzner-Lober É. and Rouvière L. 2012. Statistiques avec R (3ème édition). PRESSES UNIVERSITAIRES DE RENNES. Pratique de la statistique. pp. 296.

Coufort C., Dumas C., Bouyer D. and Liné A. 2008. Analysis of floc size distributions in a mixing tank. Chemical Engineering and Processing: Process Intensification. 47. (3). pp. 287-294.

Craig V. S. J. 2004. Bubble coalescence and specific-ion effects. Current Opinion in Colloid & Interface Science. 9. (1-2). pp. 178-184.

Craig V. S. J. 2011. Do hydration forces play a role in thin film drainage and rupture observed in electrolyte solutions? Current Opinion in Colloid & Interface Science. (0).

CTGREF 1980. Les preformances des systèmes d'aération des procédés d'épuration: Méthodes de mesure et résultats.

Czarnota Z. and Hahn T. 1995. Effect of horizontal flow on aeration. Document Flygt.

Deckwer W.-D., Louisi Y., Zaidi A. and Ralek M. 1980. Hydrodynamic Properties of the Fischer-Tropsch Slurry Process. Industrial & Engineering Chemistry Process Design and Development. 19. (4). pp. 699-708.

Déronzier G., Gillot S., Duchene P. and Héduit A. 1996. Influence de la vitesse horizontale du fluide sur le transfert d'oxygène en fines bulles dans les bassins d'aération. Tribune de l'eau (5-6). pp. 91-97.

Descoins N., Deleris S., Lestienne R., Trouvé E., Maréchal F. 2012. Energy efficiency in wastewater treatments plants: optimization of activated sludge process coupled with anaerobic digestion. Energy 41. pp. 153–164.

Dhaouadi H., Poncin S., Hornut J. M. and Wild G. 2006. Solid effects on hydrodynamics and heat transfer in an external loop airlift reactor. Chemical Engineering Science. 61. (4). pp. 1300-1311.

Dietrich N., Francois J., Jimenez M., Cockx A., Guiraud, P., Hébrard, G. 2015 Fast measurements of the gas-liquid diffusion coefficient in the gaussian wake of a spherical bubble. Chemical Engineering and Technology, 38(5), pp. 941-946

Dieudé-Fauvel E., Van Damme H. and Baudez J. C. 2009. Improving rheological sludge characterization with electrical measurements. Chemical Engineering Research and Design. 87. (7). pp. 982-986.

Domínguez L., Rodríguez M. and Prats D. 2010. Effect of different extraction methods on bound EPS from MBR sludges. Part I: Influence of extraction methods over three-dimensional EEM fluorescence spectroscopy fingerprint. Desalination. 261. (1-2). pp. 19-26.

Dubus M. 1994.Moulage par injection de poudres réalisation d'un rhéomètre capillaire et application à l'étude du comportement de pâtes chargées. II-105 f. multigr. + annexes.

Dubus M. and Burlet H. 1997. Rheological behaviour of a polymer ceramic blend. Journal of the European Ceramic Society. 17. (2-3). pp. 191-196.

Duchène P. 1995. Comment réussir un essai d'aérateur en eau propre. 36 p. + annexes.

Dupuis D. 2008. Mesure de la viscosité - Viscosimètres et rhéomètres. Techniques de l'ingénieur. Métrologie relative aux fluides - Vitesses et débits. Base documentaire : TIB402DUO. (Ref. article : r2351).

Elskens M. 2010. Analyse des eaux résiduaires Mesure de la pollution. Techniques de l'ingénieur Analyses dans l'environnement. base documentaire : TIB382DUO. (ref. article : p4200).

Fayolle Y. 2006.Modélisation de l'hydrodynamique et du transfert d'oxygène dans les chenaux d'aération. Thèse de Doctorat, INSA Toulouse, 247 p. + annexes.

Fayolle Y., Cockx A., Gillot S., Roustan M. and Héduit A. 2007. Oxygen transfer prediction in aeration tanks using CFD. Chemical Engineering Science. 62. (24). pp. 7163-7171.

Fayolle Y., Cockx A., Legendre D. and Gillot S. 2011. Analysis of bubble populations obtained in full-scale aeration tanks in clean water. GLS 10 - Gas liquid and gas liquid solid reactor engineering congres. 26/06/2011-29/06/2011. Braga, Portugal.

Fayolle Y., Gillot S., Cockx A., Bensimhon L., Roustan M. and Heduit A. 2010. In situ characterization of local hydrodynamic parameters in closed-loop aeration tanks. Chemical Engineering Journal. 158. (2). pp. 207-212.

Forster C. F. 1982. Sludge surfaces ans their relation to the rheologie of sewage sludge suspensions. Chem Tech Biotech. 30. (3). pp. 799-807.

Forster C. F. 1983. Bound water in sewage sludge and its relationship to sludge surfaces and sludge viscosities. Chem. Tech. Biotechnol. 33B. pp. 76-84.

Forster C. F. 2002. The rheological and physico-chemical characteristics of sewage sludges. Enzyme and Microbial Technology. 30. (3). pp. 340-345.

Fransolet E., Crine M., Marchot P. and Toye D. 2005. Analysis of gas holdup in bubble columns with non-Newtonian fluid using electrical resistance tomography and dynamic gas disengagement technique. Chemical Engineering Science. 60. (22). pp. 6118-6123.

Freitas C. and Teixeira J. A. 2001. Oxygen mass transfer in a high solids loading three-phase internal-loop airlift reactor. Chemical Engineering Journal. 84. (1). pp. 57-61.

Frølund B., Palmgren R., Keiding K. and Nielsen P. H. 1996. Extraction of extracellular polymers from activated sludge using a cation exchange resin. Water Research. 30. (8). pp. 1749-1758.

Gabelle J.-c. 2012.Analyse locale et globale de l'hydrodynamique et du transfert de matière dans des fluides à rhéologie complexe caractéristiques des milieux de fermentation. + annexes.

Gabelle J. C., Jourdier E., Licht R. B., Ben Chaabane F., Henaut I., Morchain J. and Augier F. 2012. Impact of rheology on the mass transfer coefficient during the growth phase of Trichoderma reesei in stirred bioreactors. Chemical Engineering Science. 75. (0). pp. 408-417.

Gaddis E. S. and Vogelpohl A. 1986. Bubble formation in quiescent liquids under constant flow conditions. Chemical Engineering Science. 41. (1). pp. 97-105.

Garcia-Ochoa F. and Gomez E. 2009. Bioreactor scale-up and oxygen transfer rate in microbial processes: An overview. Biotechnology Advances. 27. (2). pp. 153-176.

Gardener M. 2012. Statistics for ecologist using R and excel. Exeter, Pelagic publishing.

Germain E., Nelles F., Drews A., Pearce P., Kraume M., Reid E., Judd S. J. and Stephenson T. 2007. Biomass effects on oxygen transfer in membrane bioreactors. Water Research. 41. (5). pp. 1038-1044.

Gillot S. 1997.Transfert d'oxygène en boues activées par insufflation d'air. Mesure et éléments d'interprétation. Thèse de Doctorat, Université Paris XII - Val de Marne, 145 p. + annexes.

Gillot S., Capela-Marsal S., Roustan M. and Héduit A. 2005. Predicting oxygen transfer of fine bubble diffused aeration systems—model issued from dimensional analysis. Water Research. 39. (7). pp. 1379-1387.

Gillot S., Capela S. and Heduit A. 2000. Effect of horizontal flow on oxygen transfer in clean water and in clean water with surfactants. Water Research. 34. (2). pp. 678-683.

Gillot S. and Héduit A. 2000. Effect of air flow rate on oxygen transfer in an oxidation ditch equipped with fine bubble diffusers and slow speed mixers. Water Research. 34. (5). pp. 1756-1762.

Gillot S. and Héduit A. (2003). Predicting oxygen transfer in annular ditches equipped with fine bubble diffusers and mixers. 75th annual conference WEFTEC'03: Oxygen transfer, Los Angeles, USA, October 2003.

Gillot S. and Vanrolleghem P. A. 2003. Equilibrium temperature in aerated basins, comparison of two prediction models. Water Research. 37. (15). pp. 3742-3748.

Gillot S. and Héduit A. 2004. Prédiction des capacités d'oxygénation en eau claire des systèmes d'insufflation d'air. Antony, Cemagref Editions.

Gillot S., Capela-Marsal S., Roustan M. and Héduit A. 2005. Predicting oxygen transfer of fine bubble diffused aeration systems—model issued from dimensional analysis. Water Research. 39. (7). pp. 1379-1387.

Gillot S. and Héduit A. 2008. Prediction of alpha factor values for fine pore aeration systems. Water Science and Technology. 57. (8). pp. 1265-1269.

Gillot S. 2010. Optimisation du traitement biologique des eaux résiduaires; de la mesure à la modélisation. Habilitation à diriger des recherches. Université de Montpellier II. Ecole Doctorales Sciences des Procédés - Sciences des Aliments.

Harmathy T. Z. 1960. Velocity of large drops and bubbles in media of infinite or restricted extent. AIChE Journal. 6. (2). pp. 281-288.

Hebrard G. 1995.Etude de l'influence du distributeur de gaz sur l'hydrodynamique et le transfert de matière gaz-liquide des colonnes à bulles. [8]-174-[179] f + annexes.

Hebrard G., Zeng J. and Loubiere K. 2009. Effect of surfactants on liquid side mass transfer coefficients: A new insight. Chemical Engineering Journal. 148. (1). pp. 132-138.

Henkel J., Lemac M., Wagner M. and Cornel P. 2009. Oxygen transfer in membrane bioreactors treating synthetic greywater. Water Research. 43. (6). pp. 1711-1719.

Henkel J. 2010.Oxygen Transfer Phenomena in Activated Sludge. Technische Universität Darmstadt, + annexes.

Henzler H.-J. 1980. Begasen höherviskoser Flüssigkeiten. Chemie Ingenieur Technik. 52. (8). pp. 643-652.

Henzler H. J. and Kauling J. 1985. Scale-up of mass transfer in highly viscous liquids. 5th European Conference in Mixing; Würzburg/Germany. (30). pp. 303-312.

Higbie R. 1935. The rate of absorption of a pure gas into still liquid during short periods of exposure. New York,

Hreiz R., Latifi M.A., Roche N. 2015. Optimal design and operation of activated sludge processes: State-of-the-art. Review. Chemical Engineering Journal. 981. pp. 900-920.

Ishii M. and Zuber N. 1979. Drag coefficient and relative velocity in bubbly, droplet or particulate flows. AIChE Journal. 25. (5). pp. 843-855.

Jamialahmadi M., Zehtaban M. R., Müller-Steinhagen H., Sarrafi A. and Smith J. M. 2001. Study of Bubble Formation Under Constant Flow Conditions. Chemical Engineering Research and Design. 79. (5). pp. 523-532.

Jamnongwong M., Loubiere K., Dietrich N. and Hebrard G. 2010. Experimental study of oxygen diffusion coefficients in clean water containing salt, glucose or surfactant: Consequences on the liquid-side mass transfer coefficients. Chemical Engineering Journal. 165. (3). pp. 758-768.

Jimenez M. 2013.Etude du transfert de matière gaz/liquide en milieux complexes : quantification du transfert d'oxygène par techniques optiques. 210 p. + annexes.

Jin B. and Lant P. 2004. Flow regime, hydrodynamics, floc size distribution and sludge properties in activated sludge bubble column, air-lift and aerated stirred reactors. Chemical Engineering Science. 59. (12). pp. 2379-2388.

Jin B., Wilén B.-M. and Lant P. 2003. A comprehensive insight into floc characteristics and their impact on compressibility and settleability of activated sludge. Chemical Engineering Journal. 95. (1–3). pp. 221-234.

Jin B., Yin P. and Lant P. 2006. Hydrodynamics and mass transfer coefficient in three-phase air-lift reactors containing activated sludge. Chemical Engineering and Processing. 45. (7). pp. 608-617.

Johansen S. T. and Boysan F. 1988. Fluid dynamics in bubble stirred ladles: Part II. Mathematical modeling. Metallurgical Transactions B. 19. (5). pp. 755-764.

Karamanev D. G. 1994. Rise of gas bubbles in quiescent liquids. AIChE Journal. 40. (8). pp. 1418-1421.

Kawase Y. and Hashiguchi N. 1996. Gas-liquid mass transfer in external-loop airlift columns with newtonian and non-newtonian fluids. The Chemical Engineering Journal and the Biochemical Engineering Journal. 62. (1). pp. 35-42.

Kawase Y. and Kumagai T. 1991. Apparent viscosity for non-Newtonian fermentation media in bioreactors. Bioprocess and Biosystems Engineering. 7. (1). pp. 25-28.

Kazakis N. A., Mouza A. A. and Paras S. V. 2008. Experimental study of bubble formation at metal porous spargers: Effect of liquid properties and sparger characteristics on the initial bubble size distribution. Chemical Engineering Journal. 137. (2). pp. 265-281.

Kestin J., Sokolov M. and Wakeham W. A. 1978. Viscosity of liquid water in range -8°C to 150°C. Journal of Physical and Chemical Reference Data. 7. (3). pp. 941-948.

Khare A. S. and Joshi J. B. 1990. Effect of fine particles on gas hold-up in three-phase sparged reactors. The Chemical Engineering Journal. 44. (1). pp. 11-25.

Khongnakorn W., Mori M., Vachoud L., Delalonde M. and Wisniewski C. 2009. Rheological properties of sMBR sludge under unsteady state conditions. Desalination. 250. (2). pp. 824-828.

Krampe J. and Krauth K. 2003. Oxygen transfer into activated sludge with high MLSS concentrations. Water Science and Technology. 47. (11). pp. 297-303.

Kulkarni A. A. and Joshi J. B. 2005. Bubble Formation and Bubble Rise Velocity in Gas−Liquid Systems: A Review. Industrial & Engineering Chemistry Research. 44. (16). pp. 5873-5931.

Lotito, V., Spinosa, L., Mininni, G., Antonacci, R., 1997. The rheology of sewage sludge at different steps of tretment. Water Sci. Technol. 36(11), pp. 79–85.

Laera G., Giordano C., Pollice A., Saturno D. and Mininni G. 2007. Membrane bioreactor sludge rheology at different solid retention times. Water Research. 41. (18). pp. 4197-4203.

Leifer I., Patro R. K., and Bowyer P. 2000. A Study on the Temperature Variation of Rise Velocity for Large Clean Bubbles. Journal Of Atmospheric And Oceanic Technology. 17. pp. 1392 – 1402.

Li H., Wen Y., Cao A., Huang J. and Zhou Q. 2014. The influence of multivalent cations on the flocculation of activated sludge with different sludge retention times. Water Research. 55. (0). pp. 225-232.

Li H., Wen Y., Cao A., Huang J., Zhou Q. and Somasundaran P. 2012. The influence of additives (Ca2+, Al3+, and Fe3+) on the interaction energy and loosely bound extracellular polymeric substances (EPS) of activated sludge and their flocculation mechanisms. Bioresource Technology. 114. (0). pp. 188-194.

Li H. Z., Mouline Y. and Midoux N. 2002. Modelling the bubble formation dynamics in non-Newtonian fluids. Chemical Engineering Science. 57. (3). pp. 339-346.

Li X. Y. and Yang S. F. 2007. Influence of loosely bound extracellular polymeric substances (EPS) on the flocculation, sedimentation and dewaterability of activated sludge. Water Research. 41. (5). pp. 1022-1030.

Lide D. R. 2004. Handbook of Chemistry and Physics. 85th Edition. Florida, CRC Press LLC.

Lin T. J., Tsuchiya K. and Fan L. S. 1998. Bubble flow characteristics in bubble columns at elevated pressure and temperature. AIChE Journal. 44. (3). pp. 545-560.

Littlejohns J. V. and Daugulis A. J. 2007. Oxygen transfer in a gas-liquid system containing solids of varying oxygen affinity. Chemical Engineering Journal. 129. (1-3). pp. 67-74.

Lo C. S. and Hwang S. J. 2003. Local hydrodynamic properties of gas phase in an internal-loop airlift reactor. Chemical Engineering Journal. 91. (1). pp. 3-22.

Lopez J., Moreau A., Gil J.A., van der Graaf J.H.J.M., van Lier J.B., Ratkovich N. 2015. MBR activated sludge viscosity measurement using the Delft filtration characterization method. Journal of Water Process Engineering. 5. pp. 35-41

Maldonado J. G. G., Bastoul D., Baig S., Roustan M. and Hébrard G. 2008. Effect of solid characteristics on hydrodynamic and mass transfer in a fixed bed reactor operating in co-current gas–liquid up flow. Chemical Engineering and Processing: Process Intensification. 47. (8). pp. 1190-1200.

Maldonado M., Quinn J. J., Gomez C. O. and Finch J. A. 2013. An experimental study examining the relationship between bubble shape and rise velocity. Chemical Engineering Science. 98. (0). pp. 7-11.

Masutani G. and Stenstrom M. 1991. Dynamic Surface Tension Effects on Oxygen Transfer. Journal of Environmental Engineering. 117. (1). pp. 126-142.

Mena P., Ferreira A., Teixeira J. A. and Rocha F. 2011. Effect of some solid properties on gas-liquid mass transfer in a bubble column. Chemical Engineering and Processing: Process Intensification. 50. (2). pp. 181-188.

Mena P. C., Rocha F. A., Teixeira J. A., Sechet P. and Cartellier A. 2008. Measurement of gas phase characteristics using a monofibre optical probe in a three-phase flow. Chemical Engineering Science. 63. (16). pp. 4100-4115.

Mena P. C., Ruzicka M. C., Rocha F. A., Teixeira J. A. and Drahos J. 2005. Effect of solids on homogeneous-heterogeneous flow regime transition in bubble columns. Chemical Engineering Science. 60. (22). pp. 6013-6026.

Metz B., Koosen N. W. F., Suidjan J.C. 1979. The rheology of mould suspensions. Advances in chemical engineering. Vol 2. Springer Verlag, New York. pp 1103-156

Mezger E. 1946. Loi de variation de la tension superficielle avec la température.

Mikkelsen L. H. 2001. The shear sensitivity of activated sludge: Relations to filterability, rheology and surface chemistry. Colloids and Surfaces A: Physicochemical and Engineering Aspects. 182. (1-3). pp. 1-14.

Mikkelsen L. H. and Keiding K. 2002. Physico-chemical characteristics of full scale sewage sludges with implications to dewatering. Water Research. 36. (10). pp. 2451-2462.

Mineta R., Salehi Z., Yoshikawa H. and Kawase Y. 2011. Oxygen transfer during aerobic biodegradation of pollutants in a dense activated sludge slurry bubble column: Actual volumetric oxygen transfer coefficient and oxygen uptake rate in p-nitrophenol degradation by acclimated waste activated sludge. Biochemical Engineering Journal. 53. (3). pp. 266-274.

Mori M., Isaac J., Seyssiecq I. and Roche N. 2007. Effect of measuring geometries and of exocellular polymeric substances on the rheological behaviour of sewage sludge. Chemical Engineering Research and Design. 86. (6). pp. 554-559.

Mori M., Seyssiecq I. and Roche N. 2006. Rheological measurements of sewage sludge for various solids concentrations and geometry. Process Biochemistry. 41. (7). pp. 1656-1662.

Moustiri S., Hebrard G., Thakre S. S. and Roustan M. 2001. A unified correlation for predicting liquid axial dispersion coefficient in bubble columns. Chemical Engineering Science. 56. (3). pp. 1041-1047.

Ndoye F. T., Erabit N., Flick D. and Alvarez G. 2013. In-line characterization of a whey protein aggregation process: Aggregates size and rheological measurements. Journal of Food Engineering. 115. (1). pp. 73-82.

Nishikawa M., Kato H. and Hashimoto K. 1977. Heat Transfer in Aerated Tower Filled with Non-Newtonian Liquid. Industrial & Engineering Chemistry Process Design and Development. 16. (1). pp. 133-137.

Painmanakul P. and Hébrard G. 2008. Effect of different contaminants on the [alpha]-factor: Local experimental method and modeling. Chemical Engineering Research and Design. 86. (11). pp. 1207-1215.

Pittoors E., Guo Y., Van Hulle S.W.H. 2014. Oxygen transfer model development based on activated sludge and clean water in diffused aerated cylindrical tanks. Chemical Engineering Journal. 243, pp. 51-59.

Pöpel H. J. and Wagner M. 1996. Oxygen Transfer in Deep Diffused Aeration Tanks - Theory and Practical Results. Tribune de l'eau. (5-6). pp. 59-67.

Quinn J. J., Maldonado M., Gomez C. O. and Finch J. A. 2014. Experimental study on the shape–velocity relationship of an ellipsoidal bubble in inorganic salt solutions. Minerals Engineering. 55. (0). pp. 5-10.

Racault Y., Stricker A. E., Husson A. and Gillot S. 2011. Monitoring the variations of OTR in a full-scale membrane bioreactor using daily mass balances. Water Science & Technology. 63.(11). pp. 2651-2657.

Ratkovich N., Horn W., Helmus F. P., Rosenberger S., Naessens W., Nopens I. and Bentzen T. R. 2013. Activated sludge rheology: A critical review on data collection and modelling. Water Research. 47. (2). pp. 463-482.

Redmon D., Boyle W. C. and Ewing L. 1983. Oxygen Transfer Efficiency Measurements in Mixed Liquor Using Off-Gas Techniques. Journal (Water Pollution Control Federation). 55. (11). pp. 1338-1347.

Riboux G. 2008. Hydrodynamique d'un essaim de bulles en ascension. Toulouse, INP Toulouse.

Riboux G., Risso F. and Legendre D. 2010. Experimental characterization of the agitation generated by bubbles rising at high Reynolds number. Journal of Fluid Mechanics 643. pp. 509-539.

Rosenberger S., Kubin K. and Kraume M. 2002. Rheology of Activated Sludge in Membrane Bioreactors. Engineering in Life Sciences. 2. (9). pp. 269-275.

Rosso D., Huo D. L. and Stenstrom M. K. 2006. Effects of interfacial surfactant contamination on bubble gas transfer. Chemical Engineering Science. 61. (16). pp. 5500-5514.

Rosso D., Iranpour R. and Stenstrom M. K. 2005. Fifteen Years of Offgas Transfer Efficiency Measurements on Fine-Pore Aerators: Key Role of Sludge Age and Normalized Air Flux. Water Environnement Research. 7. (3). pp. 266-272.

Rosso D. and Stenstrom M. K. 2006. Surfactant effects on [alpha]-factors in aeration systems. Water Research. 40. (7). pp. 1397-1404.

Roustan M. 1996. Quels sont les critères d'extrapolation pour les systèmes d'aération? Tribune de l'Eau. (1). pp. 53–58.

Sanchez Pérez J. A., Rodriguez Porcel E. M., Casas López J. L., Fernández Sevilla J. M. and Chisti Y. 2006. Shear rate in stirred tank and bubble column bioreactors. Chemical Engineering Journal. 124. (1-3). pp. 1-5.

Sardeing R., Painmanakul P. and Hébrard G. 2006. Effect of surfactants on liquid-side mass transfer coefficients in gas–liquid systems: A first step to modeling. Chemical Engineering Science. 61. (19). pp. 6249-6260.

Schumpe A. and Deckwer W. D. 1987. Viscous media in tower bioreactors: Hydrodynamic characteristics and mass transfer properties. Bioprocess and Biosystems Engineering. 2. (2). pp. 79-94.

Seyssiecq I., Ferrasse J.-H. and Roche N. 2003. State-of-the-art: rheological characterisation of wastewater treatment sludge. Biochemical Engineering Journal. 16. (1). pp. 41-56.

Seyssiecq I., Marrot B., Djerroud D. and Roche N. 2008. In situ triphasic rheological characterisation of activated sludge, in an aerated bioreactor. Chemical Engineering Journal. 142. (1). pp. 40-47.

Sheng G.-P., Yu H.-Q. and Li X.-Y. 2008. Stability of sludge flocs under shear conditions. Biochemical Engineering Journal. 38. (3). pp. 302-308.

Spicer P. T., Pratsinis S. E., Raper J., Amal R., Bushell G. and Meesters G. 1998. Effect of shear schedule on particle size, density, and structure during flocculation in stirred tanks. Powder Technology. 97. (1). pp. 26-34.

Stewart C. W. 1995. Bubble interaction in low-viscosity liquids. International Journal of Multiphase Flow. 21. (6). pp. 1037-1046.

Stricot M. 2008.Bioréacteurs à membranes à configuration externe influence de la configuration du procédé sur la structuration des matrices biologiques et le colmatage des membranes. 1 vol. (263 p.) + annexes.

Stricot M., Filali A., Lesage N., Spérandio M. and Cabassud C. 2010. Side-stream membrane bioreactors: Influence of stress generated by hydrodynamics on floc structure, supernatant quality and fouling propensity. Water Research. 44. (7). pp. 2113-2124.

Sutapa I. D. A. 1996.Propriétés Physico-chimiques et decantabilité des boues activées en relation avec le transfert d'oxygène et la biofloculation. Thèse de Doctorat, Institut National Polytéchnique de Lorraine, 170 p + annexes.

Thomasi S., Cerri M. and Badino A. 2010. Average shear rate in three pneumatic bioreactors. Bioprocess and Biosystems Engineering. 33. (8). pp. 979-988.

Tixier N. 2003.Approche des propriétés rhéologiques de suspensions biologiques floculées. Thèse de Doctorat, Université de Limoges, 141 + annexes.

Tixier N., Guibaud G. and Baudu M. 2003. Determination of some rheological parameters for the characterization of activated sludge. Bioresource Technology. 90. (2). pp. 215-220.

Urbain V., Block J. C. and Manem J. 1993. Bioflocculation in activated sludge: an analytic approach. Water Research. 27. (5). pp. 829-838.

Vasconcelos J. M. T., Rodrigues J. M. L., Orvalho S. C. P., Alves S. S., Mendes R. L. and Reis A. 2003. Effect of contaminants on mass transfer coefficients in bubble column and airlift contactors. Chemical Engineering Science. 58. (8). pp. 1431-1440.

Vermande S. 2005.Modélisation hydrodynamique et biologique des bassins d'aération. Doctorate, INSA de Toulouse, + annexes.

Wagner M. and Pöpel H. J. 1996. Surface active agents and their influence on oxygen transfer. Water Science and Technology. 34. (3-4). pp. 249-256.

Wagner M. R. and Pöpel H. J. 1998. Oxygen transfer and aeration efficiency — Influence of diffuser submergence, diffuser density, and blower type. Water Science and Technology. 38. (3). pp. 1-6.

Wagner M., Cornel P. and Krause S. 2002. Efficiency of different aeration systems in full scale membrane bioreactors. Proc. 75th WEFTEC conference, Chicago, IL. 10 p.

Wallis G. B. 1969. One Dimensional Two-Phase Flow. Mcgraw-Hill.

Whalley, P. B. and Davidson, J. F. 1974. Liquid circulation in bubble columns. Proceedings of the symposium on multiphase flow systems, Symp ser, No. 38.J.5, Ichem, London, 1-5.

Wilén B.-M., Jin B. and Lant P. 2003. Impacts of structural characteristics on activated sludge floc stability. Water Research. 37. (15). pp. 3632-3645.

Wilén B.-M., Lumley D., Mattsson A. and Mino T. 2008. Relationship between floc composition and flocculation and settling properties studied at a full scale activated sludge plant. Water Research. 42. (16). pp. 4404-4418.

Xia M., Wang Z., Wu Z., Wang X., Zhou Z. and Lu J. 2009. Simulation and assessment of sludge concentration and rheology in the process of waste activated sludge treatment. Journal of Environmental Sciences. 21. (12). pp. 1639-1645.

Yang F., Bick A., Shandalov S., Brenner A. and Oron G. 2009. Yield stress and rheological characteristics of activated sludge in an airlift membrane bioreactor. Journal of Membrane Science. 334. (1-2). pp. 83-90.

Yang W., Wang J., Wang T. and Jin Y. 2001. Experimental study on gas-liquid interfacial area and mass transfer coefficient in three-phase circulating fluidized beds. Chemical Engineering Journal. 84. (3). pp. 485-490.

Zahradník J. and Fialová M. 1996. The effect of bubbling regime on gas and liquid phase mixing in bubble column reactors. Chemical Engineering Science. 51. (10). pp. 2491-2500.

Zahradník J., Fialová M., Růžička M., Drahoš J., Kaštánek F. and Thomas N. H. 1997. Duality of the gas-liquid flow regimes in bubble column reactors. Chemical Engineering Science. 52. (21–22). pp. 3811-3826.

Zlokarnik M. 1979. Sorption characteristics of slot injectors and their dependency on the coalescence behaviour of the system. Chemical Engineering Science. 34. (10). pp. 1265-1271.

LIST OF FIGURES

CHAPTER I

CHAPTER II

CHAPTER III

CHAPTER IV

CHAPTER V

CHAPTER VI

LIST OF TABLES

CHAPTER I

CHAPTER II

CHAPTER III

CHAPTER IV

CHAPTER V

CHAPTER VI

APPENDIX

APPENDIX 1

Some design characteristics and removal efficiency of the wastewater treatment plants of Marolles/Saint Vrain and Briis-sous-Forges.

Appendix table 1. Design features of the Saint Vrain/Marolles and Briis-sous-Forges wastewater treatment plants.

	Feature	Units	Saint Vrain	Briis-sous-Forges
Aerated basin	Geometry	-	Annular	Rectangular
	Liquid Height	m	5	5.5
	Liquid Volume	m^3	4478	898.2
Influent Load	Flow rate	m^3/d	4300	4208
	Mixed liquor suspended solids (MLSS)	kg/d	2540	1930
	Biochemical oxygen demand (BOD)	kg/d	1320	1117
	Chemical oxygen demand (COD)	kg/d	3640	2824
	Total Kjehdal nitrogen (TKN)	kg/d	400	257
	Total Phosporus (TP)	kg/d	76	40

Appendix table 2. Removal efficiency (%) in the Saint Vrain/Marolles and Briis-sous-Forges wastewater treatment plants during the periods of the oxygen transfer measurements performed on site: 2012 and 2013 respectively.

Parameter	Saint Vrain (2012)	Briis-sous-Forges (2013)
Mixed liquor suspended solids (MLSS)	98.2	98.8
Biochemical oxygen demand (BOD)	97.9	98.1
Chemical oxygen demand (COD)	94.6	96.2
Total Kjeldahl nitrogen (TKN)	95.8	96.4
Global nitrogen (GN)	92.9	82.8
Total phosporus (TP)	96.0	92.8

APPENDIX 2

Protocol description of the gas-phase oxygen analysis to estimate the OTE_c

The ambient air and the off-gas flow are alternatively drawn into the oxygen analyser by means of a set of valves. For each of these air flows, the air flow rate is fixed to 1 L min^{-1} and air pressure of 20 hPa using two rotameters and two manometers installed in the analysis unit.

Before oxygen analysis, the airflow passes through a column packed with silica gel crystals and sodium hydroxide pellets in order to remove the water vapour and carbon dioxide fractions respectively.

The oxygen partial concentration in the airflow is measured with an electrochemical gas-phase oxygen transducer (Teledyne Analytical Instruments – Class E2). The analyser response for an oxygen flow is a voltage output proportional to the oxygen partial pressure (and concentration), respectively noted I_i and I_e. With a constant airflow pressure in the measurement unit, the following relation can be written:

$$I_i/{y_i}' = I_e/{y_e}' \qquad \text{Ap. Eq. 1}$$

OTE_c can be then estimated using Ap. Eq. 2:

$$OTE_c = 1 - \frac{{y_e}'(1-{y_i}')}{{y_i}'(1-{y_e}')} = \frac{I_i - I_e}{I_e - {y_i}' I_e} \qquad \text{Ap. Eq. 2}$$

where

I_i sensor response for the ambient (injected) air flow (mV)

I_e sensor response for the off-gas air flow (mV)

${y_i}'$ oxygen molar fraction of the injected air flow free of water vapor and carbon dioxide (${y_i}'$=0.2095)

The air tightness in the oxygen analysis unit is verified before usage drawing in an inert gas stream (nitrogen). The oxygen sensor response must then be near zero (±0.6%). The linearity of the oxygen probe is also tested before use by drawing in the ambient air at two different airflow rates and measuring the respective sensor response air flow pressures. The ratio of the analyser response to the airflow pressure must remain constant (±0.4%) after the air flow rate variation, because the oxygen molar fraction do not depend on the airflow.

APPENDIX 3

Analysis of Covariance (ANCOVA) using the statistics software R for comparing two linear regressions

The analysis of covariance allowed analyzing the effect of independent variables (quantitative and qualitative) on a dependent variable Y. The analysis presented in this study is based on the method proposed by Cornillon *et al.* (2012). The analysis required considering only two independent variables: X (quantitative) and Z (qualitative), the latter considered in different modalities I. The relation between X and Y may be different for the different modalities I of the qualitative variable Z.

In a simplified way, a linear regression is written for each of the modalities i as follows:

$$Y_{ij} = \alpha_i + \gamma_i X_{i,j} + \varepsilon_{i,j} \ ; \ i = 1, \dots, I \ ; \quad j = 1, \dots, n_i$$

Where

α_i intercept of the linear model for the modality i

Y_i slope of the linear model for the modality i

ε_i model residual for the modality i

In this analysis of covariance it is considered that all residuals (ε_i) have the same variance (σ^2).

By integrating an average intercept (α) and an average slope (γ) to the linear regression, the model is written as:

$$Y_{ij} = \alpha + \alpha_i + (\gamma + \gamma_i) X_{i,j} + \varepsilon_{i,j} \ ; \ i = 1, \dots, I \ ; \quad j = 1, \dots, n_i$$

To evaluate if the variable Z has an effect on the relation between Y and X, the analysis of covariance examines if the intercepts and slopes of different linear models can be considered as statistically equal.

Using the experimental data, three models, represented in Figure Ap. 1 are written:

1. A *'complete'* model with two different slopes and two different intercepts (Figure Ap. 1a).
2. A model with a *'unique slope'* and two different intercepts (Figure Ap. 1b).

   $$Y_{ij} = \alpha_i + \gamma X_{i,j} + \varepsilon_{i,j} \ ; \ i = 1, \dots, I \ ; \quad j = 1, \dots, n_i$$

3. A model with a *'unique intercept'* and two different slopes (Figure Ap. 1c)

$$Y_{ij} = \alpha + \gamma_i X_{i,j} + \varepsilon_{i,j} \ ; \ i = 1, \dots, I \ ; \quad j = 1, \dots, n_i$$

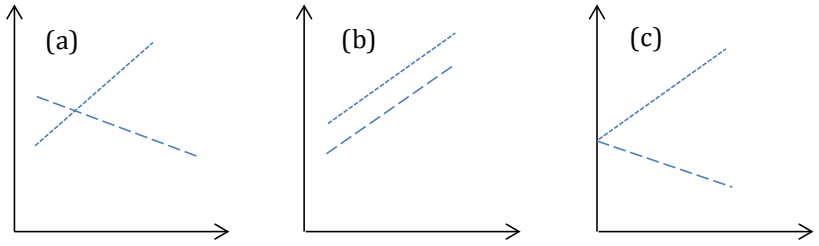

Figure Ap. 1. Representation of the written linear models for the analysis of covariance (from Cornillon *et al.,* 2012) .

The slopes and intercepts of the model 1 (complete) are respectively compared to the model of unique slope (model 2) and unique intercept (model 3) by means of an Anova analysis.

In the software R, the three respective linear models (**lm**) are written as follows:

```
> complete=lm(Y~-1+Z+Z:X,data=experimentaldata)
> Uslope=lm(Y~-1+Z+X,data=experimentaldata)
> Uintercept=lm(Y~Z:X,data=experimentaldata)
```

The comparison between the models is written using the **anova** fonction:

```
> anova(Uslope,complete)
> anova(Uintercept,complete)
```

For each of these two comparisons, the analysis results provide the degrees of freedom, the sum of squared residuals, the mean squared residuals, the statistical F value for the test and the critical probability (Pr(>F)) or p-value. If the latter is higher than the significance level (5%), the null hypothesis (Ho) is accepted. Consequently the slopes and the intercepts of the *'complete'* model can be considered as equivalent to the ones of the respective models of unique slope and unique intercept. Hence it can be deduced that the modality I of the qualitative variable Z do not affect the relationship between the variables X and Y.

The Appendix table 3 presents the p-values resulting from the analysis of covariance for different quantitative variables X and Y and different studied modalities (I) of qualitative variables Z.

Appendix table 3. Results of the analysis of covariance obtained for different quantitative variables X and Y and different studied modalities (I) of qualitative variables Z.

X vs. Y	Studied Modalities I of the variable Z	*Uslope* p-value	*Uintercept* p-value
k_La vs. U_G	Reoxygenation method Off-gas method	0.53	-
Rheogram τ vs. $\dot{\gamma}$	Large or small volume: 10L, 40L	0.17	0.34
	Agitation Speed: 40, 80, 120.	0.98	0.99
	Storage time: D_0, D+1 or D+2 days.	0.29	0.59

The shown p-values result from comparing the 'complete' model respectively with the Uslope and Uintercept model.

Since the experimental function k_La=f(U_G) must have an intercept equal to zero, the analysis of covariance did not include the creation of a linear model with a 'unique intercept' and for that reason no p-value is observed in the column *Uintercept* in Appendix table 3

APPENDIX 4

Development of the equation to estimate the gas hold-up in the bubble column by means of two hydrostatic pressure probes submerged at a constant depth at the top and the bottom of the aerated volume

In a volume with constant cross-sectional area, the overall gas hold-up (ε_G) can be expressed in terms of the gas and liquid height as:

$$\varepsilon_G = \frac{V_G}{V_T} = \frac{H_G}{H_T} \qquad \text{Ap. Eq. 3}$$

with

ε_G overall gas hold-up (-)

V_G gas volume (m^3)

V_T gas-liquid mixture volume (m^3)

H_G height occupied by the gas (m)

H_T height occupied by the gas-liquid mixture (m)

Under *non-aerated* conditions, the difference between the hydrostatic pressure of the two submerged probes corresponds to the pressure exerted by the liquid column:

$$\Delta P_1 = \rho_L g H_{1L} \qquad \text{Ap. Eq. 4}$$

with

ΔP_1 hydrostatic pressure difference between the top and bottom pressure probes under non-aerated conditions (Pa)

ρ_L liquid density (kg m^{-3})

g gravity (m s^{-2})

H_{1L} liquid height between the two oxygen probes under non-aerated conditions (m)

Under *aerated* conditions, the difference between the hydrostatic pressure of the two submerged probes corresponds to the pressure exerted by the liquid and the gas column:

$$\Delta P_2 = g(\rho_L H_{2L} + \rho_G H_G) \qquad \text{Ap. Eq. 5}$$

with

ΔP_2 hydrostatic pressure difference between the top and bottom pressure probes under aerated conditions (Pa)

ρ_G gas density (kg m^{-3})

g gravity (m s^{-2})

H_{2L} liquid height between the two oxygen probes under aerated conditions (m)

H_G gas height between the two oxygen probes under aerated conditions (m)

The gas height (H_G) corresponds to the difference in liquid height under non-aerated (H_{1L}) and aerated conditions (H_{2L}):

$$H_G = H_{1L} - H_{2L} \qquad \text{Ap. Eq. 6}$$

From the equations above defining ΔP_1, ΔP_2 and considering that $\rho_{air} \ll \rho_{eau} \approx \rho_{sludge}$, the gas height (H_G) can be estimated with:

$$H_G = \frac{\Delta P_1 - \Delta P_2}{g\rho_L} \qquad \text{Ap. Eq. 7}$$

The height of the gas-liquid mixture (H_T) corresponds to the liquid height separating the two pressure probes (H_{1L}) and can be obtained from Ap. Eq. 4. The overall gas hold-up (ε_G), determined in the volume limited by the two pressure probes, can then be estimated with:

$$\varepsilon_G\,(-) = \left(1 - \frac{\Delta P_2}{\Delta P_1}\right) = \left(1 - \frac{\Delta P_{with\ air}}{\Delta P_{without\ air}}\right) \qquad \text{Ap. Eq. 8}$$

APPENDIX 5

Development of the equation to estimate the shear stress and the shear rate in a tubular section for Newtonian fluids

a) Shear stress, τ_r , for a Newtonian fluid

Hypothesis:

- Fluid slip at the wall is zero (there is no wall slip)
- The fluid is incompressible
- The system is isothermal
- There is no thixotropy

The next figure shows the equilibrium of horizontal forces in an infinitesimal section of a tube:

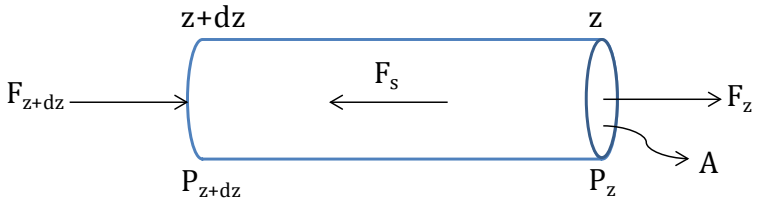

Figure Ap. 2. Schematic of equilibrium forces in an infinitesimal section of a tube

With:

A	cross-sectional area	$A = \pi r^2$	Ap. Eq. 9
P_z	pressure at the outlet section of the capillary	$P_z = \frac{F_z}{A}$	Ap. Eq. 10
P_{z+dz}	pressure at the inlet section of the capillary	$P_{z+dz} = \frac{F_{z+dz}}{A}$	Ap. Eq. 11
F_z	pressure force at the outlet section of the capillary	$F_z = \mathrm{P_z} \cdot \pi \mathrm{r}^2$	Ap. Eq. 12
F_{z+dz}	pressure force at the inlet section of the capillary	$F_{z+dz} = \mathrm{P_{z+dz}} \cdot \pi \mathrm{r}^2$	Ap. Eq. 13
F_S	shear force at the tube wall	$Fs = \tau(r) 2\pi \mathrm{r} \cdot dz$	Ap. Eq. 14
$\tau(r)$	shear stress at a radius r	$\tau(r) = \frac{F_s}{S}$	Ap. Eq. 15
S	surface layer	$S = 2\pi r \cdot dz$	Ap. Eq. 16

The pressure force at the inlet section of the capillary tube tends to accelerate the flow. The equilibrium of forces is written as follows:

$$F_z - F_{z+dz} + Fs = 0 \qquad \text{Ap. Eq. 17}$$

Replacing Eqautions from Ap. Eq. 12 to Ap. Eq. 14 in Ap. Eq. 17:

$$P_z \cdot \pi r^2 - P_{z+dz} \cdot \pi r^2 + \tau(r) 2\pi r \cdot dz = 0 \qquad \text{Ap. Eq. 18}$$

$$P_z - P_{z+dz} + \frac{2\tau(r) \cdot dz}{r} = 0 \qquad \text{Ap. Eq. 19}$$

Defining the pressure at the inlet as:

$$P_{z+dz} = P_z + \frac{dP}{dz} dz \qquad \text{Ap. Eq. 20}$$

And replacing the equation Ap. Eq. 20 in Ap. Eq. 21 it is possible to obtain $\tau(r)$ as follows:

$$\tau(r) = \frac{r}{2} \cdot \frac{dP}{dz} \qquad \text{Ap. Eq. 21}$$

Assuming a steady state flow, the shear stress $\tau(r)$ is constant in the direction z. Then,

$$\frac{dP}{dz} = \frac{\Delta P}{L} \qquad \text{Ap. Eq. 22}$$

With:

ΔP pressure loss in a tube between two points separated by a length L.

Thus, the shear stress $\tau(r)$ can be expressed at the tube wall as τ_w:

$$\tau_w = \tau = \frac{r}{2} \cdot \frac{\Delta P}{L} \qquad \text{Ap. Eq. 23}$$

The shear stress τ_w, is independent from the type of fluid considered. In a tube of known geometry, the τ_w applied, can be obtained by measuring the fluid pressures at different points of the tube length.

b) Shear rate, $\dot{\gamma}$, for a Newtonian fluid

The shear, γ, and the shear rate, $\dot{\gamma}$, in a tube are defined by the following equations:

γ Shear or deformation $\qquad \gamma = \frac{dx}{dz}$ $\qquad$ Ap. Eq. 24

$\dot{\gamma}(r)$ Shear rate

$$\dot{\gamma}(r) = \frac{dx}{dzdt} = \frac{dU}{dz} \qquad \text{Ap. Eq. 25}$$

With:

U as the fluid velocity in the tube.

When considering the flow (dQ) through an infinitesimal annular section of a capillary tube, with thickness dr, placed at a distance r from the tube axis, as shown in the figure below:

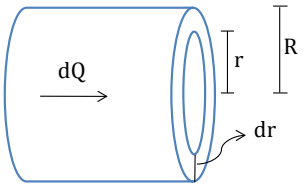

Figure Ap. 3. Schematization of the flow in an annular section of a tube

the shear rate in the annular section is written as:

$$\dot{\gamma}(r) = \frac{dU(r)}{dr} \qquad \text{Ap. Eq. 26}$$

And the flow rate, Q, in this annular section of the tube is defined as:

$$Q = S \cdot U \qquad \text{Ap. Eq. 27}$$

$$dQ = (2\pi r \cdot \mathrm{d}r)(U(r)) \qquad \text{Ap. Eq. 28}$$

Thus, the total flow rate in the tube is:

$$Q = \int_0^R (2\pi r \cdot \mathrm{d}r)(U(r)) \qquad \text{Ap. Eq. 29}$$

The velocity in a tube is a decreasing parabolic function of the radial distance to the axe of the tube defined by:

$$U(r) = U_0\left(1 - \frac{r^2}{R^2}\right) \qquad \text{Ap. Eq. 30}$$

Thus, replacing the equation Ap. Eq. 30 in Ap. Eq. 29, it results:

$$\mathrm{Q} = 2\pi U_0 \int_0^R \mathrm{r}\left(1 - \frac{r^2}{R^2}\right) \cdot \mathrm{dr} \qquad \text{Ap. Eq. 31}$$

Integrating the Equation Ap. Eq. 31 and developing for U_0:

$$U_0 = \frac{2\mathrm{Q}}{\pi R^2} \qquad \text{Ap. Eq. 32}$$

Now, from Ap. Eq. 26, and deriving the equation Ap. Eq. 30, it results:

$$\dot{\gamma}(r) = \frac{dU(r)}{dr} = -\frac{2U_0 r}{R^2} \qquad \text{Ap. Eq. 33}$$

and replacing Ap. Eq. 32 in Ap. Eq. 33, it is possible to find the mathematical expression for the shear rate as a function of the tube radius as follows:

$$\dot{\gamma}(r) = -\frac{4\mathrm{Q}r}{\pi R^4} \qquad \text{Ap. Eq. 34}$$

Because it is agreed to calculate the shear rate at the wall in a capillary tube ($r = R$), the equation defining $\dot{\gamma}$ is:

$$\dot{\gamma}_R = \dot{\gamma} = -\frac{4\mathrm{Q}}{\pi R^3} \qquad \text{Ap. Eq. 35}$$

c) Shear rate, $\dot{\gamma}$, for a non-Newtonian fluid

Given that for a non-Newtonian fluid the velocity profile results in a change of the viscosity with the radius of the tube in relation to the fluid Newtonian character, the approach to calculate the shear rate differs from the one applied for the Newtonian fluids, thus, integrating by parts the Eqaution Ap. Eq. 29, and assuming that there is no wall slip ($U(R) = 0$) :

$$Q = [\pi \mathrm{r}^2 \cdot U(r)]|_0^R - \pi \int_0^R \mathrm{r}^2 \frac{dU(r)}{dr} \mathrm{dr} = -\pi \int_0^R \mathrm{r}^2 \dot{\gamma} \cdot \mathrm{dr} \qquad \text{Ap. Eq. 36}$$

Making a variable change $\tau = \frac{r}{R} \cdot \tau_w$ in the Equation Ap. Eq. 36, Q is then expressed by:

$$Q = -\pi \int_0^{\tau_w} \dot{\gamma} \left(\frac{\mathrm{R}\tau}{\tau_\mathrm{w}}\right)^2 \frac{\mathrm{R}}{\tau_\mathrm{w}} \cdot \mathrm{d}\tau \qquad \text{Ap. Eq. 37}$$

$$\frac{{\tau_\mathrm{w}}^3}{\mathrm{R}^3} \cdot Q = -\pi \int_0^{\tau_w} \dot{\gamma}\tau^2 \cdot \mathrm{d}\tau \qquad \text{Ap. Eq. 38}$$

Deriving both sides of the Equation Ap. Eq. 38 in respect to τ_w, it results:

$$\frac{{\tau_\mathrm{w}}^3}{\mathrm{R}^3}\frac{dQ}{d\tau_\mathrm{w}} + Q\frac{3{\tau_\mathrm{w}}^2}{\mathrm{R}^3} = -\pi {\tau_w}^2 \dot{\gamma}_w \qquad \text{Ap. Eq. 39}$$

With:

$\dot{\gamma}_w$ shear rate at the wall

Thus, the shear rate at the wall, $\dot{\gamma}_w$, can be expressed by:

$$\dot{\gamma}_w = \dot{\gamma}_R = -\frac{1}{\pi \mathrm{R}^3}\left[3Q + \tau_\mathrm{w}\frac{dQ}{d\tau_\mathrm{w}}\right] \qquad \text{Ap. Eq. 40}$$

Replacing $dQ = Q \cdot d(Ln\ Q)$ and $d\tau_\mathrm{w} = \tau \cdot d(Ln\ \tau)$ in the equation Ap. Eq. 40 and assuming that $\tau_\mathrm{w} = \tau$, it results:

$$\dot{\gamma}_w = -\frac{4\mathrm{Q}}{\pi R^3}\left(\frac{3n+1}{4n}\right) \qquad \text{Ap. Eq. 41}$$

Where n is the flow index in the Ostwald-de Waele rheological model. It can be estimated as:

$$n = \frac{d(Ln\ \tau)}{d(Ln\ Q)}\ or\ \frac{d(Ln\ \tau)}{d(Ln\ 4Q/\pi R^3)} \qquad \text{Ap. Eq. 42}$$

The term $\left(\frac{3n+1}{4n}\right)$ is called the Rabinowitsch-Mooney correction.

The equation Ap. Eq. 41, calls in the expression for the shear rate $\dot{\gamma}$ found before in Ap. Eq. 35 for Newtonian fluids. Thereby, regardless of the fluid rheological behaviour, the shear rate can be determined by the measurement of the flow rate through the capillary tube.

APPENDIX 6

Calculation of measurement uncertainty with respect to viscosity using the tubular rheometer by the method of partial derivatives

The partial derivatives method to calculate the measurement uncertainty requires deriving the function that defines the studied variable in respect to each measured variable and to know the accuracy of the used instruments. The instruments accuracy and the tubes manufacturing tolerance are presented in Appendix table 4.

Appendix table 4. Tubes manufacturing tolerance and instruments accuracy in the tubular rheometer

Measured Variable	*Instrument*	*Range*	*Tolerance or Accuracy*
Radius (R)	Tube	4, 7, 12, 14 mm	±0.01 mm
Length (L)	Tube	0.4, 0.8, 1.0, 1.0 m	±1 mm
Weight (W)	Scale	Up to 30 kg	±1g
Differential Pressure (ΔP)	Micromanometers	Up to 500 Pa Up to 2500 Pa	If ΔP<100 Pa→0.2% ±0.8 Pa If ΔP>100 Pa→0.2% ±1.5 Pa 0.2%±2Pa
Density (ρ)	Correlation ρ_{water}=f(T)	from 5 to 25°C	±0.03%
Temperature (T)	Thermometer	Up to 300°C	±1°C

Density is considered in the calculation of uncertainty since measuring the flow rate (Q) with the use of a scale requires the determination of the fluid density. Sludge density is assumed to be equivalent to the water density (on the basis of laboratory measurements) which can be defined as a function of temperature as follows:

$$\rho_{(T)} = -0.0038T^2 - 0.0477T + 1000.4465 \qquad \text{Ap. Eq. 43}$$

The latter correlation provides the density values with an accuracy of ±0.03% in comparison with theoretical values (Lide, 2004). This error is then included in the uncertainty calculation. Besides, the uncertainty in the measurement of temperature induces an error on the estimation of the fluid density using Ap. Eq. 43. Consequently, the temperature accuracy is also included in the uncertainty calculation.

The calculation of uncertainty was based on the viscosity equation for Newtonian fluids. According to the Poiseuille's law the dynamic viscosity of a fluid in a tubular section can be determined as follows:

$$\mu = \frac{R^4 \Delta P \pi}{8QL} \qquad \text{Ap. Eq. 44}$$

where

μ fluid viscosity (Pa.s)

R tube radius (m)

L tube length (m)

ΔP differential pressure between two points separated by a distance L (Pa)

Q flow rate in the tube ($m^3\ s^{-1}$)

The density (ρ) and temperature (T) are introduced in the viscosity equation by replacing $Q = m/\rho$ and $\rho_{(T)}$ in the equation Ap. Eq. 44.

Thus, the measurement absolute uncertainty of the apparent viscosity ($\Delta\mu$) is given by:

$$\Delta\mu = k\left(\frac{d\mu}{dR}\Delta R + \frac{d\mu}{dL}\Delta L + \frac{d\mu}{dW}\Delta W + \frac{d\mu}{d\Delta P}\Delta(\Delta P) + \frac{d\mu}{d\rho}\Delta\rho + \frac{d\mu}{dT}\Delta T\right) \qquad \text{Ap. Eq. 45}$$

where

k coverage factor for expanded uncertainty

ΔR tube radius manufacturing tolerance

ΔL tube length manufacturing tolerance

ΔW balance accuracy

$\Delta(\Delta P)$ manometer accuracy

$\Delta\rho$ density model accuracy

ΔT thermometer accuracy

The respective derivates are given by the following equations:

$$\frac{d\mu}{dR} = \frac{4R^3 \Delta P \pi}{8QL} \qquad \text{Ap. Eq. 46}$$

$$\frac{d\mu}{dL} = \frac{R^4 \Delta P \pi}{8QL^2} \qquad \text{Ap. Eq. 47}$$

$$\frac{d\mu}{dW} = \frac{R^4 \Delta P \pi \rho}{8L(Q\rho)^2} \quad \text{Ap. Eq. 48}$$

$$\frac{d\mu}{d\Delta P} = \frac{R^4 \pi}{8LQ} \quad \text{Ap. Eq. 49}$$

$$\frac{d\mu}{dT} = \frac{R^4 \Delta P \pi}{8mL}(2 \cdot 0.0038T + 0.0477) \quad \text{Ap. Eq. 50}$$

$$\frac{d\mu}{d\rho} = \frac{R^4 \Delta P \pi}{8LQ\rho} \quad \text{Ap. Eq. 51}$$

The uncertainty is computed for a given fluid viscosity (μ) at 20°C within the range of applied flow rates (Q) and shear rates ($\dot{\gamma}$) in the different tube geometries (L, R) and the associated differential pressure (ΔP). The uncertainty is estimated within a confidence level of 95% (k=2).

For a fluid as viscous as water (μ=1mPa.s), the uncertainty of the viscosity (μ) measurement is presented in Appendix table 5 for different tube geometries, flow rates (Q) and shear rates ($\dot{\gamma}$). When the flow conditions are not laminar (Re>2000), uncertainty values are not indicated (empty cells).

Appendix table 5. Estimated measurement uncertainty (±%) on viscosity for water ($\boldsymbol{\mu}$=1 mPa.s) for each tube in the range of applied shear rate ($\dot{\boldsymbol{\gamma}}$) and flow rate ($\boldsymbol{Q}$). For the empty cells the flow is not laminar (Re>2000).

Tube	Q (L/h)	5	10	15	20	25	30	35	40	45	50
D4	$\dot{\gamma}$	221.0	442.1	663.1	884.2						
	% uncertain.	7.8%	7.7%	7.1%	6.8%						
D7	$\dot{\gamma}$	41.2	82.5	123.7	165.0	206.2	247.5	288.7	330.0		
	% uncertain.	12.5%	8.2%	6.8%	6.1%	5.7%	6.6%	6.2%	5.9%		
D12	$\dot{\gamma}$	8.2	16.4	24.6	32.7	40.9	49.1	57.3	65.5	73.7	81.9
	% uncertain.	61.6%	32.3%	22.5%	17.6%	14.7%	12.7%	11.3%	10.3%	9.5%	8.8%
D14	$\dot{\gamma}$	5.2	10.3	15.5	20.6	25.8	30.9	36.1	41.2	46.4	51.6
	% uncertain.	111.4%	57.1%	39.0%	29.9%	24.5%	20.9%	18.3%	16.3%	14.8%	13.6%

For fluids with a viscosity 1.5 times the water dynamic viscosity, the estimated uncertainty on the viscosity measurements is presented in Appendix table 6.

Appendix table 6. Estimated measurement uncertainty (±%) on viscosity for each tube in the range of applied shear rate ($\dot{\gamma}$) and flow rate ($\boldsymbol{Q}$) and for a fluid with a *viscosity* ***1.5 times the water dynamic viscosity*** (for Newtonian fluids). For the empty cells the flow is not laminar (Re>2000).

Tube	Q (L/h)	5	10	15	20	25	30	35	40	45	50
D4	$\dot{\gamma}$	221.0	442.1	663.1	884.2	1105.2	1326.3				
	% uncertain.	8.2%	7.1%	6.7%	6.7%	6.6%	6.5%				
D7	$\dot{\gamma}$	41.2	82.5	123.7	165.0	206.2	247.5	288.7	330.0	371.2	412.5
	% uncertain.	9.6%	6.8%	5.8%	6.6%	6.1%	5.7%	5.5%	5.3%	5.1%	5.0%
D12	$\dot{\gamma}$	8.2	16.4	24.6	32.7	40.9	49.1	57.3	65.5	73.7	81.9
	% uncertain.	42.0%	22.5%	16.0%	12.7%	10.8%	9.5%	8.5%	7.8%	7.3%	6.8%
D14	$\dot{\gamma}$	5.2	10.3	15.5	20.6	25.8	30.9	36.1	41.2	46.4	51.6
	% uncertain.	75.2%	39.0%	26.9%	20.9%	17.2%	14.8%	13.1%	11.8%	10.8%	10.0%

For fluids with a viscosity 7 times the water dynamic viscosity, the estimated uncertainty on the viscosity measurements is presented in Appendix table 7.

Appendix table 7. Estimated measurement uncertainty (±%) on viscosity for each tube in the range of applied shear rate ($\dot{\gamma}$) and flow rate ($\boldsymbol{Q}$) and for a fluid with a **viscosity 7 times the water viscosity** (for Newtonian fluids). For the empty cells the flow is not laminar (Re>2000).

Tube	Q (L/h)	5	10	15	20	25	30	35	40	45	50
D4	$\dot{\gamma}$	221.0	442.1	663.1	884.2	1105.2	1326.3	1547.3	1768.4	1989.4	2210.5
	% uncertain.	6.6%	6.3%	6.2%	6.1%	6.1%	6.1%	6.1%	6.0%	6.0%	6.0%
D7	$\dot{\gamma}$	41.2	82.5	123.7	165.0	206.2	247.5	288.7	330.0	371.2	412.5
	% uncertain.	6.2%	5.1%	4.7%	4.5%	4.4%	4.3%	4.3%	4.2%	4.2%	4.2%
D12	$\dot{\gamma}$	8.2	16.4	24.6	32.7	40.9	49.1	57.3	65.5	73.7	81.9
	% uncertain.	11.3%	7.1%	5.7%	5.0%	4.6%	5.6%	5.2%	4.9%	4.7%	4.5%
D14	$\dot{\gamma}$	5.2	10.3	15.5	20.6	25.8	30.9	36.1	41.2	46.4	51.6
	% uncertain.	18.3%	10.5%	7.9%	6.6%	5.9%	5.3%	5.0%	4.7%	4.5%	5.7%